Effects of Transients on High Voltage Cable Insulation

Wu, Jiayang

DOI
10.4233/uuid:0d800572-337c-405c-bf40-c4867020b601

Publication date
2020

Document Version
Final published version

Citation (APA)
Wu, J. (2020). *Effects of Transients on High Voltage Cable Insulation*. [Dissertation (TU Delft), Delft University of Technology]. https://doi.org/10.4233/uuid:0d800572-337c-405c-bf40-c4867020b601

Effects of Transients on High Voltage Cable Insulation

Dissertation

for the purpose of obtaining the degree of doctor
at Delft University of Technology
by the authority of the Rector Magnificus, prof. dr. ir. T. H. J. J. van der Hagen
chair of the Board for Doctorates
to be defended publicly on
Friday 28 February 2020 at 12:30 o'clock

by

Jiayang WU

Master of Science
in Electrical Engineering, Information Technology and Computer Engineering
RWTH Aachen University, Germany

born in Nanjing, China

This dissertation has been approved by the promotors.

Composition of the doctoral committee:

Rector Magnificus,	chairperson
Prof. dr. J. J. Smit	Delft University of Technology, promotor
Prof. dr. ir. P. Bauer	Delft University of Technology, promotor
Dr. ir. A. Rodrigo Mor	Delft University of Technology, copromotor

Independent members:

Prof. dr. R. Ross	Delft University of Technology
Prof. dr. ing. R. Plath	Technische Universität Berlin, Germany
Prof. dr. ir. F. Garnacho Vecino	Universidad Politecnica de Madrid, Spain
Dr. ir. S. Mousavi Gargari	TenneT TSO B.V.
Prof. ir. P. T. M. Vaessen	Delft University of Technology, reserve member

This research was financially supported by TenneT TSO B.V., Arnhem, The Netherlands.

ISBN: 978-94-6366-255-0

Summary

Occasionally sporadic defects in high voltage cable insulation may escape from detection by commissioning or maintenance tests. Usually these tiny defects will not initiate significant partial discharges or cause breakdown in the cable insulation system under normal AC operating condition and normal transient situations. However, nowadays more often complex transient's behaviour occurs in power systems. For example, in a mixed line and cable system, superimposed transients with large overvoltage can occur due to switching operations. Such transients may have unexpected influences on the partial discharge behaviour and degradation of the cable insulation. This thesis aims to investigate which potential effects such transients have on the insulation condition of the HV cable system, in particular in one of its weakest links, the cable joint.

To investigate the effects of transients on the cable insulation, several diagnostic technologies for evaluating the insulation condition, e.g. breakdown strength testing, measurement of partial discharge (PD) and of dielectric properties have been used. This thesis first focuses on cable insulation material samples to test the voltage endurance with and without transients. Next, the focus is on cable model experiments to evaluate the partial discharge behaviour under different waveforms including superimposed transients, as in practice. Both types of investigations are conducted in the high voltage laboratory conditions.

Using a set-up for measuring breakdown voltage of material samples, it is shown for XLPE and epoxy resin that the breakdown strength of the insulation materials is much higher under DC voltage than under AC voltage and that the higher the AC frequency, the lower the breakdown strength is. For superimposed voltage waveform, consisting of a high frequency sine wave in superposition with the 50 Hz AC voltage, insulation samples break down at lower AC voltage when the superimposed sine wave has larger amplitude.

PD investigation is firstly performed on MV cable models consisting of MV cable with accessories, since these are easier installed and manipulated in the laboratory than HV cable. Several pieces of 4-meter length 6/10 kV MV XLPE cables and cold-shrink accessories are used to produce the MV cable models. Two types of artificial defects are introduced in the cable joints: by inserting a metal wire into the joint, a small void is left most probably at the tip of the wire at the interface. By inserting a plastic tie-wrap strip into the joint till the connector, air gaps are created along the interface. The measured phase-resolved PD patterns confirmed the causing of internal and surface discharges.

For generating the superimposed transients and applying them on the cable model, a Marx impulse generator is connected with an AC supply through a blocking capacitor. In order to measure PD signals during the application of impulses, which last for milliseconds, the unconventional PD measurement method is used. It is observed that, PD could be initiated from the artificial defects by superimposing transients. For those initiated PD, some extinguish after the AC voltage condition returns, however some others persist. The PD initiation and persistence are related to several factors in particular the electric field condition, the charge distribution within the defect and the aging status of the insulation. The application of transient changes some of the factors, which may further stimulate the PD initiation and persistence.

Secondly, the cable model investigation is extended to a 16-meter full-scale 150 kV HV XLPE cable including accessories with an adjustable defect in the cable joint. Partial discharge measurements on HV cable insulation are conducted based on the knowledge and experience with the MV cable tests. For this the set-up of MV cable is adjusted to enable the application of the higher voltage and impulse strike, and to satisfy the protection purpose of human and devices. The PD measuring system is designed consisting of cascaded high frequency current transformers (HFCT), band-pass filters and transient voltage suppressors (TVS), which are responsible for signal measurement, noise suppression and protecting, respectively. The introduced artificial defect is adjustable to generate PDs with different inception and extinction voltages. In our test, the HV cable model has been subjected to both pure impulses and superimposed transients, which are realistic transients as occurring in practice. It is observed that, under positive impulse voltage, PDs firstly initiate during the front time with positive polarity, which are recognized as main discharges, and then initiate during the tail time with negative polarity, which are referred to as reverse discharges. For superimposed transients, our results for the HV cable model show that, for the defect being such adjusted that the cable model would pass the PD criterion as in the maintenance test for a cable system in service, PDs can be initiated by superimposed transients producing overvoltage larger than $1.4U_0$. The initiated PDs can persist for a certain period of time up to more than ten seconds after the voltage returns to AC operating conditions. It is observed that the PD initiation and persistence are influenced by the transient voltage wave shapes, in particular the peak overvoltage value, the AC voltage level and the phase angle of impulse application. Those factors influence the number, the probability and the duration of PD occurrence (i.e. PD persistence), as well as the PD amplitude. With the defect being such adjusted that the cable model would pass the same PD criterion as in the commissioning test for new installed cable systems, no PD is observed that is initiated by the transients adding up to an overvoltage up to $2.1U_0$.

In practice, the transient situations can be more complex and various other factors are of influence such as long cable length and electromagnetic disturbances, which need to be considered. The knowledge gained about measuring PD initiation under transient can be useful reference for future cable condition assessment in practice.

Contents

Chapter 1

Introduction

With the growing demand of power and the integration of large-scale renewable energy, the transmission system operators (TSOs) and distribution system operators (DSOs) have been facing the necessity of expanding and upgrading the electricity power grid. As an alternative to overhead lines (OHLs), underground cable systems (UGC), i.e. medium voltage (MV) and high voltage (HV) cable systems, have been installed more and more around the world on both transmission and distribution levels [1] [2]. The technical structure of the Dutch grid is shown in Table 1.1 as an example. By 2006, although the majority of circuits are still overhead lines, a total length of 32917 km of AC land cables were in service all over the world [3]. In perspective of voltage levels, as reported in [4], underground cable circuits have been applied more at HV level (50-219 kV) than that at EHV level (220-500 kV), shown in Figure 1.1a. Among the cable population in service, 57% are cross-linked polyethylene (XLPE) insulating cables, and 70% of all accessories are extruded types [3]. The extruded polymeric insulating cables are used more at HV voltage level (Figure 1.1b). Not only that, they also increasingly dominate the new installation for all the levels of AC voltage. The large increase in the use of extruded cables, especially XLPE cables, is due to their higher efficiency brought by the lower dielectric constant, higher operating temperature and easier manufacturing process [5].

Table 1.1: Structure of the electricity grid in the Netherlands [6].

Extra high voltage (EHV)	Transmission level	380 kV, 220 kV
High voltage (HV)	Transmission level	150 kV, 110 kV
Intermediate voltage (MV)	Distribution level	3 - 30 kV, 50 kV

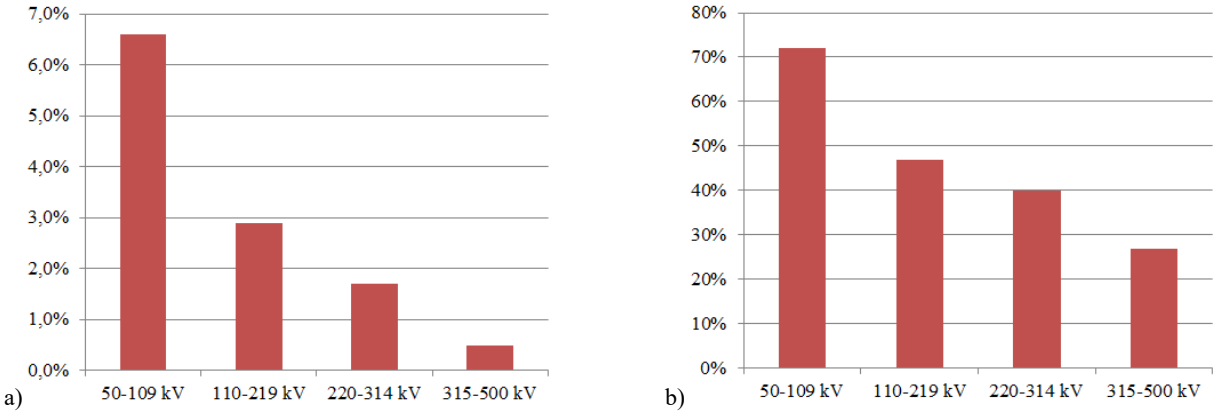

Figure 1.1: AC cable circuit population: a) percentage of the total AC circuit length that is underground for each of the voltage levels, b) percentage of the AC underground cable having extruded polymeric insulation.

1.1 Underground Power Cable Systems

Cable systems are designed to have a lifetime in the range of 40 to 50 years. Failures of cable systems are mainly the failures in the cable insulation. On a short term, initial breakdown occurs in the insulation directly. On a long term, partial discharge activities initiate and accelerate the aging / degradation process, which lead to failures in the end.

The failure distributions of power cables in service classified by components, insulation types and voltage levels are summarized in Figure 1.2, according to the power cable failure investigation based on a total of approximately 170 individual cases over the period from 1997 until 2014 [7]. Around two thirds of the failures occurred in the cable accessories, including cable joint and terminations, while one third of the failures occurred in the cables (Figure 1.2a). Hereby, cable accessories are the weak part having higher risk of failure than the cable body. Regarding to the cable insulation types, as the widely applied modern insulating material, cross-linked polyethylene (XLPE) insulated cables share a high failure proportion of around three forth (Figure 1.2b). [8] also concludes that the internal failure rates of accessories, especially on XLPE cable, are higher than other components. Considering the voltage classes, the majority of failures occur in cable systems at voltage level from 36 to 230 kV. Slightly less failures occur in cable systems at voltage level lower than 36 kV. A low proportion of 14% failures is located in EHV cable systems, which is due to the smaller population of installed EHV cable systems (Figure 1.2c).

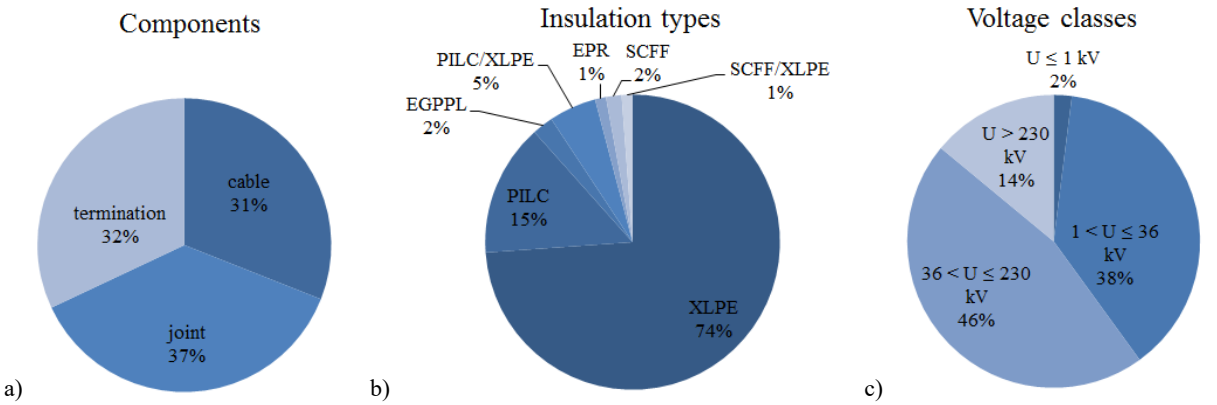

Figure 1.2: Distribution of cable failures: a) by components, b) by cable insulation types, c) by voltage classes.

By analysing the failure cases, the causes of failures are also given in [7] and shown in Figure 1.3. For cables, failures mainly result from production, installation and external damage related issues (Figure 1.3a). While for cable accessories, more than half of the failures are caused by installation related defects (Figure 1.3b), since all cable accessories have to be installed in the field where the conditions are not ideal. This, in turn, contributes to the higher failure distribution in cable accessories in general (Figure 1.2a).

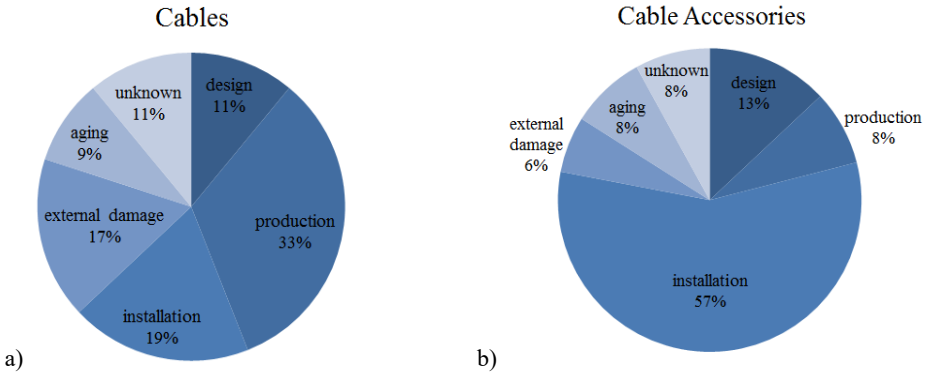

Figure 1.3: Failure causes: a) for cables, b) for cable accessories.

As a result, the HV XLPE cable accessories are the parts undergoing the highest risk, which consequently, needs more attention.

For new installed cable systems where the transportation and installation activities just happened, the defects which may lead to failures are mainly coming from the manufacturing quality, the poor installation problems, or the third party damages [9, 10]. For cable systems which have been installed and put in service decades ago, especially the ones that are approaching or already past their anticipated life, a higher proportion of age-related symptoms or failures have been reported. This is the result of intrinsic aging or degradation process caused by the aging factors [11]:

- Thermal stresses
- Electrical stresses
- Mechanical stresses
- Environmental stresses

The increasing failure rate would adversely affect the cable system reliability. The 'bathtub curve' (Figure 1.4) is often used to describe the failure likelihood. Early failures due to manufacturing or installation occur in the new installed cable systems in the phase of 'infant mortality'. As time progresses, defects arise due to aging and degradation processes in the dielectric, which result in an increasing failure rate in the phase of 'wear out'.

In order to improve the reliability of the cable system currently and in the future, utilities need to assess the cable system (cables and accessories) condition and correspondingly take actions to avoid outages. Various cable system diagnostic techniques are available and have been applied to detect cable system defects and degradation condition [12]. Different diagnostic technologies assess different characteristics of cable systems. They are selected and applied for different purposes. In some cases, more than one technology is used to assess the cable condition. For new installed cable systems, since the cable accessories are installed in field, commissioning tests are required after the installation, which aims to detect defects if there is any and ensure the cable system can be put into service. Usually, partial discharge (PD) test is accompanied to the AC withstand test. Cable systems that pass the commissioning tests are supposed to be "PD-free" without detectable defects. For aged cable systems, defects can be

induced due to the aging process. Maintenance tests are then needed to check the cable insulation condition and to verify the serviceability of the cable system. Commissioning tests and maintenance tests will be explained more in details in section 3.2.5.

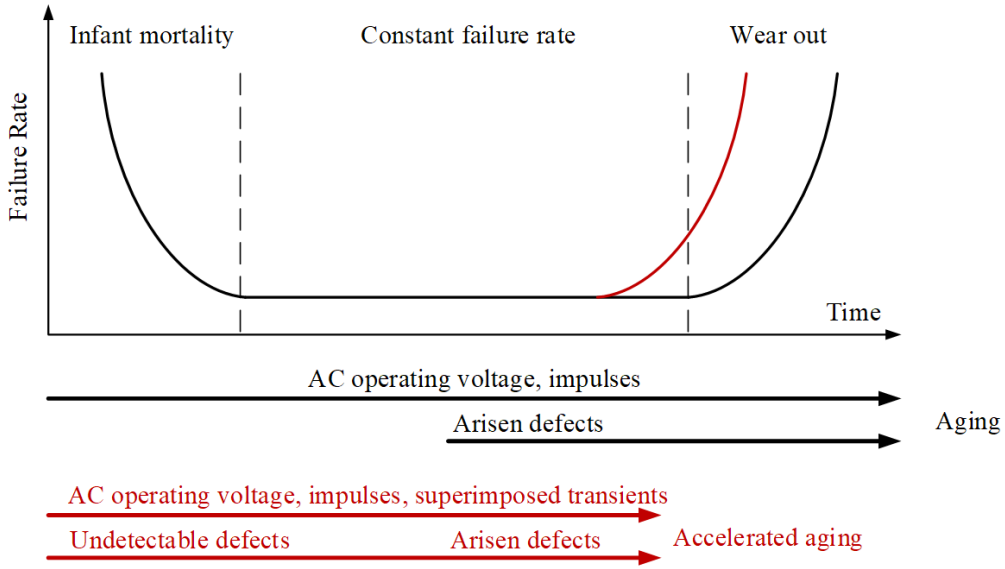

Figure 1.4: Theoretical bathtub curve.

1.2 Risks in Mixed Overhead Line and Cable Systems

In the Netherlands, the extension of distribution and transmission grid is necessary in order to guarantee the reliability and adequacy of electricity supply. In the Dutch 380 kV HV grid, two mixed line-cable connections are projected, in the so-called Randstad, of which the South ring was already in use since 2013 and the North ring had just been commissioned in October 2019, in which underground cable systems are applied.

In service, the power cable systems are subjected not only to the normal operating condition and the transient conditions such as lightning impulse and switching impulse, but also occasionally to the superimposed transient conditions, where the impulses are superimposed on the normal AC voltage. In the mixed overhead line and cable system, the presence of the underground cable system has impacts on the grid performance, especially the transient behaviour, which may lead to large overvoltage and high frequency oscillations [13]. Such transient situations create abnormal over-stress on the HV equipment, including the underground cable system. The power cable systems, which are well designed to withstand the normal operating and transient conditions, now are facing the challenges brought by the superimposed transient conditions.

For any defects existing in the cable insulation such as cavities, they are expected to be detected through PD test during commissioning tests or maintenance tests. However, it is also true that the PD measurement techniques cannot detect all possible cable insulation defects [11, 14]. In case there are defects existing in the cable systems but the PD test fails to detect them, such undetectable defects will remain in the cable system and the cable system will be put into service. Since the defects are undetectable under commissioning or maintenance PD test with overvoltage (see details in section 3.2.5), they will not initiate partial discharges under normal operating conditions. However, in the mixed overhead line and cable systems, if superimposed transient overvoltage occurs and reaches the underground cable system with a large overvoltage being higher than the PD inception voltage, then

partial discharge is likely to be initiated within those defects, which initiates the aging process earlier. In a worse case that the partial discharge, initiated by the transient overvoltage, continues under normal AC voltage, the aging process will be accelerated. This is depicted by the modified bathtub curve with the red line indicating the earlier wear out phase (Figure 1.4).

1.3 Research Objective

Cable accessories are the vulnerable parts in the cable system. For new cable accessories, the defects are mostly installation-related and introduced during the in-field installation. After-laying tests are performed in order to detect such defects. For installed cable accessories, defects may appear due to degradation in service. Maintenance tests are performed to detect these defects. Cable and accessories which pass these tests are regarded as serviceable. However, there are defects that escape from being detected by the commissioning or maintenance test. In this thesis we call these hidden defects. Having hidden defects, the cable and accessories may pass the commissioning or maintenance test unintentionally. Basically, the cables and accessories should be able to withstand the normal AC and transient stresses. However, some defects show partial discharges only under transient electrical stresses, and hereby may start or accelerate a degradation process, while at normal stresses no PDs occur. For instance, due to switching of mixed line and cable systems transients can occur that superimpose high-frequent oscillations upon the AC voltage, resulting in a larger overvoltage than normal. Therefore, it is important to know whether those transients could initiate partial discharges and then a degradation process of the insulation system. So far, knowledge of the effects that transients may have on the cable insulation has been scarcely published.

Nowadays an arising problem is, that TSOs and DSOs fear that more transients in their networks may cause unexpected insulation failures, in particular in critical connections such as high voltage cables. These failures are called unexpected in the sense, that these escape from detection by the usual partial discharge and dielectric strength measurements in commissioning and maintenance tests.

To fill the gap between the lacking knowledge about the influences of exceptional transients on high voltage insulation systems and the effectiveness of condition assessment of HV cables in preventing unexpected failures, the main research objective is set as:

To detect, reveal and understand the effects of transients on partial discharge phenomena and breakdown in high voltage cable insulation, which could potentially lead to an unexpected insulation failure.

For this purpose, research questions were set as below:

1. What are the possible transient situations in the power system, e.g. in mixed overhead line and cable systems?
2. What are the typical insulation defects occurring in cable accessories? How to design and prepare a proper HV research object that can incorporate the characteristics of the defects and possible problems brought by the defects?
3. How to investigate the effects of superimposed voltages on breakdown of a cable insulation by HV experiments? What are the effects?
4. How to investigate the effects of transients on partial discharge behaviour of the cable insulation system by HV experiments? What are the effects?
5. What kind of diagnostic knowledge should be acquired to obtain an early warning of the onset of partial discharges or degradation activated by transients, which can be used for power cable condition monitoring?

To answer the research questions, the following approach and techniques were used:

- Perform a literature review of the state-of-art of the effects of transients in cable insulation.
- Collect information about transient situations and insulation defects occurring in practice.
- Perform breakdown tests under superimposed voltage – a high frequency modulated voltage - on material samples, which are used as cable insulation.
- Investigate partial discharges that initiated by superimposed transient voltage in MV cable models with artificial defects.
- Investigate partial discharges that initiated by impulses and superimposed transient voltages in a HV cable model with artificial defects, using the preliminary knowledge gained from the experiments with MV cable models.
- Analyse and summarize the measured effects of transients on partial discharges in MV and HV cable insulation.

1.4 Thesis Outline

Chapter 2 starts with introducing transients that occurred in the power grid, especially in the mixed line and cable system. Simulations and field measurements of transients in the Dutch 380 kV mixed line and cable system are reviewed, which will be the origin of the transients designed and used in this research. Typical insulation defects in the cable systems are also described in chapter 2, together with their locations and causes, in particular the ones existing in the cable accessories. Different degradation mechanisms occurring in the cable system are then presented and explained.

Chapter 3 explains the principle of electrical breakdown and partial discharge in solid dielectric, which provides the theoretical foundation for analysing the physical phenomena observed in the practical experiments in later chapters. Moreover, the PD processes occurring under AC, impulse and superimposed voltages are presented theoretically. Chapter 3 also introduces the measurement of partial discharges. The basic method of measuring partial discharges is first given, followed by the PD tests applied to power cable systems including commissioning and maintenance tests. At last, a review on the PD measurement in power cable under transients is presented.

Chapter 4 describes the breakdown tests performed on the different types of polymeric materials under DC, AC with different and superimposed voltages. Weibull distribution, which is applied to analyse the measurement results for statistic purpose, is then introduced. The resulting dependencies between the applied voltage waveforms and breakdown are summarized and discussed.

Chapter 5 investigates partial discharges in MV cable models - which are easier to be installed and manipulated - with artificial defect under superimposed transient voltages. The experimental set-up consisting of test object, generation of superimposed transients and the lab-developed PD measuring system is described. The MV cable model used as the test object is explained which consists of MV cable, cable terminations and joint. Artificial defects are then introduced to the cable model. Different PD behaviour under transients are measured and described. The measured PD signals are analyzed and described by phase-resolved PD (PRPD) patterns, time-resolved PD (TRPD) pulse waveforms, and usual PD parameters. The obtained PD information describes different scenarios of PD initiation under the impulse, as well as the behavior of those impulse-initiated PD under AC voltage after the impulses are finished. By interpreting the PD behavior, the effects of impulse transients on PD are derived and summarized.

Chapter 6 presents the methodology used for PD measurement in a HV cable model under transient voltage. The experimental set-up which is adjusted to fulfil the HV level test is depicted. The lab-

developed PD measuring system which is designed specifically for the experiment is described in details. The measurement results of PDs under AC, impulse and superimposed voltages are then interpreted.

Chapter 7 investigates partial discharges in the HV cable model with an artificial defect under impulse voltages and superimposed transient voltages. Different PD behaviour under different pure impulse voltages are firstly presented. Then the PD measurement results are shown when the HV cable model is exposed to different superimposed transient situations with different parameters. The measured PDs are again analyzed and described by PRPD patterns, TRPD pulse waveforms, and usual PD parameters. The effects of the transient parameters on the PD behaviour are hereby analysed and depicted.

Chapter 8 summarizes the results of measurements performed in this research and answers the research questions. Conclusions are drawn based on the measurement results and recommendations are given for future work.

Chapter 2

Transients and Insulation Defects in Underground Power Cable Systems

Ideally, a well-designed and -manufactured power cables and accessories should be able to withstand normal operating stresses as well as transient stresses in service. However, it is possible that there are undetectable or so-called hidden defects in the new installed cable system, or the defects have arisen in the aged cable system due to an aging process during service. In case those defects are exposed under extreme conditions such as transients, they can 'awake' and initiate partial discharge or other degradation processes. In particular, with the presence of mixed overhead line and cable system, the transients occurring in underground cable systems may have different behaviour and different effects on the cable systems. Therefore, it is of interest to know whether such transients can have adverse effects on the cable system performance. This chapter reviews the transients in the transmission grid, especially in the mixed overhead line and cable system, as well as the insulation defects which could exist in the cable system. To have an overview of transients in the mixed overhead line and cable system, the researches based on the Dutch 380 kV grid are presented in the first section. The second section of this chapter is devoted to the insulation defects in cable systems. Typical defects with their causes are described. The degradation mechanisms in the cable system are then discussed. The information given in this chapter is important in determining and designing the experiments later in this thesis.

2.1 Transients in the Power Grid

Transients in the electrical power grid are mainly caused by lightning strikes and switching operations. The lightning - either directly striking on power transmission lines, or terminating on a structure or on a ground surface near the transmission lines - can induce high voltage impulses in the power grid, especially close to the cable terminations resulting from back flashover [15]. Usually, the cables are protected against lightning impulses by surge arresters at the transition points. Switching operations, such as line energization/re-energization, capacitor/inductor switching, load rejection, breaker opening, faults etc., are more common in the electrical network, which could be a planned or unplanned event. The resulting oscillation in voltages and currents propagate as travelling waves through the power grid. Inside the cable system, the transient voltage can become significant high due to the reflected waves.

With the extension of the power grid, underground cables are more applied. The presence of underground power cables in the power grids has impact on the power system performance during both steady state and transient situations [13]. It is important to know about the possible transient situations in particular in mixed overhead line and cable systems, not only for better decision-making during operation, but also for better understanding of possible insulation degradation as well as better development in diagnosis and monitoring of cable insulation condition.

2.1.1 Transients in the Dutch 380 kV transmission grid

The Dutch 380 kV transmission network is being extended with two new 380 kV connections, namely the North-ring and the South-ring in the region of Randstad, which is referred to as the Randstad 380 kV project. In particular, the 380 kV connections consist of mixed overhead line and underground power cable systems. The complete Dutch 380 kV network is shown in Figure 2.1a. The section of mixed overhead line and cable system between two substations Wateringen (WTR) and Bleiswijk (BWK) is depicted in Figure 2.1b. The transition points of cable and line are indicated as OPS14 and OPS32.

a)

b)

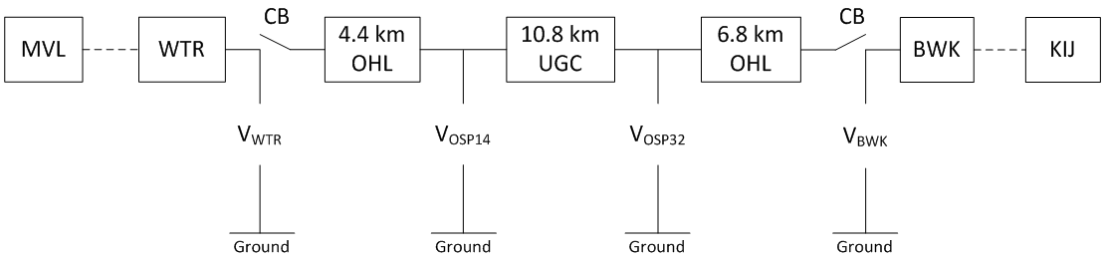

Figure 2.1: Dutch 380 kV transmission system: a) TenneT grid including 380 kV connections by 2019. Source: TenneT NL, b) connection between WTR-BWK [13].

There have been several research investigations focusing on the behaviour of the Dutch 380 kV mixed overhead line and cable system, especially during the transient situations. Some representative results are described in the following paragraphs.

Simulations of transients in 380 kV mixed overhead line and cable system [13]

To evaluate the transients in the Dutch 380 kV mixed overhead line and cable system, a transient simulation model of the system is built up in [13]. The representative simulation results of transients under different scenarios are obtained. Hereby only the worst case scenario related to the transient voltage conditions are obtained.

The energization transients, at the locations of substations Wateringen (WTR) and Bleiswijk (BWK), cable-line transition points OPS14 and OPS32, are studied when the cable circuit is switched on by the circuit breaker. Figure 2.2 shows the voltages of the scenario when the connection is switched on at substation WTR, while the BWK side is left open. It is noted that, there are oscillations in all the phases, and the voltage peak reaches 500 kV (Figure 2.2a) and 550 kV (Figure 2.2d) at WTR and BWK respectively.

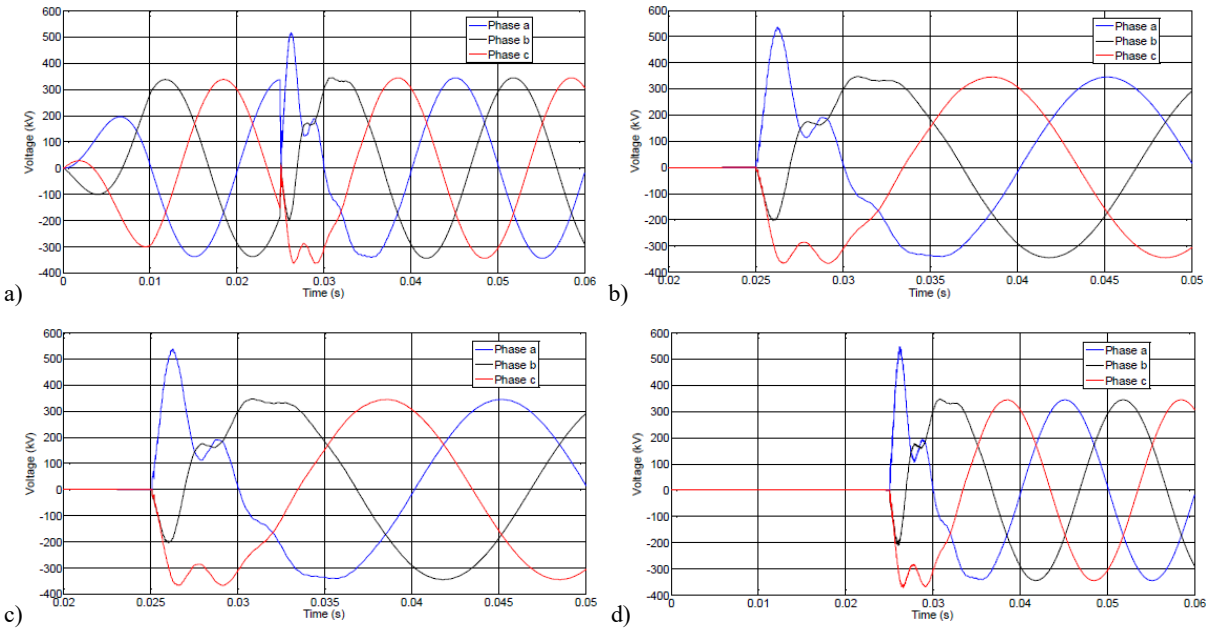

Figure 2.2: Connection switched on at substation WTR, voltage response at: a) Wateringen side, b) OSP14, c) OSP32, d) Bleiswijk side.

The similar switching action is then performed with the connection switched on from BWK side and WTR left open. The voltage transients at both substations are shown in Figure 2.3. Larger oscillations are observed, and the peak voltage at WTR exceeds 600 kV (Figure 2.3b).

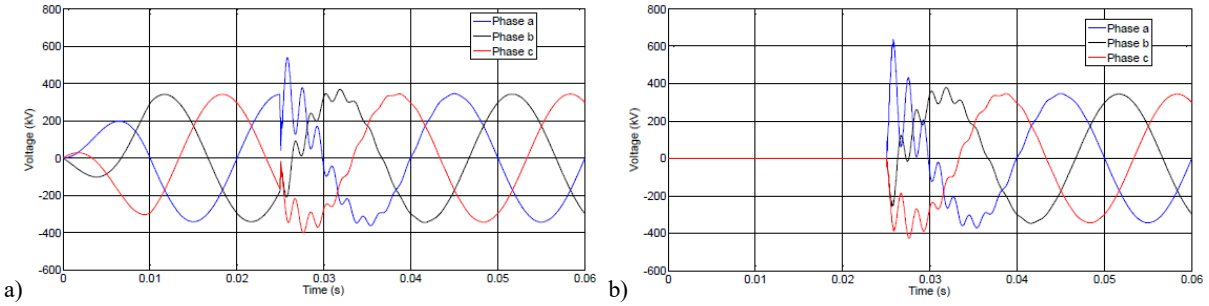

Figure 2.3: Connection switched on at substation BWK, voltage response at: a) Bleiswijk side, b) Wateringen side.

Transients were also studied in [16] based on the simulation of a hypothetical future transmission line connecting the western side of the 380 kV ring to the eastern side with underground cable. Similarly, overvoltages were observed with oscillations.

Field measurements of transients in 380 kV mixed overhead line and cable system [17]

The switching transients were also measured in the field [17]. In November 2016, a set of switching events were planned and executed in the Dutch 380 kV system for research purposes. Measurements of the switching transients were performed by the research group from Eindhoven University of Technology. Figure 2.4 shows one of the worst scenarios measured at the transition point OPS14 when the switching action was performed at BWK side. The results are presented in per-unit (p.u.).

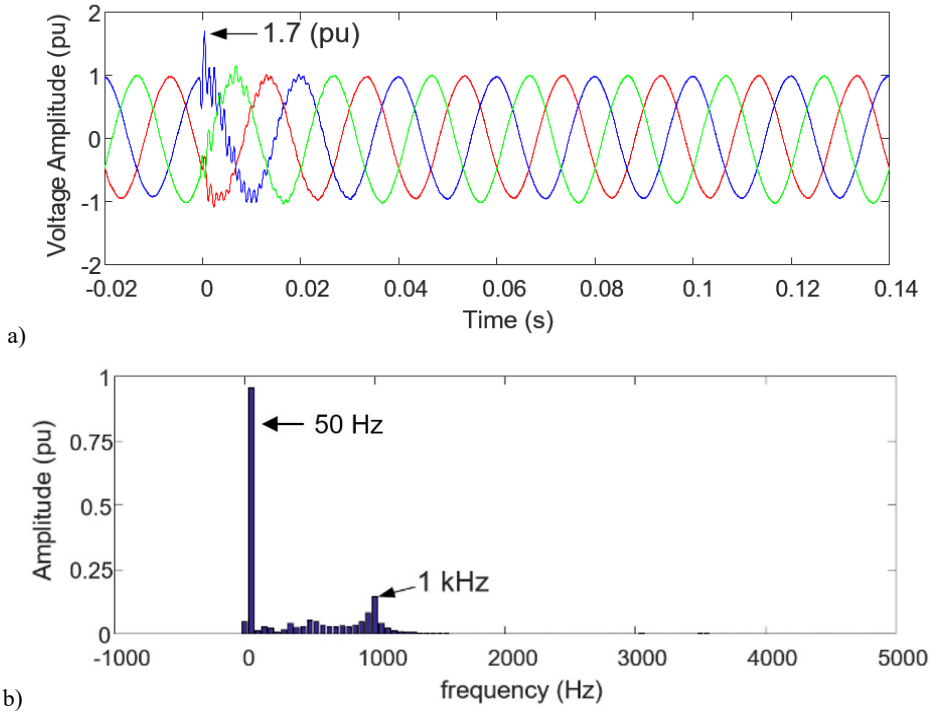

Figure 2.4: Field-measured transients in 380 kV system: a) voltage waveform of the field-measured transients, b) FFT of the field-measured transient.

The measured switching transients are assessed. As it can be observed in Figure 2.4a, that the three-phase voltages have been modulated by the transient for around one 50 Hz cycle. During the transient period, the overvoltage goes up to 1.7 p.u.. The frequency spectrum of the transient is given in Figure 2.4b, which indicates that the transient contains a series of harmonics, in which 1 kHz is dominant.

Both the simulation and field measurement results of the transients in this mixed overhead line and cable system reveal that, the transients occurred lead to overvoltages and oscillating at higher frequencies. The overvoltage level, which is in the range of 1.5 to 1.7 p.u. obtained from the above measurements, constitutes a severe stress to the system and its components. Therefore, it is important to know, whether such transient situation can have an effect on degrading the condition of the cable and accessories. The overvoltage level shown in the above researches will be used to design the test voltage for investigating the cable system in this thesis.

2.1.2 Effects of transient on cable insulation

It has been reported that, the repeated application of impulse voltages can reduce the life of XLPE insulation [18]. So far, many researches have studied the effects of standard impulses on the aging

process of cable insulation by measuring usual PD parameters such as PD inception voltage (PDIV) and extinction voltage (PDEV). However, not many studies focused on the effects of AC superimposed with impulse transients and PD initiation under these conditions. With PD measurements on XLPE cable pieces with terminations, Abdolall et al. confirm that the PD magnitude (in pC) did not change after the samples were subjected to switching impulses [19]. However another author states that PD behavior was observed to be different before and after XLPE cable samples were aged by impulses in [20] and [21]: the measured PDIV and PDEV decreased with aging by impulses, whilst the PD magnitude increased. Similar influence has been observed in EPR cable insulation under AC voltages with superimposed impulses by Cao et al. [22]. There are also material studies of the PD initiation under pure impulses and AC with superimposed impulse transients. In [23] Densley et al. describe the features of discharges that initiated under impulse. In [24] PDs were measured under AC with superimposed impulse voltage, showing that, PDs initiated by impulses could continue with AC under certain conditions. However, these results are based on polymeric material samples instead of cable samples. Furthermore, up to now, the measured PD are described in a classical way, i.e. by means of phase-resolved PD (PRPD) patterns and usual PD parameters. Time-resolved PD (TRPD) current waveforms were measured under impulses by Zhao et al.[25], which revealed the difference in characteristics of discharges occurring under impulses. However, it was still on material samples.

2.2 Insulation Defects and Degradation in Power Cable Systems

The failure statistics presented in section 1.1 indicates that the majority of failures occurred in the cable accessories. The main failure cause is due to the imperfect handling, including transportation and installation, which brings various defects into the cable accessories. Most defects, by interacting with single or synergistic aging factors, will initiate partial discharge and consequently severer degradation processes. By performing a commissioning test and maintenance test, defects should be detected and then repaired. However, there are few types of defect that can stay undetectable as hidden defects. Either the defect is not discharging so that it cannot be detected by PD tests, such as water treeing, or the discharges are too small to be detected. Or the defect needs a certain voltage to get PD initiated, which is, however, not achieved during the tests. In case such defects are exposed to impulse voltages that are higher than their PDIV, PDs may occur. In this section, the typical defects in the cable insulation systems are presented. In particular, the defects appearing in the most vulnerable part – interfaces in cable accessories- will be described in detail. The possible causes of the defects are also discussed.

2.2.1 Insulation defects in power cable systems

Typical defects

Based on practical experience, obtained by reviewing literature and technical brochures [26-29], consulting experts from utility and research institutes, and visual inspections, typical defects in the cables and accessories are as listed in Table 2.1. The causes of the defects are also given and will be described in detail below. As seen from the table, major defects are existing at the interface in the cable accessories induced by handling issues. Other parts of cable accessories are also at risk of getting defects during handling. However, those defects are relatively easy to observe or detect and to be mitigated. Compared to the cable accessories, the cable bodies have smaller chance to contain defects. The interface defects will be described below.

- Contaminants / impurities:
  During the installation, the prepared cable end is exposed to the environment. It happens that external particles are attached to the surface of the cable end and remain there. If the particles are conductive, they will increase the local electrical stress in the cable.
- Insulation damages:
  The insulation might be damaged during installation. The damage could be cavities, cut, scratch or rough surface on the surface, which may create an air gap in the insulation. PD activities will firstly start at the air gap.
- Semi-conductive layer problems:
  During the peeling of the semi-conductive layers, tips or gaps might be created by poor workmanship. Also small parts of semi-conductive layer might remain on the insulation surface.
- Mechanical pressure loosing:
  The long-term operation may lead to the migration or loosing of the grease at the interface, which will lead to the air gap between the interface, which is a big problem related to insulation.
- Moisture penetration:
  Moisture penetration also happens during the installation. However, such defect will be detected by the DC over sheath test [27] immediately, or leads to a long-term erosion.

Table 2.1: Typical defects in MV and HV cable insulation.

Locations		**Defects**	**Causes**
Cable accessories	Interface	Conductive or semi-conductive contaminants (impurities)	Manufacturing Handling In service
		Insulation damages Incision, cavities, scratches, rough surface	Manufacturing Handling In service
		Semi-conductive layer problems Too long/short layer, tip, unsmooth edge	Handling
		Local increase of electrical stress	Handling
		Mechanical pressure loosing	In service
		Air gap	Handling
		Tracking	In service
		Moisture penetration	Handling In service
	Stress cone	Voids in stress cone Poor adherence of components within stress cone Dislocation / incorrect positioning	Manufacturing Handling
	Conductor	Bad connection on conductor Conductor movement within accessories	Handling In service
	Connector	Sharp edge on connector	Handling
	Axis	Misaligned axial direction	Handling
	Sheath	Loss of earthing connection to sheath Cracking of sheath plumbs	Handling In service
	Joint jacket	Full cut on joint	Handling
Cable body		Insulation damages Incision, cavities, scratches, rough surface	Manufacturing Handling In service
		Moisture penetration	Handling In service

Root cause

The causes of the defects can be categorized to three groups considering the life phases of cable system [30]:

- Manufacturing imperfections:
  Although the manufacturing of cables and accessories is under controlled conditions, it still happens that defects are induced, such as insulation damage and contaminants in insulations etc. In addition, imperfect design can also bring defects unexpectedly. Usually, qualification and factory acceptance tests, to a large extent, help to eliminate the defects so that the delivered cables and accessories are defect free. However, even though the right tests are performed, a poor interpretation of the test results may still leave the defects behind. Moreover, some slight defects may be too small to be detected during the tests, which size may increase later [7].

- Handling problems:
  Problems arisen during transportation and installation are regarded as handling problems. During transportation, incompetent handling can damage the cable insulation or protection layers. During installation in the field, usually the jointers need to ensure the proper installation of accessories under adverse conditions [8, 31]. However, it still happens that the cable or accessories get contaminated in case of insufficient cleanness and protection. The contaminations may stay in the accessories, especially at the interface between cable and accessory insulation. In case of poor workmanship lacking of experience or skills, the jointers may damage the insulation during manipulation, or install the accessories improperly. Most defects are induced in the phase of installation. Those defects are the main causes leading to failures. Usually, after installing the cable systems and before putting them into service, commissioning tests (or after-laying tests) need to be performed, which aims to detect the defects that introduced from handling, or even from manufacturing.

- In service damage or aging:
  During the service, natural aging process occurs in the insulation systems. The mechanism is described later. Apart from normal aging process, cable systems can be damaged by external agents. Around 70% failures are caused by mechanical work. Failure statistics show that, for HV extruded cables, the failure rate caused by third-party mechanical damage is three times higher than that of internal failures. For EHV cables, an even higher factor of five times is reported [32]. The mechanical damage can cause fast failure or induce other degradation processes. The surrounding environment also can be aggressive to the cable systems. The humidity surrounding may lead to the moisture penetration into the insulation systems. The high temperature will apply thermal or mechanical stresses on the cable systems. The soil surrounded can cause the erosion of the jacket or even more parts of the cable systems. All those may introduce new defects or accelerate the aging process.

We intended to choose the realistic and worse cases from the typical insulation defects listed in Table 2.1 for our investigations. Since major defects exist at the interface in the cable accessories, and most of the interface problems lead to air gaps/cavities, we decided to mimic cavities in joints as the artificial defects for study.

2.2.2 Degradation mechanisms

The aging factors given in section 1.1 – thermal, electrical, mechanical and environmental - can result in intrinsic aging / degradation by causing changes in properties of insulation materials [11, 33]. The

aging factors can also interact with insulation defects and result in extrinsic aging [33], which begins in localized regions and propagates through the insulation. For extruded cable systems, the main degradation occurs under the electrical stress being accompanied with defects, including partial discharge, electrical treeing, water treeing and space charges as the typical aging mechanisms. During the electrical aging, thermal aging may also be arisen. Figure 2.5 illustrates the degradation mechanisms under different stresses in the power cable systems.

Since the interface has been identified as the crucial part, it is meaningful to consider the degradation of interfaces. The intrinsic electrical aging is less likely to occur since the electrical strengths along interfaces are low compared to the withstand stresses used for cables and accessories [34].

Thermomechanical and mechanical effects can cause the formation of cavities, and in a severer case, even cracks, gaps and delamination between the insulating materials. For example, at the interface, the increasing temperature caused by operation will lead to different thermal expansions in the different materials. This may cause the aforementioned defects. Thermal effects can also cause those defects by modifying the insulating materials. Within cavities or even gaps, partial discharges are easy to occur, followed by electrical treeing and other degradation. The formation of cavities or gaps is a result of a combination of several effects [35]:

- Migration of the lubricant
- Movements in the interface
- Reduction of the interface due to relaxation of materials
- Electrical aging of interface
- Contamination of the interfaces

In cables, especially cable accessories, most defects initiate partial discharge, which leads to failures through breakdown or other processes. All the thermal, mechanical and environmental aging may switch to electrical aging at a certain point, during which partial discharge is likely to occur. Therefore, partial discharge seems to be a useful indicator for evaluating the insulation condition. Partial discharge measurement is hereby applied widely. It is also chosen to be the measuring approach in this thesis to investigate the effects of transients on the cable and accessories.

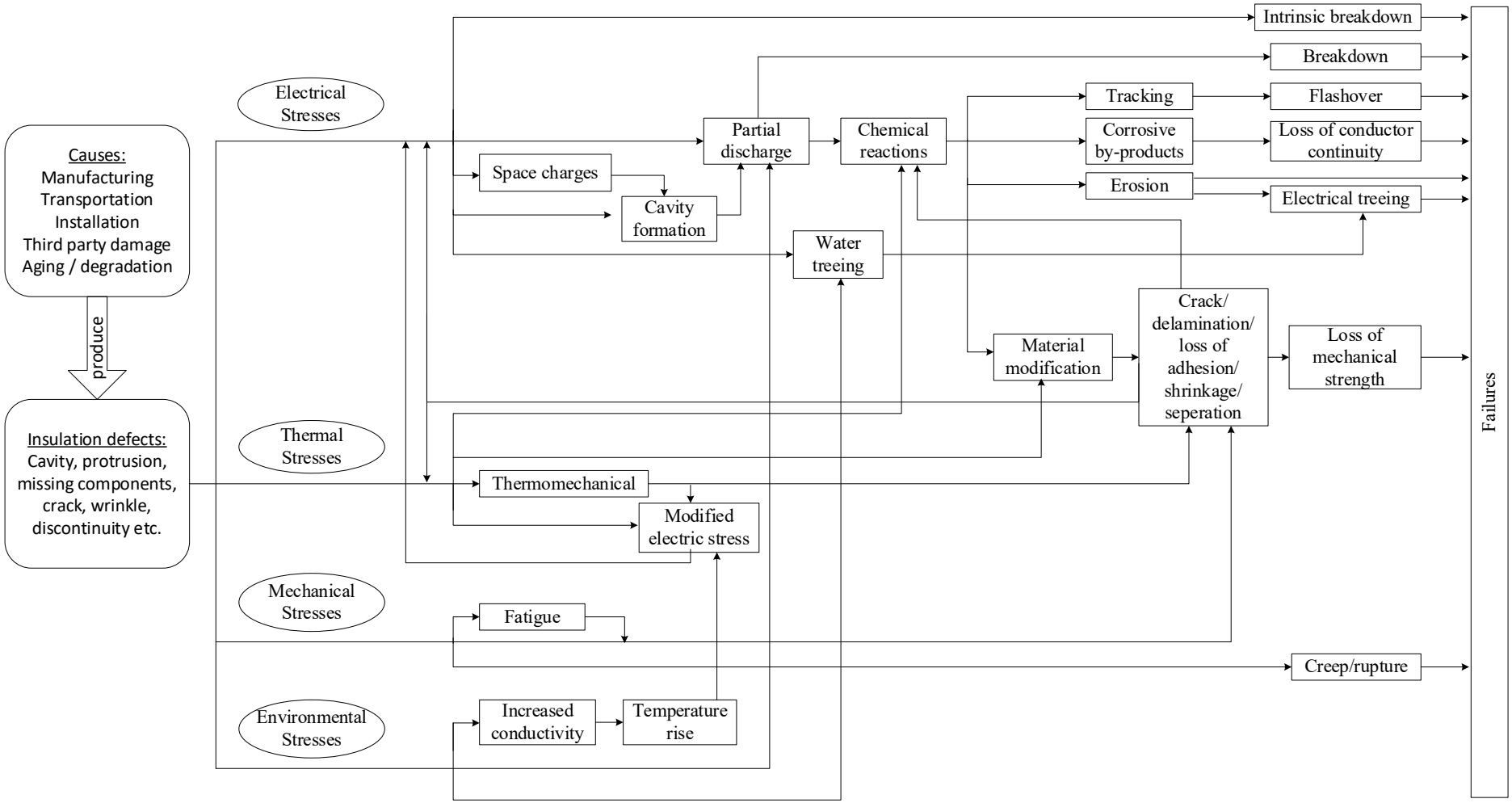

Figure 2.5: Overview of defects, degradation causes, mechanism and results in power cables [36].

Chapter 3

Breakdown and Partial Discharge Phenomena

Failures occurring in the power cable insulation system will lead to long repair time and high economic cost and in general reduce the reliability of the cable system. Insulation failures may result from electrical breakdown due to overstressing, or proceed by partial discharges in a long term degradation process. In cable systems, partial discharges are mainly caused by the occurrence of insulation defects, especially in the cable accessories. PDs are acting as an indication of the insulation condition [37]. For this reason, the measurement of partial discharges is advised to become part of the routine procedure for cable laboratory or factory testing and been suggested to be involved in on-site testing. Important typical insulation defects have been identified in Chapter 2, which are often PD activated. In this chapter, breakdown and partial discharge phenomena are described in more detail. Section 3.1 depicts the breakdown mechanism in solid dielectrics. Section 3.2 describes the partial discharge mechanism in a void, the degradation caused by partial discharges and the measurement of partial discharges.

3.1 Breakdown in Solid Dielectrics

Breakdown is the phenomenon that a dielectric between two electrodes loses its insulation function providing a conductive path under electrical stress, resulting in a short-circuit between the electrodes [38]. When occurring in solid dielectrics, especially polymeric insulators, breakdown is always catastrophic since it is irreversible and destructive with creating a narrow breakdown channel between the electrodes. All the catastrophic breakdown in solid dielectrics is driven by electrical power and ends up with a lot of thermal dissipation, which can be observed by the discharge track involving melting, carbonisation or vaporisation of the dielectric.

According to [34, 39], the processes of breakdown in solid dielectric can be categorised as follows and is shown as a function of time and electric field in Figure 3.1:

- Electric breakdown
- Electromechanical breakdown
- Thermal breakdown
- Partial discharge breakdown

Electrical, thermal and electromechanical breakdown are short-time mechanisms, which would occur within milliseconds. Partial discharge is a long-term mechanism. Usually, it takes time for partial discharge to occur, and the occurrence of partial discharge will not lead to breakdown immediately but cause degradation, which will take hours to years to reach the breakdown stage.

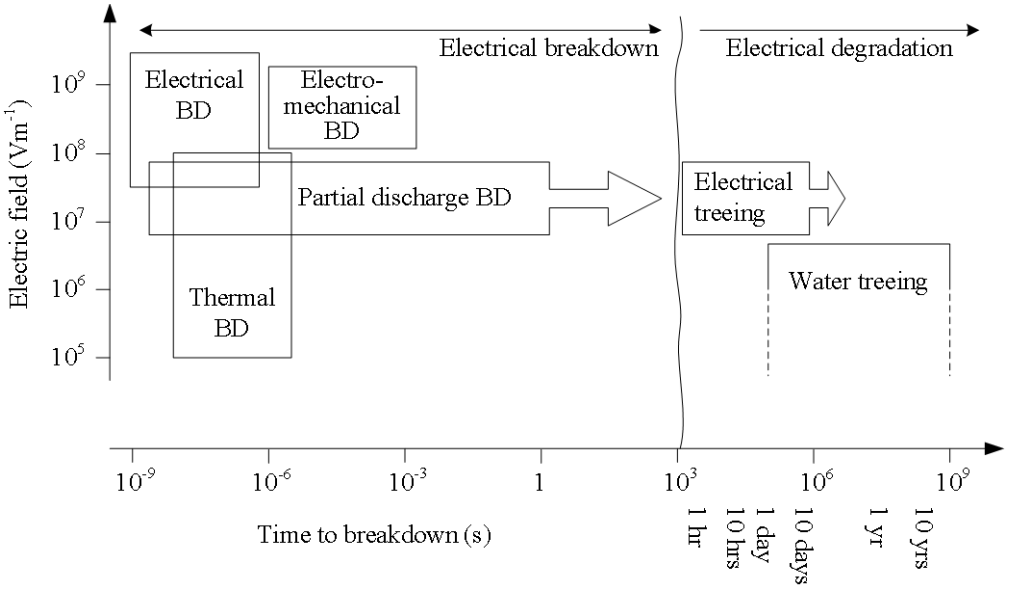

Figure 3.1: Various breakdown mechanisms with corresponding times and electric fields [34].

Electric breakdown

Electric breakdown usually occur locally under extremely high field strength needed to start the electronic avalanche multiplication [40-41]. The high field leads to a rapid increase in the number or the energy of the electrons. When they reach the unstable magnitudes, they will rise further catastrophically, which ultimately leads to destruction of the lattice of the material.

Electromechanical breakdown

Electromechanical breakdown occurs due to the Coulomb attraction of the electrodes, which exerts compressive force upon the insulation. If the mechanical pressure produced by the electrostatic attraction of the electrodes exceeds the mechanical strength of the dielectric, mechanical deformation of the material occurs and which is likely followed by breakdown. However, electromechanical breakdown does not commonly occur in polymers especially XLPE power cable, since the insulating polyethylene is crosslinked and sufficiently thick so that the effect can be neglected.

Thermal breakdown

Thermal breakdown occurs when the heat input cannot be balanced by the heat losses from the dielectrics. An ideal insulating material does not dissipate any energy since it functions as a pure capacitor. In practice, every insulating material dissipates some energy in the form of dielectric losses. The dielectric losses under applied voltage cause overheating in the insulation and result in increased temperature. If the heating rate is higher than the cooling rate, the temperature will further increase exceeding the critical value. As a result, the material will burn out leaving a channel. Such rapid breakdown bypasses the aging / degradation process and causes the failure before any intervention can be taken.

The dielectric AC power losses P are determined by the applied voltage stress U, frequency ω, the material capacitance C and the dissipation factor *tanδ* [42]:

$$P = U^2 \cdot \omega \cdot C \cdot tan\delta \qquad (3.1)$$

where: P = Dielectric losses in watt (W)
U = Voltage in volt (V)
ω = Angular frequency (rad/s)
C = Capacitance in farad (F)
$tan\delta$ = Dissipation factor

The physical origins of dielectric losses can be classified into [42-43]:

- Conduction losses
- Dipole losses
- Discharge losses
- Interface losses

The conduction losses result from the very small leakage current through the dielectric causing the *tanδ* to decrease if the frequency increases (Figure 3.2a). Further an insulation material subject to an AC electric field reverses the directions of electric dipoles continuously. The friction between the rotating electric dipoles and the material causes dipole losses in form of heat, which make contributions to the dielectric losses. Up to the Debye frequency, the tanδ increases if the frequency increases (Figure 3.2b). In the insulating material where only conduction losses and dipole losses occur, the *tanδ* mainly independent of applied voltage. Partial discharges also dissipate energy in the form of heat, light and sound, which is provided by the power supply and manifest also as *tanδ* losses [43-44], which increase with voltage (Figure 3.2c). The presence of partial discharges may lead to not only the increase in dielectric losses, but also breakdown. The losses at the interface between a loss-free dielectric and lossy dielectric can be distinguished from dipole losses by the less sharp maximum (Figure 3.2d).

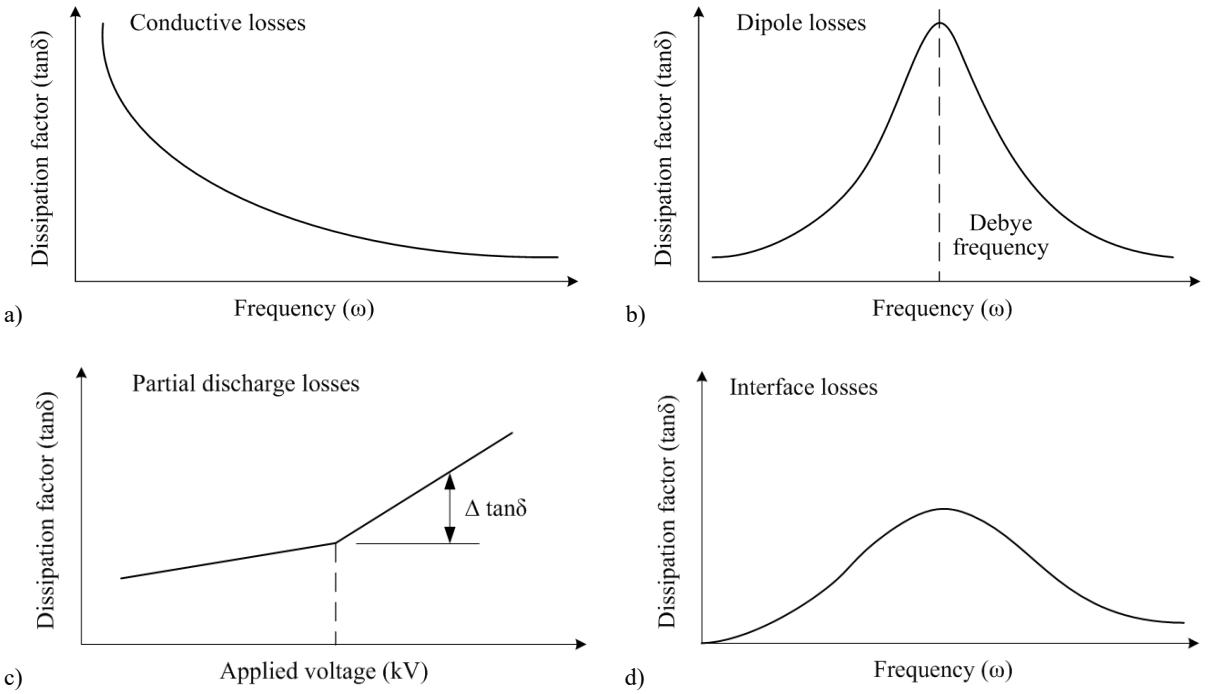

Figure 3.2: Dielectric losses characteristics: a) conduction losses, b) dipole losses, c) partial discharge losses, d) interface losses [42].

Partial discharge breakdown

Partial discharge is a localized breakdown which causes degradation and eventually leads to system breakdown. As observed, before any breakdown, there is either tracking or electrical trees, which are initiated from partial discharge. In other words, continuously occurred partial discharges will cause the erosion in the material, which can lead to breakdown in the end. Partial discharge will be discussed in the next section in detail.

3.2 Partial Discharge in Solid Dielectrics

One of the main causes of insulation breakdown in solid dielectric is partial discharges in cavities (also termed 'voids') in the dielectric. Cavities, which are usually gas filled, appear within the dielectric in different forms. Figure 3.3 shows some examples of cavities. Internal discharges usually occur in the cavities in Figure 3.3a to Figure 3.3c. Discharges would occur at the interface perpendicular to the field (Figure 3.3d) or with a substantial tangential field (Figure 3.3e). In Figure 3.3f, surface discharges take place at the edge of a sharp electrode.

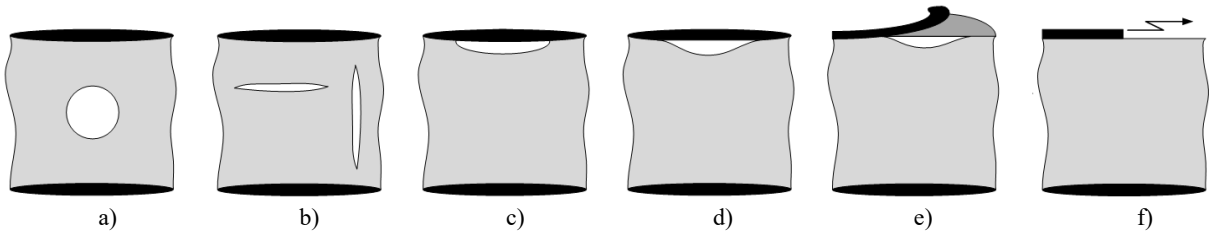

Figure 3.3: Cavities causing partial discharges in solid dielectrics: a) spherical cavity surrounded by the dielectric, b)fissures, c) electrode bounded cavity, d) non-adhering electrode, or opening between electrode and dielectric, e) interface with a longitudinal field, f) electrode edge.

The gas in the cavity has a lower permittivity than the surrounding dielectric, which leads to the enhanced field strength in the cavity. Thus, the gas will break down long before the solid dielectric reaches its breakdown strength. Therefore, the partial discharge in a cavity is the breakdown of the gas within the cavity. The theory of breakdown in gas will be used to explain the discharge mechanism in cavities.

3.2.1 Discharge mechanism

There are some necessary conditions for partial discharge to initiate: a sufficiently high voltage, i.e. electric field strength, the presence of an initiatory electron, and a dielectric material which can support the discharge process. For a PD the electric field strength needs to reach the breakdown strength of the gas in the cavity. The initiatory electron must be sufficiently far (in the direction of the electric field) from the cavity wall of the anode side [45], preferably near the cathode. In this case, the electron can be accelerated sufficiently by the electric field, so that a multiplication of the number of electrons can be generated during ionization caused by the collisions between the electrons and the gas molecules. As a result the electron avalanche can be initiated and travels towards to the anode [46]. Once the avalanche size is large enough without being stopped before reaching the cavity wall of the anode side, a breakdown channel is produced across the cavity. The breakdown process is accompanied with substantial ionization [47] and will be generating large quantities of positive and negative charges (ions). Those charges tend to drift to the walls of the cavity and deposit on the surface.

Electric field enhancement

Sufficient field strength is required for PD initiation, which is a dynamic combination of several factors. At the cavity site there is an enhancement in the electric field which drives the PD occurring. The local enhanced field E_i is composed of two contributing fields [48], as shown in Figure 3.4. The first one E_c is an enhancement of the background field E_0 inside the insulation, which is caused by the lower permittivity of the gas in the cavity and the cavity shape. The second one E_q is produced by the local space or surface charges q left by the previous PD events. The local field inside the defect is the vectorial addition of the two fields, which is expressed as:

$$\overrightarrow{E_i} = \overrightarrow{E_c} + \overrightarrow{E_q} = f \cdot \overrightarrow{E_0} + \overrightarrow{E_q} \qquad (3.2)$$

E_i is the local field inside the defect which drives PD. f is the field-modification factor that quantifies the field enhancement inside the cavity and depends on the relative permittivity of the dielectric and the cavity shape [49]. For simple shapes such as spheroidal and ellipsoidal cavities [50-51], the field within the cavity is nearly uniform. The spheroidal cavity model as shown in Figure 3.3a is used in this thesis for analysing the field conditions within the cavity.

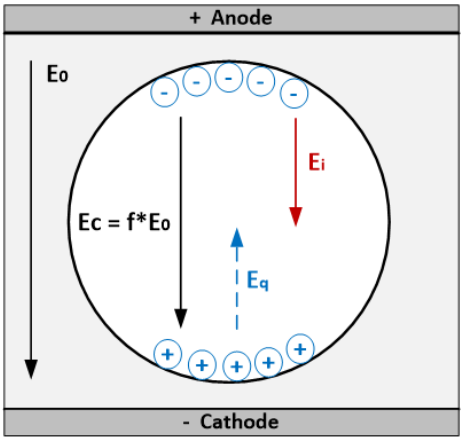

Figure 3.4: The local field composed of the enhanced background field and the field produced by the surface charges.

There exists a minimum local field which enables the avalanche and the following partial discharge when an initiatory electron is available. This field is the inception field E_{inc}, which corresponds to the PD inception voltage (PDIV). It is associated with the breakdown field strength of the gas in the cavity, which obeys the Paschen's law. E_{inc} depends on the dimension of the cavity (when considering the breakdown voltage of the gas), the pressure and contents in the defect, and the temperature [46]. In a virgin cavity, the breakdown of the gas is caused by a streamer. The voltage required to start a streamer is usually 5% higher than the voltage corresponding to the Paschen curve [42]. When this cavity has been aged by discharges for some time, organic acids are produced by chemical reactions in the gas, which will increase the conductivity of the cavity surface [52]. The conductive part on the surface acts as a cathode, and Townsend discharge can take place. In this case, the inception voltage coincides with the Paschen curve. In other words, E_{inc} in a virgin void is higher than in an aged void.

Initiatory electron

An initiatory electron is also needed to initiate PD. According to Niemeyer [48], there are two main groups of the initiatory electron generation mechanisms: volume generation and surface emission. The volume generation includes the gas ionization by energetic photons due to cosmic and background radiation, and the field detachment of electrons from negative ions. In both cases, the production rate of

the first electron depends on the electric field. The surface emission includes the detrapping of electrons from traps on the insulator surface, electron release by ion impact, and by the photon effect from both insulating and conducting surfaces.

In the virgin defect where PD has not occurred ever, volume generation is the dominating effect. The initiatory electron will be generated from the cosmic and background radiation, which is a stochastic process. Once PD has occurred in the defect, the charges produced by the previous PD will be deposited on the insulator surface and in the traps existing in the surface. The traps in the surface of the dielectric are produced by so called hot electrons with energies above around 4 eV [53]. They have an energy level within the forbidden band gap of the dielectric being closer to the conduction band than to the valence band (Figure 3.5). According to [54], traps with energy depths of the order of eV's are present at the insulator surface. Electrons stayed in such traps can be thermally excited to escape the traps and jump to the conduction band and become free electrons [40, 55]. Those electrons are potential initiatory electrons. Before discharges occur in the cavity for the first time, the number of traps in the surface is limited, and some of them are filled. Once PD has occurred, more new traps and deeper traps are formed [46, 53]. Hereby, the detrapping of electrons from surfaces is an additional initiatory electron generation mechanism.

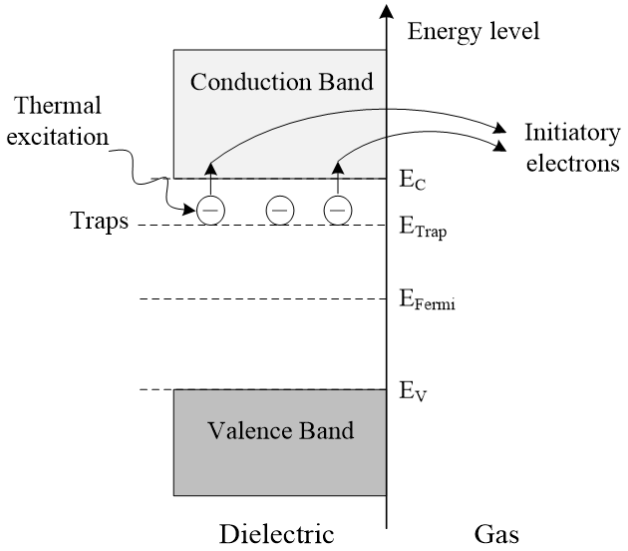

Figure 3.5: Electron traps at the surface of dielectric and electrons being excited from traps [46].

PD inception delay

Partial discharge will not necessarily take place as soon as the inception field is reached if the initiatory electron is absent. Electrons are generated by the cosmic and background radiation at a rate of about 3-4 electrons per s·cm^3·bar [45-46]. For cavity size in the magnitude order of mm^3 or smaller, the waiting time for the first electron to be generated is about minutes or even longer. If the initiatory electron is present, it must be appearing at a position within the cavity far from the anode so that it could initiate the avalanche. Otherwise, discharge cannot be initiated neither. As the voltage is raised and the electric field exceeds the inception field, the probability of discharges being initiated increases. The time needed for PD to be initiated after the inception field has been reached is the PD inception delay time t_{delay}. The average t_{delay} depends on the dimensions of the cavity, the ionization process and pressure change in the cavity, and the ratio of the applied voltage to the inception voltage [48, 56], as shown in equation (3.3).

$$t_{delay} \approx \frac{1}{\frac{\pi}{6} C_{rad} \emptyset_{rad} \left(\frac{d}{p}\right)_0 p l^3 \left(l - \left(\frac{AC}{PDIV}\right)^{-\gamma}\right)} \qquad (3.3)$$

Wherein, C_{rad} is the volume ionization parameter and $\emptyset_{rad}$ is the ionizing quantum flux density regarding an air filled cavity with gas density d and pressure p, l standing for the void dimension and γ characterizing the gas combination. PDIV is the PD inception voltage measured without inception delay. With increasing applied AC voltage, t_{delay} decreases.

The initiatory electron can also be the one which escapes from the traps in the surface. This process also causes inception delay. However, the delay caused by detrapping is much lower than that caused by the natural irradiation.

The delay in PD inception is a statistical cause of the variations in PD inception voltage (PDIV).

Charge decay and loss

The charges deposited on the surface of the cavity wall left by previous PD are also sources for an initiatory electron generation and they contribute to the field E_q as well. Those charges have a finite lifetime. They decay after PD events by ion drift, diffusion through the gas, and conduction along the insulator surface [48]. A long decay time means the charges will remain almost intact in the defect and contribute strongly to the E_q. The RC decay time constant is of the order

$$\tau_{dc} \sim \frac{\varepsilon_0 r_c}{2\sigma_s} \qquad (3.4)$$

wherein, σ_s is the surface conductivity and r_c the equivalent radius of the circumference of the conducting surface. So τ_{dc} is mainly controlled by the surface conductivity, which depends on the aging state of the defect. In the virgin defect, the surface conductivity of polymers is relatively small, so that the surface charges can survive for a long time. For the aged defect, the surface conductivity increased, so the charges will decay faster. In addition, the conducting surface will shield the defect interior from the electric field, which leads to a suppression of discharges.

The electrons, especially the ones which are trapped in the deep traps, can be diffused even deeper into the dielectric from where they can no longer be liberated. Such electron loss may lead to the discharge extinction due to the lack of initiatory electrons [57-58].

Conductivity of cavity surface

The discharge process is accompanied by chemical reactions, which produce different by-products. The by-products mainly consist of acids [59]. During the deposition of the PD by-products, the conductivity of the cavity surface is increased [60] due to the formation of acid layers on the surface [59, 61]. Consequently, the charges are deposited on the surface more homogeneously, and the initiatory electrons are spread more evenly over the surface [62]. Moreover, with more traps produced and filled, the conductivity also increases. All these results in an accelerated re-occurrence of PD. In other words, the PD repetition rate increases with a rise of the surface conductivity [46].

3.2.2 Partial discharge process under AC, impulse and superimposed voltage

Partial discharge process under AC voltage

Figure 3.6 illustrates the electric fields during PD activity under AC voltage. It is hypothesized in Figure 3.6a that the initiatory electron is always available and no charge decay is considered. The local electric field E_i follows the background electric field E_c at the beginning. When E_i reaches the inception field E_{inc}, one partial discharge occurs. The charges generated by the PD process deposite on the cavity wall and create the electric field E_q. As the vectorial addition of E_c and E_q, E_i drops to E_{ext}, where the PD extinguishes. Without considering the charge decay, E_q keeps the same and E_i tries to follow E_c again

with the offset of E_q until the next PD occurs. In Figure 3.6b, the charge decay is considered, which is depicted by the decreasing E_q between each two PD events. In practice, the statistical characteristics of PDs show strong scatter and variations. It can happen that PD doesn't occur as soon as the local field E_i reaches the inception field E_{inc}. Instead, it initiates later when the initiatory electron is available. Such PD activities considering the stochastic behaviour of the initiatory electron generation and the charge decay is shown in Figure 3.6c.

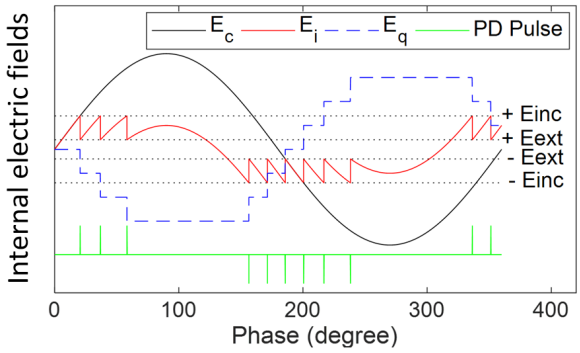

(a). Infinite initiatory electron, no charge decay.

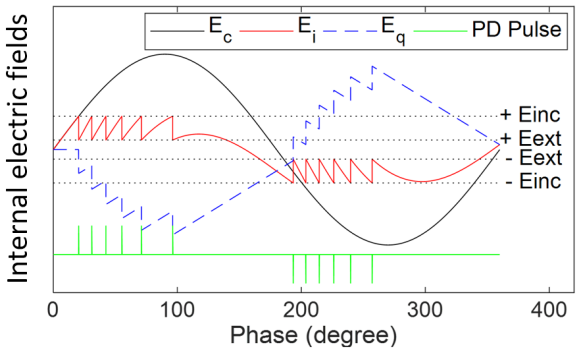

(b). Infinite initiatory electron, charge decay.

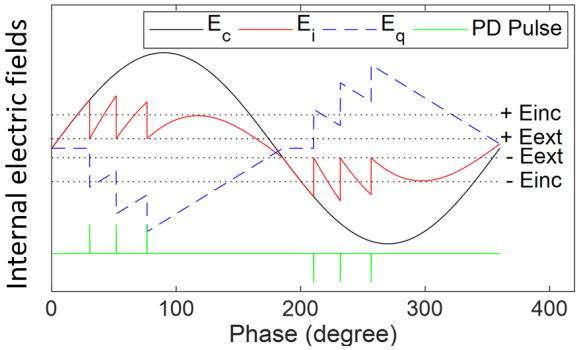

(c). Finite initiatory electron, charge decay.

Figure 3.6: Electric field conditions during PD process under AC voltage.

Partial discharge process under impulse voltages

Under impulse voltage conditions, the same partial discharge mechanism is expected to occur within the cavity. Since the impulse voltage is not periodic with only one polarity and decreases to zero in the end, the discharges initiated are not phase related but polarity related. Basically, two types of discharges can be observed under impulse voltage [24]:

- The main discharge, which occurs on the wave front of the impulse.
- The reverse discharges, which occur on the wave tail of the impulse which are opposite in direction to the main discharge.

Figure 3.7 illustrates the partial discharge process under the impulse voltage. It is hypothesized that the initiatory electron is always available and no charge decay is considered. Main discharges occur during the front time of the impulse which are same in direction with the impulse polarity. With the built up E_q, the local field E_i reverses soon after the impulse peak and the reverse discharges occur.

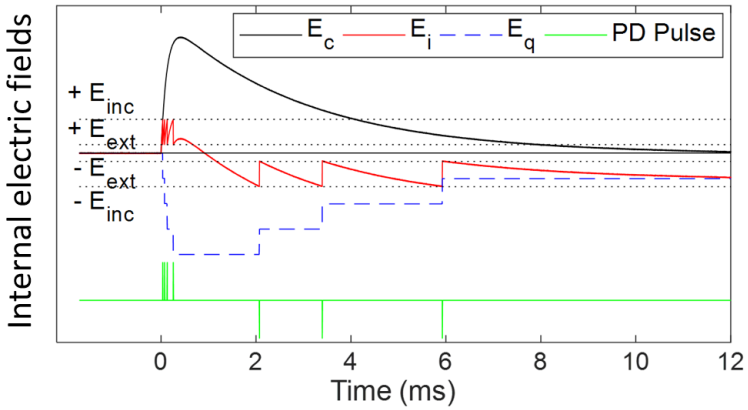

Figure 3.7: Electric field conditions during PD process under impulse voltage

According to Densley [24], single main discharge with large magnitude occurs on or near the peak of the impulse, which actually consists of many site discharges. Several reverse discharges occur with much smaller magnitude. The author of this thesis, however, believes that more than one main discharge could occur during the front wave of the impulse and not necessarily on or near the impulse peak. It is possible that only one or few main discharges are observed during the impulse front or on the impulse peak due to the PD measuring limitation. Since the voltage increases rapidly during the front time, the main discharges may occur in many sites simultaneously and consecutively with a very small time interval, which results in single discharge being observed with large magnitude. If the PD measuring system has enough time resolution, it might be possible to observe consecutively occurred main discharges. Compared to main discharges, reverse discharges occur in a relatively gentler pace under smoothly decreasing wave.

Partial discharge process under superimposed transient voltages

The partial discharge process under the superimposed transient voltage is illustrated in Figure 3.8, where a positive impulse is superimposed at the AC crest. Similar to the PD process under impulses, one or more main discharges occur during the front time of the impulse. After that, with the offset of E_q, the local field E_i decreases firstly following the impulse tail, and then increases in the opposite polarity following the E_c. After the impulse finishes, partial discharges are initiated as they are under AC voltage.

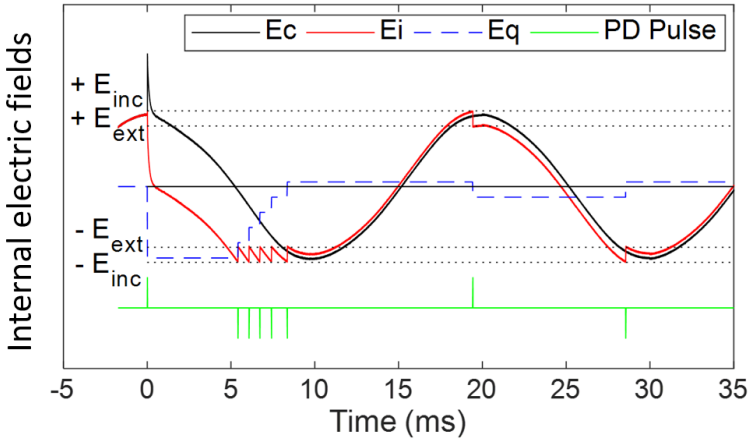

Figure 3.8: Electric field conditions during PD process under superimposed voltage

3.2.3 Degradation caused by discharges

Partial discharges in cavities in a dielectric induce degradation in the material, which eventually cause the breakdown in the dielectric. The degradation is mainly due to two processes: the chemical reaction and the physical attack by bombardment of charge carriers (electrons and ions) [63]. The chemical reactions taking place in the cavity accompanying the partial discharge process produce gaseous [64-65], liquid [59, 66-67] and solid by-products [68-69]. The PD by-products, mostly deposited on the wall of the cavity, erode the dielectric material, enhance conductivity of the surface and roughen the surface. The bombardment of the electrons and ions on the surface of the cavity wall also increase the roughness of the surface. In addition, the cavity surface may also get deteriorated by UV radiation [46]. As a result, the surface of the cavity wall is severely eroded and roughened, and the surface conductivity is increased. In a long term, a pit is then formed and growing deeper often at the edge of the cavity, which usually takes hours to even years. The field stress at the tip of the pit is hereby enhanced. Once the field stress reaches the intrinsic breakdown strength of the dielectric, breakdown occurs over a small distance, and an electrical tree starts to be formed and grows, which usually takes seconds to minutes. As soon as the tree grows and approaches the electrode, a complete breakdown occurs.

The interaction between partial discharges and degradation is a dynamic process. Partial discharges cause the degradation, in turn, the degradation process also affects the PD mechanism, such as the PD inception and extinction condition.

3.2.4 Measurement of partial discharge

The physics of partial discharge process have been described in section 3.2.1. Measuring partial discharges is basically the measurement of the charge displacement caused by the discharge. During the discharge process, the partial discharge current pulse, which is formed by the movement of electrons and positive ions in the breakdown channel, changes the field in the cavity and hereby induces the charge on the electrodes. The actual charge displacement caused by PD is not directly measurable, while the induced charge on the electrodes can be measured.

PD sensors

PD signals are measured by sensors, which responds to an input PD signal by creating a functionally related output in the form of mechanical or electrical signal. Different types of PD sensors are commonly available:

- Capacitive sensor
- Inductive sensor, most commonly in the form of high frequency current transformer (HFCT)
- Piezoelectric sensor
- Acoustic sensor

The capacitive sensor and the inductive sensor are mostly applied since the electrical measurement in forms of voltage and current can be used directly to quantify partial discharges. In this thesis, the high frequency current transformer (HFCT) is used to measure PD, which will be discussed in chapter 5 and chapter 6 in details.

Conventional and unconventional method

The shape of partial discharge pulses depends on many factors, such as the discharge source, frequency response of the system connected to the test object, detection equipment and its frequency response etc.. The duration of a single PD pulse occurring in a cable system is typically in the order of tens of nanoseconds [37, 70-71], which implies that the frequency content of a partial discharge pulse is in the

order of tens to hundreds of megahertz. Such PD pulse is measured by a suitable PD measuring system. With regard to the frequency bandwidth of measurement, PD measurement can be classified into two methods: the conventional method and the unconventional method.

The conventional method, described in IEC 60270 [72] and IEC 60885-3, applies narrow band (9 kHz $\leq \Delta f \leq$ 30 kHz, 50 kHz $\leq f_m \leq$ 1 MHz) or wide band detection (30 kHz $\leq f_1 \leq$ 100 kHz, $f_2 \leq$ 500 kHz, 100 kHz $\leq \Delta f \leq$ 400 kHz). The conventional method usually measures the discharge magnitude (in pC) with respect to phase position. The calibration of the measuring system is required for using the conventional method. For power cables the conventional method is mostly applied in laboratory tests, routine tests and type tests [73].

The unconventional method makes use of ultra-wide bandwidth in the measuring instruments with frequency up to the MHz range. By this mean it is possible to measure the shape and frequency spectrum of PD pulses. Moreover, noises at lower frequencies tend to be rejected. Therefore, the method is usually applied in the field tests.

3.2.5 Partial discharge tests in power cable system

Partial discharge measurements provide a useful tool to obtain information about discharging defects in high-voltage power cables. In power cables, PD occurs at insulation defects for instance in cable joints and terminations, especially at interfaces [74-75]. Therefore, PD measurement on cable systems can be considered a useful tool to diagnose insulation condition [76-78].

PD tests applied to power cables usually fall into two categories: laboratory tests and on-site field tests. Laboratory test is usually carried out on new cable system, which includes routine test, qualification test and factory test. The laboratory tests are usually conducted on short cable systems under controlled conditions of noise, grounding, etc. The purpose of laboratory tests is to evaluate if the cable system has a service life as specified by the manufacturers, to estimate the aging mechanism and to investigate important properties or behaviour of cable systems. The field (on-site) test includes commissioning test and maintenance test. They are going to be described more in detail in the following.

PD tests in commissioning tests

Defects may appear in the cable insulation system after installation. During the transportation, or on-site installation of new cable systems, or replacement of failed components, defects can be introduced into the cable systems, especially in cable accessories [79]. In order to ensure that the cable system is free of such life limiting defects, commissioning test is performed after the installation and before the system is put in normal service. For a commissioning test, PD tests are recommended to be performed [80].

A survey has been carried out among CIGRE-membership countries in [80] regarding the field PD testing of HV and EHV extruded cable systems. The survey showed that the most common practice for commissioning tests of extrude HV and EHV cable systems is a combination of AC withstand test with PD test. According to the feedback from cable owners of HV and EHV cable systems their experience in commissioning tests is that some partial discharge sources require some time to be active (Figure 3.9a). Moreover, the majority of PD sources have a PDIV more than $1.5U_0$ (Figure 3.9b). Consequently, a PD test with acceptance criterion in combination with AC withstand test is suggested (only HV class is given here), as given in Table 3.1.

a) 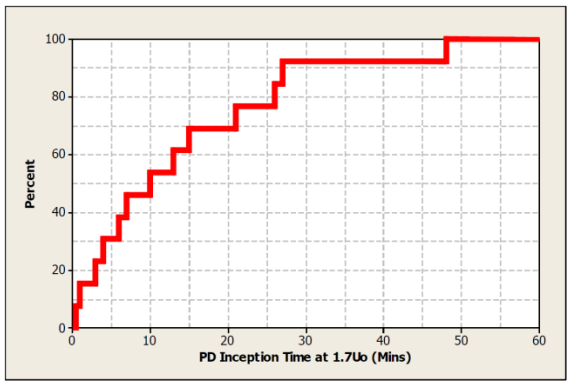

b) 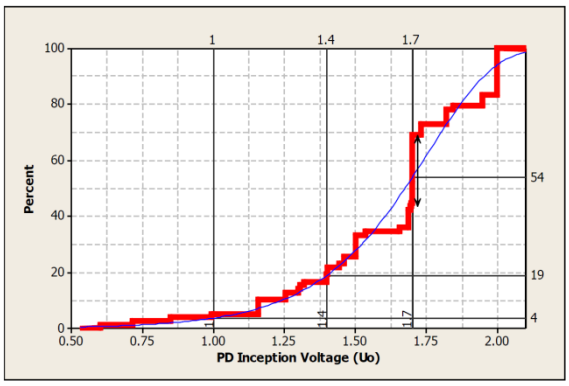

Figure 3.9: Experience in commissioning tests: a) PD on-set time at $1.7U_0$, b) distribution of PDIV (copied from [80]).

Table 3.1: Suggested commissioning test with PD test involved.

Voltage class [kV]	Withstand test			PD test
	Test level [U_0]	Frequency range [Hz]	Duration [min]	PD pass/fail criterion
150/160	1.7	10-300	60	PDEV > 1.5 U_0 (No detectable PD at 1.5U_0)

The PD test is performed during the AC withstand test with a procedure described in Figure 3.10.

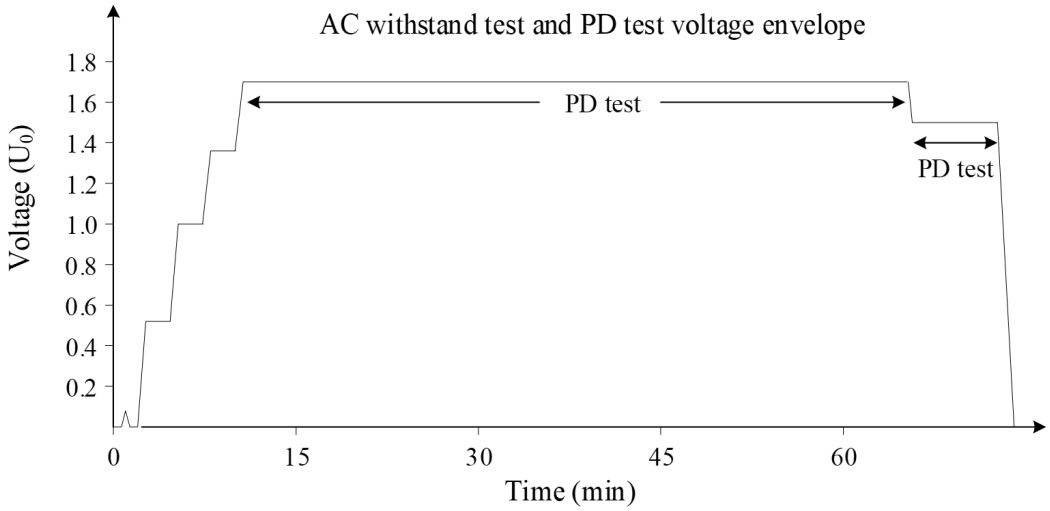

Figure 3.10: PD test procedure in commissioning test.

PD tests in maintenance tests

For aged cable systems that have been operated in service for a time, defects can be induced during the insulation aging due to operational stresses or environmental stresses. To detect degradation condition and to verify the serviceability of the cable systems, maintenance test is performed. For maintenance test, PD tests are recommended to be involved as well [80]. Regarding maintenance test for cables older than 15 years, a similar suggestion on PD test in combination with withstand test is proposed and given in Table 3.2.

Table 3.2: Suggested maintenance test with PD test involved.

Voltage class [kV]	Withstand test			PD test
	Test level [U_0]	Frequency range [Hz]	Duration [min]	PD pass/fail criterion
150/160	1.1	10-300	60	No detectable PD

Supposing the suggested PD tests are applied in commissioning test and maintenance tests, in case a defect exists which has a PDEV higher than at $1.5U_0$ or $1.1U_0$ respectively, it will pass the tests and the cable system will be put into service. With the existence of the defect, there are risks that it could be initiated by some severe situations, for example impulses or superimposed transients.

In this thesis, the cable system with defects are investigated in laboratory conditions. The defects are artificially made in such a way that they can pass either the commissioning test or the maintenance test. The details about the defects will be presented in Chapter 5 and Chapter 6.

3.2.6 PD measurement in power cable under impulses and superimposed transients

PD in power cables is normally measured under AC voltage by using the conventional technique [81]. In practice, power cables are not only subjected to AC operating voltage, but also to transient voltages such as lightning and switching impulses, which occasionally will superimpose on the normal AC voltage. Those transient voltages will have an additional stress on the cable insulation. In addition, as discussed before, defects may exist in the cable systems which can pass the commissioning test or the maintenance test but might be initiated by severe transient situations. In that regard it is important to investigate PD under impulse and superimposed voltages.

One of the challenges in measuring PD under impulse and superimposed voltages concerns the suppression of the disturbances caused by the transient voltages. In laboratory tests, the applied impulse voltage causes currents in the cable under test that disturb the PD measurement. Thus, the PD measurement system needs to have a strong suppression of the disturbance. In such a case, the conventional PD technique is not suitable anymore. The unconventional method based on the measurements of electrical signals in MHz range is of more interest as a better alternative for these conditions [78, 82-86].

Three circuits for PD detection under impulse are provided in [87] with a measurement frequency from hundreds of MHz to GHz, namely: the high frequency current transformer (HFCT) with multipole filter, the coupling capacitor with multipole filter, and the electromagnetic couplers. HFCTs or other sensors are commonly used with wide/ultra-wide bandwidth together with filters and a digital oscilloscope to detect PD in insulation specimens or models under impulses [88-93]. A coupling capacitor was used to measure PD in material samples in cases where only impulse [94] and square wave voltage were applied [5]. Those PD measuring systems were able to detect PD during the impulse even during its front time. For superimposed impulses, PD was detected in laminated paper using a current transformer and a high-pass filter by Hayakawa et al. [95]. Nikjoo et al. [96] used a wideband detection system consisting of a coupling capacitor, a detection impedance and a low-pass filter to measure PD in oil-impregnated paper. However, in both works, PD was measured during AC cycles before and after impulses instead of during the impulses. Moreover, PD measurements in the above-mentioned works were performed on material specimens. Due to the small scale of the samples and the relatively low voltage level applied, less disturbance is produced in the circuitry.

Regarding PD measurement on power cables, for off-line tests, capacitors and HFCTs are used, while on-line tests almost always use HFCTs [76], especially for testing cable accessories [97-99]. However, in the related literature, partial discharges in power cables are usually measured after the impulse has been applied, while partial discharges during the moment of impulse have been less reported.

During impulse voltage conditions the PD measuring system should fulfil two requirements. Firstly, the safety of both human and equipment need to be ensured when using the measuring system. Secondly, the measuring system should be able to detect PD from the cable joint before, during and after the impulse transient application upon the AC voltage.

Chapter 4

Breakdown in Polymeric Material Samples under Superimposed Voltages

Since the polymeric material structures are complicated and different by types, it is still difficult to apply a well-accepted theory of breakdown to the insulation materials. Moreover, the breakdown process is sensitive to many factors. It can be affected by not only internal factors such as insulation structure, but also external factors such as transients in the system [20, 100-101]. Power system transients such as lightning and switching impulses contain a wide range of frequencies [102]. Measurements of real transients in a 380 kV system in the Netherlands show switching transients from power frequency up to several kHz (Chapter 2).

Previous literature shows that there are relations between certain transient parameters and breakdown performance of insulation. For example, with decreasing front time of impulse voltages, the breakdown voltage of insulation models increases [103]. In [100], the breakdown voltage of cross linked polyethylene (XLPE) insulating material decreased with increasing frequency of the applied voltage for HVAC on-site testing.

This chapter investigates the effect of superimposed voltages on the breakdown strength of the polymeric insulating materials which are used in HV cables systems. Due to the high population of XLPE cables in service, the increasing installation of more XLPE cables, as well as the higher failure rates of XLPE cables and accessories (section 1.1), XLPE insulation with its performance are of great interest. Hereby it is chosen to be one polymeric insulating material for the investigation. In addition, epoxy resin, as another important polymeric insulating material, is also investigated in this work since it is easy to be prepared in the lab. DC voltage, AC voltage with different frequencies and superimposed voltages are applied on the insulation material samples in order to measure the breakdown voltages.

This chapter is based on:
J. Wu, H. Jin, A. Rodrigo Mor, J. J. Smit, “Effects of Transients on Breakdown of XLPE Cable Insulation”. In 20th International Symposium on High Voltage Engineering (ISH), Buenos Aires, Argentina, Sept. 2017.

4.1 Samples Preparation

Two types of XLPE material samples and one type of epoxy resin material samples were prepared for the breakdown measurements.

The first type of XLPE samples, XLPE I (Figure 4.1a), were cut from XLPE films which were produced by hot pressing. The samples are in the shape of disks with average thickness of 0.1 mm and diameter of 25 mm. Before tests, the samples were carefully cleaned with ethanol, degassed in vacuum for 2-3 days at 50-60 °C and then kept in vacuum at ambient temperature.

The second type of XLPE samples, XLPE II (Figure 4.1b), were produced from a 220/380 kV commercial XLPE cable with insulation thickness of 25 mm. Figure 4.2 illustrates how the samples are produced. Cross sections of 0.2 mm thick were sliced perpendicular to the cable axis. The XLPE samples were then cut from the cable slices which have a diameter of 25 mm and a thickness of 0.2 mm. Before tests, the XLPE samples were carefully cleaned and kept in vacuum at ambient temperature.

The epoxy resin samples (Figure 4.1c) were casted in the HV lab, with diameter of 55 mm and thickness ranged from 0.3 mm to 0.5 mm.

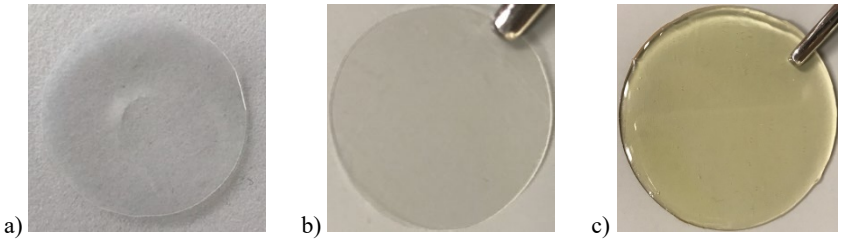

Figure 4.1: Material samples: a) XLPE sample type I, b) XLPE sample type II, c) Epoxy resin samples.

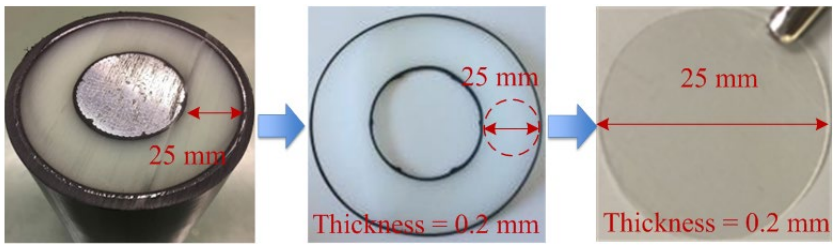

Figure 4.2: Producing XLPE II samples from 220/380 kV XLPE cable.

The dimensions of the materials samples are given in Table 4.1. The dielectric properties of the material samples were measured using a dielectric analyser (Novocontrol Alpha-A) at 3 V for different frequencies at ambient temperature. Table 4.1 gives the property values in average measured at 50 Hz and 20 °C.

Table 4.1: Dimensions and dielectric properties of material samples.

Material samples	Diameter [mm]	Thickness [mm]	Temp [°C]	freq [Hz]	ε'	ε''	tanδ	C [pF]
XLPE I	25	~ 0.1	20	50	2.23	3.55×10^{-4}	1.59×10^{-4}	47.4
XLPE II	25	~ 0.2	20	50	2.31	3.40×10^{-4}	1.47×10^{-4}	31.9
Epoxy resin	55	0.3-0.5	20	56	3.63	1.65×10^{-2}	45.5×10^{-4}	69

4.2 Breakdown Voltage Tests

4.2.1 Experimental set-up

The experimental set-up consists of a sample cell, a high voltage source and a measurement system. To avoid flashover, a pair of stainless steel Rogowski-profiled electrodes were used and samples were immersed in dielectric oil. The high voltage electrode has a diameter of 6 mm, and the ground electrode has a diameter of 11 mm. Figure 4.3 shows the schematic and physical arrangement of the sample cell.

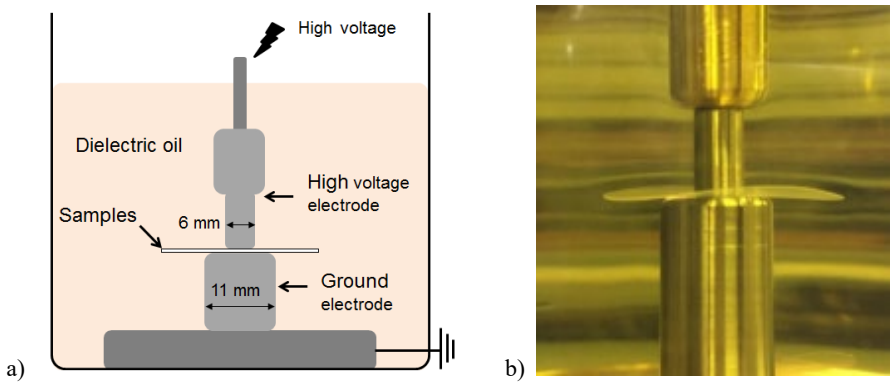

Figure 4.3: Sample cell: a) schematic of the sample cell and dimension, b) physical arrangement of sample cell.

Samples were tested for breakdown strength under high voltage DC, AC and superimposed waveforms. Breakdown tests under DC voltage were carried out using a 300 kV DC source as the high voltage source. The voltage applied on samples were measured by a volt meter. For AC breakdown tests, an arbitrary waveform generator together with a high voltage power amplifier were used to generate high voltage AC. The arbitrary waveform generator generated the test voltages with varying frequencies and amplitudes as low voltage signals, which were then amplified to high voltage level by the high voltage power amplifier with maximum output of ±30 kV and frequency up to 2.5 kHz. The voltage applied to the samples was measured by the voltage monitor of the high voltage power amplifier and then displayed on the computer. Figure 4.4 shows the set-up for AC breakdown tests. For testing breakdown under superimposed waveforms, the same set-up as AC test was used.

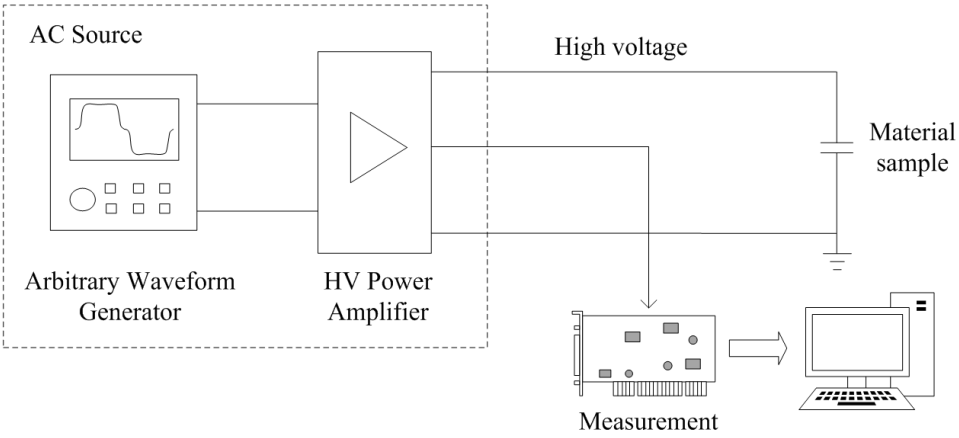

Figure 4.4: Experimental set-up for AC and superimposed voltage tests.

4.2.2 Test voltage waveform

In section 2.1.1, the transient in the 380 kV mixed overhead line and cable system measured in the field was presented. Figure 2.4 shows the characteristics of the field-measured transient having an

overvoltage of 1.7 p.u. and a dominant frequency of 1 kHz. These transient characteristics from the practical observations, i.e. overvoltage and frequency components, are used to define the test voltage waveform for the breakdown tests on the material samples. To investigate the effect of frequency on the breakdown, the material samples were tested under DC voltage and AC voltage with different frequencies. To investigate the effect of the superimposed voltage on the breakdown, superimposed waveforms were defined with both varied frequency and varied overvoltage. The test voltage waveforms are described in detail in the following.

DC and AC sinusoidal waveforms with different frequencies

DC voltage and AC voltage with different frequencies were applied to the material samples for investigating the effect of frequency on breakdown. For AC tests, in order to reflect the practical situation, the frequency of 1 kHz was included (see section 2.1.1 and Figure 2.4b). Fundamental frequency of 50 Hz was tested as the reference. The test voltage waveforms with their frequencies are listed in Table 4.2.

Table 4.2: Test voltage waveforms Testing voltages for investigating the effect of frequency.

Material samples	**DC**	**AC sinusoidal wave**						
frequency [Hz]	—	50	300	500	1000	1500	2000	2500

Superimposed waveforms

For investigating the breakdown under superimposed voltages, a waveform with a high frequency sine wave (referred to as harmonic in this thesis) being superimposed on 50 Hz AC voltage was designed as the test voltage. The overvoltage and frequency components of the field-measured transients were used as parameters to design the superimposed harmonics. Considering the practical transient presented in section 2.1.1 and Figure 2.4, the ratio between the overvoltage peak amplitude (1.7 p.u.) and the fundamental peak amplitude (1.0 p.u.) is 0.7. For the superimposed test voltages, a series of amplitude ratios were selected to design the harmonic amplitudes. The AC frequencies in Table 4.2 were applied to design the harmonic frequencies. As a result, a series of harmonics with different amplitude ratios and frequencies were superimposed on top of the fundamental voltage composing the testing voltages. Those superimposed waveforms are listed in Table 4.3. Figure 4.5 shows the V_1 waveform listed in Table 4.3 as an example. In practice, a harmonic with an amplitude ratio of 20% - 30% is more likely to occur, rather than the amplitude ratio of 80%. However, we still studied 80% as the worst case.

Table 4.3: Testing voltages for investigating the effects of superimposed waveforms.

Test voltages		**Amplitude ratio between harmonic and fundamental voltage**			
		20%	**40%**	**60%**	**80%**
Harmonic* frequency [Hz]	**500**	V_1	V_4	V_7	V_{10}
	1000	V_2	V_5	V_8	V_{11}
	2000	V_3	V_6	V_9	V_{12}

* Harmonic is defined as the high frequency sine wave which is superimposed on 50 Hz AC voltage.

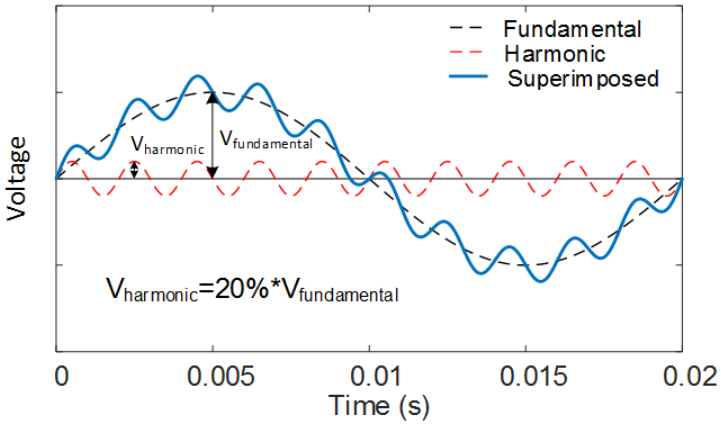

Figure 4.5: Example of superimposed waveform V_1.

4.2.3 Experimental procedure

Before testing, the entire sample cell (Figure 4.3) was degassed for 90 minutes at 70 °C. The tests were performed at ambient temperature. After breakdown occurrence, the sample thickness in the vicinity of the breakdown perforation were measured in order to calculate the electric field.

Ramp tests were performed according to IEC 60243-1 [104] and 60243-2 [105] standards. All the test voltage waveforms of Table 4.2 and Table 4.3 were applied on the samples from an initial value and increased continuously until the breakdown occurred. The initial voltages for all the testing voltages are the same 1.5 kV_{pp}. The testing voltage was increased with a rate of 1 kV_{pp}/s. The measured values were the breakdown voltages of the samples.

4.3 Statistical Analysis of Experiment Results

The breakdown results were analysed with a 2-parameter Weibull distribution, given in equation (4.1):

$$F(E) = 1 - e^{-\left(\frac{E}{\eta}\right)^{\beta}} \tag{4.1}$$

Where *F(E)* is the cumulative distribution function of breakdown, E is the breakdown strength. β is the shape parameter, also known as the Weibull slope, which is the slope of the regression line in a probability plot. η is the scale parameter, which determines the range of the distribution. η is also known as the characteristic breakdown strength. Regardless of the shape parameter β, when set $E = \eta$ in the equation 4.1, the corresponding *F(E)* will be equal to 63.2%. In other words, 63.2% of the population fails at $E = \eta$. In this way, η expresses the breakdown strength at which the failure probability is 63.2%, which is called B63-value. In Weibull analysis, a correlation coefficient ρ is used to measure how well the linear regression plot fits the data. The closer ρ is to 1, the better the plot fits [106]. Besides the 63.2% failure probability, i.e. B63-value, the breakdown strength of samples under DC and AC voltages at which the failure probability equals 10%, including 90% confidence bounds is also presented. The latter failure probability is called B10-value. It is a usual minimum requirement for safety practice, and also a simplified way of comparing different distributions according to the IEC 62539 [107] and IEEE 930-2004 [108] standards.

4.4 Breakdown under DC, AC with Different Frequencies and Superimposed Voltages

The prepared material samples were tested under the voltage waveforms given in section 4.2.2. The breakdown can be observed in Figure 4.6. The measurement results are presented in this section.

a) 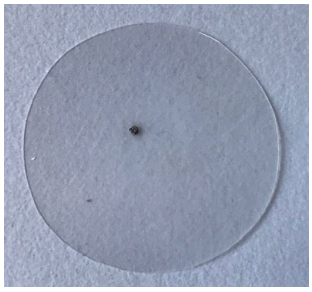 b)  c) 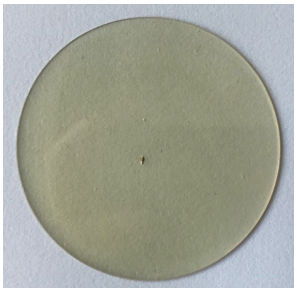

Figure 4.6: Material samples after breakdown tests: a) XLPE sample type I, b) XLPE sample type II, c) Epoxy resin samples.

4.4.1 Breakdown under DC and AC waveforms with different frequencies

All three types of material samples, XLPE I, XLPE II and epoxy resin, were tested under DC voltage and AC voltage with different frequencies. Weibull analysis was applied on the measurement results. The dependency between the breakdown strength and the frequency of the applied voltage for each material sample type was studied.

Breakdown Strength of XLPE Samples I of 0.1 mm thickness

Breakdown voltages of XLPE samples I were measured under DC and AC waveforms for four frequencies. For each waveform, six XLPE samples were tested. Figure 4.7 shows the probability of breakdown strengths of XLPE sample I under test waveforms in the 2-parameter Weibull plot within 90% confidence bounds. The corresponding distribution parameter values are given inTable 4.4. The breakdown strength under each waveform with 63.2% failure probability is given as η and plotted in Figure 4.8 with errors. The measurement results reveal a dependency between breakdown strength and AC frequency: the higher the AC frequency, the lower the breakdown strength of the XLPE samples I. The dependency is seen as a line in the double log plot in Figure 4.8. In other words, the breakdown strength decreases according to a power law, when the frequency increases. Moreover, compared to AC voltages, the XLPE samples-I have much higher breakdown strength under DC voltages.

Considering the probability distribution, the breakdown strength of XLPE samples I under DC and AC voltages at which the failure probability equals 10%, including 90% confidence bounds, is presented in Table 4.5. The relative change in breakdown strength at 10% failure probability under each testing voltage is compared to that under AC 50 Hz and given in Table 4.5 as well. The same dependency between frequency and breakdown strength of XLPE sample I can be observed for both 63.2% and 10% failure probability. The breakdown strength decreases with increasing frequency. For 10% failure probability, the breakdown strength under DC voltage is around two times higher than at AC 50 Hz. For AC voltage, the breakdown strength decreases to 36% of the 50 Hz level when frequency goes up to 2000 Hz.

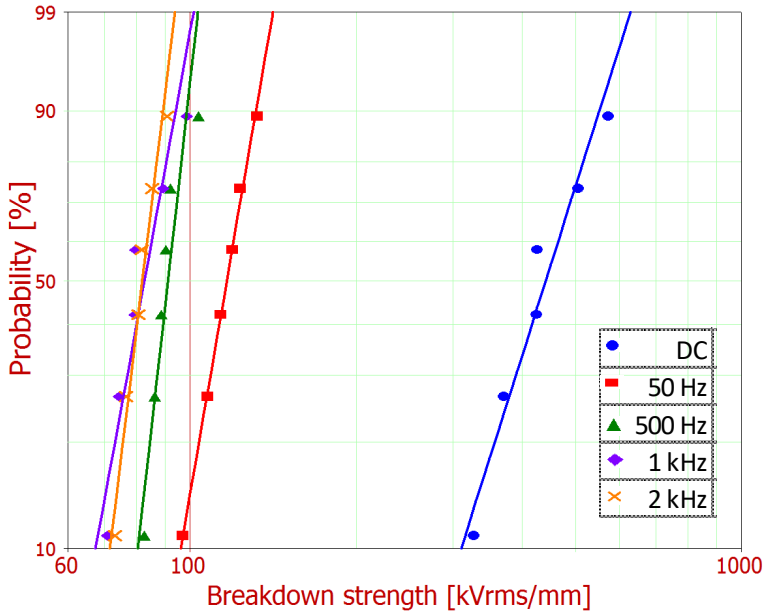

Figure 4.7: Weibull analysis of breakdown strength of XLPE samples I.

Table 4.4: Distribution parameters of breakdown strength of XLPE samples I.

Frequency of testing voltage [Hz]	η (with confidence bounds 90%) [kV_{rms}/mm]			β (with confidence bounds 90%) [kV_{rms}/mm]			ρ
	Lower	*η*	*Upper*	*Lower*	*β*	*Upper*	
DC	414	473	539	3.17	5.34	9.02	0.976
50	113	121	130	5.68	9.82	17.0	0.998
500	88.8	93.4	98.2	9.41	15.1	24.2	0.918
1000	79.6	86.0	93.0	5.60	9.23	15.2	0.942
2000	78.0	84.1	88.5	8.32	13.9	23.4	0.981

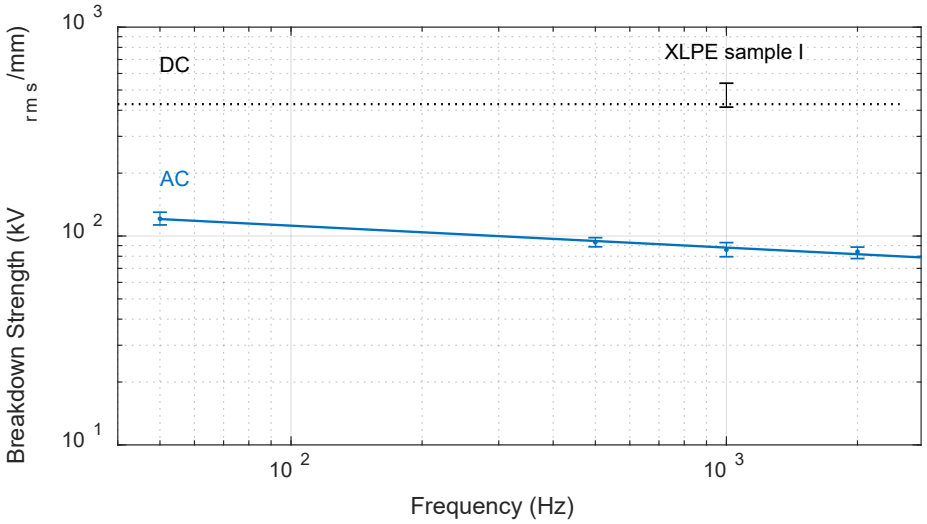

Figure 4.8: XLPE sample I: breakdown strengths with failure probability of 63.2% under AC waveforms with different frequencies in kV_{rms}/mm, and at DC conditions in kV_{DC}/mm.

Table 4.5: Breakdown strengths of XLPE Samples I at 10% Failure Probability including 90% Confidence Bounds.

Frequency of testing voltage [Hz]	Breakdown Strength		Confidence bounds 90%	
	10% Failure prob. [kV_{rms}/mm]	*Relative change*	*Lower [kV_{rms}/mm]*	*Upper [kV_{rms}/mm]*
DC	310	↑ 177%	233	412
50	112	-	82.7	112
500	80.5	↓ 28.1%	72.2	89.7
1000	67.4	↓ 39.8%	56.9	79.9
2000	71.6	↓ 36.1%	64.2	79.8

Breakdown Strength of XLPE Samples II of 0.2 mm thickness

The probability of breakdown strengths of XLPE samples II under DC and AC voltages are shown in the 2-parameter Weibull plots in Figure 4.9. Data are all within 90% confidence bounds. The corresponding distribution parameter values are given in Table 4.6. It can be observed that, the breakdown strength with 63.2% failure probability (η) of XLPE samples II under DC voltage as 493 kV_{rms}/mm is more than four times higher than that under AC 50 Hz as 95.2 kV_{rms}/mm, and even higher than AC voltage with higher frequencies. Under AC voltage, the higher the frequency, the lower the breakdown strength of XLPE samples. This dependency is illustrated in a double log plot in Figure 4.10, as the breakdown strength is decreasing according to a power law with the increasing of frequency.

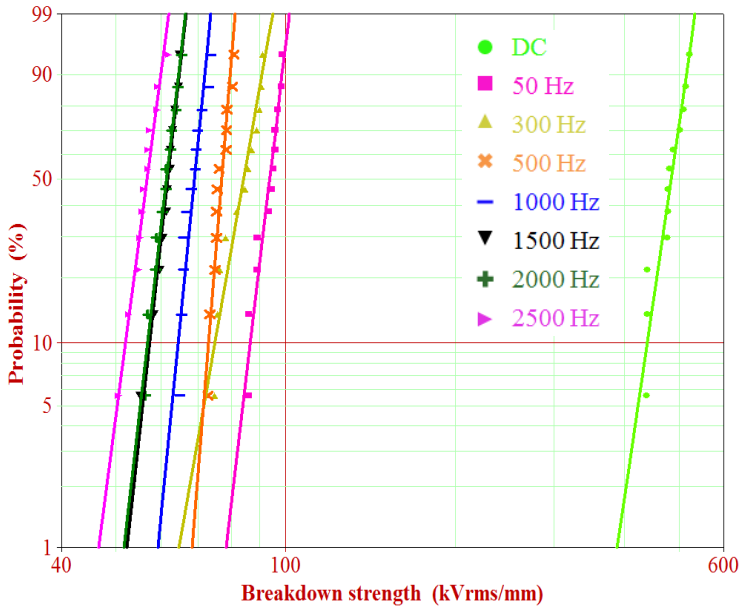

Figure 4.9: Weibull analysis of breakdown strength of XLPE samples II.

Table 4.6: Distribution parameters of breakdown strength of XLPE samples II.

Frequency of testing voltage [Hz]	η (with confidence bounds 90%) [kV_{rms}/mm]			β (with confidence bounds 90%) [kV_{rms}/mm]			ρ
	Lower	*η*	*Upper*	*Lower*	*β*	*Upper*	
DC	480	493	506	13.1	19.2	28.0	0.952
50	93.3	95.2	97.2	16.0	23.8	35.4	0.967
300	83.7	86.3	89.0	10.8	16.0	23.7	0.962
500	76.8	77.9	79.1	24.3	34.8	50.0	0.955
1000	68.5	69.8	71.2	19.8	28.2	40.2	0.936
1500	61.5	62.7	63.9	17.0	25.4	37.9	0.989
2000	61.1	62.4	63.7	16.6	24.3	35.4	0.986
2500	56.4	57.8	59.1	15.1	21.3	30.2	0.981

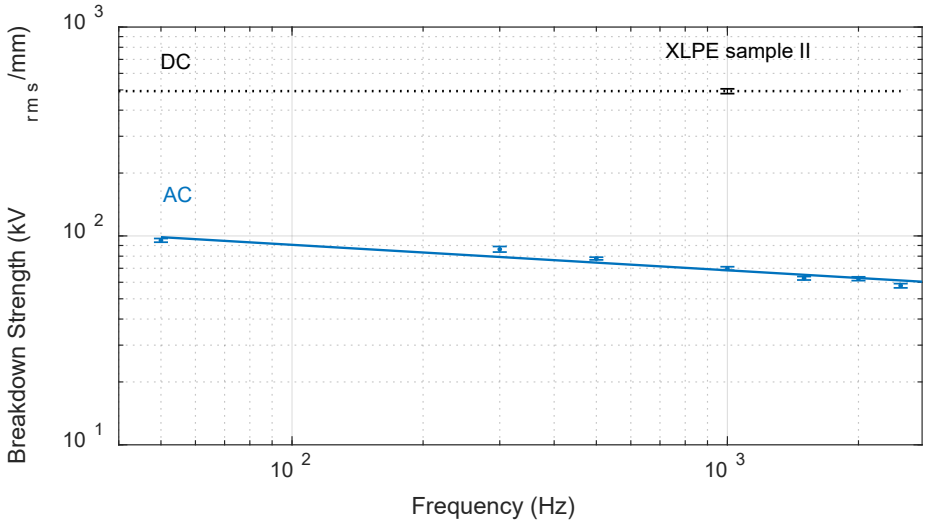

Figure 4.10: XLPE samples II: breakdown strengths with failure probability of 63.2% under AC waveforms with different frequencies in kV_{rms}/mm, and at DC conditions in kV_{DC}/mm.

The breakdown strength of XLPE samples under DC and AC voltages at which the failure probability equals 10%, including 90% confidence bounds, is presented in Table 4.7, including the relative change in breakdown strength at 10% failure probability under each testing voltage compared to that under AC 50 Hz. The same trend can be observed also at the 10% failure probability. The breakdown strength under DC voltage increases approximately four times compared to that under AC 50 Hz. For AC voltage, the breakdown strength decreases to 40% of the 50 Hz level when frequency goes up to 2500 Hz.

Table 4.7: Breakdown Strength of XLPE Samples II at 10% Failure Probability including 90% Confidence Bounds.

Frequency of testing voltage [Hz]	Breakdown Strength		Confidence bounds 90%	
	10% Failure prob. [kV_{rms}/mm]	*Relative change*	*Lower [kV_{rms}/mm]*	*Upper [kV_{rms}/mm]*
DC	438.4	↑ 406%	413.7	464.6
50	86.63	-	82.73	90.72
300	74.95	↓ 13.5%	69.89	80.37
500	73.02	↓ 15.7%	70.65	75.47
1000	64.48	↓ 25.6%	61.82	67.25
1500	57.36	↓ 33.8%	55.02	59.81
2000	56.87	↓ 34.4%	54.37	59.50
2500	51.96	↓ 40.0%	49.40	54.66

Breakdown Strength of Epoxy Resin Samples

Figure 4.11 and Table 4.8 present the probability of breakdown versus field strength for epoxy resin samples in a 2-parameter Weibull plot with 90% confidence bounds and the corresponding parameter values. Figure 4.12 shows the breakdown strength (η) as a function of frequency in double log plot. Table 4.9 gives the breakdown strength at 10% failure probability including 90% confidence bounds as well as the relative changes in breakdown strength. The dependencies between frequency and breakdown strength of epoxy resin samples are the same for both 63.2% and 10% failure probability as the breakdown strength decreases according to a power law with increasing frequency. For 10% failure probability, a decrease in breakdown strength of approximately 36% is observed at 2500 Hz. DC voltage leads to an almost five-time increase in breakdown strength compared to AC 50 Hz level.

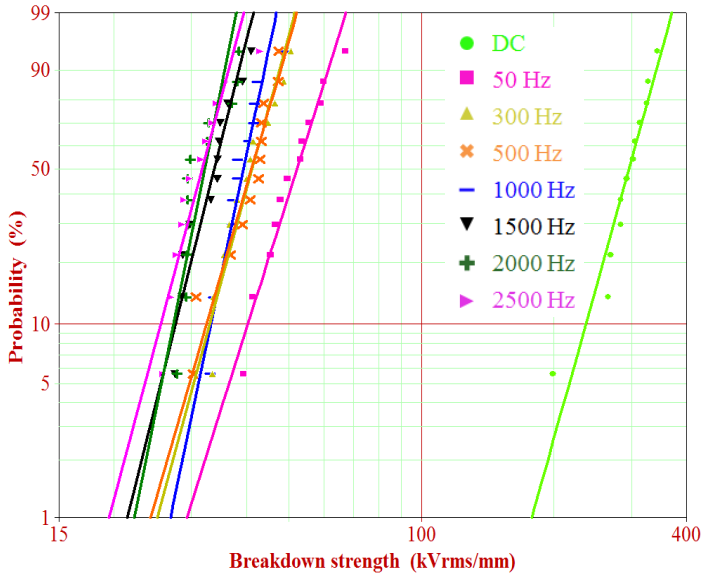

Figure 4.11: Weibull analysis of breakdown strength of epoxy resin samples.

Table 4.8: Distribution parameters of breakdown strength of epoxy resin samples.

Frequency of testing voltage [Hz]	η (with confidence bounds 90%) [kV_{rms}/mm]			β (with confidence bounds 90%) [kV_{rms}/mm]			ρ
	Lower	*η*	*Upper*	*Lower*	*β*	*Upper*	
DC	291	309	328	5.56	8.35	12.5	0.955
50	51.2	54.7	58.6	5.19	7.38	10.5	0.980
300	40.6	43.1	45.7	5.93	8.52	12.2	0.961
500	40.3	43.1	45.8	5.32	8.01	12.1	0.959
1000	38.7	40.8	43.0	8.06	11.0	15.1	0.938
1500	33.3	35.2	37.2	6.48	9.27	13.3	0.958
2000	31.4	33.3	35.2	7.69	11.5	17.1	0.853
2500	30.9	33.2	35.6	6.31	8.67	11.9	0.922

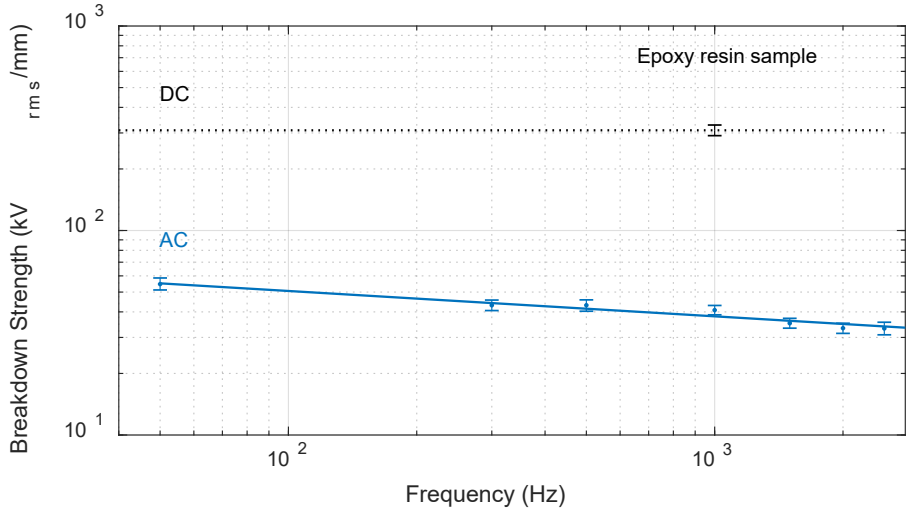

Figure 4.12: Epoxy resin samples: breakdown strengths with failure probability of 63.2% under AC waveforms with different frequencies in kV_{rms}/mm, and at DC conditions in kV_{DC}/mm.

Table 4.9: Breakdown Strength of Epoxy Resin Samples at 10% Failure Probability including 90% Confidence Bounds.

Frequency of testing voltage [Hz]	Breakdown Strength		Confidence bounds 90%	
	10% Failure prob. [kV_{rms}/mm]	*Relative change*	*Lower [kV_{rms}/mm]*	*Upper [kV_{rms}/mm]*
DC	236.1	↑ 485%	208.1	267.9
50	40.33	-	34.73	46.84
300	33.06	↓ 18.0%	28.93	37.79
500	32.51	↓ 19.4%	28.42	37.19
1000	33.26	↓ 17.6%	29.88	37.01
1500	27.63	↓ 31.5%	24.49	31.17
2000	27.32	↓ 32.3%	24.01	31.09
2500	25.57	↓ 36.6%	22.15	29.51

4.4.2 Breakdown under superimposed waveforms

XLPE sample I and epoxy resin samples were tested under superimposed waveforms to investigate the effects on the breakdown. The influence from the amplitude ratio between harmonic and fundamental waveforms as well as the harmonic frequency on the breakdown were studied.

Breakdown Strength of XLPE Samples I

Superimposed waveforms $V_1 \sim V_{12}$ as given in Table 4.3 were applied to the XLPE samples I for testing their breakdown strengths. For each waveform, six samples were tested. When breakdown occurs, the r.m.s. value of the fundamental waveform was chosen as the breakdown voltage, shown as the $V_{fundamental}$ in Figure 4.5. The relative changes in breakdown strength under each waveform compared to the 50 Hz sinusoidal waveform are given in Table 4.10. All the superimposed waveforms lead to lower breakdown strength of XLPE samples I compared to the average breakdown strength of 115.5 kV_{rms}/mm of the 50 Hz sinusoidal waveform. This indicates that, the occurrence of superimposed transients might cause faster change in material properties of XLPE insulation, which leads to a lower breakdown strength of the insulation under these conditions.

Table 4.10: XLPE samples I - Breakdown strengths and their relative changes under superimposed waveforms.

Relative changes in breakdown strength*		Amplitude ratio between harmonic and fundamental waveforms			
		20%	40%	60%	80%
Harmonic frequency (Hz)	500	↓16.6%	↓25.1%	↓48.2%	↓44. 3%
	1000	↓5.30%	↓28.7%	↓43.2%	↓43.9%
	2000	↓16.0%	↓16.4%	↓36.0%	↓41.9%

* The breakdown strengths are calculated from breakdown voltages. The breakdown voltage is the r.m.s. value of the fundamental (50 Hz) sine wave of the superimposed waveform under which the sample breaks down.

The measured breakdown strengths under superimposed waveforms are shown in Figure 4.13 as average values. As soon as the harmonics appear, the samples broke down at a lower fundamental voltage compared to the pure 50 Hz sinusoidal waveform. With the same harmonic frequency, the higher the harmonic amplitude, the lower the fundamental voltage at which samples broke down, which results in lower breakdown strength of XLPE samples. On the other hand, with the same harmonic amplitude, the change in the harmonic frequency doesn't show an obvious influence on the breakdown strength as it does for pure AC sinusoidal waveforms. The above observations are acquired with considering only the average values. However, when the standard deviations are also considered, there are overlaps observed among the result in Figure 4.13. In this sence, the dependency between the harmonic amplitude and the breakdown strength of XLPE samples becomes uncertain.

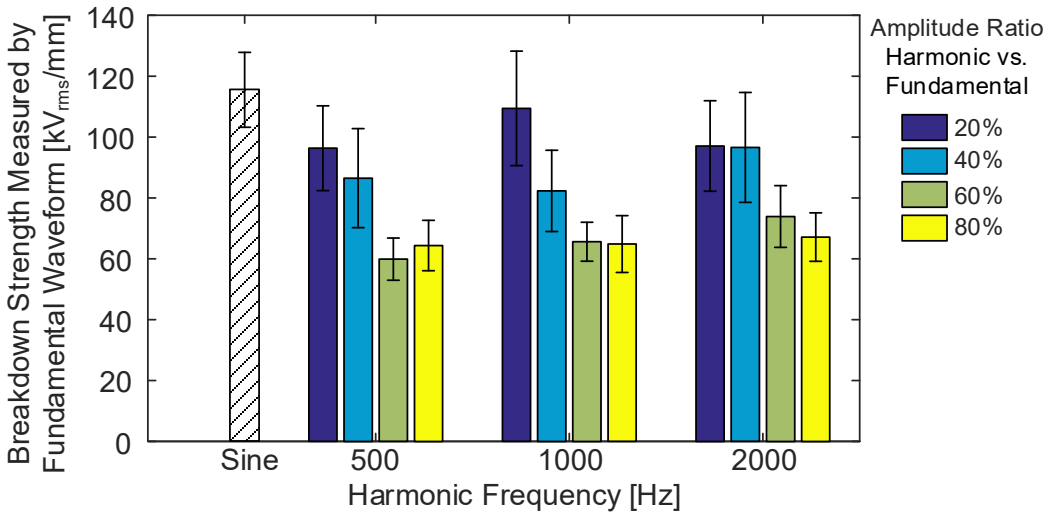

Figure 4.13: XLPE samples I - Average breakdown strengths under superimposed waveforms. The breakdown voltages are the r.m.s. value of the fundamental (50 Hz) sine wave of the superimposed waveforms under which the samples break down.

Breakdown Strength of Epoxy Resin Samples

Superimposed waveforms $V_1 \sim V_{12}$ were applied to the epoxy resin samples for testing their breakdown strengths. For each waveform, six samples were tested. The relative changes in breakdown strength under each waveform compared to the 50 Hz sinusoidal waveform are given in Table 4.11. Similar to the phenomenon with XLPE samples, all the superimposed waveforms lead to lower breakdown strength of epoxy resin samples compared to the breakdown strength of the 50 Hz sinusoidal waveform.

Table 4.11: Epoxy samples - Breakdown strengths and their relative changes under superimposed waveforms.

Relative changes in breakdown strength*		Amplitude ratio between harmonic and fundamental waveforms			
		20%	40%	60%	80%
Harmonic frequency (Hz)	500	↓26.7%	↓36.6%	↓44.0%	↓49.9%
	1000	↓23.5%	↓35.8%	↓38.3%	↓42.5%
	2000	↓29.1%	↓28.3%	↓32.1%	↓38.4%

* The breakdown strengths are calculated from breakdown voltages. The breakdown voltage is the r.m.s. value of the fundamental (50 Hz) sine wave of the superimposed waveform under which the sample breaks down..

The measured breakdown strengths under superimposed waveforms are shown in Figure 4.14 as average values. Similar trends are observed from epoxy sample as to XLPE sample I. Samples broke down at a lower fundamental voltage compared to the 50 Hz AC voltage when harmonics appear. From the perspective of only the average values without considering their standard deviations, at the same harmonic frequency, the higher the harmonic amplitude, the lower the fundamental voltage at which samples broke down, in other words, the lower breakdown strength that epoxy resin samples have. With the same harmonic amplitude, the change in the harmonic frequency doesn't have clear effects on the breakdown strength as the change in AC voltage.

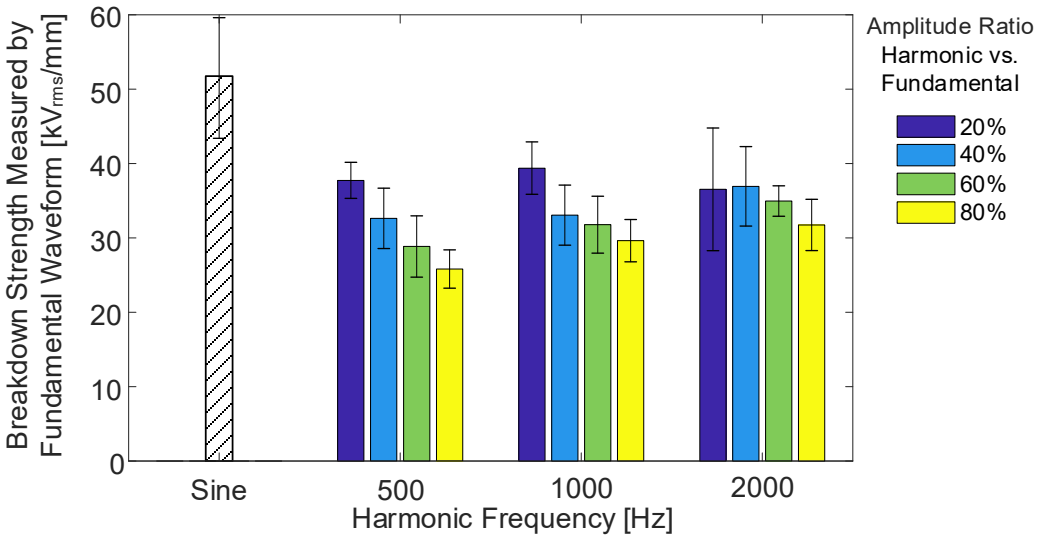

Figure 4.14: Epoxy samples - Average breakdown strengths under superimposed waveforms. The breakdown voltages are the r.m.s. value of the fundamental (50 Hz) sine wave of the superimposed waveforms under which the samples break down.

4.5 Discussions

4.5.1 AC sinusoidal waveforms with different frequencies

On behalf of the discussion, we present the *tanδ*, PD inception voltages (PDIV) and the breakdown voltages V_{BD} of all the three materials measured at 50 Hz in Table 4.12, and the dissipation factor *tanδ* measured along with frequency in Figure 4.15. The *tanδ* values have been averaged over four samples, measured at low voltage only (3 V).

Table 4.12: Measured characteristics, PDIV and breakdown voltage of material samples.

Samples	Thickness [mm]	Frequency [Hz]	C [pF]	tanδ	PDIV [kV_{rms}]	V_{BD} [kV_{rms}]
XLPE I	~ 0.1	50	47.4	1.59 x10^{-4}	8.5	15.6
XLPE II	~ 0.2	50	31.9	1.47 x10^{-4}	9.6	18.5
Epoxy resin	0.3-0.5	56	69.0	45.5 x10^{-4}	7.5	19.1

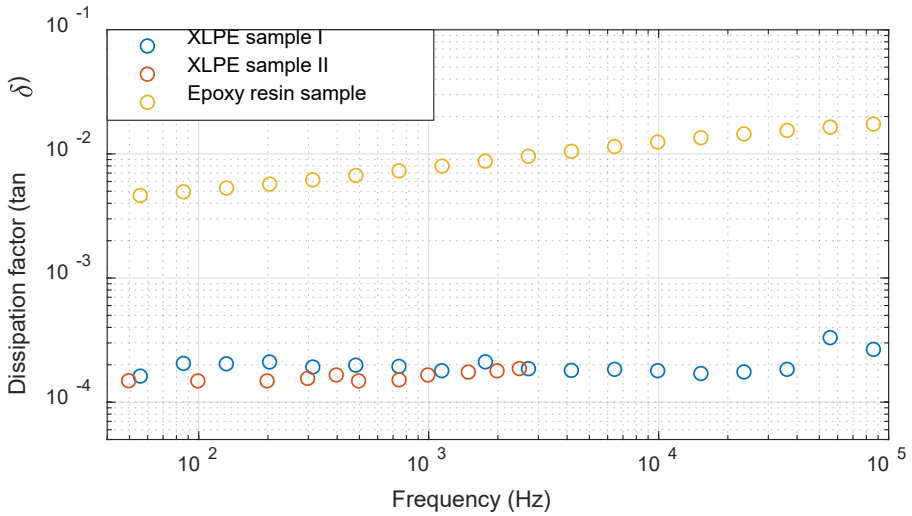

Figure 4.15: Relation between dielectric properties and frequency of material samples.

Consider the dielectric power losses with 50 Hz firstly. Recalling the formula given in equation (3.1), the dielectric power losses are the product of frequency, capacitance, *tanδ* and the square of the applied voltage U^2. As shown in Figure 3.2b (section 3.1), at low frequencies *tanδ* is low, as caused by dipole losses. When below inception voltage, no discharge losses occur due to partial discharges, and *tanδ* is almost independent of *U* (Figure 3.2c), so the dielectric power losses only increase monotonically with the square of the applied voltages. When the applied voltage reaches the PD inception voltage, partial discharges take place in the samples, which add discharge losses to *tanδ* tip-up with further increase of the voltage. Consequently, the increase of dielectric power losses are enhanced by both increasing applied voltage and increasing *tanδ*. At a certain value (V_{BD} in Table 4.12), breakdown will occur in the materials.

Considering the influence of frequency in Figure 4.15, the *tanδ* of XLPE sample I and XLPE sample II increase subtly while *tanδ* of epoxy resin samples increase faster with frequency. Apart from the U^2 and frequency factors, the increase of dielectric power losses with frequency is accelerated by increasing *tanδ* before partial discharge taking place, while *tanδ* tip-up accelerates the power losses even more after partial discharge inception. Moreover, in case of higher frequency where the voltage changes faster, more partial discharges with larger magnitude can occur, which leads to damage to the insulation material. As a result, breakdown may occur at a lower voltage. The effect of transient voltages on partial discharge behaviour will be discussed more in Chapter 5 and Chapter 7.

4.5.2 Superimposed waveforms

For superimposed waveforms, the frequency of harmonics doesn't show significant effects on the breakdown by itself. In reality, the harmonic frequency and amplitude influence the breakdown in combination, whereby amplitude dominates the scene. From the perspective of dipole losses, in the case of small harmonic amplitude, although harmonics have higher frequency compared to 50 Hz sinusoidal waveform, the resulting superimposed waveform doesn't have more zero-crossings during one 50 Hz cycle. Thus, the occurrence of dipole losses doesn't increase too much. In the case of larger harmonic amplitude, the resulting superimposed waveform reverse its polarity for more times during one 50 Hz cycle. Consequently, the dipoles reorient more frequently. However, it is unclear if the increase in dipole reorientation will lead to the increase in dielectric power losses, since the dipoles behaviour and the change in *tanδ* are unknown when subjected to superimposed waveforms. Therefore, to essentially explain the results under superimposed waveforms, it needs to be figured out how do the superimposed waveforms influence the dipole reorientation and *tanδ*.

4.6 Conclusions

The breakdown strength of XLPE and epoxy resin insulation samples were investigated under DC, AC with different frequencies and superimposed voltages are investigated. The samples were tested under different waveforms, which can either represent the transient high frequency components separately or reflect the specific composition of the transients on waves in practice, which can be seen from Figure 2.4a as the oscillation right after the 1.7 p.u. overvoltage. The main results are:

- The breakdown strength of all the material samples under DC voltage are more than three times higher than that under 50 Hz AC.
- Frequency of AC voltage has an effect on the breakdown strength of both XLPE and epoxy resin insulation. The higher the frequency, the lower the breakdown strength. This might be caused by the increasing dielectric power losses with the increasing frequency.

Under superimposed waveforms, the frequency of harmonics doesn't have significant effects on the breakdown of both XLPE and epoxy resin samples by itself. The harmonic frequency and amplitude influence the breakdown in combination overruled by amplitude. With larger harmonic amplitude, insulation samples break down at lower voltage.

During the breakdown under AC with high frequencies and superimposed voltage waveforms in material samples, partial discharge may also play a role. Thus, it would be interesting to know the effects of transient waveforms on partial discharges in material samples, which however, has already been studied by Densley in [24]. Since it is more critical if partial discharges are initiated by transients in real cables and accessories, we decided to investigate partial discharges in MV and HV cable models under transients instead of in material samples based on the knowledge collected in this chapter and provided by Densley. These investigations will be presented in chapter 5 to chapter 7.

Chapter 5

Partial Discharge in MV Cable Models under Transients

Superimposed transients may have impacts on the power cable insulation system. As shown in chapter 4 the high frequency voltage decreases the breakdown strength of insulation material. The breakdown is usually preceded by a degradation process, which may also escalate from so-called hidden defects. For MV cable systems hidden defects, which may remain unnoticed in commissioning or maintenance tests, occur mainly in the cable accessories. Therefore, we create a physical cable model of a cable section with two terminations and one joint with a "hidden" defect in the joint. As the physics of such defect depends on local fields rather than voltage class, we first learn about the PD behaviour of defects in MV cable models in this chapter, and deal with HV cable models in chapter 6 and 7. Moreover, for investigating partial discharge behaviour under transients in laboratory conditions, MV cable is a more suitable test object due to its easy installation and manipulation. This chapter investigates the partial discharge in MV cable under superimposed impulse transients. 6/10 kV cross-linked polyethylene (XLPE) MV cable samples with accessories are used as test objects, further called cable models in this thesis. A test circuit is designed and build up in the HV lab, which enables to supply the impulse transients and to measure partial discharges during the transients. The effect of transients on partial discharge is investigated based on laboratory experiments.

5.1 MV Cable and Accessories with Insulation Defects

5.1.1 MV cable and accessories

A 6/10 kV XLPE commercial cable was chosen to produce the cable samples for the test object (Figure 5.1a). Table 5.1 specifies the main data of the MV cable. Three cable samples were cut from the commercial cable with identical length of 4 meters. Each cable was then equipped with two outdoor

This chapter is based on:
J. Wu, A. Rodrigo Mor, J. J. Smit, "The effects of superimposed impulse transients on partial discharge in XLPE cable joint", International Journal of Electrical Power & Energy Systems, vol. 110, Sept. 2019, pp. 497-509.
J. Wu, L. C. Castro Heredia, A. Rodrigo Mor, J. J. Smit, "Partial Discharges at Artificial Defects in XLPE Cable Accessories under Superimposed Transients". In 2018 IEEE International Conference on High Voltage Engineering and Application (ICHVE), Athens, Greece, Sept. 2018.

cold shrink terminations (Figure 5.1b) at two ends. Two cable samples were further installed with cold shrink inline splices (Figure 5.1c) in the middle. Figure 5.1d shows a so-called cable model, which consists of the cable sample with the splice and two terminations. With the operating capacitance of 0.45 µF/km (Table 5.1), the total capacitance of each cable sample is 1.8 nF. Before introducing any artificial defects, all three cable models were tested and confirmed to be PD free (< 5 pC) up to $3U_0$, namely 18 kV_{rms}.

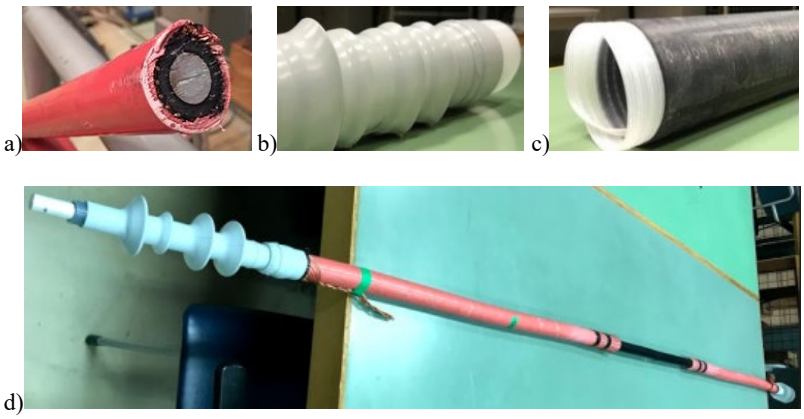

Table 5.1: MV cable data.

Conductor diameter	18 mm
Insulation	
Nominal thickness	3.4 mm
Diameter	25 mm
Earth screen (25 mm^2)	
Nominal thickness	1.2 mm
Diameter	29 mm
Outer sheath	
Nominal thickness	2.5 mm
Diameter	35 mm
Weight per meter	1.5 kg
Capacitance	0.45 µF/km

Figure 5.1: XLPE MV cable and accessories: a) 6/10 kV XLPE cable, b) outdoor cold shrink termination, c) cold shrink inline splices, d) assembled cable model with the splice and two terminations.

5.1.2 Artificial insulation defects

Artificial insulation defects were introduced into the two cable models in order to generate partial discharges. Table 5.2 gives the artificial defects made in each cable model, as well as the partial discharge produced by each defect.

Table 5.2: Cable models with defect types.

Cable model	Defects	PD
0	No defects	No PD
1	Semi-conductive remainder on XLPE surface	No PD
	Inserted metal wire which is grounded	PD Type I
2	Inserted plastic strip	PD Type II

Cable model 0

Cable model 0 is the one without cable splice and defect. This cable model is used to provide reference information.

Cable model 1

In cable model 1, a small part of the semi-conductive layer was left during peeling (Figure 5.2a), which is a typical defect that can occur in practice when installing cable joints in the field. However, this defect didn't cause PDs in cable model 1 on short term. Therefore, to simulate the defect experimentally, a thin metal wire with a diameter of 2 mm was inserted into the cable joint 65 mm along the interface between the cable and the joint insulation (Figure 5.2a). Figure 5.2b illustrates the dimension and location of the defects. In this way, a small void is left most probably at the tip of the wire at the interface.

By applying AC voltage, PDs called type I were detected due to artificial defects in cable model 1. The PRPD pattern of the detected PDs (Figure 5.3) at AC of 17 kV_{pk} is seen as internal discharges, which is

in accordance with a phase-resolved pattern of internal discharges in square cavity, given by Gulski in [109].

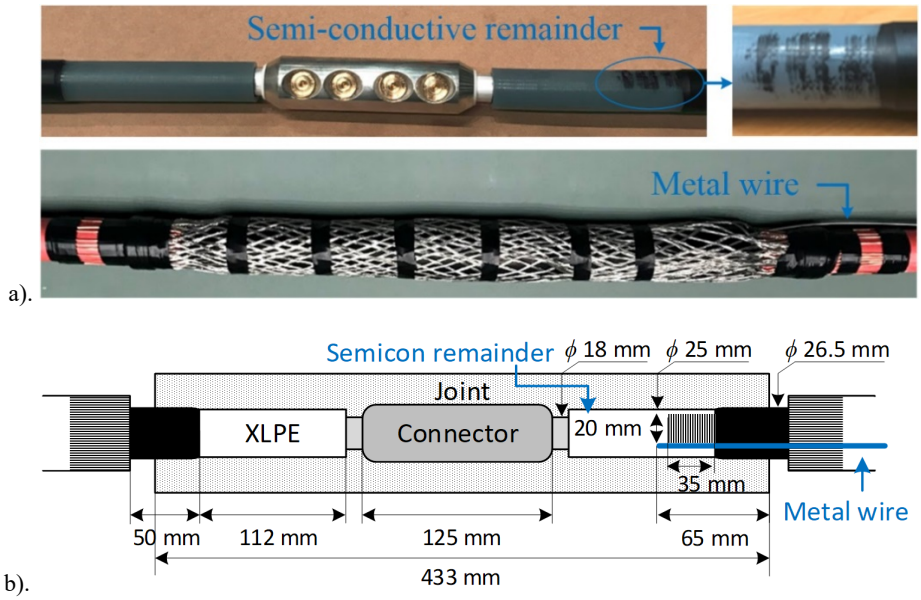

Figure 5.2: Defects in cable model 1: a) defects of semi-conductive remainder and inserted metal wire, b) Dimension and location of defects.

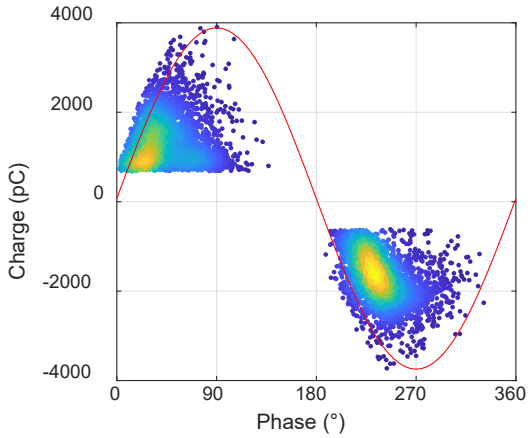

Figure 5.3: Characteristics of PD type I in cable model 1: PRPD pattern at 17 kV_{pk}

Cable model 2

In cable model 2, a plastic tie-wrap strip was put at the interface between the cable insulation and the cable splice's inner semi-conductive layer with its gear racks down to the cable insulation. Then the splice was installed (Figure 5.4a). The dimension and location of the defect is illustrated in Figure 5.4b. In this way, cavities are created by the gear racks at the XLPE surface, i.e. along the interface.

PD type II was detected in cable model 2 under AC voltage. With increasing AC voltage on the cable model, discharges firstly initiated at the negative cycle with inception voltage of 8.6 kV_{pk}. Figure 5.5a shows the PRPD pattern measured at 9.2 kV_{pk}. By further increasing the voltage, discharges started to initiate at the positive cycle with inception voltage of 14.5 kV_{pk}. Figure 5.5b shows the PRPD pattern measured at 17 kV_{pk}. PD type II behaves like the surface discharges described by Gulski [109], which is characterized by a significant difference between the positive half and the negative half of the voltage cycle [110].

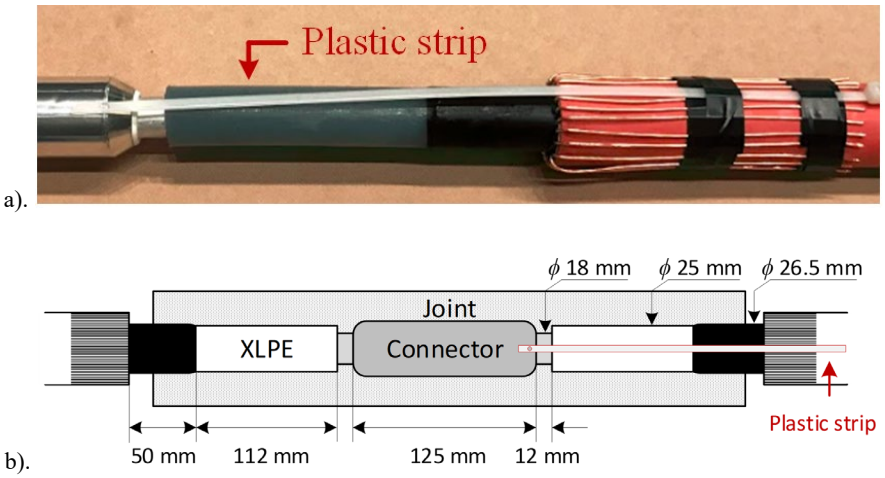

Figure 5.4: Defect in cable model 2: a) Inserted plastic tie-wrap strip until the edge of the connector, b) Dimension and location of defects.

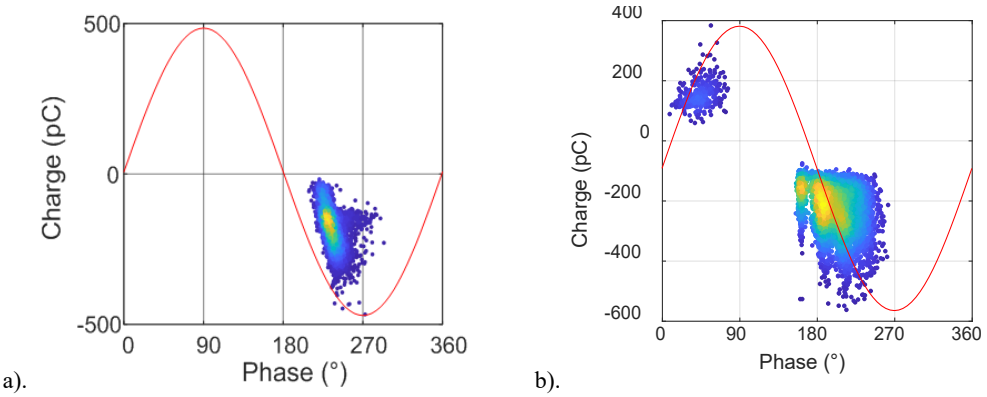

Figure 5.5: Characteristics of PD type II in cable model 2: a) PRPD pattern at 9.2 kV_{pk}, b) PRPD pattern at 17 kV_{pk}.

5.2 Experimental Set-up

An experimental circuit was designed to generate and apply superimposed transients on the cable models, and to measure partial discharges in the cable models if these occur. The circuit consists of three parts: the generation of superimposed transients, the PD measuring system (will be discussed in section 5.3), and the test objects (the cable models as discussed in section 5.1). Figure 5.6 shows the schematic diagram of the experimental circuit. Figure 5.7 gives the physical set-up build in the HV lab.

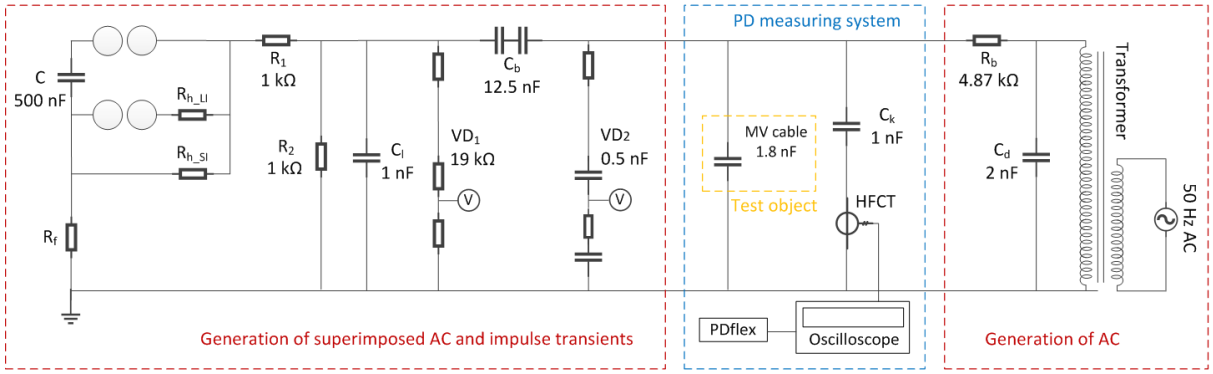

Figure 5.6: Schematic diagram of test circuit.

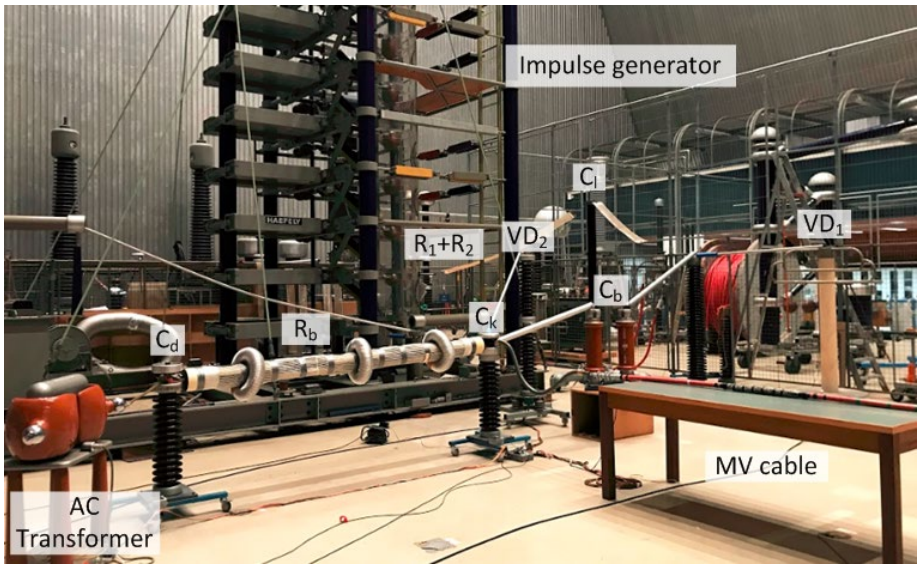

Figure 5.7: Physical experimental set-up

5.2.1 Generation of superimposed transient voltages

The transient voltage to be applied on the cable models was designed as a superimposed voltage of a 50 Hz AC voltage with an impulse voltage riding on top of it. To generate such voltage waveform, an AC supply and an impulse generator were combined as the voltage source. Some other elements were added in the circuit to protect the equipment.

High-voltage AC supply

To supply the cable models at their operating voltage level, a trefoil testing transformer was used with single phase of 50 kV output. The transformer was supplied by an AC voltage source via a variac. The HV AC supply has been tested as PD-free (< 5 pC) up to 30 kV.

Marx impulse generator

To generate impulse voltages, a 20-stage Haefely Marx impulse generator was used. Each stage has a maximum output of 200 kV and minimum output of 20 kV. For testing the 6/10 kV cable models, one stage of the impulse generator was used. Even so, the minimum 20 kV voltage is still too high for stressing the cable models, especially when it is superimposed on the AC voltage. Therefore, a resistive voltage divider with R_1=R_2=1 kΩ was placed after the impulse generator to further decrease the output voltage to half value. Both R_1 and R_2 are band resistors of woven mat type with taps.

The discharge capacitance C of one stage is 500 nF. Different impulse waveforms, i.e. different front time T_f and time to half value T_h, can be generated by adjusting the front resistor R_f and the tail resistors R_{h_LI} and R_{h_SI}. At the same time, T_f and T_h are also related to the total load capacitance C_{load}. For testing under superimposed voltages, the total load capacitance C_{load} is the combination of the MV cable, the voltage divider VD_2, the blocking capacitor C_b, the coupling capacitor C_k and the filtering capacitor C_d. In order to reach a longer front time without using a too large R_f, an additional 1 nF capacitance C_l was connected.

The desired impulse voltage was superimposed at determined phase angles of AC voltage by specifying the trigger angle in the impulse control system. The generated impulses are measured and recorded by the impulse measuring system. In this set-up, two high voltage dividers are used to measure high voltage, shown as VD_1 and VD_2 in Figure 5.6. VD_1 serves to measure the generated impulse voltages at the terminal of impulse generator, and VD_2 is used to measure the superimposed voltages at the terminal of the test object.

Blocking capacitor C_b

For generating superimposed voltages, the AC transformer and the impulse generator were both connected to the test object. In order not to stress the impulse generator with the AC voltage, a 12.5 nF blocking capacitor C_b was installed between the AC supply and the impulse supply. This attenuates the AC voltage at the impulse generator and allows the impulse voltage to be superimposed on AC voltage at the cable.

Low-pass filter: C_d and R_d

If the generated impulse reaches the test transformer, the high frequency component of the impulse may cause the overloading of the transformer winding, which will damage the test transformer. To protect the AC transformer against the impulse voltage, a low-pass filter (C_d = 2 nF, R_d = 4.8 kΩ) was designed and placed after the AC supply in order to filter the high components.

5.2.2 Test waveforms

In order to reflect the real transient situation, the field-measured transient presented in section 2.1.1 and Figure 2.4 was considered to be the test waveform at the beginning. However, due to the technical limitations in the HV lab, it is difficult to generate the same transient waveform as shown in Figure 2.4a, having an overvoltage and followed by high frequency oscillations. As an alternative, with the set-up presented in section 5.2.1, it is possible to generate a transient waveform which has an impulse being superimposed on the AC voltage, representing the overvoltage of the real transient, but without the following oscillations. Such superimposed transient waveform is simplified but still similar to and representative of the real transient, which is then used as the test waveform for the MV cable tests.

One example of the generated test voltage is shown in Figure 5.8, including the positive impulse voltage measured by VD_1 and the superimposed voltage on the test object measured by VD_2. The generated impulse is characterized by its peak value V_{peak} of 16 kV, front time T_f of 2.8 µs and time to half value T_h of 526 µs (Figure 5.8a). The superimposed voltage (Figure 5.8b) has the positive impulse riding on the AC crest, resulting in a total peak value V_{peak} of 24 kV. Several studies have established that naturally occurring transient voltages do not always resemble the lightning or switching impulse wave shape [111]. The time period of the transient condition lasts for around 3.2 ms.

In the MV cable models tests, the voltage waveform of the impulse with the front time of 2.8 µs and the time to half value of 526 µs being superimposed on the AC crest were determined as the test voltage waveform, as given in Figure 5.8a. Only the total peak value V_{peak} of the test waveform varied by changing the impulse peak value.

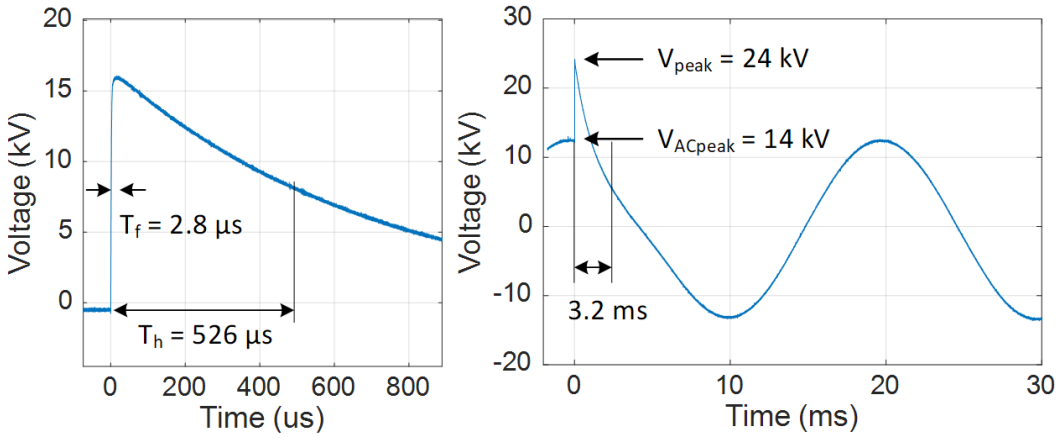

Figure 5.8: The test voltage waveform: a) generated impulse voltage, b) test voltage at the test object.

5.3 PD Measuring System

During the application of impulses, disturbances such as electromagnetic interferences and noise are also produced. The disturbance signals contain high frequency components, which are close to that of PD signals. In order to safely measure PD signals during the application of impulses in such a disturbing environment, the unconventional PD measurement method with bandwidth laying on hundreds of MHz was applied over the conventional method according to the international standards IEC 60270 [72] and IEC 60885-3 [112]. The PD measuring system build up thereby is able to measure and record signals, analyse signals and distinguish PD signals from disturbance signals.

PD signals measuring circuit

A coupling capacitor C_k of 1 nF (Figure 5.9a) is connected in parallel with the test object (see the circuit in Figure 5.6) to provide the closed circuit for the discharge displacement. The coupling capacitor is rated for 40 kV and tested to be PD free up to 30 kV.

By applying the unconventional PD measurement method, a high frequency current transformer (HFCT) with a bandwidth of 35 kHz – 60 MHz is connected in series with the coupling capacitor to sense the PD currents. The HFCT consists of five turns of flat copper strips that wound on a ferrite-core. Such HFCT has an ultra-wide bandwidth that enables the acquisition of very fast PD current pulses without heavy transient oscillation. The measured current signal is transferred to voltage signal with a gain of 9.1 mV/mA. All these above are integrated in a shielded box, as shown in Figure 5.9b.

To locate the phase angles of the measured signals, a synchronized unit was used. It generates a 50 Hz ramp voltage synchronized with the AC voltage, and records the phase angle when triggered by the PD signal.

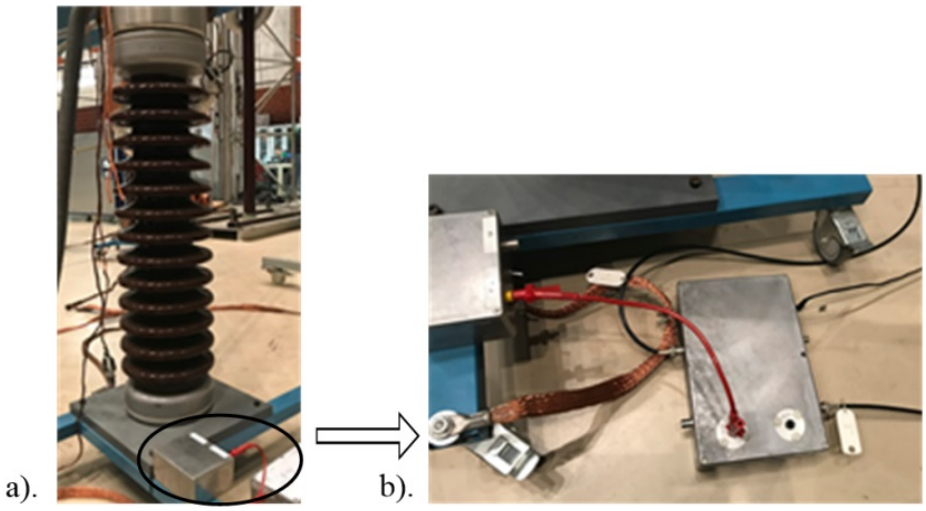

Figure 5.9: PD measuring devices: a) coupling capacitor C_k, b) HFCT sensor.

PD signals acquisition

The signals captured by the HFCT were sent to a digital oscilloscope Tektronix DPO7354C via a coaxial cable. With 8-bit vertical resolution and a 2.5 GS/s sampling frequency, this high-performance oscilloscope was able to accurately record the very fast PD pulses. The fast frame acquisition mode of the oscilloscope was used so that every triggered signal was acquired as a single frame with full information of its time-resolved pulse shape, occurrence timestamp and phase angle. The background noise can be filtered out by setting a proper trigger level during measurements. In the MV cable test, the trigger level was set as 2 mV.

PD data analysis

PDflex [113], software developed by the High Voltage Laboratory of Delft University of Technology, was used to analyse and present the PD measurement results. It is possible to present the data in time-resolved PD pulses (TRPD), phase-resolved PD pattern (PRPD) and typical PD parameters [83, 114-115]. Moreover, several clustering techniques are included for PD recognition.

PD measurement sensitivity

The sensitivity of the PD measuring system was checked by injecting standard calibration pulses. The smallest pulse that can be distinguished from noise is 20 pC. The signal of the injected 20 pC calibration pulse was measured by the HFCT sensor and is shown in Figure 5.10, with a voltage amplitude of 0.9 mV.

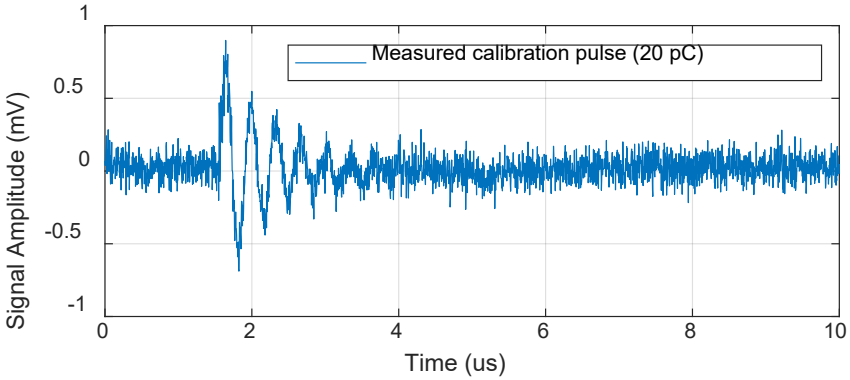

Figure 5.10: The smallest calibration pulse of 20 pC measured by HFCT sensor.

5.4 Verification of the Experimental Set-up

The experimental set-up was examined to see whether it could work properly during the impulses and whether its function could meet the requirements of PD measurements. For this purpose, the following questions had to be answered:

- Is the experimental set-up able to withstand the impulses and the PD measuring system able to keep measuring and acquiring signals during the impulse application?
- If partial discharges occur during the impulses, is it possible to distinguish the PD signals from the disturbance signals?

Moreover, some important information has to be collected as reference for later tests:

- Partial discharge behaviour from the cable model
- Disturbance or noise signals characteristics
- How to set up the acquisition appropriately in order to measure partial discharges from the cable model.

5.4.1 Measurement of disturbances

The experimental set-up was subjected to impulses in order to examine whether it could work safely during the impulse application and how do the disturbance signals look like. The set-up was tested with the PD-free cable model 0 as the test object under pure impulses and superimposed voltages. Table 5.3 gives the test voltage values for each test.

Table 5.3: Tests of disturbance under pure impulses and superimposed voltages with PD-free cable model 0.

Cable model	PD condition	Tests	Testing voltages of impulse transients		
			AC [kV_{pk}]	V_{peak} [kV_{pk}]	Amount of impulses
0	PD free up to $3U_0$	Only impulses	-	11.3	13
		Superimposed voltage	9.2	17.3	4

Disturbances under pure impulses

13 impulses were successively applied on the experimental set-up with cable model 0 as the test object, which was tested as PD free up to $3U_0$. The time interval between each two impulses is 35 seconds. The measurement results are shown in Figure 5.11.

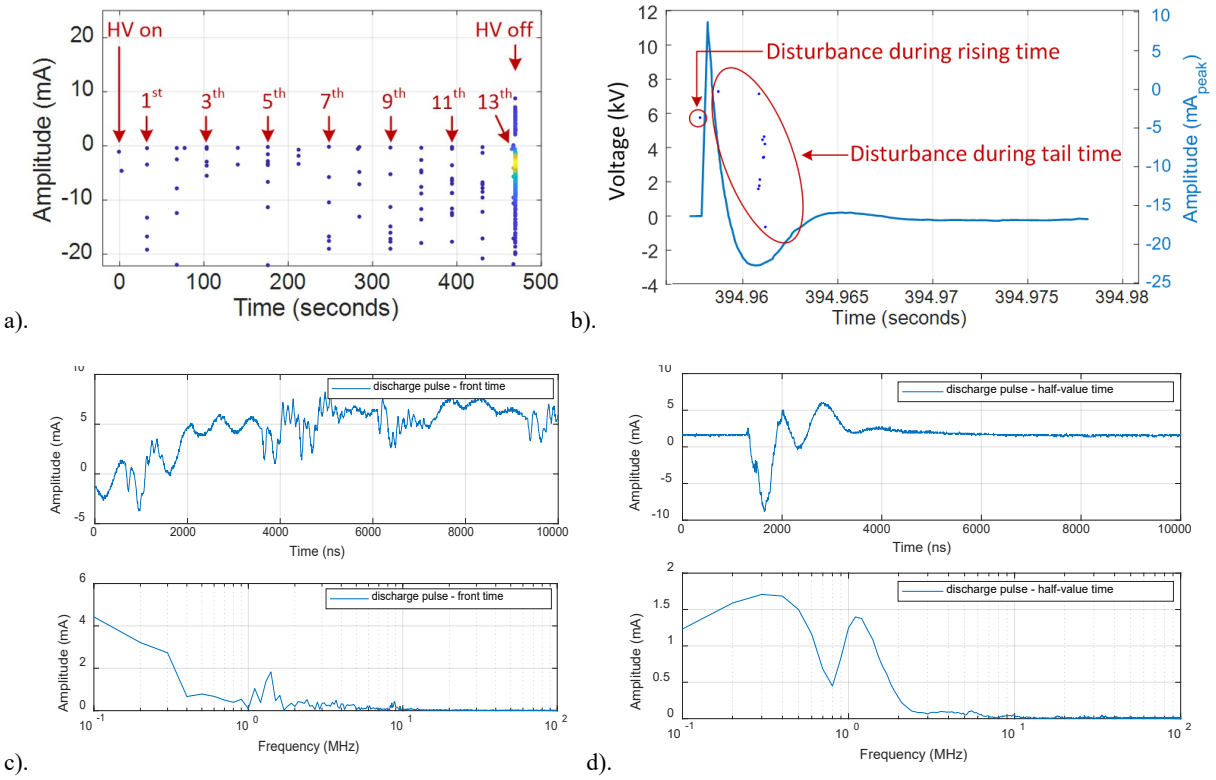

Figure 5.11: Measurement result under impulses with cable model 0 as test object: a) signals measured over time, b) signals measured during the 10th impulse moment c) pulse shape and frequency spectrum of disturbance at front time, b) pulse shape and frequency spectrum of disturbance at tail time.

The signals measured by the PD measuring system during the application of the 13 impulses are presented in Figure 5.11a. It shows the moment of each impulse application as well as the moments when the impulse generator was switched on and off. The impulse generator was switched on at time of zero and switched off immediately after the 13th impulse. Every time an impulse was applied, a few disturbance signals were produced. Those disturbances occurred in such a short time that they are seen as occurring simultaneously in the time scale in Figure 5.11a. Around 35 seconds interval is observed between each two impulses.

The signals produced by the 10th impulse are illustrated in Figure 5.11b. There are two types of pulse shape observed: the ones that occurred during the impulse rising time, having pulse shapes shown in Figure 5.11c with the dominant frequency fastened on the low frequency range. The other ones that occurred during the tail time, having pulse shapes shown in Figure 5.11d, with negative peak and a dominant frequency of 300 kHz. The whole discharge process in Figure 5.11b lasted for around 3.4 ms.

This duration nearly equals to the duration of the generated impulse as 3.2 ms, as shown in Figure 5.8b. This helps to confirm that the measured signals are disturbances produced during the impulse application.

The experimental set-up was examined to be functioning during the impulse application. The information of disturbance caused by the impulses has been collected regarding the disturbance distribution in large time scale (in the magnitude order of second), as well as the disturbance pulse shape in small time scale (in the magnitude order of microsecond) with its dominant frequency.

Disturbances under superimposed voltage

Superimposed voltage with four successive impulses were applied on the experimental set-up with cable model 0. The time interval between each two impulses is still 35 seconds. Similar measurement result was observed, given in Figure 5.12a. Apart from the disturbance pulses shown in Figure 5.11c and Figure 5.11d, another pulse shape appears during the transient voltage, as shown in Figure 5.12b. the pulse shape and corresponding frequency spectrum are given in Figure 5.12c.

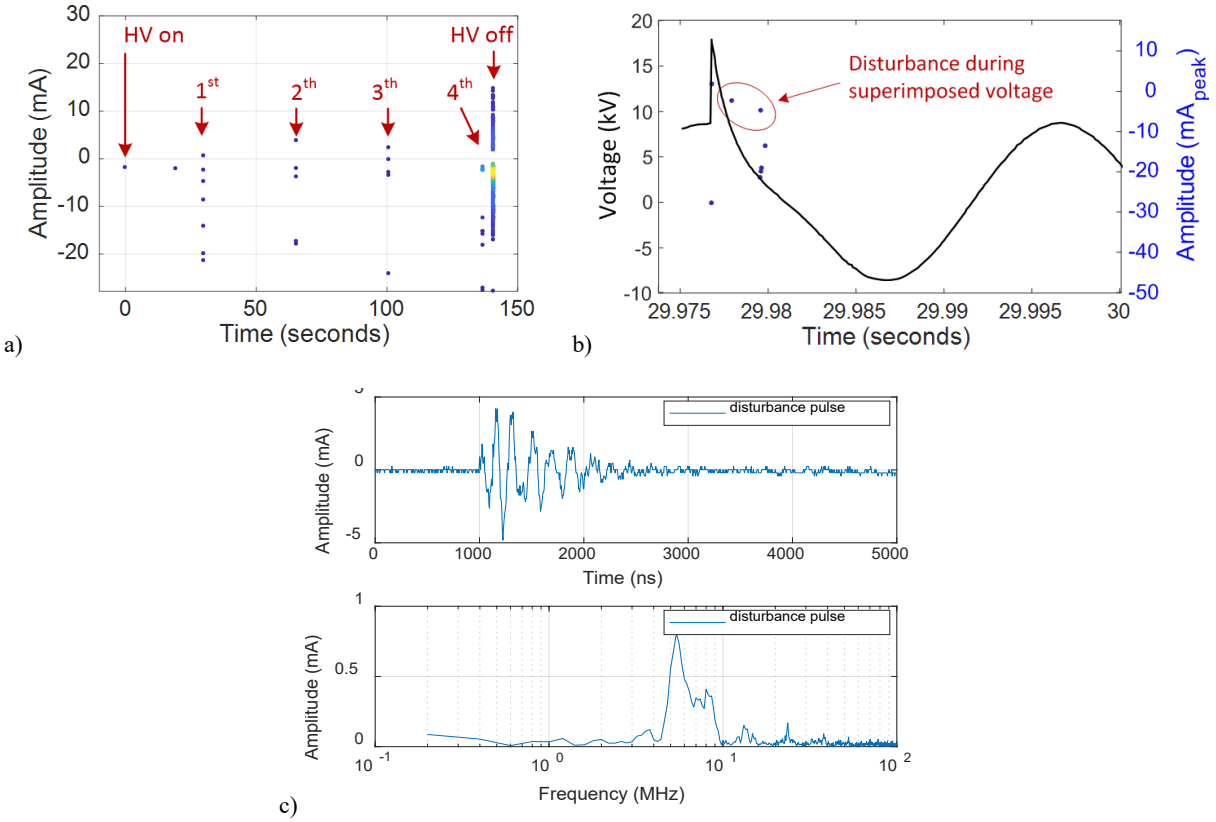

Figure 5.12: Measurement result under superimposed voltage with cable model 0 as test object: a) disturbance measured over time, b) signals measured during the 1st impulse moment, c) disturbance pulse shape.

The measurement result of disturbance shows that:

- The experimental set-up is able to withstand the impulses and the PD measuring system is able to keep measuring and acquiring signals during the impulse application.
- Disturbance signals may occur during the impulse application. The information has been recorded and analysed, which can serve as reference for tests of PD under impulse in the following.

5.4.2 Measurement of PD under pure AC

The partial discharges produced by the artificial defects in cable model 1 and 2, type I and type II, have been presented in section 5.1.2. The two cable models were connected into the experimental set-up and tested under AC voltage again. Hereby we could examine the performance of the PD measuring system, and also recognize and collect more information about the PD characteristics in the cable models.

A pure AC voltage was applied on the cable model 1 and increased gradually, until fast pulses were initiated sustainably. Figure 5.13 presents the measurement result of PD at 9 kV_{rms} in cable model 1. The PRPD pattern (Figure 5.13a), similar to Figure 5.3, reveals the PD in cable model 1 to be internal discharges. Two PD events PD1 and PD2 are presented in Figure 5.13b with their time-resolved pulse shapes. The two PDs have different polarities and amplitudes but similar pulse shapes. PD1, occurring at positive half cycle, has positive polarity while PD2 has negative polarity which occurred at negative half cycle. With similar pulse shapes, PD1 and PD2 have similar frequency spectra with dominant frequency of 900 kHz (Figure 5.13c), which are different from the frequency spectra of disturbance (Figure 5.11 and Figure 5.12). Thus, this dominant frequency was found as a helpful parameter to distinguish PD signals from other disturbance or noise signals. In Figure 5.13d, the measured PDs are clustered by their peak current values and dominant frequencies. All the measured PD signals have the dominant frequency in the range of 800-1000 kHz. The majority of PD signals drop into 900 kHz, while minor PD signals have 800 or 1000 kHz.

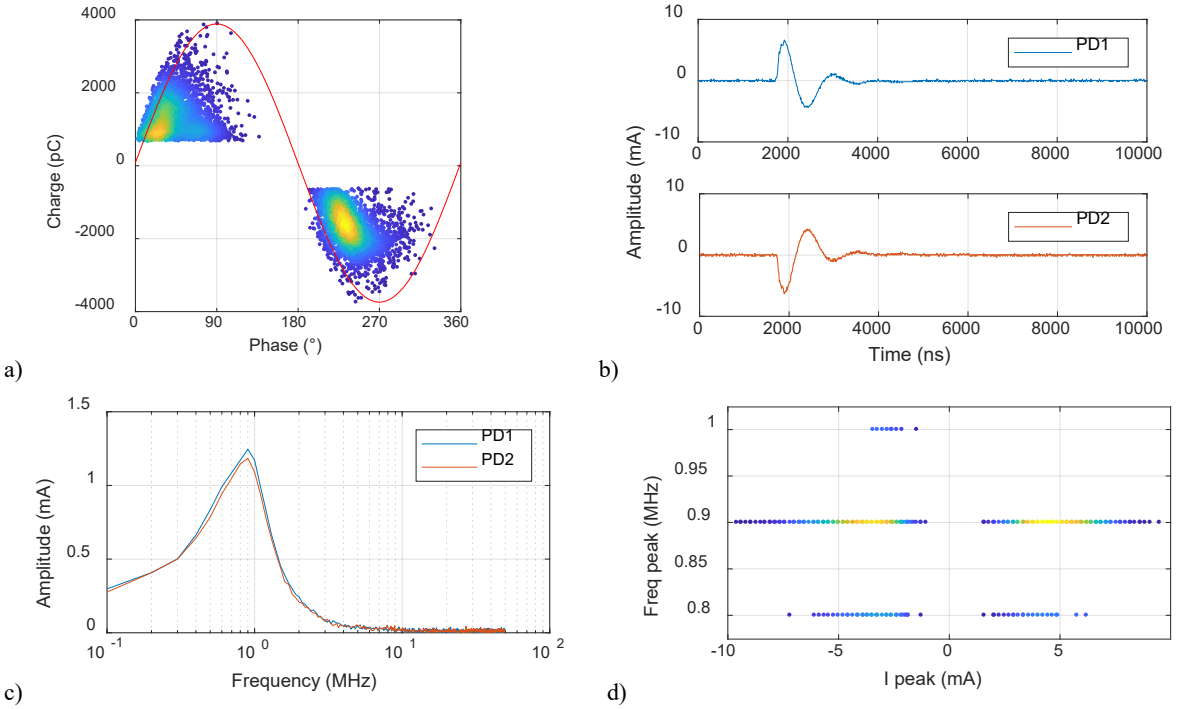

Figure 5.13: PD in cable model 1: a) PRPD pattern at 9 kV, b) TRPD shapes of PD1 and PD2, c) frequency spectra of PD1 and PD2, d) dominant frequencies of all measured PDs.

PD type II in cable model 2 was measured again in order to collect the TRPD shapes and frequency information. With lower voltage of 9.2 kV_{pk}, the TRPD pulse of PD1 in Figure 5.14a is given in Figure 5.14b, with its dominant frequency of 1 MHz. With higher voltage of 17 kV_{pk}, the TRPD pulse shape of PD1 and PD2 in Figure 5.14c are given in Figure 5.14d, with their dominant frequencies around 800 kHz.

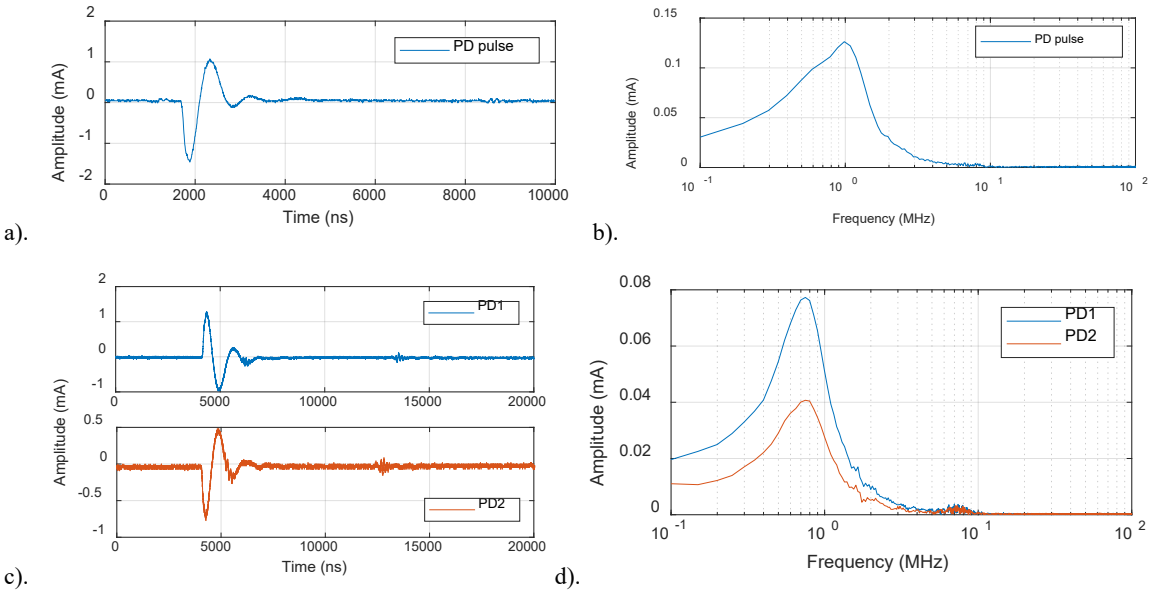

Figure 5.14: Characteristics of PD type II in cable model 2: a) TRPD pulse shape at 9.2 kV_{pk}, b) dominant frequency at 9.2 kV_{pk}, c) TRPD pulse shapes at 17 kV_{pk}, d) dominant frequency at 17 kV_{pk}.

The measurement result of PD under pure AC voltage shows that:

- Both cable model 1 and 2 produce sustained partial discharges, PD type I and II, with steady PRPD patterns under AC voltage higher than PDIV. Both PD type I and II have similar TRPD pulse shapes with lengths in the order of microsecond and dominant frequencies in the range of 800-1000 kHz. This information will be used to study the PD under transients later.
- The PD measuring system is able to measure the partial discharges from the cable model with enough time resolution. The time-resolved pulse shape and the dominant frequency helps to distinguish the PD signals from disturbance signals, which are important for the PD measurement under transients.
- The used window with 10 µs is appropriate to capture complete PD pulses from the cable model. Signals which deviate significantly from the TRPD pulse shapes as shown in Figure 5.13 and Figure 5.14 are not considered to be the partial discharges from the cable model, regardless their pulse shapes or PRPD patterns. This setting will be applied to the rest tests.

5.4.3 Measurement of PD under superimposed transients

The test voltage waveform of a superimposed transient voltage was applied on cable model 1. The AC voltage level of the testing voltage was determined as 6.8 kV_{rms}, which is lower than the PDIV of 8.6 kV_{rms}. of cable model 1. The AC voltage was firstly applied on the cable model. Then 11 impulses were applied successively. The time interval between each two impulses was 35 seconds, during which the AC voltage was kept on the cable model. The peak value of the superimposed voltage reached 13 kV. Figure 5.15 gives the measurement results.

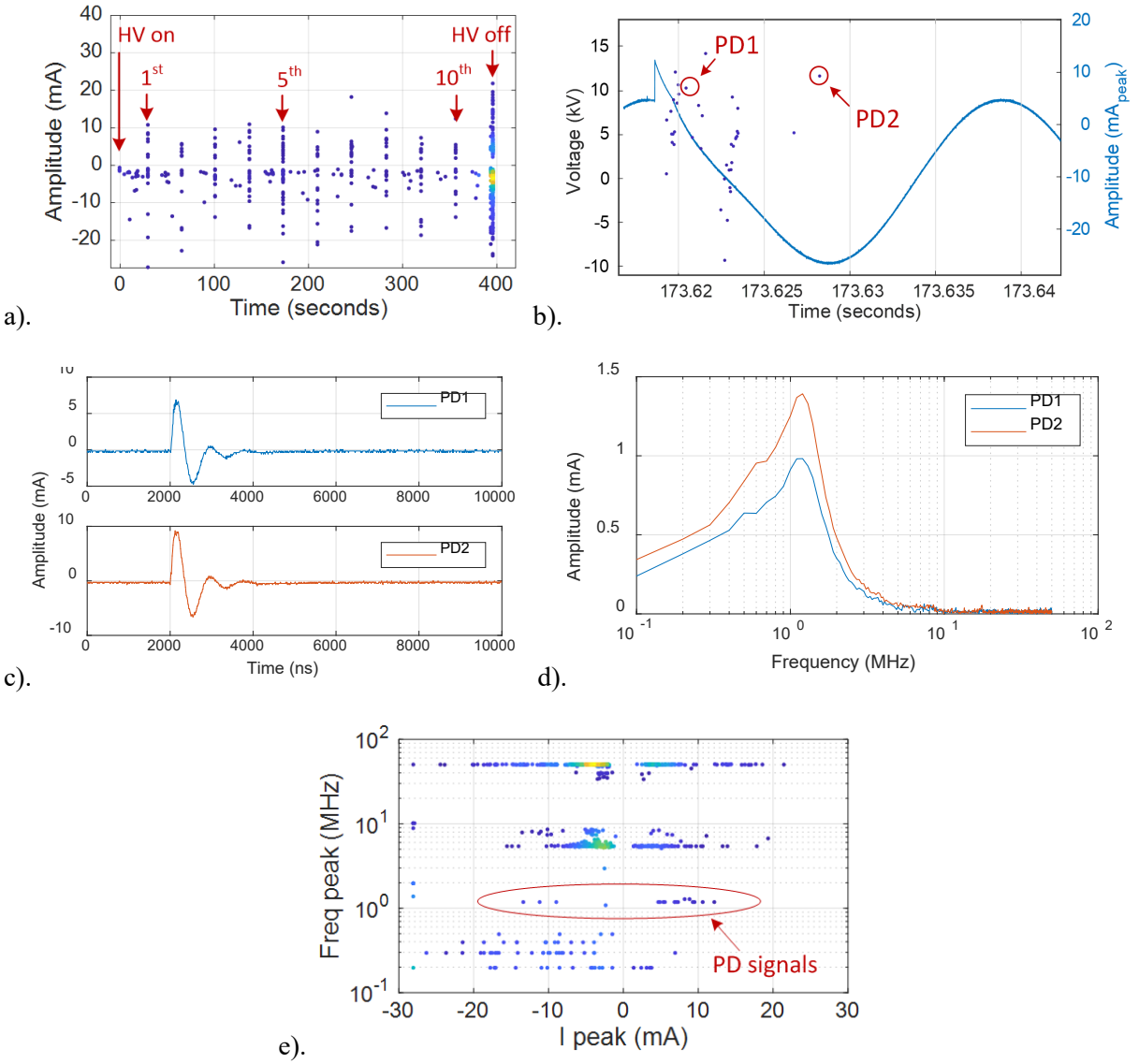

Figure 5.15: Measured results under superimposed transient with cable model 1: a) signals measured over time, b) signals measured during the impulse moment including PDs, c) TRPD shapes of PD1 and PD2, d) frequency spectra of PD1 and PD2, e) dominant frequencies of all measure signals including PDs under superimposed transients.

Figure 5.15a presents all the signals acquired during the application of the test voltage with 11 successive impulses. There are 11 groups of disturbance signals which are corresponding to the 11 impulses according to the conclusion from section 5.4.1. Figure 5.15b shows the signals during the 5th impulse. Among the acquired signals, there are two pulses being recognized as PD pulses, shown as PD1 and PD2. Their time-resolved pulse shapes (Figure 5.15c) all have positive peaks and same time length in the order of magnitude of a microsecond. The dominant frequency was used to select out PD signals. All the PD signals have dominant frequencies around 1.1 MHz (indicated in Figure 5.15e). Both the time-resolved pulse shapes and the dominant frequencies of these two signals are similar to the PD pulses that were captured under pure AC voltage as shown in Figure 5.13. Therefore, it is very probable that the two pulses are internal discharge pulses from the cable model 1.

Comparing the dominant frequencies, the measured PD pulses under impulse transients have the similar dominant frequencies with the ones measured under AC voltage as shown in Figure 5.13, which are significantly different from the ones of disturbance as shown in Figure 5.11 and Figure 5.12. The dominant frequency, hereby, can be used to distinguish the PD pulses from disturbances. Figure 5.15e

shows the dominant frequencies of all the measured signals, among which, the ones of PD pulses are clustered at 1.1-1.2 MHz as in the red circle. By this way, it is easy to select out all the PD pulses.

From the measurement results of PD under superimposed transients, it can be concluded that:

- The experimental set-up is able to measure PD under superimposed transients in MV level if any occurs. The PD measuring system can keep measuring during the impulse application without being interrupted and damaged.
- The PD measuring system is able to capture fast pulses under impulse conditions with sufficient time resolution.
- The PD measuring system is able to accurately recognize PD pulses from other discharge and disturbance pulses by means of phase-resolved pulse pattern, time-resolved pulse shape and selecting the dominant frequency of PD pulses.

5.5 Partial Discharges in MV Cable Models under Transients

In the previous section 5.4, the experimental set-up has been verified being able to measure partial discharges from the cable models under superimposed transient conditions. Moreover, the characteristics of partial discharges produced by the artificial defects in cable model 1 and 2 have been measured and collected. In this section, the cable models were subjected to the defined superimposed transient voltages. The effect of superimposed transients on the cable models regarding partial discharge behaviour has been investigated.

5.5.1 Test procedure

Partial discharges were measured in the cable models under superimposed transient voltages as shown in Figure 5.8. The test voltage waveform and the test procedure are explained in Figure 5.16. The AC voltage value was determined to be below the PD inception voltage (PDIV) and above the PD extinction voltage (PDEV). In each test, the cable model was subjected to only the determined AC voltage for several minutes in order to confirm that PD did not occur at the AC voltage level. Then the first impulse was applied on the AC voltage at the AC crest. After 30-35 seconds, the second impulse was applied on the AC crest. The impulses were applied on AC voltage at a rate of one per half minute. After the last impulse, the AC voltage was kept on the cable model until the acquisition stopped.

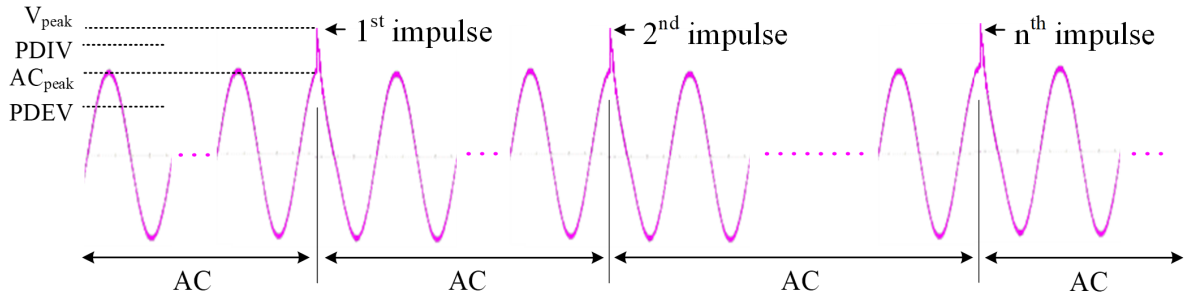

Figure 5.16: Test voltage waveform and test procedure.

Table 5.4 lists the PD tests under the designed test voltages. For each test, the cable model under test, the defect status and the PDIV / PDEV of the cable model, as well as the parameters of the applied test voltage are given. Test order tells the sequence of each test being performed. Before each test, the PDIV and PDEV of the tested cable model were measured. The applied testing voltage is described by its AC peak value and total peak value, the parameters α and β, and the number of impulses contained in the test voltage.

The two parameters, α and β, are defined in equations (5.1) and (5.2). The ratio α describes the relation between the applied AC voltage and PDIV/PDEV. The ratio β is the superimposed total peak divided by the applied AC voltage peak value.

$$\alpha = \frac{PDIV - AC_{peak}}{PDIV - PDEV} \qquad (5.1)$$

$$\beta = \frac{V_{peak}}{AC_{peak}} \qquad (5.2)$$

When the AC voltage is below PDIV and above PDEV, α is a positive value below 1. The closer that AC is to PDIV, the smaller value α has. When AC is below PDEV, α becomes larger than 1. If AC is higher than PDIV, then α turns to negative. The impulse voltages were set mostly with certain peak values so that the obtained transients had the overvoltage ratio β in the range of 1.7 to 2.0, which could happen in practice. Moreover, for all the defined testing voltages, the time period of the transient overvoltage being higher than the PDIV due to the impulse application is long enough for PD to occur.

Table 5.4: PD tests in MV cable models under superimposed transient voltages.

Test	Cable model	Test order	Defect Status	PDIV [kV_{pk}]	PDEV [kV_{pk}]	Testing voltages of impulse transients					
						Label	AC [kV_{pk}]	V_{peak} [kV_{pk}]	Amount of impulses	α	β
1	1	1	Virgin	16.9	13.0	TV_1	14.1	23.4	4	0.73	1.66
2	1	2	Virgin	19.4	15.1	TV_2	15.8	27.3	20	0.88	1.73
3	1	3	Virgin	16.3	10.9	TV_3	8.5	25.5	10	1.44	3.11
4	2	8	Virgin	8.6	8.2	TV_4	8.3	14.7	10	0.75	1.77
5	1	5	Virgin	18.4	12.3	TV_5	15.7	25.0	14	0.44	1.59
6	1	6	Aged	13.3	11.0	TV_6	12.7	24.2	1	0.30	1.91
7	1	4	Virgin	16.3	10.9	TV_7	15.7	27.2	10	0.13	1.73
8	1	7	Aged	12.3	11.46	TV_{81}	11.6	23.0	37	0.80	1.98
						TV_{82}	11.9	23.4	20	0.50	1.97
						TV_{83}	12.2	23.8	20	0.10	1.95
						TV_{84}	12.4	24.1	20	-0.10	1.94
						TV_{85}	12.7	24.5	11	-0.50	1.93

5.5.2 Measurement results of PD under impulse transients

Different PD behaviours have been observed under superimposed transients. Here four scenarios are summarized based on the observations:

- No PD being triggered by impulse transients
- PDs initiate only in the impulse period
- PDs initiate only at AC after the impulse
- PDs initiate in the impulse period and persist at AC

In the following, these four scenarios of PD behaviour are presented and discussed in detail. The physical mechanism is interpreted as well.

No PD being triggered by impulse transients

In test 1 and test 2, cable model 1 was stressed under test voltages with different value and amount of impulses. No PD were observed during the whole testing process with the application of impulses.

The reason why no PD were observed can be referred to the breakdown mechanism in gas. The time to breakdown in the gas is in the order of magnitude of a microsecond for the Townsend mechanism and 1-100 ns for the streamer mechanism [116]. In all the tests, the time period of the superimposed transient overvoltage being higher than PDIV was 1-2 ms on average. In this case, both the time period and the electric field during the overvoltage period were large enough to initiate PD. However, no PD was observed in test 1 and test 2. We can hereby infer that the initiatory electron was not present during the entire test. Since the cable model was discharged after each test, the surface and space charges flow away. Such a long inception delay is due to the stochastic generation of an electron by cosmic and background radiation.

PDs initiate only during the impulse period

Firstly, we define the impulse period as one 50 Hz cycle, i.e. 20 ms, counting from the very start of the superimposed impulse transient.

In both test 3 and 4, PD were observed in cable model 1 and 2 after applying the impulses. All the observed PDs occurred only during the impulse periods. After the impulse periods, PD did not occur anymore under AC voltage.

In test 3, PD only occurred instantaneously in the impulse periods of all the applied 10 impulses, except for the 2nd impulse, shown in Figure 5.17a. Each dot represents one PD pulse. The red lines indicate the impulses. Figure 5.17b illustrates the PD initiation under the 1st impulse. A discharge of larger magnitude and positive polarity occurred near the peak of the impulse, which we attribute this to a so-called main discharge [24]. Next, near to the beginning of the negative cycle, a discharge of smaller magnitude with negative polarity occurred. After these two discharges, PD extinguished. The TRPD pulse shapes (Figure 5.17c) and the frequency spectra (Figure 5.17d) of PD1 and PD2 are similar to the PD pulses measured under pure AC, shown in Figure 5.13. We can hereby recognize the instantaneous PD initiated by the impulse as the discharge type I in cable model 1. In this test, the occurrence of PD is highly correlated with the application of impulses, instead of being sustained by the AC voltage.

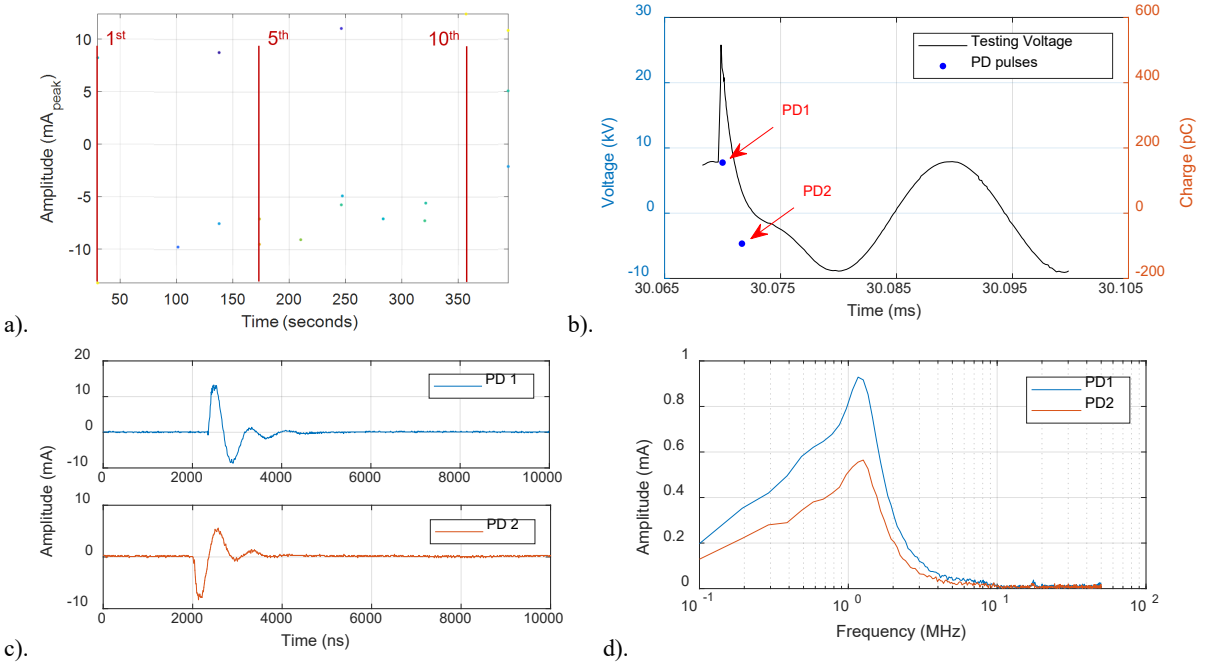

Figure 5.17: PDs in Test 3: a) PDs occurred over time, b) PD1 and PD2 occurred at 1st impulse moment, c) TRPD pulse shapes of PD1 and PD2, d) dominant frequencies of PD1 and PD2.

In test 4, a similar phenomenon was observed with cable model 2, shown in Figure 5.18a. The AC level of the testing voltage TV_4 was determined based on the inception and extinction values of discharges occurred at negative cycle. There were PD occurring at every impulse moment. However, no PD was observed near the peak of the impulse. Instead, one or two PD occurred at the negative cycle during the impulse period, as shown in Figure 5.18b. Then they extinguished. The TRPD pulse shape (Figure 5.18c) and the frequency spectrum (Figure 5.18d) of PD1 conform well with discharge type II that was measured for cable model 2 under pure AC.

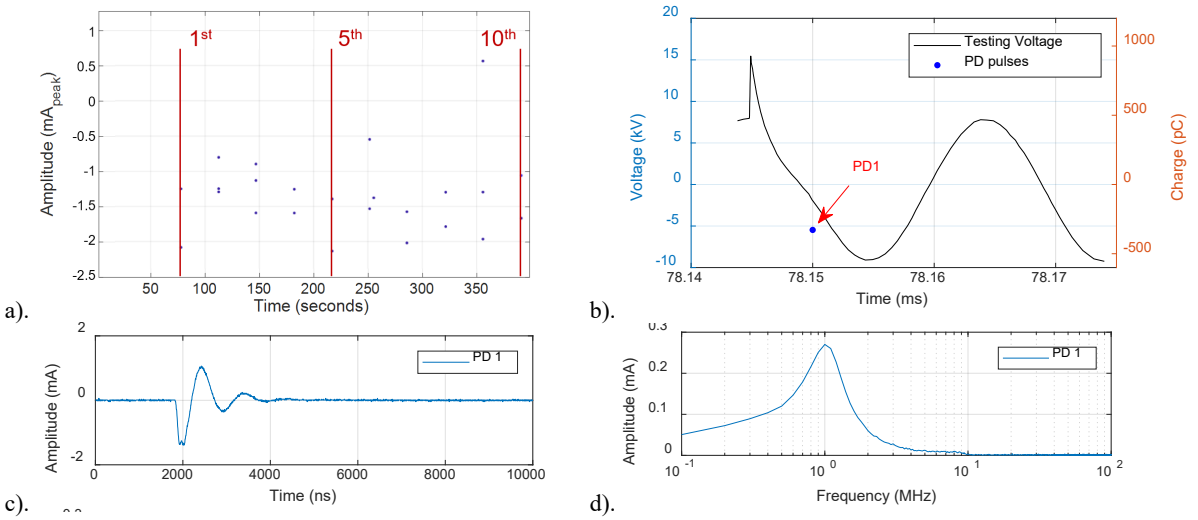

Figure 5.18: PDs in Test 4: a) PDs occurred over time, b) PD1 occurred at 1st impulse moment, c) TRPD pulse shapes of PD1, d) dominant frequency of PD1.

The observed phenomena can be explained by the PD inception criteria and the field condition in the defect. In test 3, a positive main discharge initiated at the impulse rising phase, then a negative discharge occurred near but below zero voltage, see Figure 5.17b. Afterwards PD extinguished. It is necessary to notice that, the negative discharge occurred at a field that is below the extinction field. This phenomenon can be explained based on the field conditions shown in Figure 5.19.

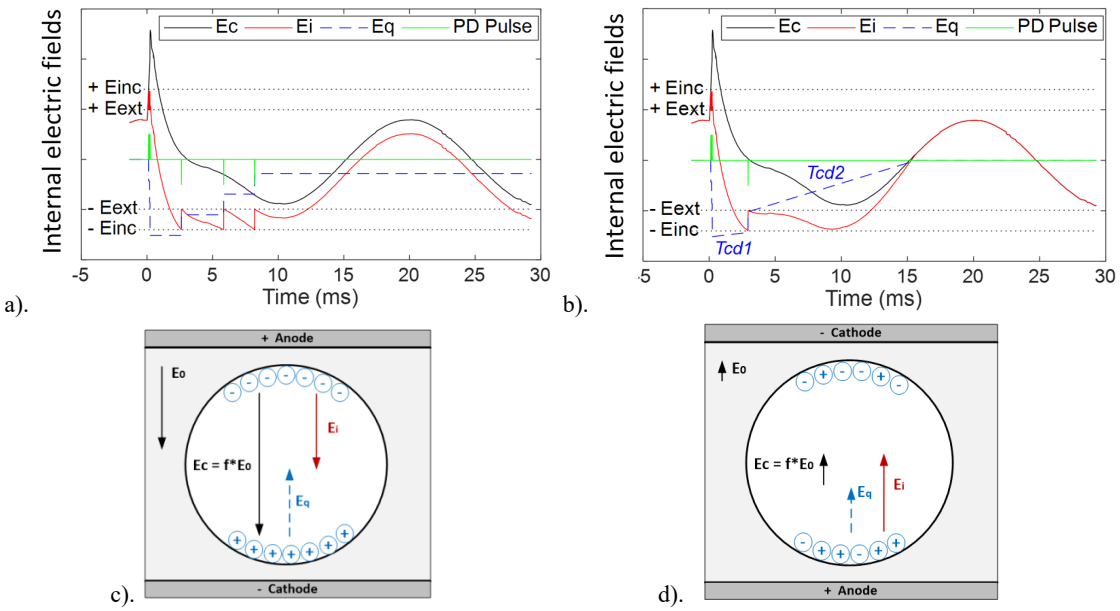

Figure 5.19: Schematical electric field conditions during PD process in test 3: a). the field changes after 1st impulse with infinite initiatory electron and no charge decay, b) the field changes after 1st impulse with infinite initiatory electron and charge decay, c) the field conditions in the void after the positive PD, E_c and E_i in positive polarity, d). the field conditions in the void after the negative PD, E_c and E_i in negative polarity.

Figure 5.19a shows how the internal electric fields change during the 1st impulse period. E_c is the enhancement of E_0, where E_0 is generated by the applied testing voltage TV_3 cross the insulation thickness. Thus, E_c follows the wave shape of TV_3. E_q is created by the surface charges. The residual local field E_i is the sum of E_c and E_q, which drives the PD occurrence. The concept of E_i, E_c and E_0 have been detailed explained in section 3.2.1. It is assumed that the initiatory electron is always available and there is no charge decay. In this case, the main discharge ignites as soon as the local field E_i reaches the inception field E_{inc} at the impulse rising phase. During the discharge process, charges from the discharge are accumulated on the insulation surface, which leads to an increasing E_q. Correspondingly, E_i reduces until it reaches the extinction field E_{ext}. At this moment, discharge extinguishes, E_q stops increasing and then keeps unchanged since there is no charge decay. The field condition is shown in Figure 5.19c. Afterwards, E_i changes with E_c until it reaches $-E_{inc}$, then a negative discharge ignites. The charges deposited on the surface by the negative discharge have an opposite polarity with the existing charges, which reduce E_q. The field condition now is shown in Figure 5.19d. After the negative discharge, E_i re-traces E_c. As a result, the negative PDs would recur periodically.

Considering the charge decays, expressed by the decay time constant τ_{cd}, the phenomenon will change as shown in Figure 5.19b. Between two PD events, the charges decay with a certain τ_{cd}, so the field E_q generated by the charges decreases. A smaller τ_{cd} means a faster charge decay and a faster change of E_q. After the positive discharge, the charges start to decay slowly with a large τ_{cd1}. E_q hereby decreases slightly. After the negative PD, due to the damage of the previous discharge, the surface conductivity may become larger, which lead to a smaller τ_{cd2} and faster decay. Moreover, the polarity of E_c reverses now, and most positive charges are accumulated at the anode side. As a result, a relatively large E_i with negative polarity is formed, see Figure 5.19d. And the surface charges are easy to drift with E_i, which means the charges decay faster. With this τ_{cd2}, E_i is unable to reach E_{inc} again and at last converges to E_c. Therefore, PD cannot be ignited any more, and there are only two PD events occurring after the impulse, which conforms to the measurement result shown in Figure 5.17b.

In test 4, discharges only occurred at the negative cycle after the impulse during the impulse period, see Figure 5.18b. This phenomenon is probably due to the change in the charges that created E_q caused by the defect. In cable model 2, the defect was made next to the metal connector. Therefore, a cavity with metal as wall on one side and insulator as wall on the other side was formed. When electric field is present, electrons can overcome the potential barrier to leave the metal into the dielectric and contribute to space charges. Under pure AC, electrons are injected from and gather near the metal wall. On the insulator wall, there are charges deposited in the traps. All these form an electric field in the direction from metal to insulator wall, shown as E_{q0} in Figure 5.20. With E_{q0}, E_i has a negative offset from E_c. This is the reason why the inception voltage in negative cycle is lower than that in positive cycle for cable model 2, shown in Table 5.4. When the impulse is applied, the high electric field may cause more electrons being injected from the metal surface and some deposited charges escaping from the traps in the insulator surface. This process will lead to an enhanced E_{q1}. Due to the relatively high PDIV for positive cycle, the resulting E_i is not sufficient to ignite PD near the impulse, but it exceeds the PDIV for negative cycle. Consequently, a discharge occurs. With considering the charge decay, E_q returns to E_{q0} after the discharge. Since E_i with offset of E_{q0} doesn't exceed the negative PDIV again, PD extinguishes.

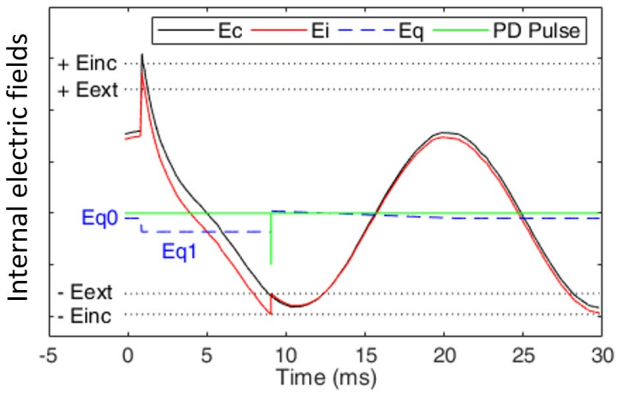

Figure 5.20: Schematical electric field condition after 1st impulse in test 4 with charge decay.

PDs initiate during the impulse period and persist at AC

PD initiated by the impulses may also persist under the AC voltage after the impulses stopped. This phenomenon was observed in test 7 and test 8. Test 7 is to be discussed here, and test 8 will be discussed in the section "Statistical analysis on the progress from PD initiation to sustained status".

In test 7, no PD initiated before the 5th impulse. When the 5th impulse was applied, two PD initiated during the impulse period and then extinguished, as shown in Figure 5.21b. After the 8th and 9th impulses, more PD initiated, recurred and extinguished. After the 10th impulse, PD initiated and then became sustained by the AC voltage. This process is shown in Figure 5.21a. Figure 5.21c and Figure 5.21d show the TRPD and frequency spectra of PD1 and PD2. PRPD patterns of PD occurred after 5th, 8th, 9th and 10th impulses are shown in Figure 5.21e.

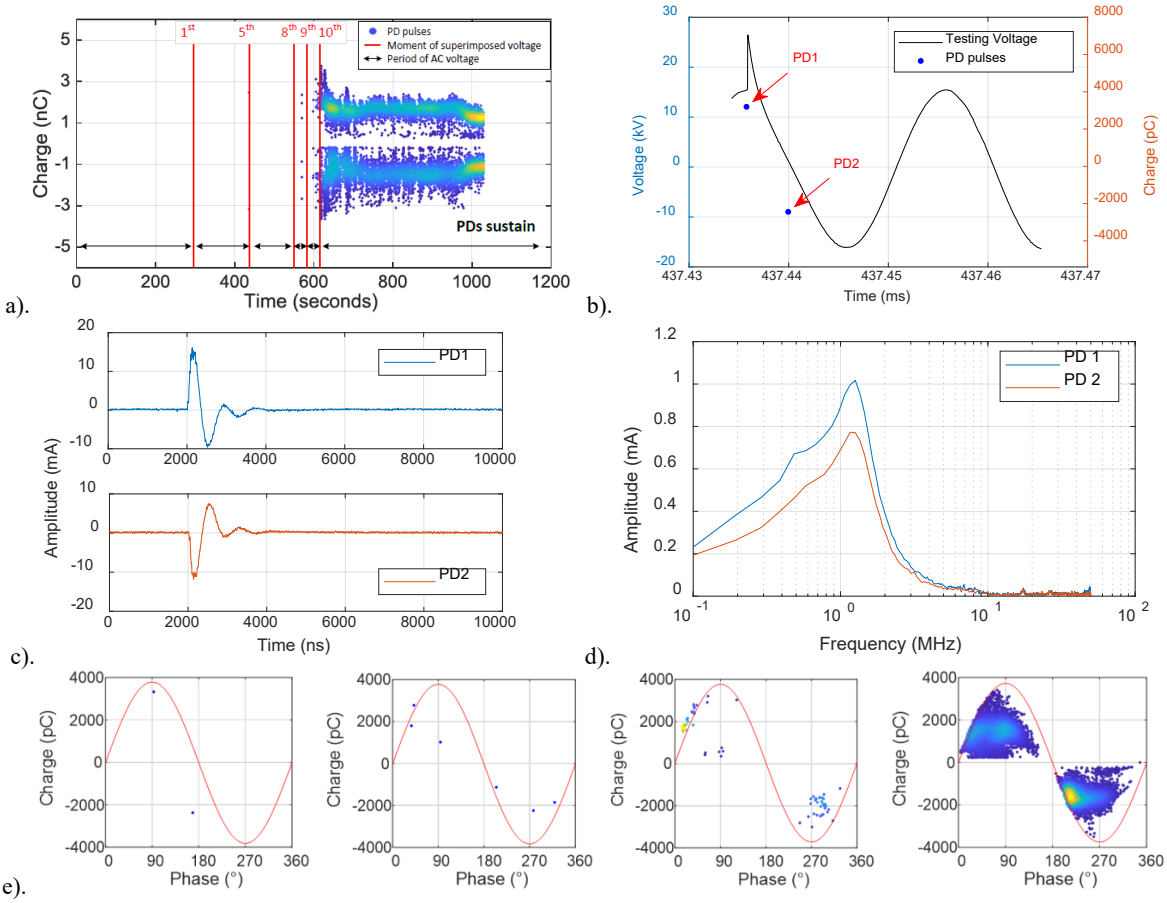

Figure 5.21: PDs in Test 7: a) PD initiation with consecutive impulses, b) PD1 and PD2 occurred at 5th impulse moment, c) TRPD pulse shapes of PD1 and PD2, d) frequency spectra of PD1 and PD2, e) PD after 5th, 8th, 9th and 10th impulses.

In test 7, PD firstly initiated in the 5th impulse period (Figure 5.21b). The explanation is similar to what happened in test 3. Figure 5.22a and Figure 5.22b illustrates the field changes in this PD process.

When neglecting the charge decay between PD events, PD will be initiated by the impulse and then recur periodically, as shown in Figure 5.22a. Figure 5.22b shows the condition considering the charge decay. After the negative PD, there is only a small number of charges left along the surface and in the traps, which contributes to the charges created E_q. After a short time, the residual surface charges all decay. A tiny E_q is left, which is kept by the deposited charges in the traps. The detrapping process may take time, which will affect the PD activity in two ways. Firstly, the tiny E_q causes an offset of E_i from E_c. With this offset, E_i may exceed E_{inc}, shown as the negative peak of E_i in Figure 5.22b. Secondly, there might be an absence of a free electron. In this case, even though E_i exceeds E_{inc}, PD will not be ignited. This is why PD extinguished after the negative PD, as shown in Figure 5.21b and Figure 5.22b.

After the 8th impulse, PD initiated under AC voltage instead of being ignited in the impulse period. A negative PD initiated firstly and followed by a positive PD, then PD extinguished. A couple of milliseconds later, PD initiated and extinguished again in a same way. In general, PD recurred intermittently after the 8th impulse. This phenomenon is explained by the schematic in Figure 5.22c. Assuming the absence of a free electron, PD cannot be ignited even with E_i exceeding $-E_{inc}$. At a certain moment, the electron deposited in the surface traps detraps successfully. When E_i exceeds $-E_{inc}$ again, a negative PD ignites. Then E_i follows E_c with an offset of E_q, until it exceeds E_{inc} in the positive cycle and causes a positive PD. After that, the decreased E_i re-tracks E_c with considering the charge decay until all the surface charges disappear. Then the same situation happens again as described in Figure 5.22b. With absence of initiatory electron, PD extinguishes with an exceeding E_i.

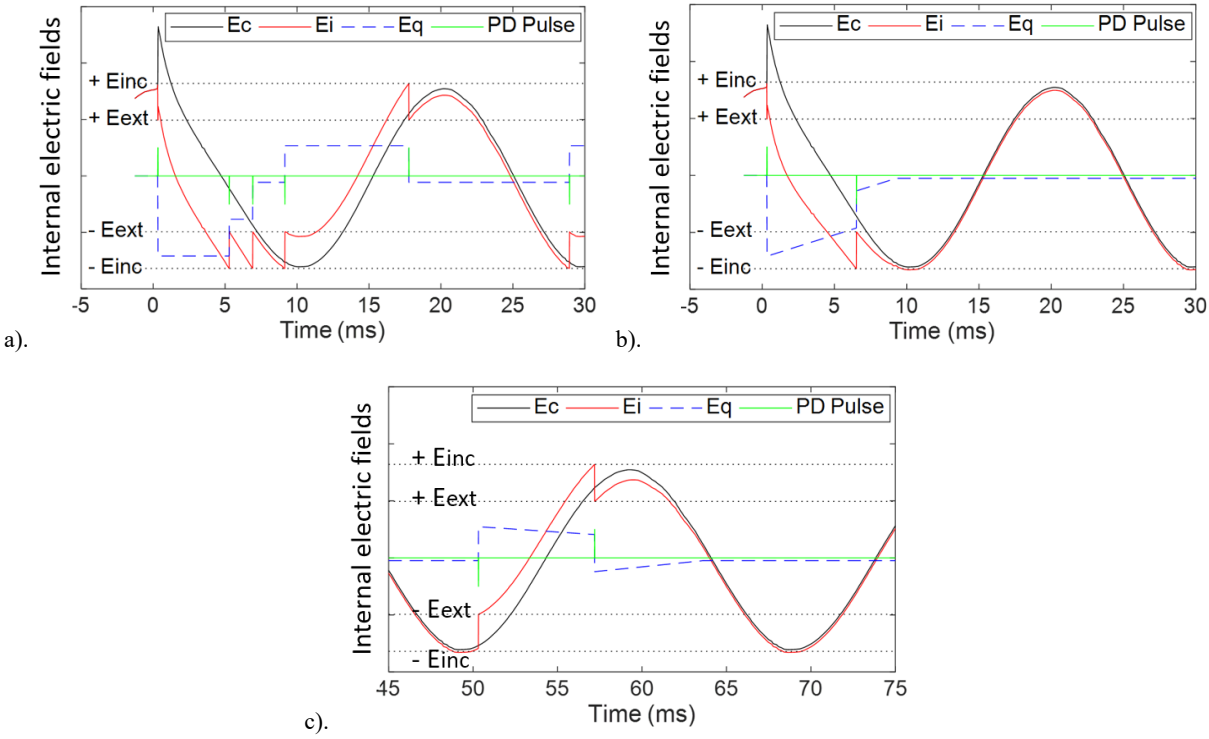

Figure 5.22: Schematical electric field conditions during PD process in test 7: a) the fields change after 5th impulse with infinite initiatory electron and no charge decay, b) the fields change after 5th impulse with infinite initiatory electron and charge decay, c) the fields change after 8th impulse.

Such intermittent PD behaviours also happened after the 9th and 10th impulses. After the 9th impulse, PD initiated earlier, and the time interval between the intermittent PD events was shorter. After the 10th impulse, PD initiated even earlier and very soon they became sustained under AC voltage. PD can persist

under AC voltage which is far below the inception voltage [42], provided the charges decay slowly as in the virgin defect, and there are always surface or deposited charges that generate E_q. From the previous analysis, the charges decay fast, and it may happen that all charges decay so that there is not a sufficient E_q supporting E_i to exceed E_{inc}. In this case, PD cannot persist under AC voltage anymore. Then, the sustained PD might be explained by another reason.

Apart from the dimension and condition of the defects, the PD inception delay t_{delay} also depends on the applied voltage [48], as shown in equation 3.3. With the same PDIV, a higher applied voltage will lead to a shorter t_{delay}. According to [56], the strong increase of the time lag with decreasing field strength is due to the increase of the critical length, which restricts the active volume available for avalanche development. Wester et al. [116] presents the dependency between t_{delay} and the applied 50 Hz voltage measured with different specimens. For each specimen, the delay time is considerably short for higher voltages and rather long for lower voltages. In the current work, t_{delay} of cable model 1 in virgin status was measured under 50 Hz AC voltages. The result is shown as the solid line with point A, B and C in Figure 5.23. Point A indicates the PDIV, at which PD initiated with t_{delay} of milliseconds and kept sustained. At point B, PD initiated around 20 minutes after applying AC of 15.7 kV_{pk}. In test 7 where the AC voltage was 15.7 kV_{pk}, PD initiated and kept sustained after 10 impulses, i.e. around 630 seconds, which is shown as point B' in Figure 5.23. It is believed by the author that, the application of impulses contributes to this decrease in t_{delay} under 15.7 kV_{pk}.

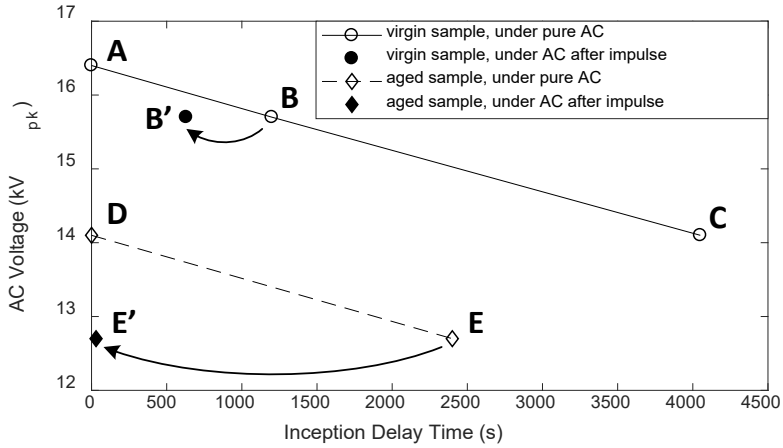

Figure 5.23: The waiting time of PD inception in cable model 1.

PDs initiate at AC after the impulse finished

In some cases, PD did not initiate during the impulse period. However, after the impulses finished, PDs were observed under AC voltage. This phenomenon was observed in test 5 and test 6.

In test 5, no PD were detected in cable model 1 during the application of 14 impulses. After the impulses finished, PDs were observed under the continuing AC voltage, shown in Figure 5.24a. The PRPD (Figure 5.24b), further proves that the occurred discharges were sustained by the AC voltage rather than being initiated by the impulses. PD1 and PD2 are further described with their TRPD pulse shapes (Figure 5.24c) and their frequency spectra (Figure 5.24d), which confirm with that in Figure 5.13.

In test 6, cable model 1 has encountered only one impulse. No PDs were observed during the impulse period. After the impulse finished, PD initiated under the AC, which persisted actively with the AC. This is shown in Figure 5.25a and Figure 5.25b. PRPD pattern (Figure 5.25c), TRPD pulse shapes and frequency spectrum (Figure 5.25d) confirm the observed PD being the type I discharges characteristic for cable model 1.

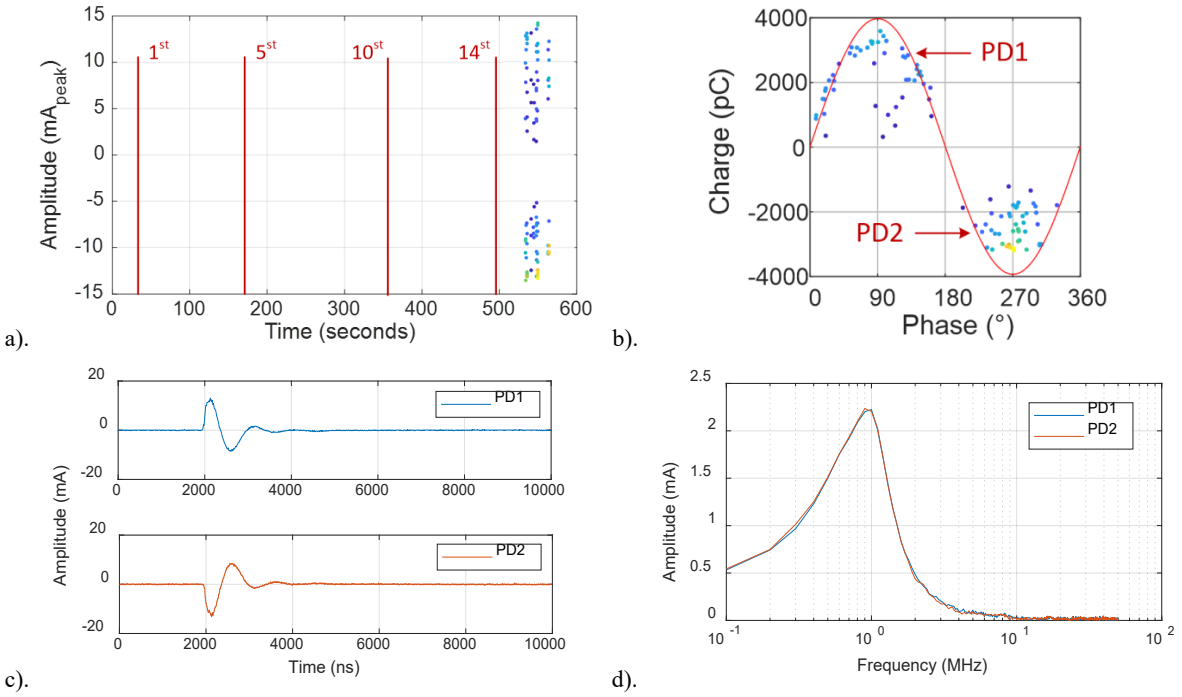

Figure 5.24: PDs in test 5: a) PDs occurred after 14th impulses, b) PRPD pattern, c) TRPD pulse shapes of PD1 and PD2, d) peak frequencies of PD1 and PD2.

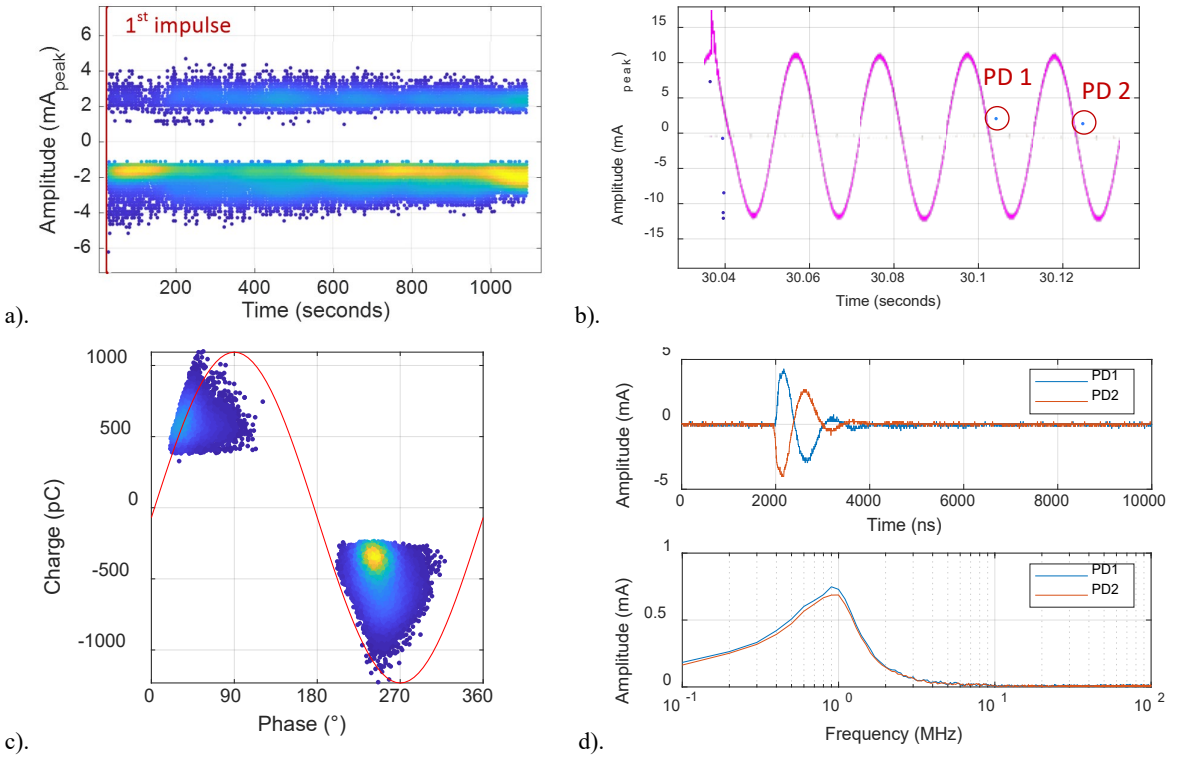

Figure 5.25: PDs in test 6: a) PD occurred over time, b) PD occurred after 1st impulse , c) PRPD pattern, d) TRPD pulse shape and peak frequency.

In test 5, after being subjected to AC voltage of 15.7 kV_{pk} for 120 seconds and the following TV_5 for 530 seconds, i.e. 650 seconds in total, PD initiated in the cable model 1 (Figure 5.24a). It is likely that the application of impulses helps to liberate the electron and hereby enable PD to initiate. Under this

assumption, the waiting time of PD inception t_{delay} as 650 seconds in total locates itself at point B' in Figure 5.23 approximately.

After being stressed by more than two hundred impulses, during which partial discharges occurred, the defect in cable model 1 was supposed to be deteriorated by discharges (section 3.2.3). Thus, t_{delay} of cable model 1 was checked again under 50 Hz AC voltages, shown as the dash line in Figure 5.23. The PDIV was measured as 14.1 kV_{pk} with t_{delay} of milliseconds, indicated as point D, which is decreased compared to that of virgin cable model. At AC of 12.7 kV_{pk}, t_{delay} was around 40 minutes, shown as point E. Test 6 was performed on the aged sample. When applying TV_6, PD did not initiate under 12.7 kV_{pk} before the impulse but initiated three cycles after the impulse and kept sustained by the 12.7 kV_{pk} AC, which is also indicated by point E' in Figure 5.23.

Statistical analysis on the progress from PD initiation to sustained status

A similar phenomenon was observed in test 8 as in test 7, that PD initiated by the impulses persist under the AC voltage after the impulses stopped. In test 8, five sets of testing voltages were applied to cable model 1 uninterruptedly. The AC voltage levels of TV_{81}, TV_{82} and TV_{83} were set below PDIV, whilst the AC voltage levels of TV_{84} and TV_{85} were set higher than PDIV. Figure 5.26a shows the PD measurements under the five testing voltages.

In this test, PD always initiated in the impulse periods. However, PDs behaved differently under the different AC voltages of different testing voltages. Under TV_{81}, PDs were initiated by each impulse and lasted for a couple of seconds, then they stopped. Several seconds later, they recurred again for a short time, and so forth. This is shown in Figure 5.26b. Such an intermittent PD behaviour was also observed under TV_{82}, shown in Figure 5.26c. Under TV_{83}, the same intermittent behaviour was observed for the first six impulses. After the 6^{th} impulse, PD occurred more continuously and extensively, and became sustained at last, as shown in Figure 5.26d. Under TV_{84} and TV_{85}, PDs were occurring sustainably. All the PRPD patterns confirm the PDs to be the type I discharge from cable model 1.

The whole progress under one impulse transient - PD being initiated firstly, then recurring intermittently, and at last occurring sustainably - has been investigated in test 7. In test 8, such progress has been repeated for multiple times for statistical purpose. The pulse count distribution *HN* is used to analyse the discharge behaviour after each impulse application, which shows the number of discharges after each impulse application as a function of the time in second. The expression of *HN* is given in Equation (5.3). HN_i is the pulse count distribution after the i^{th} impulse. N_j is the number of discharges occurred during the $(j-1)^{th}$ second and the j^{th} second after the impulse application. Since the time interval between each two impulses is around 35 seconds, j counts from 1 to 35. As an example, Figure 5.27 shows the pulse count distribution after the 3^{rd} impulse HN_3 and after the 13^{th} impulse HN_{13} under the test voltage TV_{83}. After the 3^{rd} impulse, illustrated as the blue bar, around 18 discharges occurred during the 1^{st} second, and 10 discharges occurred during the 2^{nd} second. After five seconds, discharges extinguished. After the 13^{th} impulse, illustrated as the yellow bar, discharges occurred continuously over the 35 seconds.

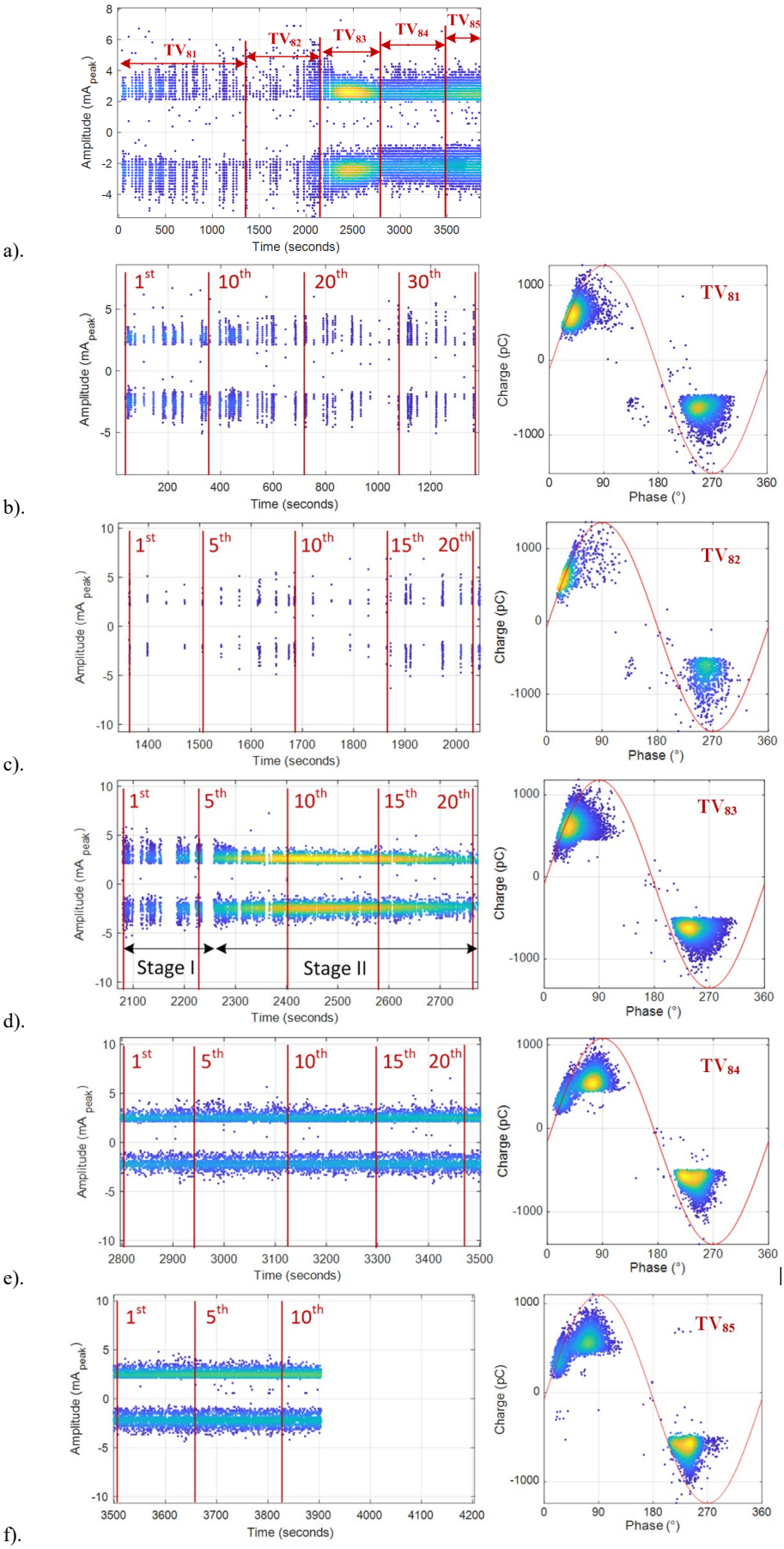

Figure 5.26: PDs in test 8: a). PD under five sets of testing voltage, b) PD under testing voltage TV_{81}, c) PD under testing voltage TV_{82}, d) PD under testing voltage TV_{83}, e) PD under testing voltage TV_{84}, f) PD under testing voltage TV_{85}.

$$HN_i\,(N_j) = [N_1, N_2, \cdots\cdots N_{35}] \qquad i = i^{th}\ impulse, j = 1, 2, \cdots\cdots, 35 \qquad (5.3)$$

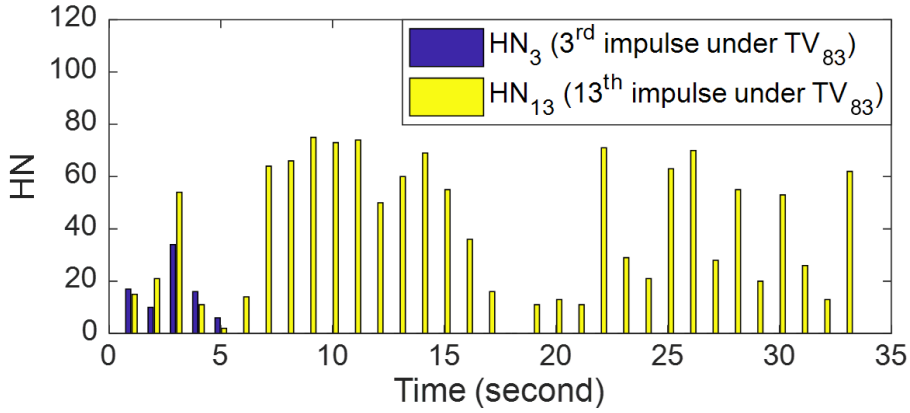

Figure 5.27: The pulse count distribution after the 3rd impulse HN3 and after the 13th impulse HN13 under the TV_{83}.

Figure 5.27 shows the pulse count distribution after single impulse application. In test 8 under TV_{83}, 20 impulses were applied. In order to evaluate the effects of impulse transients on the PD progress statistically, the average pulse count distribution *HN'* was defined, which is described in Equation (5.4) and (5.5). Assuming k impulses are applied, HN_1 to HN_k are then acquired for each impulse. For the pulse count distribution after the mth impulse HN_m, $N_{m,j}$ is the number of discharges occurred at jth second. The average pulse count distribution HN' for all the k impulses is an array containing the mean values of $N_{1,j}$ to $N_{k,j}$ at each second, that is, the mean value of each column in Equation (5.4). Thus, the time base of *HN'* is also 35 seconds. In case of an average pulse count distribution for the mth - nth impulses, at each second the mean value of $N_{m,j}$ to $N_{n,j}$ is calculated, as shown in Equation (5.3). The PD repetition rate keeps at 1-2 PD per cycle during the entire test since the AC level of the testing voltages closely approximate the PDIV. Therefore, a larger *HN'* means PDs occur in more AC cycles, i.e. PD occurring more extensively.

$$\begin{bmatrix} HN_1 \\ HN_2 \\ \vdots \\ HN_m \\ \vdots \\ HN_n \\ \vdots \\ HN_k \end{bmatrix} = \begin{bmatrix} N_{1,1},\ N_{1,2}, \cdots\cdots N_{1,35} \\ N_{2,1},\ N_{2,2}, \cdots\cdots N_{2,35} \\ \vdots \\ N_{m,1},\ N_{m,2}, \cdots\cdots N_{m,35} \\ \vdots \\ N_{n,1},\ N_{n,2}, \cdots\cdots N_{n,35} \\ \vdots \\ N_{k,1},\ N_{k,2}, \cdots\cdots N_{k,35} \end{bmatrix} \qquad (5.4)$$

$$HN' = \frac{\sum_n^m HN_i}{m-n} = \left[\frac{\sum_n^m N_{i,1}}{m-n}, \frac{\sum_n^m N_{i,2}}{m-n}, \cdots\cdots, \frac{\sum_n^m N_{i,35}}{m-n}\right] \qquad m, n \in 1, 2, \cdots, k \qquad (5.5)$$

In Figure 5.27, there is a significant difference between the pulse count distributions HN_3 and HN_{13} under the test voltage TV_{83}. PDs occurred after the 13th impulses are more active and last longer. This phenomenon is also seen in Figure 5.26d. The PD activity basically went through two stages: during the first five impulses, regarded as stage I, PDs occurred intermittently. In stage II from the 6th impulse, PDs occurred more sustainably and intensively. In the following, the average pulse count distribution HN' is to be calculated for the stage I (1st-5th impulses) and stage II (6th-20th impulses) respectively under test voltage TV_{83}.

Similarly, for all the other test voltages from TV_{81} to TV_{85}, the PD process was analysed based on the pulse count distribution. According to the pulse count distribution, the PD process under each test voltage was divided into several stages. In each stage, the pulse count distributions after every impulse are similar to each other. Then the average pulse count distribution was calculated for all the stages, which can represent the PD process in each stage. By showing the PD process in the way of stages, the development in PD is presented. Figure 5.28 shows the average pulse count distributions HN' under five testing voltages.

With TV_{81} and TV_{82}, the AC levels are far below PDIV, the observations are shown in Figure 5.28a and Figure 5.28b. In Figure 5.28a, during the stage I (1^{st} – 25^{th} impulses) under TV_{81}, the PD processes after each impulse are similar, that the initiated PD re-ignited intermittently and extinguished at last. Such PD behaviour was also observed during the stage II (26^{th} -37^{th} impulses), i.e. the application of impulses had not affected the PD progress. The effect of impulses on PD rises up with TV_{82}, which is shown in Figure 5.28b. During the stage I (1^{st} -8^{th} impulses), the initiated PD extinguished fast within 10 seconds. With applying more impulses, during the stage II (9^{th} - 20^{th} impulses), the initiated PD recurred more extended and extinguished after 30 seconds. This is due to the conductivity of the insulation surface caused by the accumulated damage. With more impulses being applied, more surface charges are accumulated. Consequently, the probability of PD initiating and recurring under AC becomes higher.

Figure 5.28c shows the HN' under TV_{83}, whose AC level is closely approaching to PDIV. As discussed before, during the stage I (1^{st}-5^{th} impulses), the initiated PD recurred with receding occurrence, then extinguished after 30 seconds. With more impulses being applied, during the stage II (6^{th}-20^{th} impulses), the initiated PDs were able to persist with the same occurrence extension. In this case, the initiated PDs transferred from an intermittent status to a sustained status. This can be explained as the decreasing of the inception delay time during the application of TV_{83}. With more impulses being applied, t_{delay} under the AC of TV_{83} has been decreased. Thus, the AC voltage became sufficient to ignite PD, which leads to the sustained PDs. Under TV_{84} and TV_{85} where the AC levels exceed PDIV, impulses did not have a significant effect on PD behaviour. PDs were sustained all through the AC voltage (Figure 5.28d and Figure 5.28e).

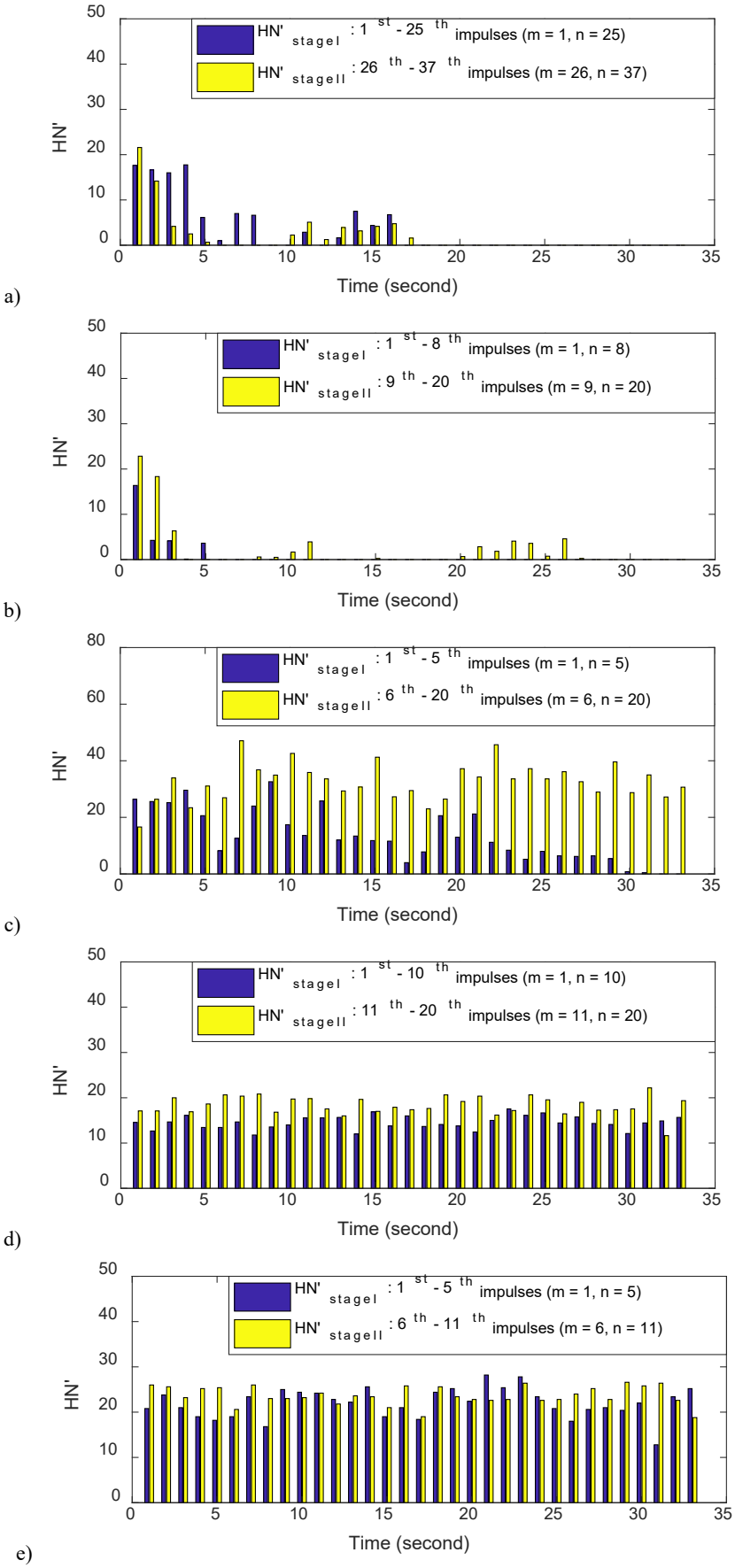

Figure 5.28: Statistical distribution of PD pulse count in test 8: a) PD pulse count distribution under TV_{81} with 37 impulses, b) PD pulse count distribution under TV_{82} with 20 impulses, c) PD pulse count distribution under TV_{83} with 20 impulses, d) PD pulse count distribution under TV_{84} with 20 impulses, e) PD pulse count distribution under TV_{85} with 11 impulses.

5.5.3 Discussions

By observing the parameter α of virgin cable model 1, in test 7 where the applied AC is close to PDIV and far from PDEV, indicated by α of 0.13, PDs have been triggered with less number superimposed voltages and stay sustained under AC. In test 5 where AC gets further from PDIV with α of 0.44, more superimposed voltages are needed to trigger PDs. And the triggered PDs are not sustained. For test 2 with α of 0.88 and even more superimposed voltages, no PD has been observed. Therefore, the closer the AC voltage to PDIV and further from PDEV, then with less number of superimposed voltages PDs could be triggered, and the more active and sustained activities of PDs occur.

The different PD behaviour under impulse transients has been interpreted. Hereby, the effects of impulse transients on PD can be summarized by the flowchart as shown in Figure 5.29 and are explained below.

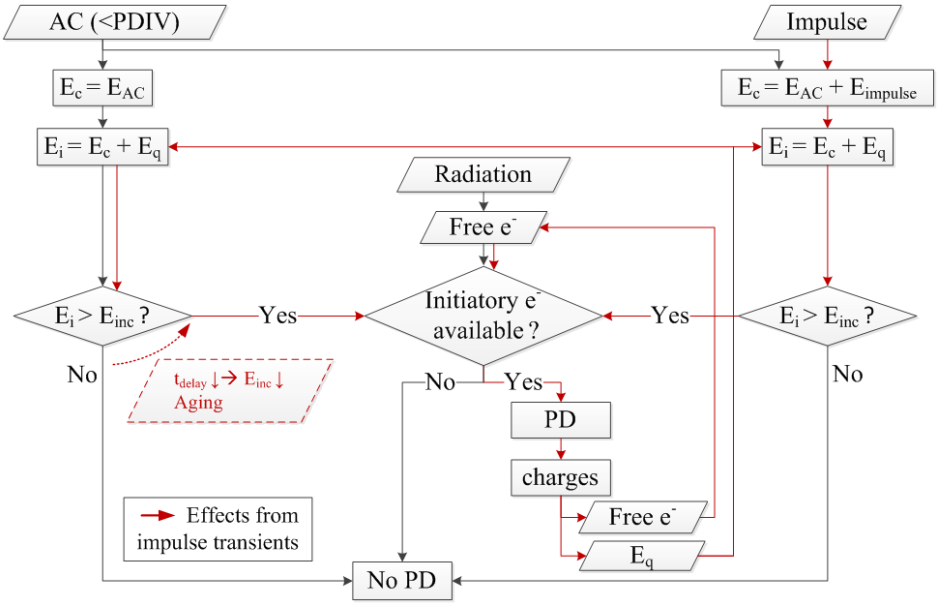

Figure 5.29: The effects of impulse transients on PD.

With only AC voltage being applied on the cable, which is below PDIV, the local field is not sufficient for PD to initiate (E_i<E_{inc}, E_q=0). When the impulse occurs, the background field in the defect E_c is enhanced. This results in a very high local field E_i which can ignite PD (E_i>E_{inc}, E_q=0). Once the initiatory electron generated by radiation is present, PD initiates. Those PDs always occur in the impulse periods. The charges created by PDs deposit along the insulation surface in the surface traps. Consequently, the surface charges become another source of the initiatory electrons, and also generate a field E_q, which will superpose on the original E_c. The resulting E_i may exceed E_{inc} even after the impulse finished. As a consequence, PDs will recur under only AC voltage (E_i>E_{inc}, E_q≠0). However, since PDEV is quite close to PDIV, the initiated PDs recur and extinguish intermittently.

The initiated PDs may also become sustained under AC voltage after the impulses. In that case, PDs are sustained by a sufficient electric field (E_i>E_{inc}), where the E_{inc} is not the original one any more. The application of impulses may leads to an accumulated strengthening of the electric field, and hereby a shorter t_{delay}, i.e. a decreased E_{inc}. Moreover, it used to be the streamer breakdown taking place in the defect, with an inception voltage that is usually 5% higher than the Paschen curve. With the defect being deteriorated by the impulses, Townsend breakdown starts to occur with the inception voltage being coincident with the Paschen curve [42]. As a result, the PDIV becomes lower than before, leading to E_i above E_{inc}. Thus, the initiated PD can be sustained by the AC voltage.

5.6 Conclusions

The PD behaviour in artificial defects in MV XLPE cable models under impulse transients were investigated. An experimental set-up was designed and built to measure partial discharges in MV cable under superimposed transients. Measurements were firstly performed with the built-up experimental set-up to verify its function and the results show that:

- The experimental set-up is able to withstand the impulses in MV level.
- The PD measuring system is able to keep measuring and acquiring signals during the impulse application without being interrupted or damaged.
- The PD measuring system is able to measure PD under superimposed transients with enough time resolution if any PD occurs.
- The PD measuring system is able to accurately recognize PD pulses from other discharge and disturbance pulses by means of the phase-resolved pulse pattern, the time-resolved pulse shape and the dominant frequency of pulses.

The cable models with different defects were subjected to an AC voltage which was below PDIV without generating PD. When applying impulses, different scenarios of PD initiation and development have been observed:

- No PD could be initiated by the impulse transients.
- PDs were initiated by the impulses in the impulse period, and extinguished when the impulse stopped.
- PDs were initiated by the impulses in the impulse period. The initiated PDs recurred intermittently and persisted actively under AC voltage when the impulse was gone.
- PDs didn't initiate during the application of impulses but initiated under AC voltage when the impulse was gone.

In addition, it is observed that the initiation of PD partially depends on the AC voltage level and the peak value of the superimposed voltage, as well as PDIV and PDEV. If the peak value of the superimposed voltage is significantly higher than PDIV, and the AC voltage is slightly lower than PDIV, PDs might be triggered and be sustained by the AC voltage after the transient. With the AC level getting further from PDIV and closer to PDEV, more superimposed voltages are needed to trigger PDs, and the triggered PD activities become less active and sustained.

The differences in PD behaviour under impulse transients are interpreted theoretically based on the local electric field condition, the charges in the defects, and the aging status of the insulation. According to the interpretation, the following processes occurred:

- PD cannot initiate because the initiatory electron is not available due to the stochastic generation of an electron by cosmic and background radiation.
- During the impulse moment, the local field E_i is sufficient to initiate PD. When the impulse is gone, E_i goes back to the original value which is not sufficient for PD initiation. And due to the charge decay, the field E_q cannot contribute to enhance the field E_i. As a result, PD extinguishes.
- After the impulse, E_q builts up by the charges deposited in the insulator traps, may stay and contribute to E_i. As soon as the initiatory electron is available, PDs initiate again. This leads to the intermittent recurrence of PDs.
- The application of impulses may contribute to a decrease in t_{delay}. As a result, PDs can be sustained by AC voltage after the impulses.

Therefore, we conclude the effects of impulse transients on PDs as following:

- When at operating voltage there is a non-discharging defect existing in the cable, especially in the cable accessories, PD can be initiated by the impulse transients.
- Once PDs being initiated by the impulses, the generated surface charges will increase the probability of PD occurrence by contributing to the local field and providing free electrons.
- The application of multiple impulses may decrease the PD inception delay time or accelerate the aging process, which can both result in PD occurrence.

Based on the effects of transients on PDs, risk warnings as following are given:

- The initiated PD may not lead to breakdown immediately, but may affect the degradation. In particularly, the PDIV may get decreased, which will cause more PD occurrence and accelerate the degradation. Moreover, such intermittent PDs can switch to sustained PDs, which endangers the cable insulation.
- The commissioning tests and the maintenance tests are usually performed to evaluate the cable insulation conditions after cable installation or cable operation. Cable systems which pass those tests will be put into service. However, there is still a risk existing: it happens in practice that defects can exist in the cable insulation system, which however are not detectable by the commissioning tests or the maintenance tests. According to the above conclusion, PD can be initiated by the impulses within certain defects. In case PDs are triggered by the impulses at the undetectable defects in the cable system, situations with higher risk as discussed above can be resulted in. Such risk situation of PD being initiated within the defects in the cable system, which are not detectable during commissioning tests or the maintenance tests, are to be investigated in the HV cable system in Chapter 6.

Chapter 6

Methodology for Partial Discharge Measurement in HV Cable Model under Transients

In chapter 5, the effects of the superimposed transients on MV cable models with an artificial joint defect have been investigated and discussed. Superimposed transients initiated partial discharges, which developed into different scenarios under AC voltage after the transient was finished. In chapter 6 and chapter 7, we investigate the HV cable insulation system, when exposed to transients. A methodology for partial discharge measurement in HV cable models under transients is presented in chapter 6, including the experimental set-up, measurement of PDs using the set-up, and the interpretation of the measured PDs. Similar experimental set-up as used in the MV cable tests is applied with certain adjustments to fulfil the purpose of testing at high voltage level. Since HV cable accessories are considered to be the most vulnerable location for a hidden insulation defect to occur, a HV cable model is prepared as the test object, which consists of a HV cable section, two terminations and a joint with controlled defect size. For measuring partial discharges, a PD measuring system according to the unconventional method (section 3.2.4) is investigated and implemented, which enables PD measurement during high-level impulses and discrimination of PDs from disturbances. By interpreting the PDs measured by the set-up, we learn about the characteristics of PDs from the cable joint as well as how to properly use the experimental set-up. The presented methodology is applied to investigate the effects of transients on PDs in the HV cable model, when subjected to different impulse voltages and superimposed transient voltages. This will be presented in chapter 7.

6.1 HV Cable and Accessories with Insulation Defects

6.1.1 HV cable and accessories

The HV cable model used as the test object consists of a 16-meter long 150 kV XLPE extruded power cable, two terminations and one joint. The cable structure is shown in Figure 6.1. Some important data

This chapter is based on:
J. Wu, A. Rodrigo Mor, P. V. M. van Nes, J. J. Smit, "Measuring method for partial discharges in a high voltage cable system subjected to impulse and superimposed voltage under laboratory conditions", International Journal of Electrical Power & Energy Systems, vol. 115, Feb. 2020.

of the HV cable are given in Table 6.1. With 0.24 µF/km operating capacitance (Table 6.1), the total capacitance of the cable section is 3.75 nF. The HV cable is terminated with two outdoor-type terminations, termination 1 and 2, and a pre-moulded joint in between, as shown in Figure 6.2. The cable joint is located ten meters from the termination 1. The cable is grounded at the cable terminations.

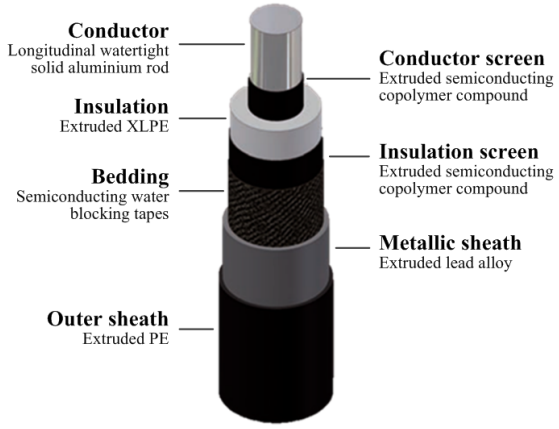

Figure 6.1: 150 kV XLPE insulated cable with its structure [117].

Table 6.1: 150 kV XLPE insulated cable data.

Rated voltage	U_0/U = 87/150 kV U_m = 170 kV U_p = 750 kV
Conductor material	Aluminium
Nominal cross-sectional area of conductor	1200 mm^2
Outer diameter with Al conductor	95 mm
Operating capacitance	0.24 µF/km

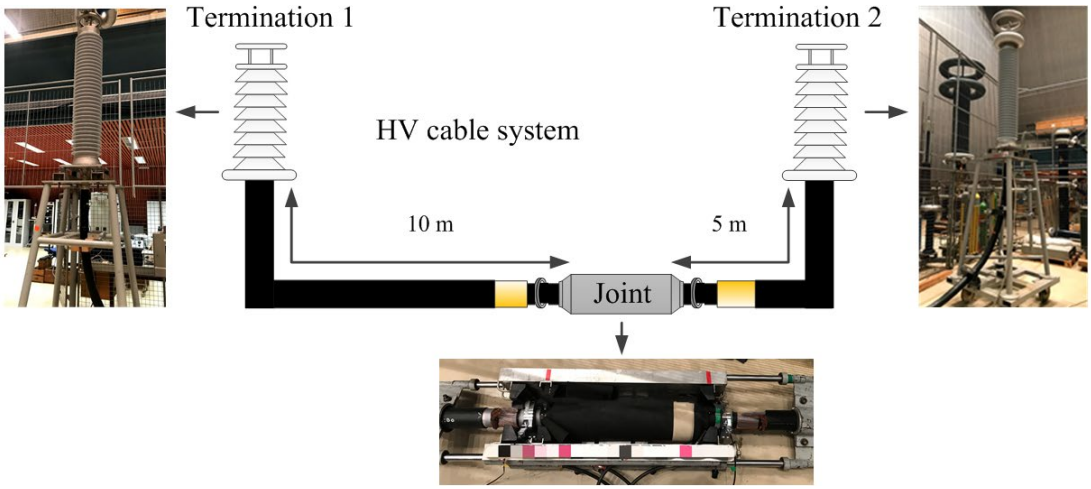

Figure 6.2: HV cable model: a XLPE cable installed with two terminations and a pre-moulded cable joint in between.

6.1.2 Artificial insulation defects in the joint

In order to produce partial discharges in the HV cable model, an artificial defect was created by manipulating the joint. The connector in the joint was prepared in such a way that the cable can be pulled out of the joint at the side near to termination 2 for a certain distance (Figure 6.3). In practice, this outbound displacement of cable will not happen in a properly mounted cable joint. Whereas for laboratory testing, this defect can generate under AC voltage detectable partial discharges. We refrain from a definite interpretation of the defect and the cause of partial discharges, since the cable joint was not inspected for investigation after all the tests. With different outbound displacements of cable - by pulling the cable out for different distances D - partial discharges with different inception voltages (PDIV) and extinction voltages (PDEV) can be obtained, which are given in Table 6.2 as average values. Figure 6.4 shows the phase-resolved (PRPD) pattern of partial discharges measured at 108 kV_{rms} with a defect dimension due to an outbound displacement D of 7 mm.

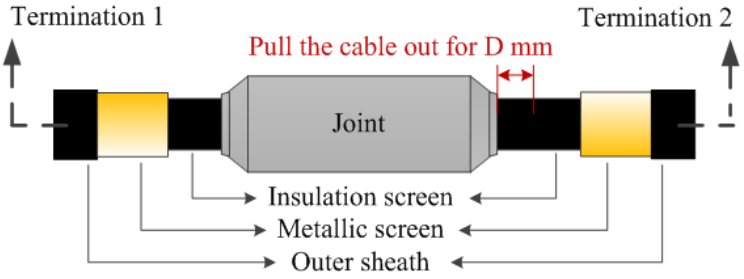

Figure 6.3: Artificial defect introduced in the HV cable joint.

Table 6.2: Average PDIV and PDEV of PD generated at different cable displacements.

Displacement D [mm]	PDIV [kV_{rms}]	PDEV [kV_{rms}]
14	47	32
9	83	58
7	104/97	90
6	150	139
0	PD free up to $1.8U_0$	

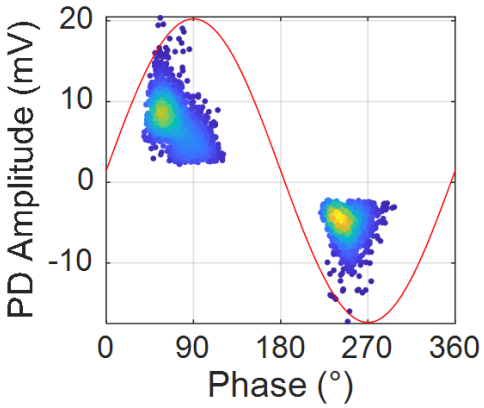

Figure 6.4: PRPD pattern pf PD measured at 108 kV_{rms} with a defect dimension D of 7 mm.

6.2 Experimental Set-up

The experimental circuit for investigating the effect of transients on the HV cable is similar to the circuit used for the MV cable measurement, which consists of the generation of superimposed transients, the test object (the HV cable system as discussed in section 6.1), and the PD measuring system (will be discussed in section 6.3). Figure 6.5 shows the schematic diagram of the experimental circuit. Values of all the elements are given except for the resistors in the impulse generator, which are adjusted according to the required waveforms of impulse voltages. In the investigation, the HV cable system was tested under 50 Hz AC voltage, impulse voltage and superimposed voltage. For testing under impulse voltages, part of the circuit denoted by the grey area in Figure 6.5 was connected. For testing under superimposed voltages, the entire circuit was connected. To localize and measure PD in the HV cable system, an unconventional PD measuring system was installed at the cable joint. A conventional PD measuring system applying IEC standard was also used. Figure 6.6 shows the schematic diagram of the set-up and the physical set-up built in the HV lab based on Figure 6.5.

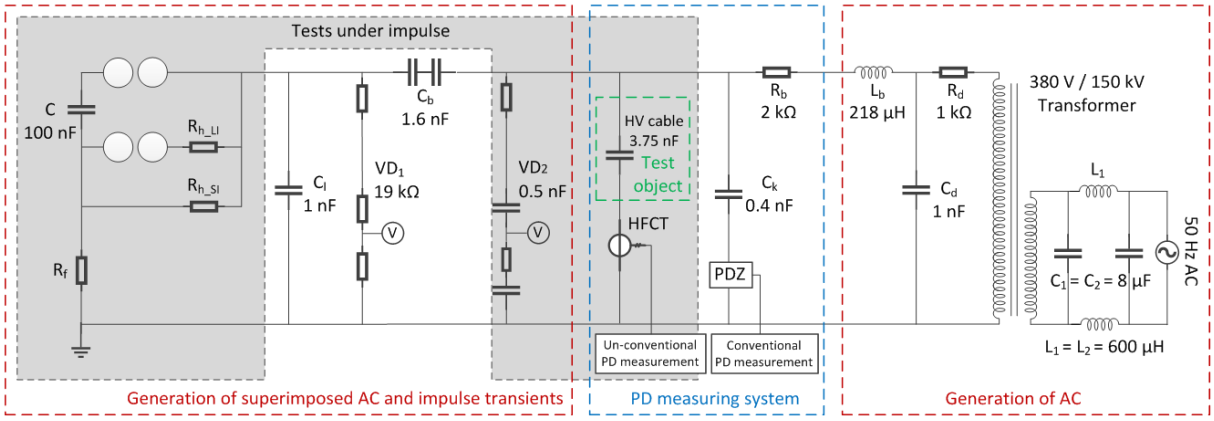

Figure 6.5: Experimental circuit for testing HV cable model under transients.

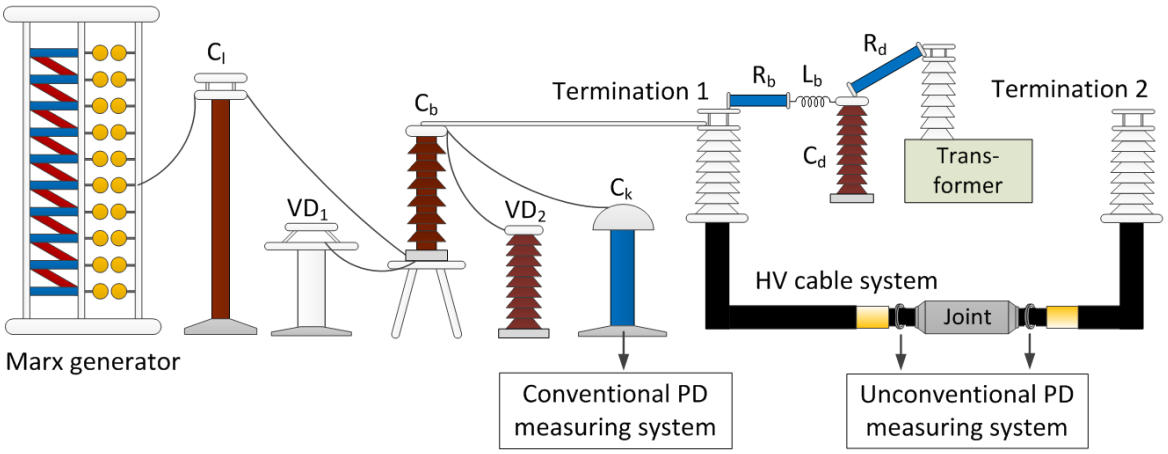

a)

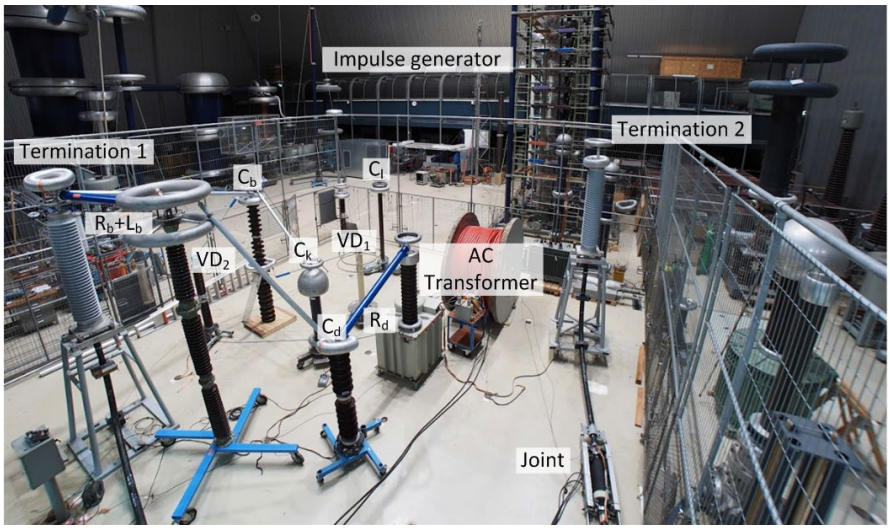

b)

Figure 6.6: Experimental set-up: a) schematic diagram of the set-up, b) physical set-up built in the HV lab.

6.2.1. Generation of impulse and superimposed transient voltages

The experimental circuit is able to provide 50 Hz AC voltage, impulse voltage and superimposed voltage. The principle of the experimental circuit is the same as that for testing the MV cable.

To supply AC voltage, a 380 V/150 kV AC transformer was connected to the HV cable. A LC low-pass filter (L_1, L_2, C_1, C_2) was added at the low-voltage side of the transformer to filter out the line noise (Figure 6.5).

For testing the 150 kV cable system with impulse voltages, five stages of the Marx impulse generator were used. The total discharge capacitance C of the five stages is then 100 nF. Different impulse waveforms, i.e. different front time T_f and time to half value T_h, can be generated by adjusting the front resistor R_f and the tail resistors R_h_LI and R_h_SI. Since T_f and T_h are also influenced by the total load capacitance in the circuit, the additional capacitance C_l of 1 nF was still connected in order to reach a longer front time without using a too large R_f.

For generating superimposed voltages when the AC transformer and the impulse generator were both connected to the cable, a 1.6 nF blocking capacitor C_b together with a 2 kΩ resistor R_b were connected between the AC supply and the impulse supply, so that the AC voltage will not stress on the impulse generator (Figure 6.6). This attenuates the AC voltage at the impulse generator and allows the impulse voltage to be superimposed on the AC voltage at the cable. The AC transformer was protected against the impulse voltages by a RC low-pass filter (R_d, C_d). One voltage divider VD_1 was used to measure the generated impulse voltages at the impulse generator, and another VD_2 served to measure the composite voltages at the cable termination 1.

The settings of the impulse generator for generating different impulses are given in Table A.1in the Appendix.

6.2.2. Test waveforms

The HV cable system model was tested under AC voltage, impulse voltage and superimposed transient voltage. In the impulse test, the impulse voltage waveforms (Figure 6.7a), with different peak values V_{peak}, front times T_f and times to half value T_h, were applied to the HV cable system. In the superimposed transient voltage test, superimposed voltage waveforms as shown in Figure 6.7b were applied. Due to the limitations as mentioned in section 5.2.2, it is difficult to generate the same transient waveform as the real one shown in Figure 2.4a. Thus, the simplified but representative superimposed waveform was used to test the HV cable insulation system. In Figure 6.7b, an impulse voltage with front time T_f and time to half value T_h is riding on the AC wave crest. The total peak value V_{peak} of the test voltage is the combined value of the AC peak value V_{ACpeak} and the superimposed impulse voltage. During the test, the parameters such as the front time T_f, the time to half value T_h, the AC peak value V_{ACpeak}, the total peak value V_{peak}, as well as the phase angle at which the impulse was superimposed on the AC voltage, were varied in order to study their effects on the HV cable system.

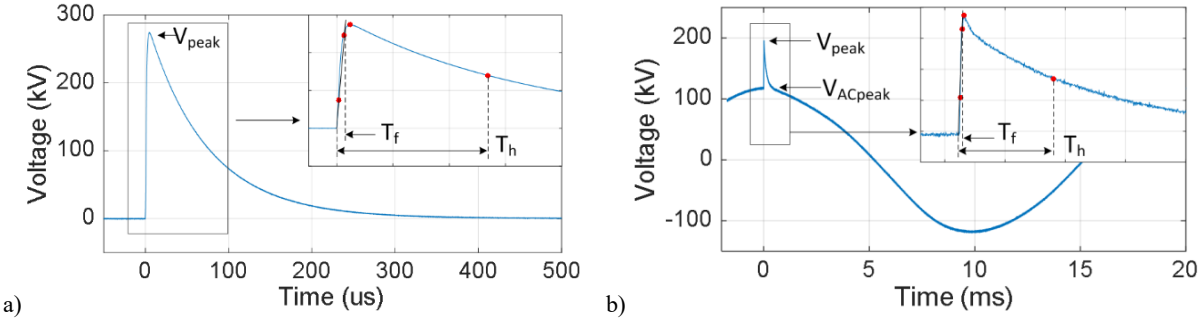

Figure 6.7: Test voltage waveforms: a) impulse voltage, b) superimposed voltage.

6.3 PD Measuring System

The unconventional method was again applied for the PD measurement in the HV cable system. PD signals were measured by high frequency current transformers together with filter/suppressor protection units, and then acquired by the oscilloscope. After analysis, the PD data were presented as time-resolved PD pulses (TRPD), phase-resolved PD pattern (PRPD) and by typical PD parameters.

6.3.1 PD sensors

Two identical high frequency current transformers (HFCT) were used as PD sensors to detect PD from the cable joint, with a gain of 3 mV/mA and a bandwidth of 100 kHz - 40 MHz [118]. The two HFCTs were mounted at both ends of the joint with the same polarity, as shown in Figure 6.8. The one near to termination 1 is named as HFCT 1, and the other one near to termination 2 is named as HFCT 2. When the PD occurs externally to the cable joint, i.e. from the cable section near termination 1 or termination 2, the PD signals measured by HFCT 1 and HFCT 2 from PD event have the same polarities and similar magnitudes. If the PD occurs in the cable joint, the PD is generated between the two HFCTs and splits propagating in both directions. In this case the PD pulses measured by HFCT 1 and HFCT 2 have opposite polarities and similar magnitudes. By using this polarity recognition, it is possible to discriminate between discharges produced in the joint and outside the joint.

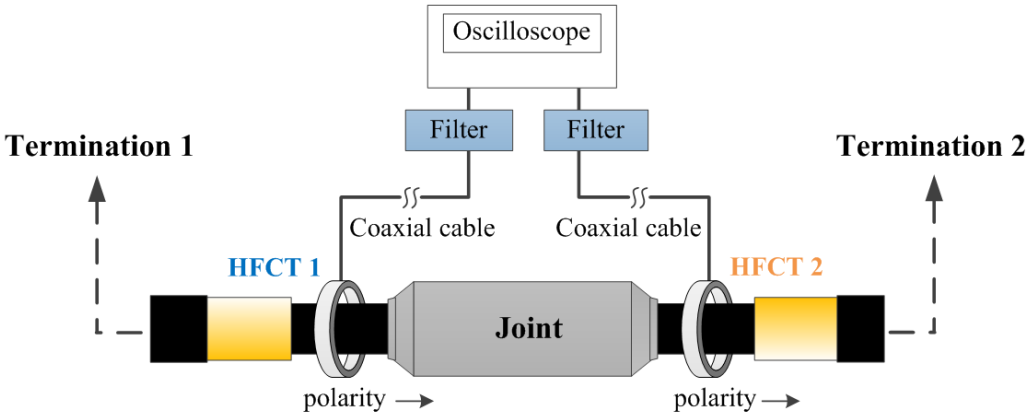

Figure 6.8: Two HFCTs installed at two ends of the cable joint.

During the application of impulse voltages, the inrush currents in the cable system induce a high voltage signal in the HFCTs, which is regarded as disturbance during the PD measurement. Figure 6.9 presents the disturbance measured by the HFCT during the application of the impulse. The signal was measured with a HV probe. The applied impulse has a waveform as shown in Figure 6.7a with V_{peak} of 274 kV and T_f / T_h=3 / 2000 µs. As shown in Figure 6.9, the amplitude of the measured disturbance is in the range of kilovolt, which far exceeds the maximum input voltage of the oscilloscope. Such large disturbance will cause a damage to the oscilloscope. Therefore, in order to protect the oscilloscope, a filter/suppressor protection unit, named 'Filter', was applied before the oscilloscope (Figure 6.8). A transient voltage suppressor (TVS) together with a spark gap (SG) were used to clip the voltage at 12 V. A band-pass filter was added before the TVS and the spark gap. All the three elements are integrated in one box.

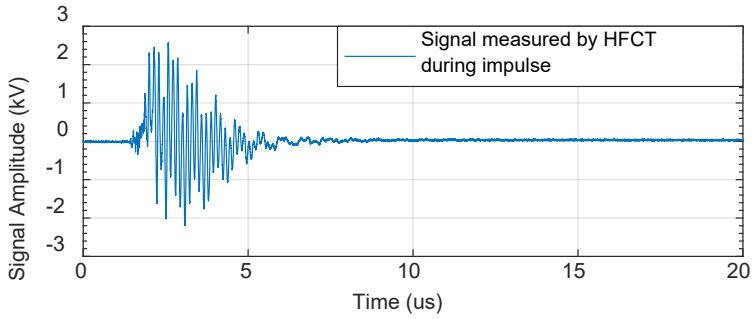

Figure 6.9: Signal measured by HFCT during the impulse with V_{peak} = 274 kV and T_f / T_h=3 / 2000 µs.

Two configurations using such unit were applied in the measurements, which are illustrated in Figure 6.10. In configuration I, only one unit was used before the oscilloscope. The filter A in it has a bandwidth of 114 kHz - 48 MHz, which helps to reinforce the power attenuation outside the sensor's bandwidth. The physical configuration I is shown in Figure 6.10c. In configuration II, another unit was added before unit filter A, which also consists of a band-pass filter, a TVS and a spark gap. The filter B in it has a bandwidth of 1.38 MHz – 90.2 MHz. The transfer functions of the HFCT as well as the measuring system using configuration I and II are characterized by using the method in [119] and given in Figure 6.11. The two configurations have their own advantages and disadvantages, which will be discussed in the next and in section 6.4.1.

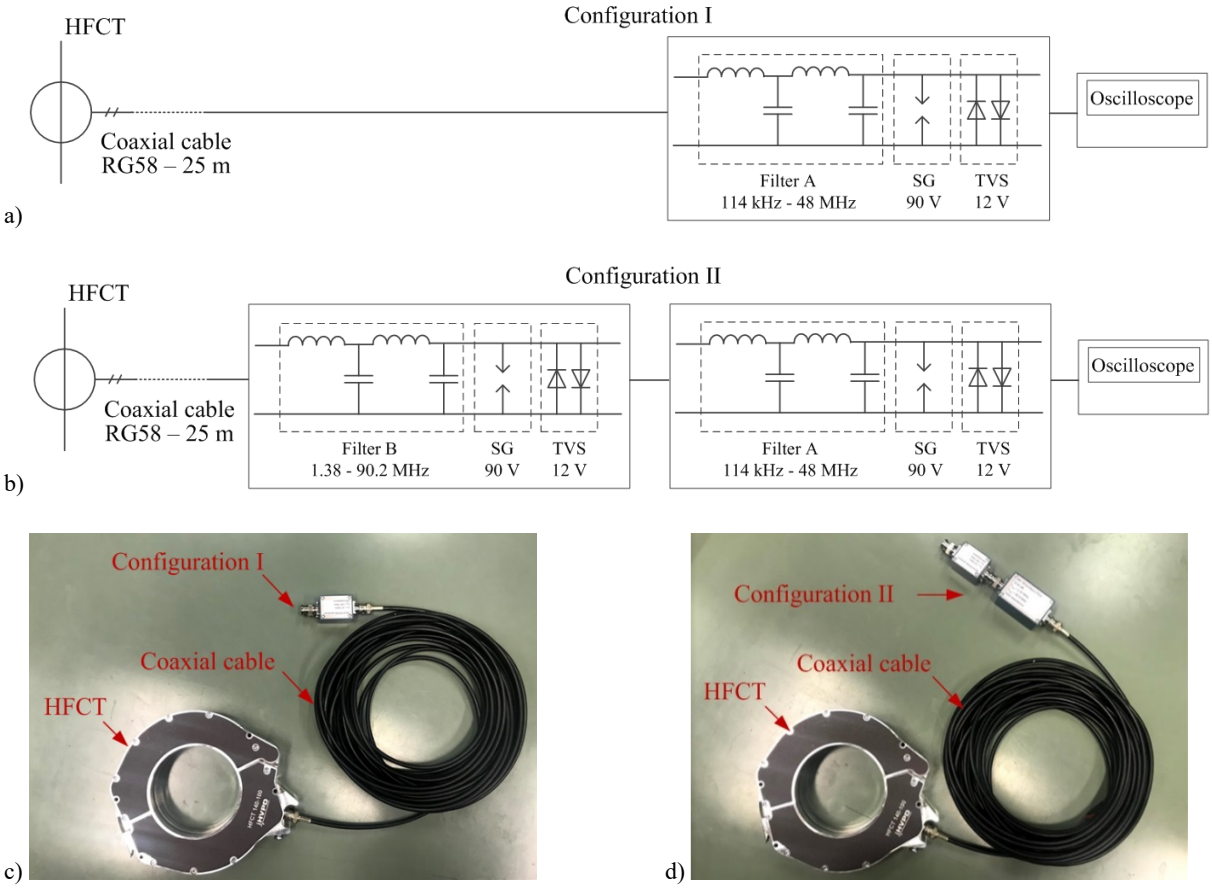

Figure 6.10: Configuration of the measuring system: a) configuration I, b) configuration II, c) connection of configuration I, d) connection of configuration II.

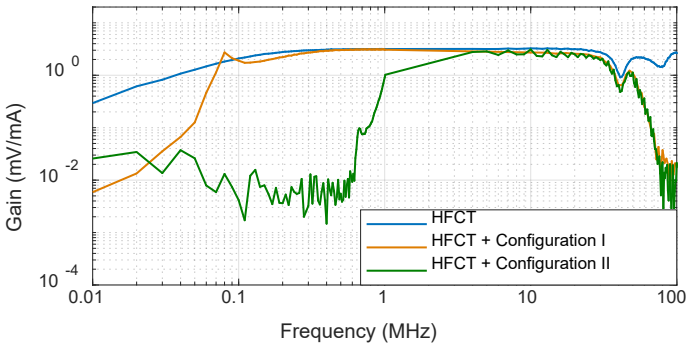

Figure 6.11: Transfer functions of the HFCT, HFCT + configuration I and HFCT + configuration II.

To evaluate the effectiveness of the units, signals were measured with the HFCT in two different configurations and applying the impulse voltage shown in Figure 6.7a with V_{peak} of 274 kV and T_f / T_h = 3 / 2000 µs. Figure 6.12 shows the measured signal in frequency and time domains. In the frequency domain (Figure 6.12a), the magnitudes of the disturbance measured with configuration I and II have been attenuated from tens of volt to tens of millivolt. In the time domain (Figure 6.12b), the disturbance, which used to be in the kilovolt range (Figure 6.9), now is in the volt range measured with configuration I. The large disturbance lasts for around 100-150 µs. This period is regarded as the detection dead zone, to be defined in Figure 6.13. The signals shown in Figure 6.13 were taken from a measurement in which the HV cable with artificial defect was subjected to the impulse (T_f / T_h = 3 / 2000 µs). During the impulse application, both disturbance and partial discharges were measured, as shown in Figure 6.13a. Once the impulse was applied, a large disturbance was captured, which started from 1000 µs. The disturbance is shown in Figure 6.13b for details. One partial discharge occurred at 4857 µs (Figure 6.13a) and is depicted in Figure 6.13c, with a pulse amplitude of around 20 mV. It will be seen in the later section 6.4.1 that, the generated partial discharge signals have amplitudes in the range of millivolts. In order to capture the PDs in the millivolt range, the vertical resolution in the oscilloscope was usually set in the range of several to tens mV/div. In this measurement, the vertical resolution was set as 5 mV/div, resulting in a vertical range of ±50 mV. With this vertical range, the disturbance is so large that it exceeds the vertical range. The time period that the signals exceed 80% of the vertical range is determined as detection dead zone. In Figure 6.13b the dead zone is 140 µs starting from 1000 µs and ending up at 1140 µs. If partial discharges, such as the one shown in Figure 6.13c, occur within the dead zone, the measured signal will be a superposition of the disturbance and the PD signals. In case PDs occurred at the moment where the disturbance was larger than the 12 V threshold of the TVS, the PD signals would be clipped. If PDs occurred when the disturbance was smaller than 12 V but larger than the vertical range set in the oscilloscope, they would still be clipped. Although PDs were within the observation window, it might be difficult to decouple them from the disturbance. As a result, partial discharges are undetectable if they occur within the dead zone. With configuration II, the disturbance has been suppressed and the dead zone has been reduced to around 40 µs (Figure 6.12b). This means, configuration II provides more chances to detect PD during the impulse application compared to configuration I.

It is possible to increase the vertical range in the oscilloscope. But in this case, the signal (in millivolt) to noise (in volt) level is too small so that it is still impossible to decouple the PD signals from the disturbance signals. Only if PDs occurred when the disturbance remained within the observation window, there was a chance to observe them. There are several options to cope with this issue. The signals can be measured with a higher threshold TVS, and a larger vertical range of the oscilloscope. However, in this way, the signal to noise issue still exists. Another option is to use a coaxial attenuator to attenuate the captured signals. Nevertheless, both the PD signals and the disturbance signals will be

attenuated. Thus, for measuring PD, using an attenuator is considered not suitable. Consequently, using configuration II is considered to be the best option.

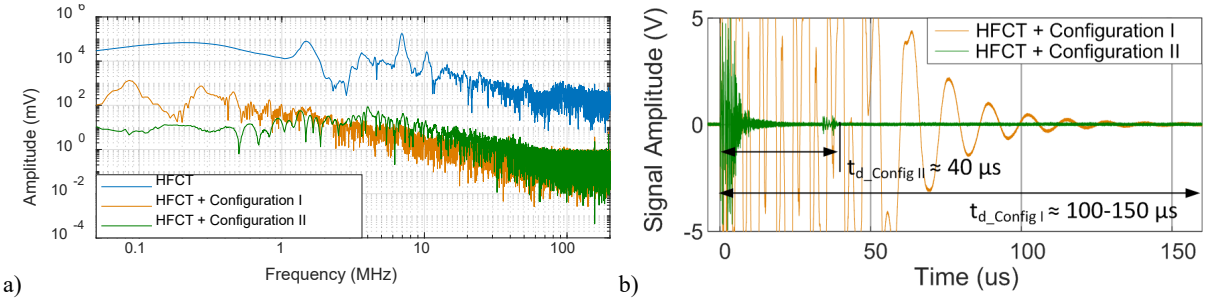

Figure 6.12: Disturbance during impulse (T_f / T_h = 3 / 2000 µs) application measured with different configurations: a) measured disturbance in frequency domain, b) measured disturbance in time domain shown on oscilloscope.

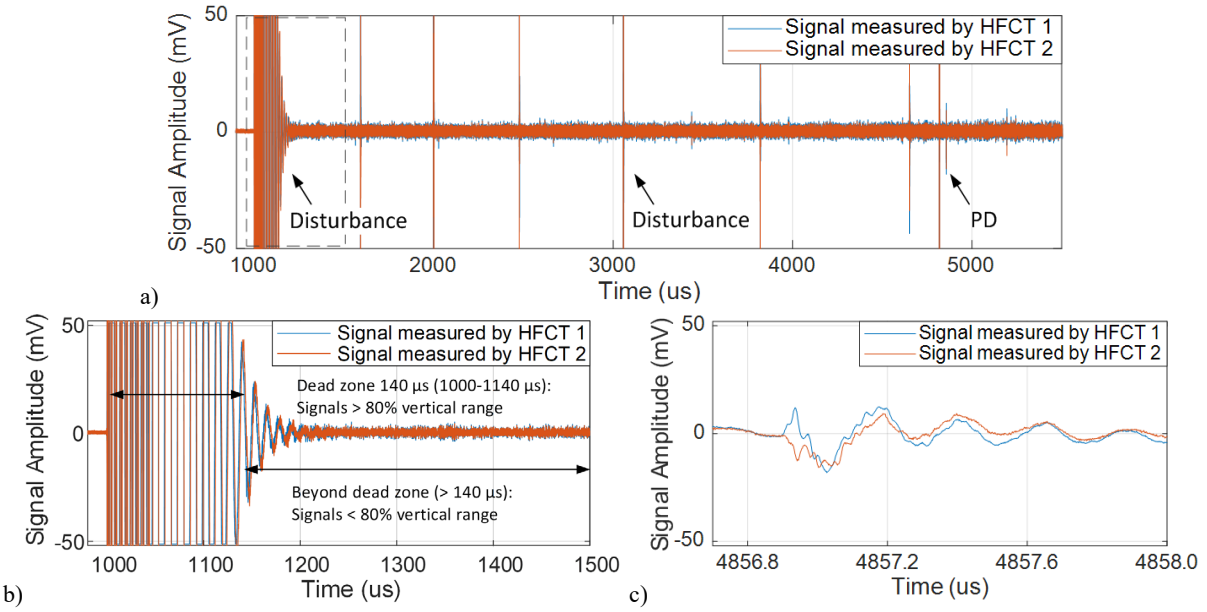

Figure 6.13: Signals measured during impulse (T_f / T_h = 3 / 2000 µs) application: a) measured disturbance, b) zoom-in of disturbance in a) with dead zone indicated, c) zoom-in of PD in a).

In the impulse tests, impulses with short front time and long front time were applied. For impulses with short front time, the dead zones resulting from both configurations are still longer than the front time, which may lead to obstruction in detecting partial discharges during the front time. For impulses with long front time, configuration II with smaller dead zone gives more chances to observe partial discharges if they occur during the front time. This is illustrated in Figure 6.14.

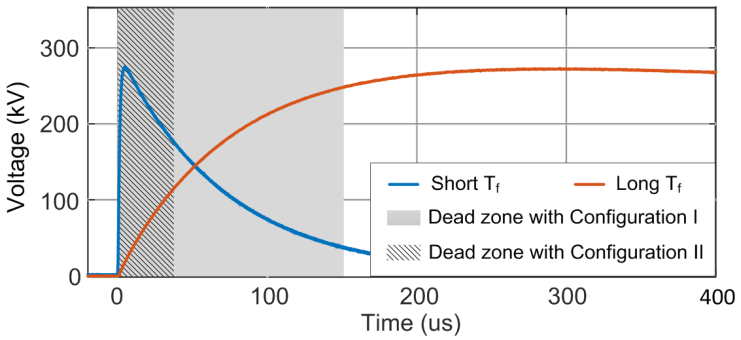

Figure 6.14: Dead zones of two configurations and impulses with different front times.

The disturbance was also measured under impulse voltages with different voltage values. With higher voltage and longer time of the impulse, the disturbance tended to have a larger amplitude and longer dead zone. In all cases, configuration II helped to suppress the disturbance and to decrease the dead zone.

6.3.2 PD signals acquisition

The PD signals captured by the two HFCTs were transmitted through two 20-meter identical coaxial cables and then acquired by a digital oscilloscope Tektronix MSO58. The transmission line was matched using an external 50 Ω coaxial resistor connected in parallel to the oscilloscope acquisition channel which is terminated with 1 MΩ. The PD acquisition channels were set with a bandwidth of 250 MHz, and the sampling frequency was set to 1.25 GS/s. The fast frame acquisition mode of the oscilloscope was used to collect all the captured signals with the time-resolved pulse shapes, timestamps, and phase angles with the help of a synchronization unit. The background noise was filtered out by setting the trigger level at 2.4 mV.

6.3.3 PD data analysis

The acquired PD data were analysed by PDflex [113]. The results were presented in phase-resolved PD patterns (PRPD), time-resolved PD pulses (TRPD) and typical PD parameters [114-115]. Clustering techniques were applied to separate PD from noise [120].

6.3.4 Verification of PD measuring system

To verify the PD measuring system if it is able to properly identify and measure partial discharges that occurring in the HV cable model, different types of pulses were injected in the cable model from different locations. Table 6.3 lists the verifying pulses and the test voltages under which they were tested.

Table 6.3: Verifying pulses and their testing voltages.

PD source		Locations	Test voltage
Injected pulse from calibrator	Single	Ternimation1 Termination 2	No voltage applied
	Dual	Cable joint	No voltage applied
Corona discharge under high voltage		Termination 1	AC = 16 kV_{rms}

Pulse injection verification (single and dual)

Pulses of 1 nC were injected from different locations to the HV cable model. Externally at terminations, pulses were injected from one termination to another termination, which flowed through the two HFCTs in the same direction. This is called single injected pulse. Internally to the cable joint, pulses were injected and flowed through the two HFCTs in bi-direction. This is called dual injected pulse. Figure 6.15 illustrates how these pulses were injected by the calibrator.

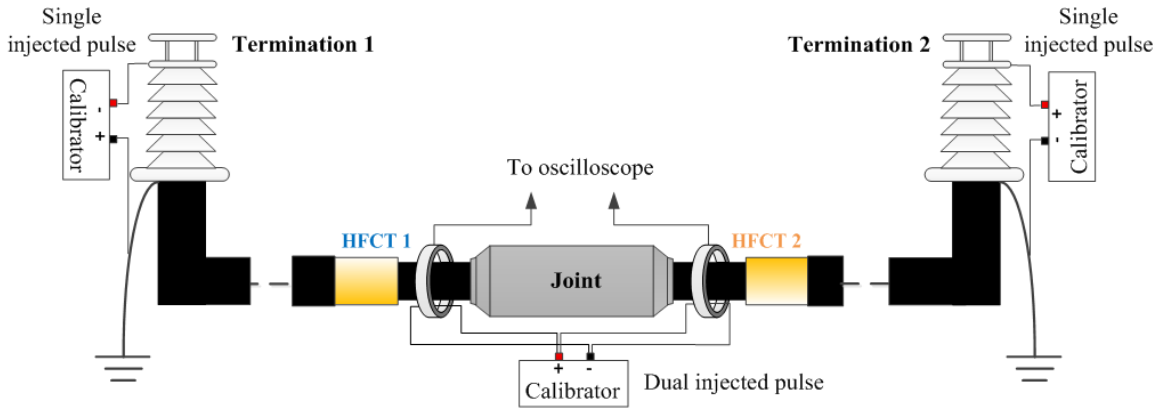

Figure 6.15: Pulses injected to the HV cable model by the calibrator.

The pulse signals recorded by HFCT 1 and HFCT 2 are shown in Figure 6.16. When the single pulse was injected from termination 1, the measured signals always have positive polarities and similar amplitudes, as shown in Figure 6.16a. When the single pulse was injected from termination 2, the measured signals show negative polarities, as shown in Figure 6.16b. In Figure 6.16c when the dual pulses were from the cable joint, the pulse captured by HFCT 1 shows a negative polarity while the pulse captured by HFCT 2 shows a positive polarity.

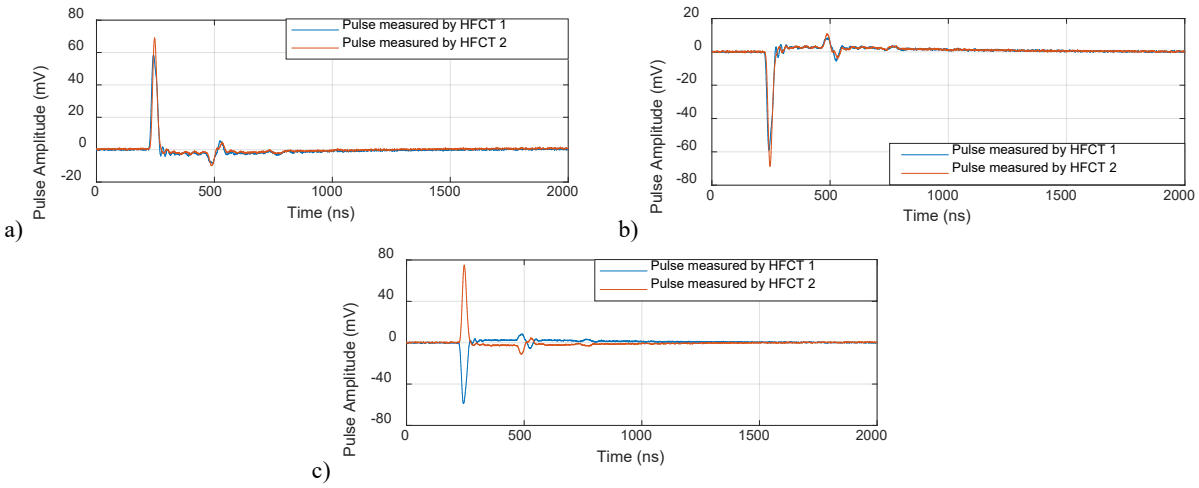

Figure 6.16: Injected pulses measured by HFCTs: a) pulse injected from termination 1, b) pulse injected from termination 2, c) pulse injected between two HFCTs.

With the injected pulses, the applied PD measuring system is able to indicate whether the pulses are internal or external to the cable joint by polarity recognition. If there are PD occurring in the joint while disturbances are produced outside the joint, such polarity recognition can also help to separate PD from disturbances.

Corona discharge

To test real PD external to the cable joint, corona discharge was generated by a metal needle installed at termination 1 under an AC voltage of 16 kV_{rms}. Figure 6.17a and Figure 6.17b show the PRPD patterns of the corona measured by HFCT 1 and HFCT 2. Both patterns indicate that the corona discharges occurred at the peak of the negative AC cycle. Figure 6.17c shows the TRPD pulses of one corona discharge measured by the two HFCTs. The two PD pulses have the same positive polarities. This indicates that the corona source is external to the cable joint and from the cable section near to termination 1, which conforms to the result of injected pulse as shown in Figure 6.16a.

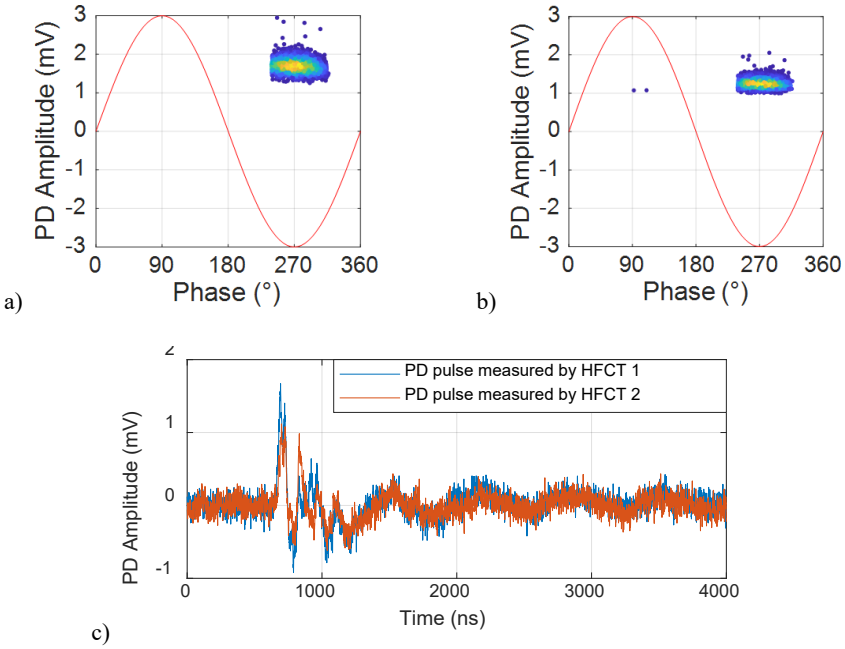

Figure 6.17: Corona discharge at termination 1: a) PRPD patterns of corona discharges measured by HFCT 1, b) PRPD patterns of corona discharges measured by HFCT 2, c) TRPD pulses of one corona discharge.

6.4 Measurement and Interpretation of PDs from HV Cable Model

The PD measuring system had been verified. Then the entire experimental set-up was examined to see whether it can properly measure partial discharges under high voltage impulse and superimposed voltage conditions, and whether the PD measurement could meet the requirements of the investigation purpose. The following questions are to be answered:

- Is the set-up able to withstand the impulse voltages, and the PD measuring system able to keep measuring and acquiring signals during the impulse application?
- If partial discharges from the cable joint occur during the impulses, is the set-up able to identify and measure them properly, and separate them from other disturbances?
- How to set up the acquisition properly?
- What are the circumstances to use filter configuration I and configuration II respectively?

To answer the questions, the set-up was tested with both filter configurations to:

- Measure partial discharges from the cable joint under AC voltage
- Measure partial discharges from the cable joint under impulse voltages
- Measure partial discharges from the cable joint under superimposed transient voltages

6.4.1 Measurement of PD under AC voltage

Measured with the PD measuring system (unconventional method)

The partial discharges generated by the artificial defect in the cable joint under AC voltage were measured with applying configuration I and configuration II. For both cases, the defect dimension – the outbound displacement of cable D - was set as 7 mm, and the AC voltage was set as 108 kV_{rms} which is higher than the PDIV of 104 kV_{rms} at 7 mm. The measurement results are shown in Figure 6.18 and Figure 6.19 respectively.

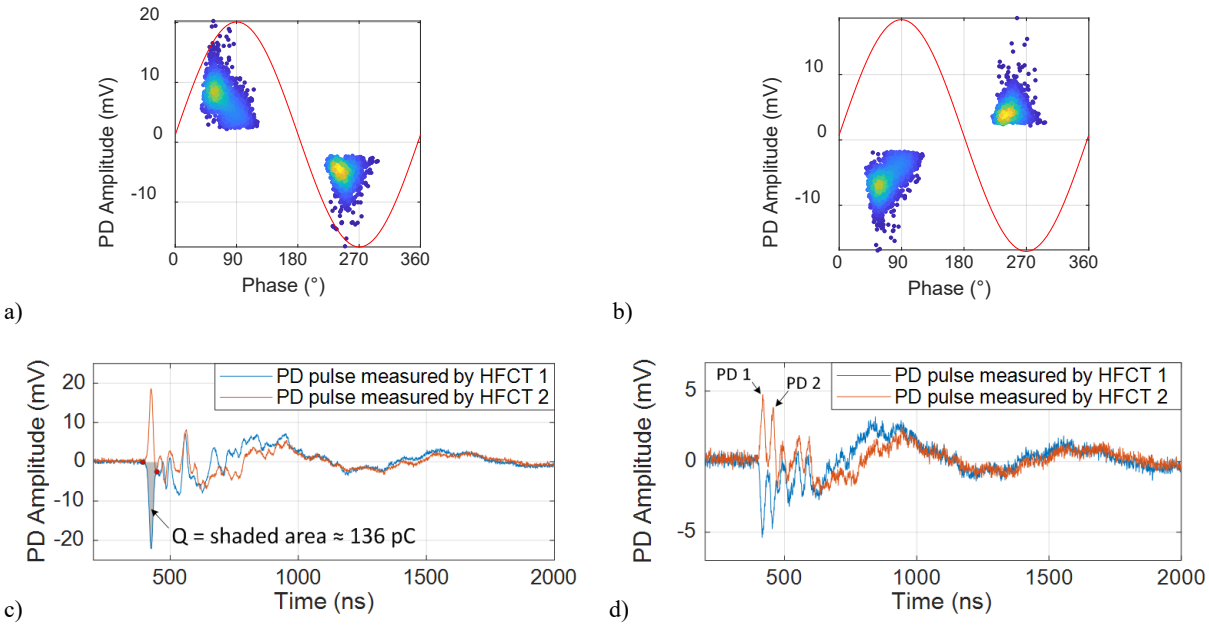

Figure 6.18: Partial discharges at 108 kV_{rms} measured with configuration I: a) PRPD patterns measured by HFCT 1, b) PRPD patterns measured by HFCT 2, c) TRPD pulses of one PD at negative cycle of 108 kV_{rms}, b) TRPD pulses of two partial discharges in series at 108 kV_{rms}.

The PRPD patterns of the partial discharges measured by HFCT 1 (Figure 6.18a) and HFCT 2 (Figure 6.18b) are mirrored. In other words, the signals measured by the two HFCTs from every discharge event always have opposite polarities, which confirms that the PDs originate from the cable joint. One partial discharge event, that occurred during the negative half cycle, is shown in Figure 6.18c in TRPD representation. The first peaks of both pulses having opposite polarities reach the peak values at the same time. After the first peak, both pulses start to oscillate with attenuation and become in phase due to the circuit configuration and cable reflections. Based on the pulse characteristics, only the first peak of each pulse was used to analyse the PD information. Due to the opposite polarity, these two pulses indicate that the partial discharge source is localized in the cable joint. Since the duration of the first peak is in the range of 40 to 50 ns, two PDs within a time interval longer than 40 ns should be detectable. Figure 6.18d shows a case in which two PD events occurred in series with a time interval of 40 ns.

It is worth mentioning that since the magnitude of the partial discharges is in the order of millivolts, the partial discharges would not be clipped by the TVS.

The apparent charge (measured in pC), which is the integrated PD current pulse, is usually used as the PD magnitude in conventional PD measurement. With un-conventional method, the measured PD signal is the induced PD current. Theoretically, it is possible to estimate the PD charge based on the PD current. Figure 6.18c also gives an estimation of the charge magnitude of the PD pulse measured by HFCT 1. The apparent charge Q, with estimated value of 136 pC, is calculated as the integral of the first peak over time by applying the method in [114-115]. Such estimation is valid when the PD pulse is not critically affected. However, since the cable length under test is quite short, the impact on PD pulse shape increases a lot due to pulse propagation and reflections. This situation will be shown in later sections. In such case, the estimation of apparent charge is not accurate any more. Consequently, the calibration of PD value based on the measured PD pulse becomes difficult. Thus, we directly use the voltage amplitude of the first PD pulse to describe the PD level instead of the charge magnitude.

With configuration II, the PRPD patterns of the partial discharges measured by HFCT 1 (Figure 6.19a) and HFCT 2 (Figure 6.19b) are also oppositely. The TRPD pulse shapes of one PD event is given in Figure 6.19c. The opposite polarity appears at the first peak and the reversed at the second peak.

Afterwards the two pulses oscillate in phase. Based on this feature, given the case as shown in Figure 6.19d, PD 2 was recognized as another PD event right after PD 1 instead of the residual oscillation of PD 1.The shape distortion produced by the configuration II doesn't jeopardize the pulse polarity recognition.

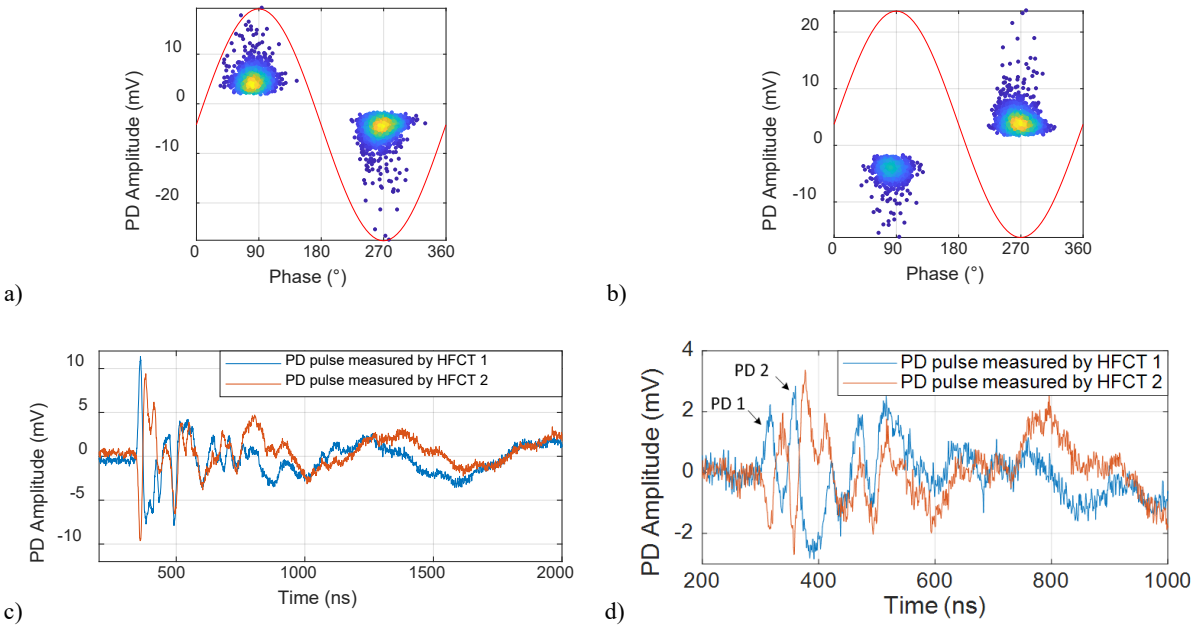

Figure 6.19: Partial discharges at 108 kV_{rms} measured with configuration II: a) PRPD patterns measured by HFCT 1, b) PRPD patterns measured by HFCT 2, c) TRPD pulse shapes of one PD event, d) TRPD pulse shapes of two PD events in series.

Using configuration II may lead to a decrease in the measured PD amplitude. Figure 6.20 shows the pulses of one PD event simultaneously measured with configuration I and II under 108 kV_{rms} AC. By using configuration II, the amplitude of the measured PD signal has been decreased around 50%. In case the decreased signal is close to the trigger level, it is very likely that this PD signal will not trigger the acquisition. As a result, using configuration II may influence the detection of small PDs.

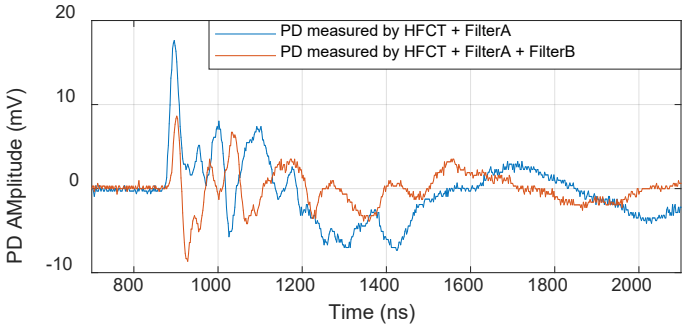

Figure 6.20: Pulse shapes of one PD event measured with Configuration I and Configuration II.

Measured with conventional method

As stated in [121], depending on the test object and the PD measuring system there is no obvious correlation between the apparent charge level measured with the conventional and the unconventional methods. Moreover, in short cables the PD measurements are affected by the multiple PD reflections which makes the calibration process difficult. However, to provide some reference information, a conventional PD measuring system was also applied in the test circuit to measure PD under the same AC condition. A 400 pF coupling capacitance C_k was connected to the cable termination 1 (Figure 6.6). A Haefely DDX9101 PD detector complying with IEC 60270 [72] was used to measure PD through a

PD coupling impedance PDZ. The PD measurement result acquired by the conventional method is given in Figure 6.21. For the same defect dimension and the same AC condition of 108 kV_{rms} as in Figure 6.18, Figure 6.21 shows a comparable PRPD pattern to Figure 6.18a and Figure 6.18b. The average discharge magnitude of 514 pC, which was measured with a filter bandwidth of 50 kHz – 400 kHz, which is in the same order of magnitude as the estimated charge value as shown in Figure 6.18c. In addition, the conventional PD calibrator also helped to check the sensitivity of the PD measurement. A sensitivity around 10 pC was reached by diminishing calibration pulses injected into the cable system until it cannot be observed.

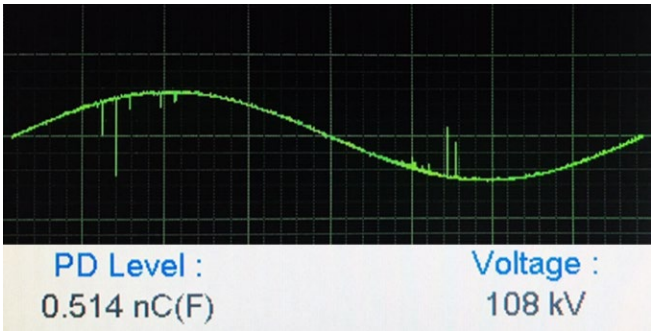

Figure 6.21: Partial discharges at 108 kVrms measured by conventional method.

6.4.2 Measurement of PD under impulses

In section 6.4.1, the experimental set-up has been determined to be able to identify partial discharges from the cable joint with the help of the polarity recognition. The PD characteristics from the cable joint have been collected as well. To further evaluate the intended capability of the PD measuring system under impulses, the cable system was then tested under impulse voltage waveforms (Figure 6.7a). The test voltages with their parameters are given in Table 6.4.

Table 6.4: Impulse voltages for testing HV cable system

Waveform	Test	T_f / T_h [µs]	Values [kV]		Filter unit
			V_{ACpeak}	V_{peak}	
Impulse	1	3 / 56	-	274	Configuration I
	2	3 / 2000	-	274	Configuration I
	3	300 / 2650	-	274	Configuration II

In test 1, a short impulse voltage with T_f = 3 µs and T_h = 56 µs was firstly applied on the cable. Configuration I was used for the PD measuring system. The observed PDs under this impulse are shown in Figure 6.22 with their polarities and amplitudes. The presented PDs were measured by HFCT 1, with which the polarity of measured PD is the same as the polarity of the applied voltage (see Figure 6.19). All PDs were detected on the wave tail with negative polarities, which are referred to as reverse discharges (RD) according to Densley [23]. The pulse shapes of the reverse discharges RD7 and RD8 measured by the two HFCTs are given in Figure 6.22b. The pulse measured by HFCT 1for RD7 and RD8 are both negative. The opposite polarities for each PD event as observed by HFCT 2 confirm that the discharges originate from the cable joint internally.

The impulse application generated a lot of disturbance which was also captured by the HFCTs. Figure 6.22c shows typical disturbances. The two signals from the two HFCTs are always in phase, which indicates that the disturbance is external to the cable jonit. Such polarity recognition contributes to separate PD from disturbance in the analysis stage.

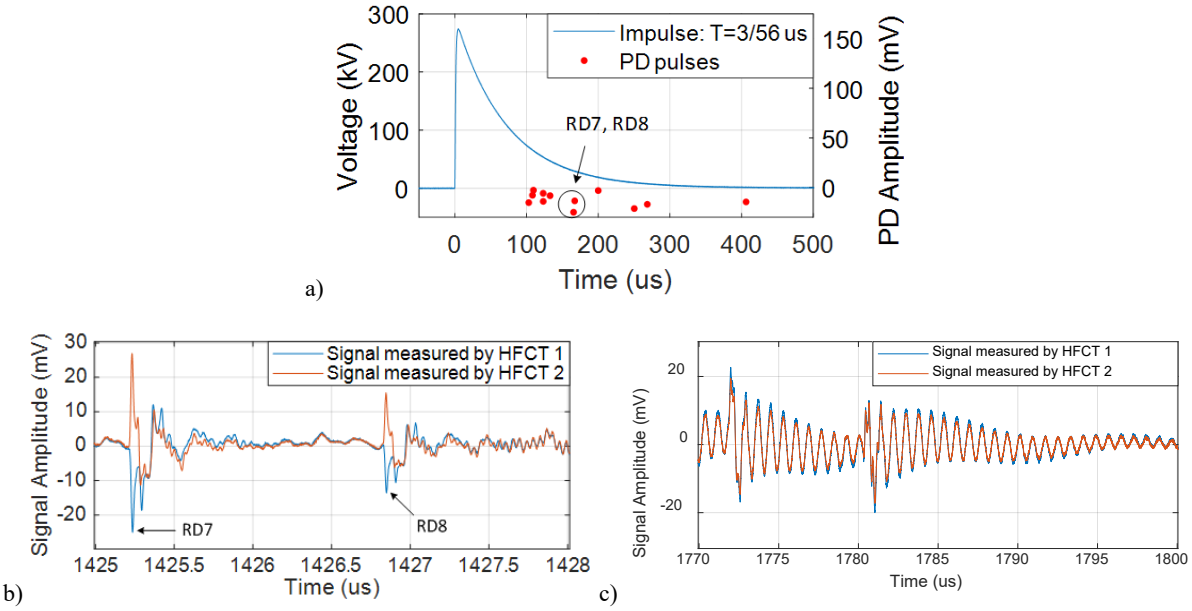

Figure 6.22: PD under impulse voltage in test 1: a) PD occurrence measured under impulse, b) TRPD pulses of partial discharges RD7 and RD8 under impulse voltage, c) time-resolved pulses of measured disturbance under impulse voltage.

In test 2, a longer impulse voltage with T_f=3 µs and T_h=2000 µs was applied to the cable. Configuration I was still in use. The observed PDs are shown in Figure 6.23a. Similar to test 1, PDs were only detected on the wave tail with negative polarities. Figure 6.23b shows the pulse shapes of the three reverse discharges RD5, RD6 and RD7, which occurred in series.

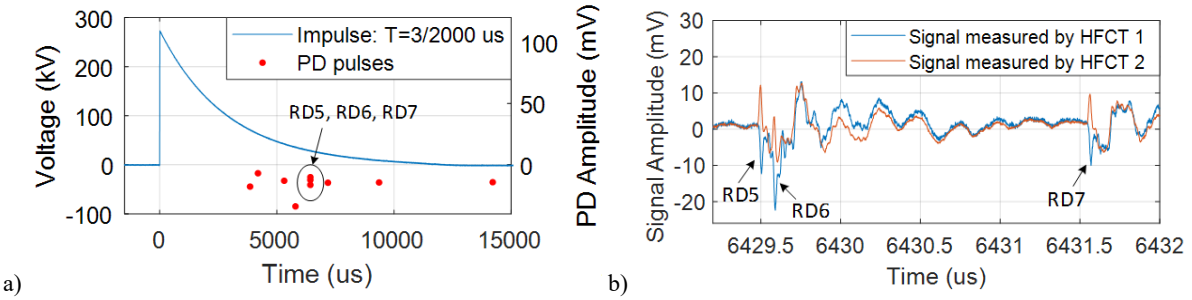

Figure 6.23: PD under impulse voltage in test 2: a) PD occurrence measured under impulse, b) TRPD pulses of RDs measured under impulse voltage.

Test 1 and test 2 show that, the PD measuring system is able to measure signals, including PD and disturbance, during the impulse application. Moreover, using the pulse shape and pulse polarity, it is possible to identify PD from the cable joint and separate PD from disturbance.

According to Densley [23], PD initiates at the impulse both during the front time and the tail time. PD occurring during the front time near the peak of the impulse is referred to as main discharge with positive polarity. PD occurring during the tail time is referred as reverse discharge with negative polarity. However, in both test 1 and test 2, only reverse discharges (RD) were detected during the tail time. No main discharges (MD) have been observed during the front time. This obstruction in observing PDs during the front time of impulses is due to the large disturbance generated by the impulse application (Figure 6.9). When there is this disturbance, the signal captured by the HFCT is a superposition of the induced disturbance and the PD signals. In section 6.3.1, two configurations of filter unit were proposed in order to protect the equipment. In test 1 and test 2, configuration I was used, which filtered and clipped the captured signal. The PD magnitude is in the order of milivolt measured with configuration I (Figure

6.18). Therefore, for measurement purpose, the vertical range on the oscilloscope was set to 20-30 mV/division and the signal was then clipped as well by the vertical range. In the end, the signal on the oscilloscope displayed a large disturbance being clipped lasting for the dead zone period. After the dead zone, the disturbance was gone and the PD signals could be observed clearly. This has already been explained in section 6.3.1. Based on the performance shown in Figure 6.12b, using configuration II will lead to a smaller dead zone and hereby more chance to observe PDs during the front time. However, the dead zone of configuration II is still not enough for testing the short impulses applied in test 1 and test 2 (Figure 6.14). Therefore, a longer impulse with T_f = 300 µs and T_h = 2650 µs was applied in test 3, where configuration II was used. The observed PDs are shown in Figure 6.24a. In this test, main discharges with positive polarities were detected during the front time near the impulse peak at 237.4 µs and 239.7 µs, indicated as MD1 and MD2. During the impulse tail time, more reverse discharges occurred. Figure 6.24b shows the pulse shapes of the two main discharges MD1 and MD2. Figure 6.24c shows one reverse discharge RD6.

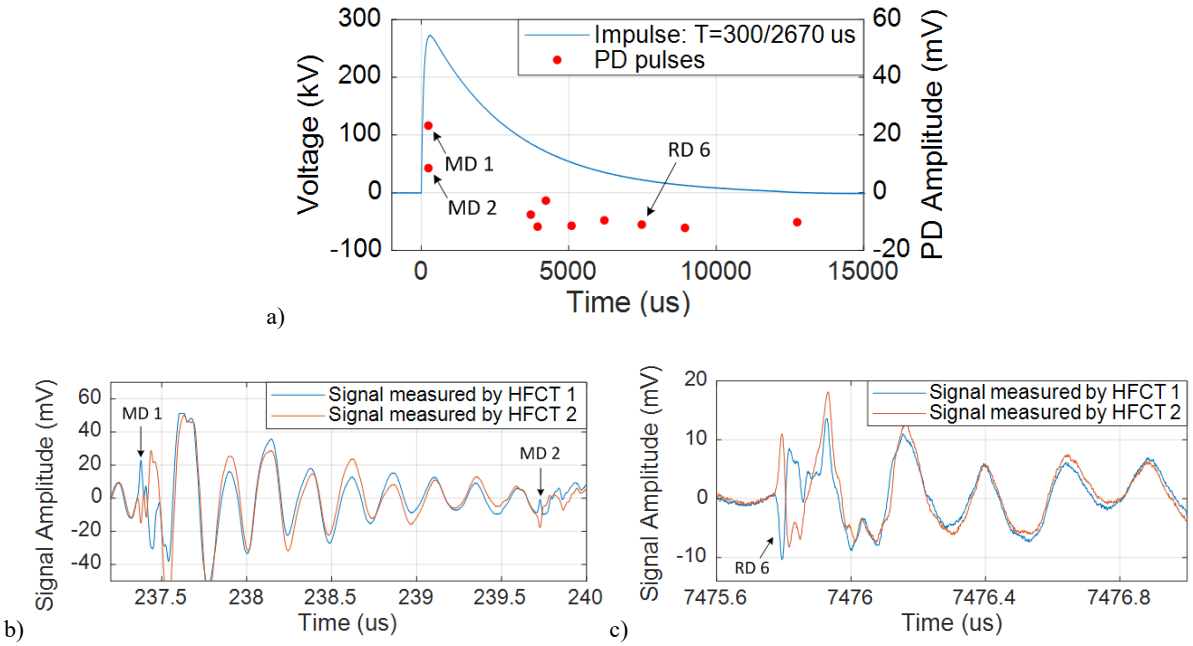

Figure 6.24: PD under impulse voltage in test 3: a) PD occurrence measured under impulse, b) TRPD pulses of MD1 and MD2 measured under impulse voltage, c) TRPD pulses of RD6 measured under impulse voltage.

6.4.3 Measurement of PD under superimposed transients

In 6.4.3, the HV cable system and the PD measuring system were tested under the impulse voltage waveforms. In this section, they were subjected to the superimposed voltages (Figure 6.7b). The test voltages with their parameters are given in Table 6.5.

Table 6.5: Superimposed voltages for testing HV cable system

Waveform	Test	T_f / T_h [µs]	Values [kV]		Filter unit
			V_{ACpeak}	V_{peak}	
Superimposed voltage	4	3 / 91	124	196	Configuration I
	5	93 / 714	124	196	Configuration I
	6	93 / 845	124	194	Configuration II

In test 4, configuration I was used in the PD measuring system. The AC voltage was set at 124 kV_{ACpk}, which is the nominal operating voltage of the cable system. Since this AC voltage is below the PDIV of 147 kV_{ACpk}, no PD would occur. The applied impulse voltage with T_f= 3 µs and T_h= 91 µs made the superimposed voltage to reach to a peak value of 196 kV_{pk}, which is well above the PDIV. During the test, the AC voltage was continuously applied before the impulse, under which no PD occurred. Then the impulse was superimposed on the AC voltage. After the impulse, the AC voltage was continuously applied until no more PDs were observed. The measurement results are shown in Figure 6.25.

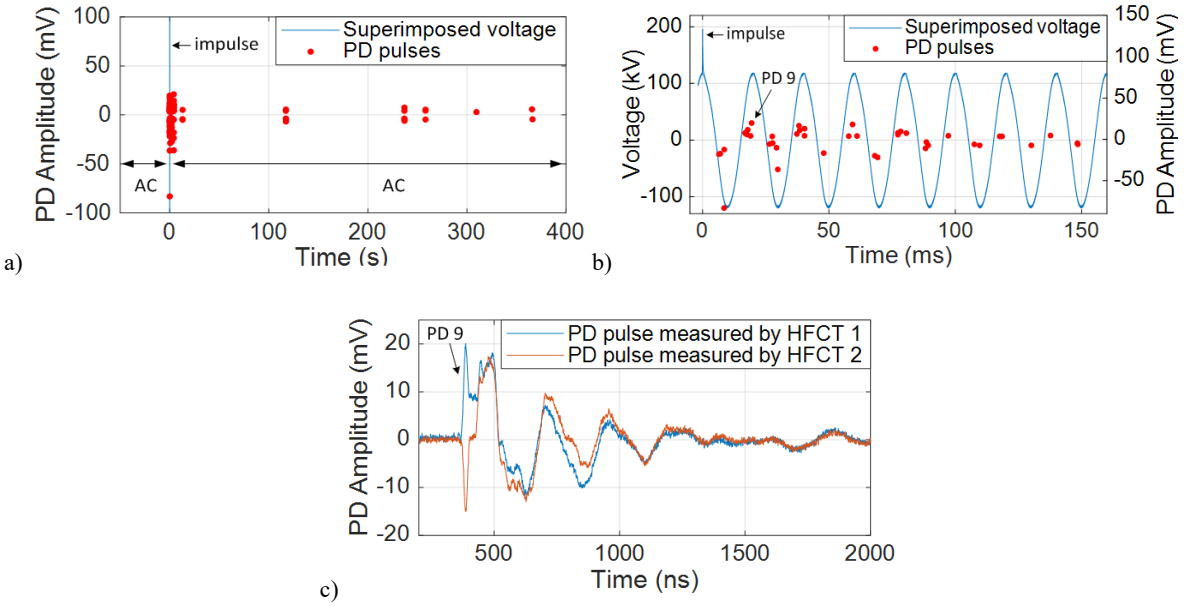

Figure 6.25: PD under superimposed voltage in test 4: a) PD occurrence under superimposed voltage over time, b) PD occurrence during the first eight cycles after the impulse, c) TRPD pulses of PD9.

Figure 6.25a shows the observed PD activity over time under the superimposed voltage. Before the impulse, no PD occurred under the AC voltage as expected. When the impulse was applied on the cable, PD initiated, and then reoccurred for around 360 seconds under AC voltage. Figure 6.25b shows the PD occurrence during the first eight cycles after the impulse. During the impulse moment, no PD could be observed. From the first negative cycle after the impulse, PD started to occur. With time, the number of PD decreased. The pulse shape of one PD from the positive cycle is given as PD9 in Figure 6.25c.

Test 4 shows that, the PD measuring system is able to measure signals under superimposed voltages. However, PDs were only observed when the impulse was finished but not during the impulse moment due to the disturbance. In order to prove that PD could occur during the front time under superimposed voltages, configuration II was used then, and longer impulses were to be superimposed on the AC voltage.

In test 5 and 6, the same voltage waveform as in test 4 but with longer impulse front time of T_f = 93 µs was applied to the cable system. The AC level of 124 kV_{ACpk} and the total peak value of 196 kV_{pk} were kept the same. In test 5, configuration I was applied, while in test 6 configuration II was used. The measurement results in test 5 are given in Figure 6.26. Similar to test 4, PDs were initiated by the impulse starting from the first negative cycle, and lasted for around 22 seconds under AC voltage. No PD could be detected during the impulse moment. In test 6, main discharges were detected during the front time near the impulse peak at 91.6 µs, shown as MD1 and MD2 in Figure 6.27a. The pulses shapes of MD1, MD2 near the impulse peak and PD1 under AC are given in Figure 6.27b and Figure 6.27c.

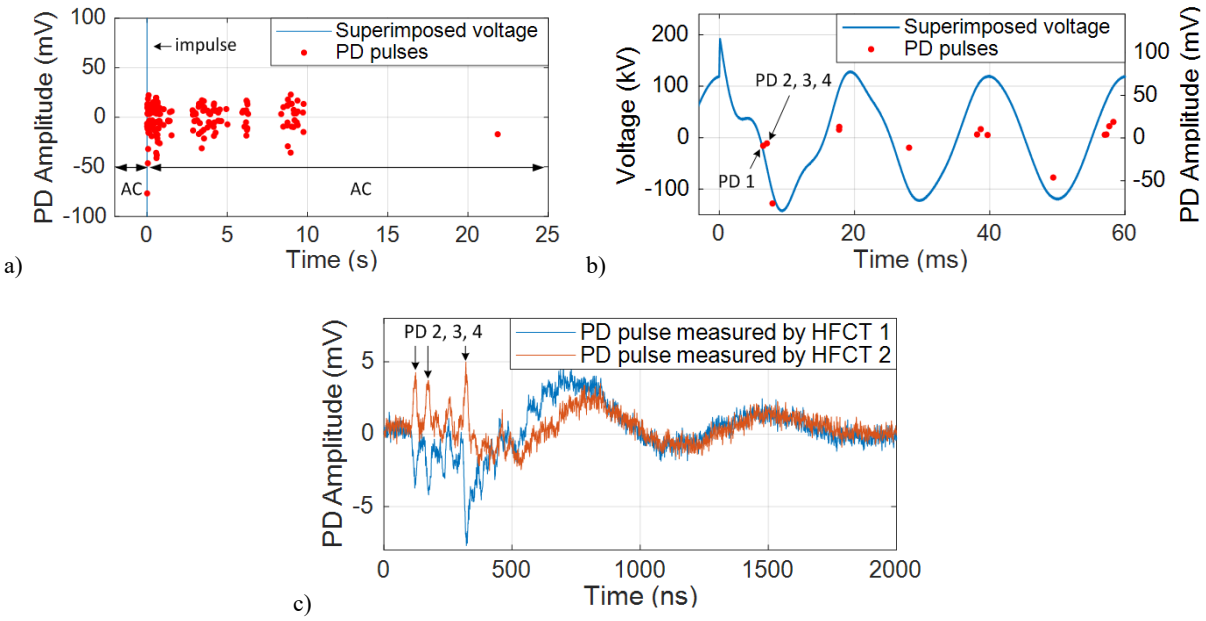

Figure 6.26: PD under superimposed voltage in test 5: a) PD occurrence over time, b) PD occurrence during the first three cycles, c) TRPD pulses of PD2, PD3 and PD4.

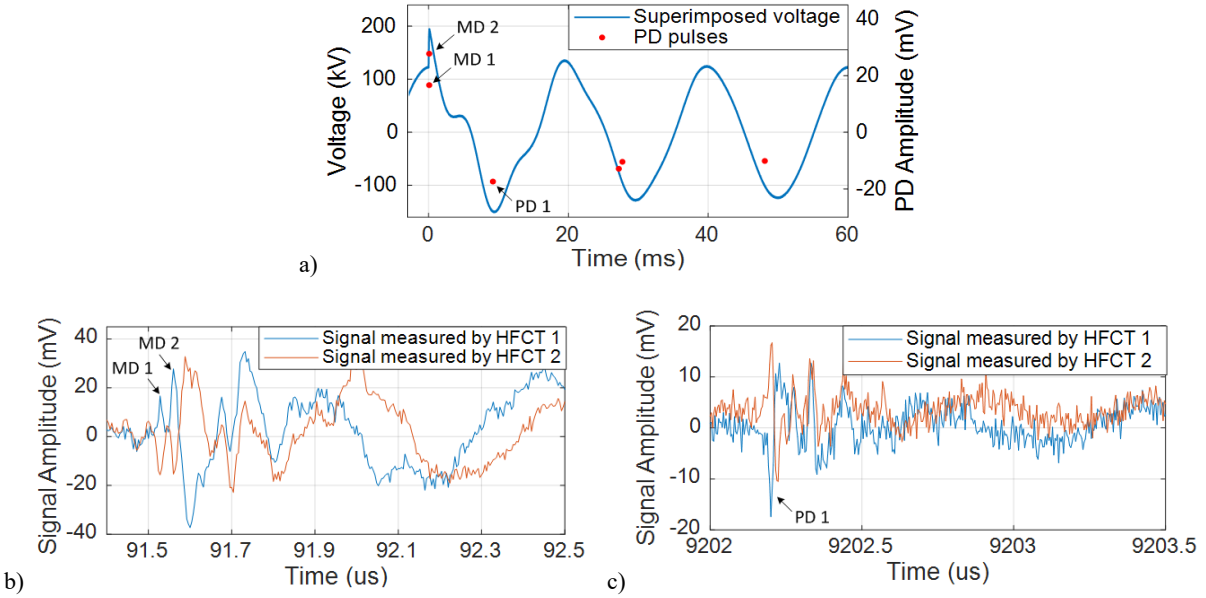

Figure 6.27: PD under superimposed voltage in test 6: a) PD occurrence, b) TRPD pulses of MD1 and MD2 measured under impulse voltage, c) TRPD pulses of PD1 measured under impulse voltage.

With configuration II, the PD measuring system is able to measure both main discharges during the front time as well as the reverse discharges during the tail time, as long as the impulse voltage has a front time longer than the dead zone of the PD measuring system.

6.5 Conclusions

The measurements under impulse and superimposed voltages show that:

- The experimental set-up is able to withstand under impulses and superimposed voltages in HV level, and to keep on measuring PDs from the cable joint during the impulse conditions without and with AC superposition. Under these conditions the safety of equipment and human is ensured by using filter and transient voltage suppressor units.
- The installed HFCTs measure the signals internally to the cable joint with opposite polarities while externally to the joint with equal polarities. Such polarity recognition allows us to identify PD from the cable joint, and to discern PD from disturbances. The disturbance separation obtained by the polarity recognition and filtering units is considered useful especially during the impulse test, since many disturbances enter the measuring system during the impulse application.
- The applied band-pass filters, spark gaps and transient voltage suppressors contribute to disturbance suppression and safety, which is a challenge in PD measurements under impulse. Configuration I, equipped with filter A, a TVS and a spark gap, helps to protect the oscilloscope. By adding filter B unit in configuration II, the extra band-pass filter helps to further suppress the disturbance and reduce the detection dead zone without detriment to the polarity recognition and having a good balance between pulse shape distortion and pulse attenuation. As a result, PD can be detected during the impulse front time.
- Using configuration II can help to suppress the disturbance and to decrease the dead zone so that PDs occurred during the front time can be observed. On the other hand, small PD signals might be missing during the acquisition, due to attenuation produced by the extra filter B and the trigger level. As a conclusion, using configuration I or II depends on the purpose of the test. If it is aimed to detect PDs during the entire impulse or superimposed transient moment, using configuration II will help to decrease the dead zone. If it is more important to observe all the PD activities, using configuration I will increase the chance of the detection of small PD events at least beyond the dead zone.

The presented PD measuring system is instrumental for investigating the effect of transients on a HV cable system model in laboratory conditions. The effect of transients on HV cable insulation system are to be discussed in Chapter 7.

Chapter 7

Results of PD Measurements on HV Cable Model under Transients

Partial discharges were observed being initiated by superimposed transients from the artificial defect in MV cable models in chapter 5. Based on the knowledge and experience gained through PD measurements in MV cable models, a methodology for PD measurement in a HV cable model, including experimental set-up, PD measuring and data interpretation, has been presented in chapter 6. The methodology has been verified and proved to work well. By applying this methodology, partial discharges from the HV cable model with artificial defect are investigated in chapter 7. Section 7.1 presents the measured partial discharges under different pure impulse voltages. In section 7.2, the defect as described in chapter 6 is first adjusted in such a way that the cable model could pass the maintenance test. Then superimposed voltages with different waveforms are applied to the HV cable model and PDs are measured. The effects of transients are analysed based on the measurement results. Next, the defect is adjusted to the situation that the cable model could pass the commissioning test and similar measurements are performed on the cable model.

7.1 Partial Discharges in HV Cable Model under Impulses

For impulse tests, impulses with long wave and short wave were applied to the HV cable system model, which has been described in chapter 6. For long impulses, the relatively long front time and tail time were such defined that, the impulses can represent the standard switching impulse, and meanwhile the test circuit is able to withstand the impulses. The same holds for the short impulse voltages, which were defined with relatively shorter front time and tail time to approach the standard lightning impulse and to avoid any test circuit failure. Only one dimension of the defect as D = 7 mm (section 6.1.2) was investigated. Configuration II was used in order to detect PDs during the front time of impulses.

This chapter is based on:
J. Wu, A. Rodrigo Mor, J. J. Smit, "Partial discharges activated by impulses and superimposed voltages in a high voltage cable model", International Journal of Electrical Power & Energy Systems, submitted.

7.1.1 Test procedure

Table 7.1 lists all the tests performed on the HV cable model under impulse conditions. For all the tests, the defect dimension D - the outbound displacement of cable – was set as 7 mm. In each test, the HV cable system was subjected to only one impulse voltage. The PD measuring system kept acquiring data until no more signals were captured.

Table 7.1: Impulse tests on HV cable model with defect dimensions D of 7 mm.

Defect dimension D [mm]	PDIV [kV_{rms}]	PDEV [kV_{rms}]	Impulses	Tests
7	104 / 97	90	Long impulses	L1 – L6
			Short impulses	S1 – S11

7.1.2 Partial discharges under long impulses

The long impulse voltages, which were applied to the HV cable system model, are described in Table 7.2 with their peak values, front times and tail times. In test L1-L4, the applied impulse voltages had the same shape with a front time T_f of 410 µs and a tail time T_h of 2535 µs. The peak value of the impulses V_{pk} increased with a step of 20% from L1 to L4. Partial discharges were measured during the impulses in test L1-L4, and the results are given in Figure 7.1. In test L4-L6, the peak values of the applied impulses were kept the same at 274 kV, while the front times and the tail times were getting shorter. For each impulse, the same test was repeated six times. Partial discharges measured in test L4-L6 are presented in Figure 7.2.

Table 7.2: Long impulses with their characteristics.

Tests	T_f / T_h [µs]	Peak value V_{pk} [kV]	Number of repeated tests	Number of PD (average)
L1	410 / 2535	147	1 × L1	0
L2		176	1 × L2	2
L3		220	1 × L3	9
L4		274	6 × L4	13
L5	374 / 1612	274	6 × L5	11
L6	232 / 690	274	6 × L6	14

PDs occurred under the impulses having the same shape (T_f/T_h) and different peak values in test L1-L4 are illustrated in Figure 7.1a. During the tail time of V_{L4}, the first PD initiated, shown as the red dot RD1, has a negative polarity with an amplitude of -7.1 mV. RD1 occurred at V_{L4} = 97 kV, indicated by the red circle on the wave tail. Similarly, during the tail time of V_{L3} the first PD initiation occurred at V_{L3} = 41 kV, and during the tail time of V_{L2} the first PD initiation occurred at V_{L2} = 9 kV. No PD has been observed under V_{L1}. With the same impulse shape, the higher the peak value of the impulse, at higher voltage PD initiates during the impulse tail time. From another perspective, the higher the peak value of the impulse, the earlier PD initiates. This can be seen from Figure 7.1a as the PDs under V_{L4} (red dot) appear firstly, then the PDs under V_{L3} (blue dot) ignite and at last the PDs under V_{L2} (green dot) occur.

The PD occurrence during the front time of the impulse is zoomed in and shown in Figure 7.1b. The first PD detected during the front time of V_{L4} is indicated as MD1, which has a positive polarity. The voltage at which the first PD initiated under V_{L4} (red) is the highest voltage while the voltage at which the first PD initiated under V_{L2} (green) is lowest. However, the initiation moments seem to be random.

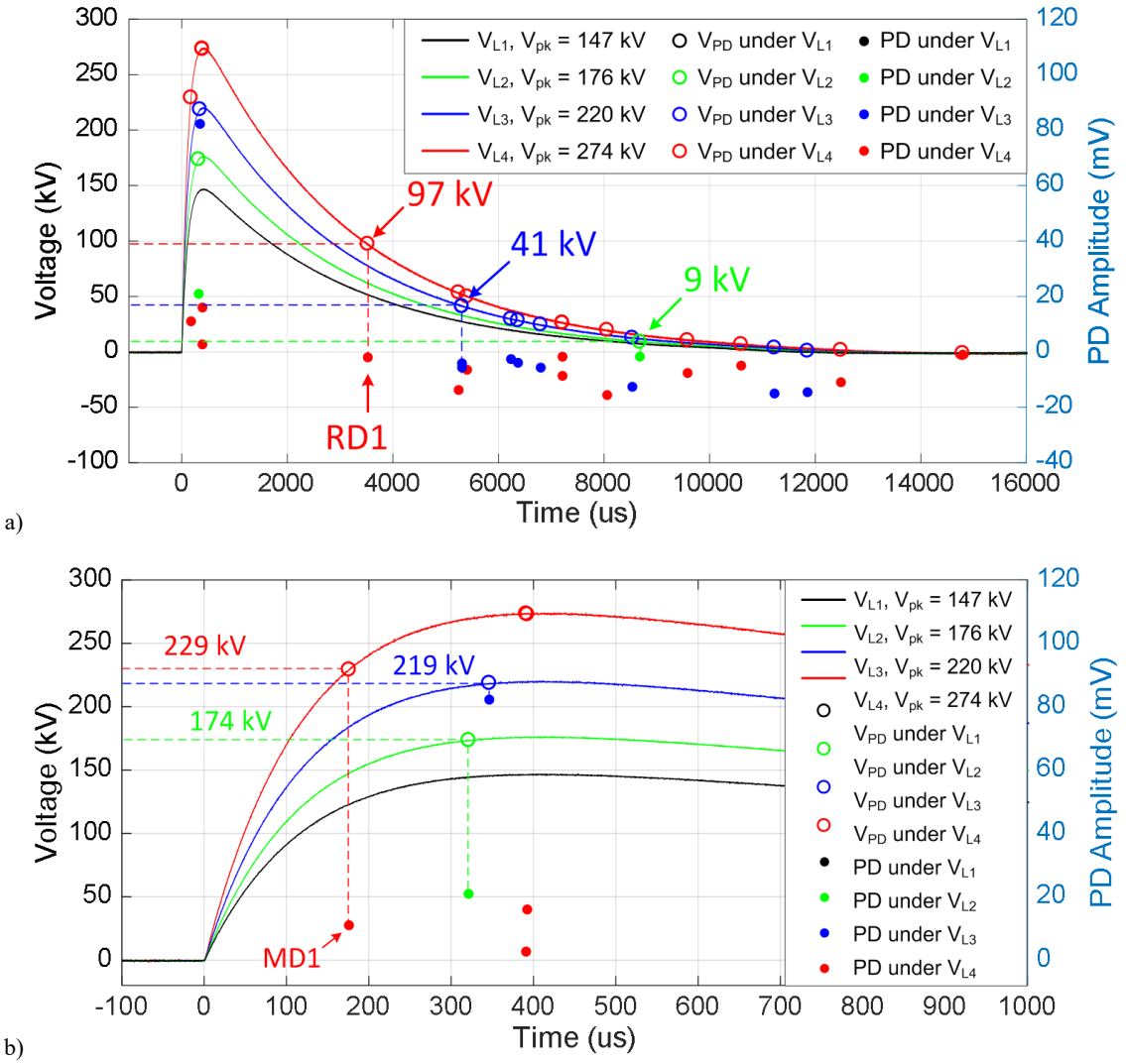

Figure 7.1: PD occurrence under long impulses with the same shape of T_f/T_h = 410/2535 µs and different peak values in test L1-L4: a) PD occurrence during the entire impulses, b). PD occurrence during the front time.

In test L4-L6, PDs were measured for three different impulse shapes, having the same peak value. Each test was repeated for six times for each impulse shape, and the results of 18 tests are shown collectively in Figure 7.2a. During the tail time of the impulse V_{L6}, the voltage level at which PD initiated for the six tests varies from 64 kV to 84 kV, resulting in an average value of 76 kV (indicated as the dash green line) with standard deviation SD of 9 kV. The average PD initiation voltage under V_{L4} and V_{L5} is 77 kV (SD = 17) and 73 kV (SD = 20) respectively. The minimum and maximum PD initiation voltages among all the 18 tests are given as a range of 50-105 kV, shown as the gray band in Figure 7.2a. It shows that, the PD initiation voltage during the tail time of different impulse shapes is similar. In other words, PD initiates when the impulse voltage decreases into a certain range, in this case the gray band of 50-105 kV, regardless of the impulse shapes. This is why the PDs under V_{L6} (green dot) initiate at the earliest as the impulse voltage drops into the range firstly. And the PDs under V_{L4} (red dot) occur in the latest since the impulse voltage drops into the range latest.

A similar phenomenon is observed for the PD occurrence during the front time, as shown in Figure 7.2b. PD initiates when the impulse voltage reaches a certain level near to the wave crest in the range of 225-267 kV under V_{L4}, V_{L5} and V_{L6}.

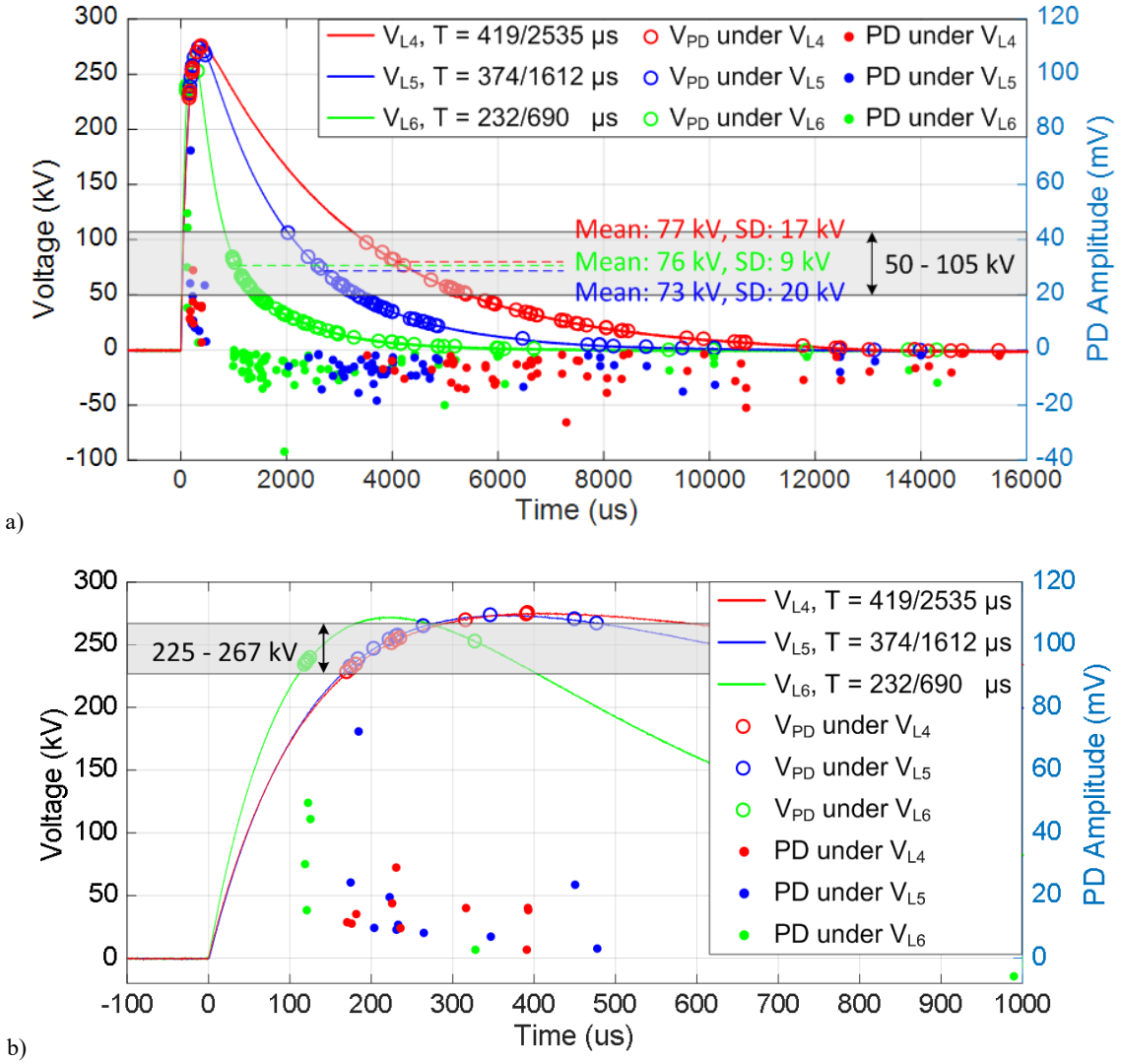

Figure 7.2: PD occurrence under long impulses with the same peak value of 274 kV and different shapes in test L4-L6: a) PD occurrence during the entire impulses, b). PD occurrence during the front time.

Considering the amount of PD occurring under different impulse waveforms (Table 7.2), with the same impulse shape (T_f/T_h), the higher the peak value, the more PDs occur. With the same peak value and different impulse shapes, the number of PD occurring doesn't show an obvious trend.

7.1.3 Partial discharges under short impulses

Same sort of tests were performed under short impulse voltages. Table 7.3 gives the short impulse voltages with their characteristics. Impulse voltages with the same shape of T_f/T_h = 3/56 µs and different peak values were applied in test S1-S4. The peak values of the impulse voltages increased with a step of 20% from S1 to S4. In test S4-S11, impulse voltages with the same peak value of 274 kV and different shapes were applied. Partial discharges measured in test S1-S4 and S4-S11 are shown in Figure 7.3a and Figure 7.3b respectively.

Table 7.3: Short impulses with their characteristics

Tests	T_f / T_h [µs]	Peak value V_{pk} [kV]	Number of repeated tests	Number of PD (average)
S1	3 / 56	150	1 × S1	0
S2		176	1 × S2	2
S3		226	1 × S3	6
S4		274	6 × S4	10
S5	3 / 26	274	6 × S5	8
S6	3 / 84	274	6 × S6	12
S7	3 / 174	274	6 × S7	11
S8	3 / 409	274	6 × S8	10
S9	3 / 782	274	6 × S9	9
S10	3 / 1630	274	6 × S10	11
S11	3 / 2006	274	6 × S11	13

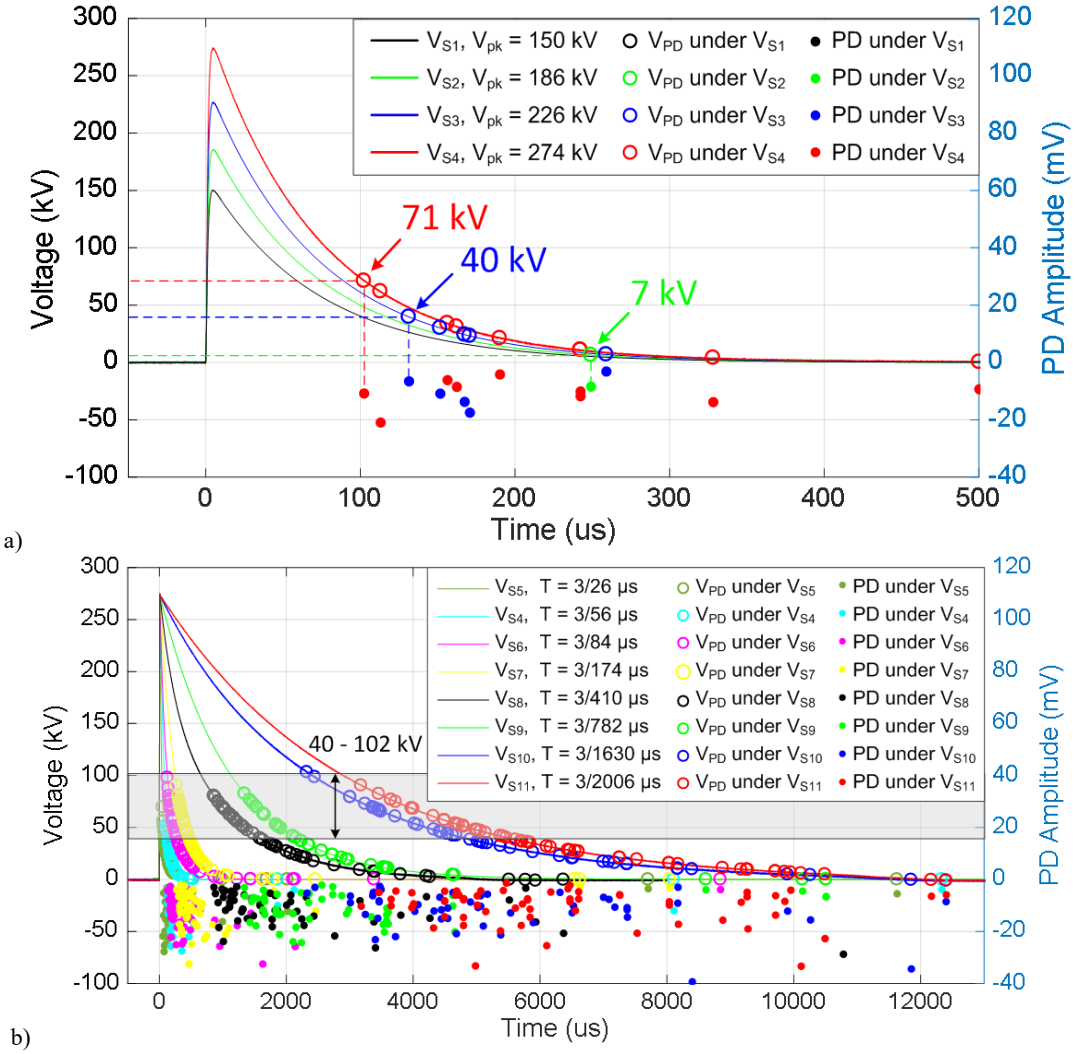

Figure 7.3: PD occurrence under short impulses: a) PD occurrence under short impulses with the same shape of T_f/T_h = 3/56 µs and different peak values in test S1-S4, b) PD occurrence under short impulses with the same peak value of 274 kV and different shapes in test S4-S11.

According to [23], both main discharges during the front time and reverse discharges during the tail time of the impulse are supposed to be observed. However, the front time of the short impulse is so short that the rising phase of the impulse is within the detection dead zone caused by the PD measuring system (section 6.3). Thus, any main discharge during the front time is not detectable. Based on this, in the case of short impulse application, we are going to focus only on the reverse discharges during the tail time.

For the PD occurrence under short impulse voltages with the same shape of T_f/T_h = 3/56 µs and different peak values in test S1-S4, similar phenomenon was observed to that under long impulses as shown in Figure 7.1a. PDs under V_{S4} (red) initiated at V_{S4} = 71 kV, PDs under V_{S3} (blue) ignited at V_{S3} = 40 kV, and PDs under V_{S4} (green) occurred at V_{S4} = 7 kV. With the same impulse shape, the higher the peak value of the impulse, at the higher voltage initiates PD during the impulse tail.

The PD occurrence under short impulse voltages with the same peak value and different shapes is given in Figure 7.3b. Each test was repeated for six times under each impulse shape. During the tail time, the PD initiation voltages of all the 48 tests under V_{S4} to V_{S11} are in the range of 40-102 kV. When the impulse voltage decreases to this range, PD initiates. Therefore, the shorter the impulse shape, the earlier PDs initiate.

The amount of PD occurring under different impulse waveforms (Table 7.3), is similar to the number of PDs for long impulses of the same shape (T_f/T_h), and that more PDs occurred under impulse with higher peak value. No obvious trend is observed for the number of PD under the impulses with the same peak value and different impulse shapes.

7.1.4 Discussions

The observation of different PD occurrence patterns under different impulse shapes and peak values can be explained by the electric field condition within the defect.

Figure 7.4 shows internal local electric field conditions within the defect under long impulses V_{L1} to V_{L4} corresponding to test L1-L4. E_c is the enhancement of E_0, where E_0 is generated by the applied testing voltage, e.g. V_{L1} cross the insulation thickness. Thus, E_c follows the wave shape of V_{L1}. E_q is created by the surface charges. The residual local field E_i is the sum of E_c and E_q, which drives the PD occurrence. The concept of E_i, E_c and E_0 have been detailed explained in section 3.2.1. During the front time of every impulse (Figure 7.4a), main discharge initiates as soon as the local electric field E_i reaches the PD inception field. After the first PD, E_q is created by the charges left from the discharge process, which has an opposite direction to E_c. Due to the arisen E_q, the local electric field E_i deviates from the background field E_c. Assume no charge decays, E_q stays same and E_i increases with E_c again. When it reaches the PD inception field, PD reoccurs. Based on the assumption that there is no charge decay, PD occurs under all the four impulses as shown in Figure 7.4a. However, in practice, the PD measuring system used in this work has an observation limitation: PD cannot be detected, or be separated from the disturbance signal during the dead zone after applying the impulse. For the case of applying long impulse, the detection dead zone is around 130 µs, which means, any PD that occurs within 130 µs after the impulse application may not be observed. Therefore, the first main discharge being observed is MD1. This can explain why we observed the PD initiation likewise in Figure 7.1b, which actually occurred beyond the detection dead zone (Figure 7.4a).

The development of the local electric field E_i further influences the PD initiation during the tail time. As shown in Figure 7.4b, E_i of V_{L4} reaches the negative PD inception field firstly, which causes the first reverse discharge RD1. The first reverse discharge under V_{L3} appears later and under V_{L2} in the latest. Moreover, with PD being initiated earliest, more PDs could occur under V_{L4} within the same impulse

duration. This is why an increasing number of PD was observed with increasing peak value of impulses in Table 7.2.

Figure 7.4 gives a qualitative analysis simulating the electric field conditions with the assumption that there is no charge decay. In real defects, the charges deposited on the insulator surface from previous PD processes may decay by ion drift and diffusion. This will influence the E_q created by the charges and hereby the E_i. As a result, the PD occurrence will be slightly different and random, but still follows the physical principle as explained above.

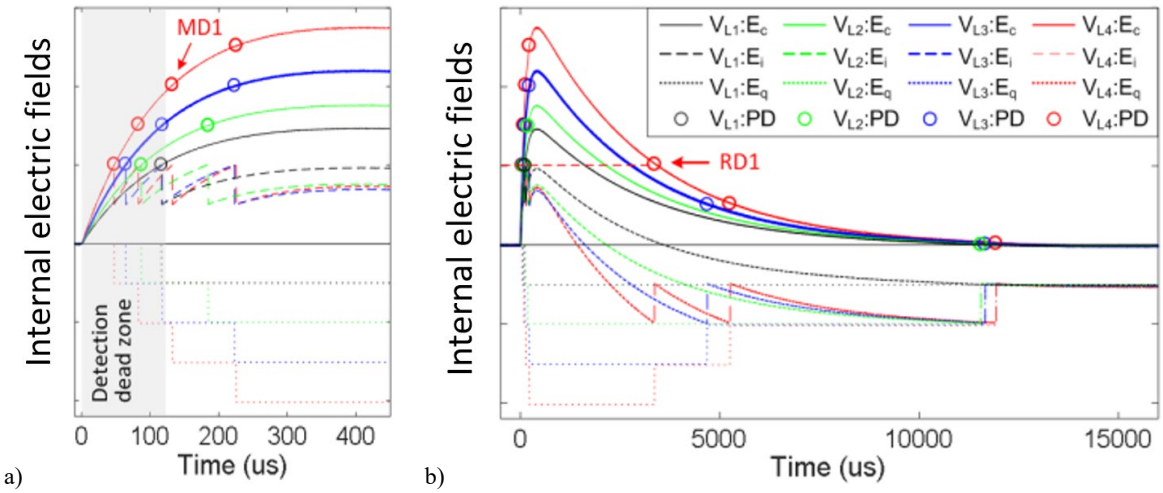

Figure 7.4: Schematical electric field conditions under long impulses in test L1-L4: a) during front time, b) during tail time.

For impulses V_{L4} to V_{L6} corresponding to test L4-L6, due to the detection dead zone, we could only observe the PDs occurred after the dead zone, as shown in Figure 7.5a. E_i of V_{L6} starts to decrease firstly. Together with the biggest slope of V_{L6}'s tail wave, E_i of V_{L6} reaches the negative PD inception field earliest, while V_{L6} drops into the range of 50-105 kV (Figure 7.5b). This leads to the earliest PD occurrence under V_{L6}. E_i of V_{L4} and V_{L5} start to decrease almost at the same time. But V_{L4} has the smallest slope. Therefore, PDs under V_{L4} (red) occur the latest.

Since PD occurred under V_{L6} the earliest, and the biggest slope of V_{L6}'s tail wave makes the E_i reaching the negative PD inception field faster, more PDs are supposed to occur during the impulse period. However, with shorter T_f/T_h, the impulse V_{L6} finishes earlier, which suppresses PD to occur. Therefore, the number of PD under different impulse shapes doesn't show an obvious change.

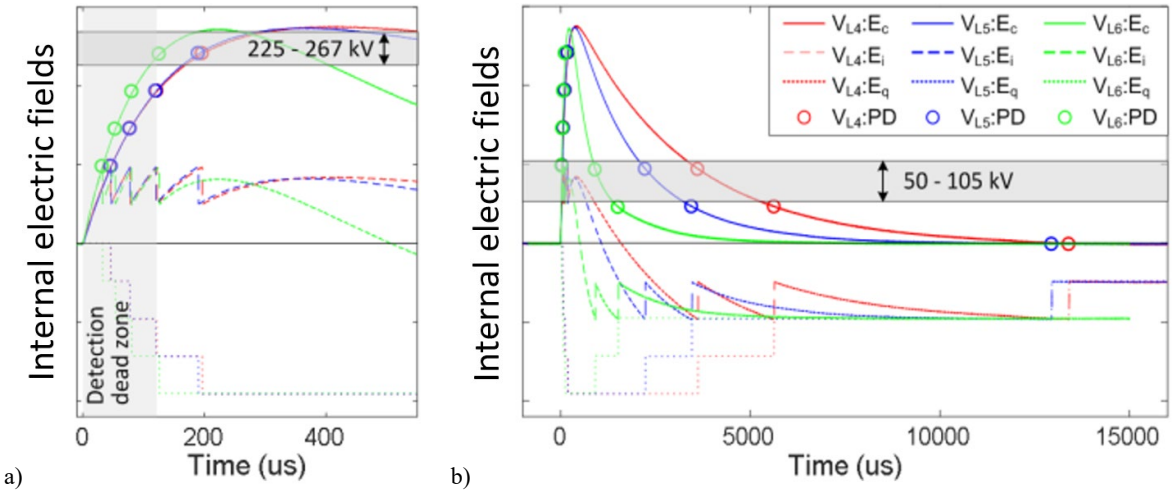

Figure 7.5: Schematical electric field conditions under long impulses in test L4-L6: a) during front time, b) during tail time.

The field conditions with the defect under short impulses in test S1-S11 are shown in Figure 7.6 and Figure 7.7. For impulses V_{S1} to V_{S4} with the same shape and different peak values (Figure 7.6), main discharges are supposed to occur during the front time as soon as the local electric field E_i reaches the PD inception field. During the tail time, due to the largest arisen E_q, the resulting E_i of V_{S4} reaches the negative PD inception field firstly, which causes the first reverse discharge. The first reverse discharge under V_{S3} occurs then and the one under V_{S2} initiates at the latest. Moreover, with PD being initiated earliest, more PDs could occur under V_{S4} within the same impulse duration. The analysis is in accordance to the observation in Figure 7.3a. However, in practice, since the front time is shorter than the dead zone, no main discharges during front time but only reverse discharges during the tail time were observed.

For impulses V_{S4} to V_{S11} with the same peak values and different shapes (Figure 7.7), the shorter the tail wave, the bigger the wave slope, the earlier E_i starts to decrease and reaches the negative PD inception field. The first reverse discharges under every impulse occur when the voltage drops into the range of 40-102 kV as shown in Figure 7.3b.

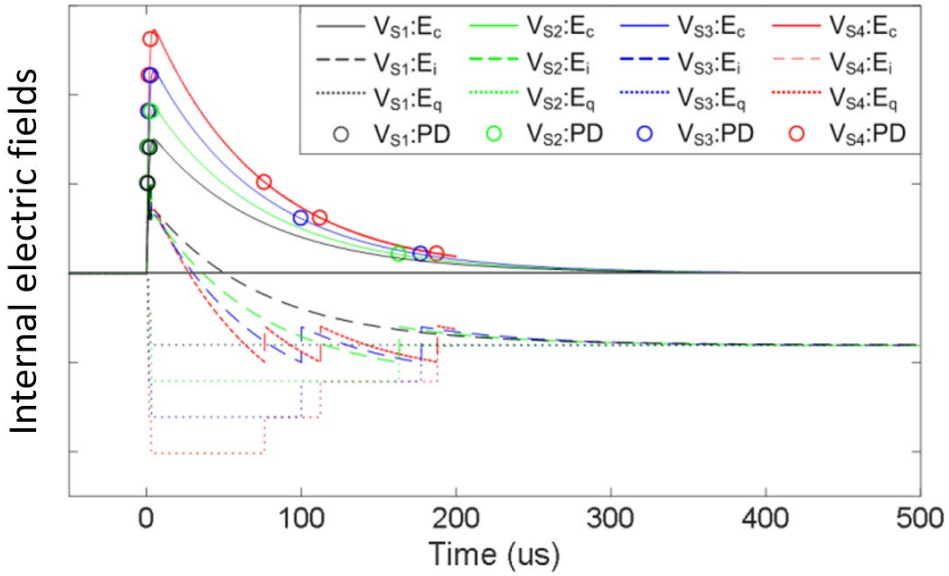

Figure 7.6: Schematical electric field conditions under short impulses in test S1-S4.

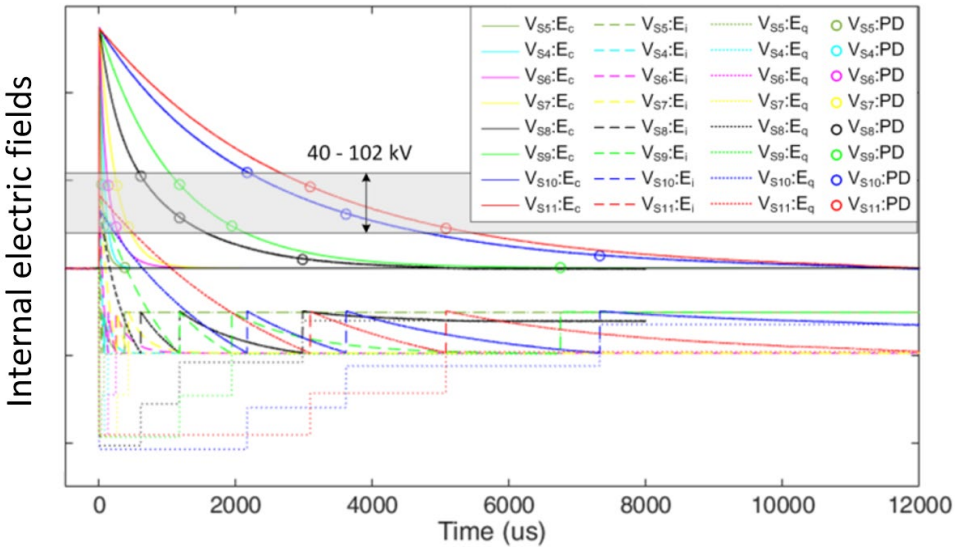

Figure 7.7: Schematical electric field conditions under short impulses in test S4-S11.

7.1.5 Conclusions

The measurement results of partial discharge under impulse voltages show that:

- Impulse voltage of sufficient voltage level can initiate partial discharges. Several main discharges initiated during the front time of the impulses, but not necessary to be near the impulse crest. More reverse discharges occurred during the tail time of the impulses until the impulse finished.
- The PD initiation under impulse voltages is determined by the electrical field condition. When the local field E_i reaches the PD inception field, PD may occur. For the impulse voltages with the same shape (T_f/T_h), the higher the peak value, the faster E_i reaches the PD inception field, the earlier PD would initiate and the more PDs would occur during the entire impulse. While for the impulse voltages with the same peak value and different shapes, the shorter the impulse, the faster E_i will reach the PD inception field, the earlier PD would initiate. However, the wave shape doesn't influence the average number of PD occurring.

As a conclusion, the peak value of impulse voltage has more significant effect on partial discharges than the impulse shape. Thus, impulse voltage with high peak value needs more attention.

7.2 Partial Discharges in HV Cable Model under Superimposed Transients

For superimposed voltage tests, the voltage waveform of impulses being superimposed on AC voltage (Figure 6.7b) was defined as the test voltage with varying parameters. All of the defect dimensions as shown in Table 6.2 were investigated under superimposed voltages. Section 7.2.1 describes the test voltage, test procedure and the defects under tests. The defect with dimension which can pass the maintenance test was investigated and presented in section 7.2.2. The defect with dimension which can pass the commissioning test was studied and described in section 7.2.3. Both Configuration I and II were used to detect PDs during the superimposed voltages.

7.2.1 Test content and procedure

To investigate the partial discharge under superimposed transient voltages, waveform as shown in Figure 6.7b was applied to the HV cable system. With a specific defect dimension, due to the outbound displacements of cable, the PDIV and PDEV were measured, and an AC voltage was determined to be below the PDIV and above the PDEV. In each test, the HV cable system model was firstly subjected to the determined AC voltage for several minutes to confirm that no PD occurred. Then the defined impulse was applied, followed by the same AC voltage until no PD was detected anymore (Figure 7.8).

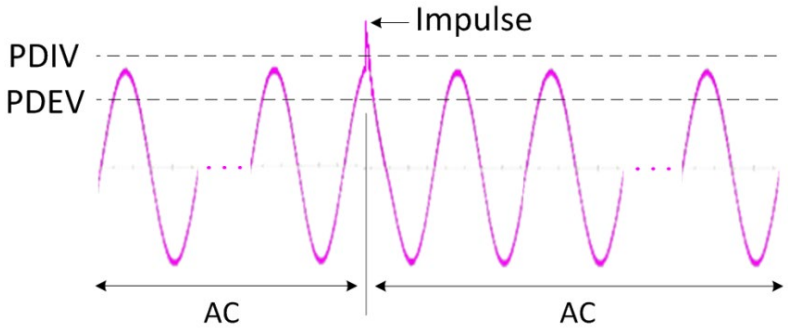

Figure 7.8: Test waveform and test procedure.

In section 6.1.2, the artificial insulation defect was introduced to the cable joint to generate partial discharges. As expected in none of the cases PDs came from the insulation of the cable itself. Only insulation internal to the joint produced PD if activated.

The defect information in Table 6.2 is given again in Table 7.4 including the defect dimensions, and their corresponding PDIV and PDEV. The AC voltage was determined for each defect dimension based on the given PDIV and PDEV. In the case of defect due to a displacement of 7 mm, the PDIV was measured as 104 kV_{rms}, which is more than $1.1U_0$. Such defect can pass the PD test in the maintenance test at overvoltage [80]. This case of defect Type A is to be studied in section 7.2.2. A smaller defect due to a displacement of 6 mm has the PDIV more than $1.7U_0$ and the PDEV more than $1.5U_0$. Such defect is able to pass the PD test in after-laying commissioning test at overvoltage. This case of defect Type B is to be studied in section 7.2.3. For the defect dimensions due to displacements of 14 mm and 9 mm, the same tests were performed as well. However, since defect with such dimension will be detected during the commissioning test or the maintenance test, the measurement results have limited value, which will not be presented here.

Table 7.4: Defects and their test voltages.

Displacement D [mm]	PDIV [kV_{rms}]	PDEV [kV_{rms}]	AC levels [kV_{rms}]	Applicable tests with their PD pass criterion	Case
14	47	32	35	NA	-
9	83	58	70	NA	-
7	104/97	90	87	Maintenance test at overvoltage: No detectable PD at $1.1U_0$ for cables > 15 years	Type A
6	150	139	87	After-laying commissioning test at overvoltage: No detectable PD at $1.5U_0$	Type B
0	PD free up to $1.8U_0$		-	OK	-

7.2.2 Case study of defect Type A

The effect of transients on partial discharges in HV cable system model were investigated under superimposed voltage waveforms (Figure 6.7b). The defect dimension was adjusted so that it can pass the maintenance test as described in section 3.2.4. To study the influence from the transients, different waveforms with different parameters were applied to the cable system, which are given in Table 7.5. The parameter *Ratio* and φ are explained as following:

- Ratio: the ratio of the total peak voltage V_{peak} and the AC voltage peak value V_{ACpeak}.
- φ: the phase angle that the impulse is superimposed on AC voltage. The positive AC crest is set as $\varphi = 0^o$

The PD inception voltage was always measured just before the tests. Each measurement started with applying pure AC voltage on the HV cable system without observing any partial discharges for 5-10 minutes. After the impulse was applied, the cable system stayed under the AC voltage until no more partial discharges can be observed. In this way it is ensured that the partial discharges observed during the measurement were initiated by the latest superimposed transient.

In each test, one specific waveform was applied on the HV cable system and partial discharges were measured. The measurement under the same waveform was repeated for six times. The results described in the table and figures for each test are seen to be the most typical and representative of the six

measurements in each test. To describe the PD behaviour qualitatively and quantitatively, PD related parameters are presented in Table 7.5 as follows:

- PD magnitude: as mentioned in section 6.4.1, since the PD pulse shape is affected by the pulse propagation and reflections, the PD charge estimated based on the PD pulse is not accurate. Therefore, we directly use the peak voltage/current amplitude of the first PD pulse as the PD magnitude to describe the PD level instead of the charge magnitude. In particular, the maximum PD magnitude / peak amplitude is evaluated, which can reflect the effect of the impulse transients.
- PD number: is the total number of PDs measured after applying the superimposed transients.
- Duration: is the time duration of PD occurrence counted from the moment of impulse application to the moment the last PD occurred.
- PD probability: in each test, the same measurement was repeated for six times. PD probability describes that in how many measurements out of six PDs were initiated by the superimposed transients.
- PD occurrence during first five cycles: is a PD pattern showing the PD magnitude and the occurring moment under the applied waveform during the first five cycles after the impulse application.
- PD occurrence under transients: is a PD pattern showing the PD magnitude and the occurring moment over time from the moment of impulse application until PD extinguished.
- PD density pattern: in [72], the average discharge current is defined as the sum of the absolute values of individual apparent charge magnitudes during a selective reference time interval divided by this time interval. Since the measured PD signal is the PD current in this work, we define a similar parameter density based on the peak value of individual PD current, which is the sum of the absolute peak values of individual PD current during one AC cycle:

$$PD_{Density} = \frac{\sum_1^n |I_i|}{T_{cycle}} \qquad (5.1)$$

  where I_i is the peak value of individual PD current, T_{cycle} is the period of one AC cycle which is 20 ms, and n is the total number of PDs occurred during one T_{cycle}. The PD density pattern depicts the PD densities over cycles.

PD patterns of each test are given in Figure 7.9. In Figure 7.9, each row shows the results from one test, and each column gives a certain PD pattern of all the tests. For example, Figure 7.9-1a shows the PD occurrence during the first five cycles of test 1. Figure 7.9-2c shows the PD density of test 2.

Table 7.5: Tests on HV cable under superimposed voltages with PD that pass maintenance tests.

T_f / T_h [µs]	AC [kV_{rms}]	Ratio = $\frac{V_{peak}}{V_{ACpeak}}$	φ [°]	PDIV [kV_{rms}]	Test	Max PD magnitude [mV]	PD number	Duration [s]	PD probability
3 / 91	88	1.8	0	97	1	43.2	180	2.92	6 / 6
		1.7	0		2	27.0	110	1.87	6 / 6
		1.7	0	104	3	64.0	95	1.20	6 / 6
		1.6	30		4	106.6	61	1.13	6 / 6
		1.2	60		5	56.9	64	0.71	1 / 6
		1.0	90		6	-	-	-	0 / 6
		1.7	180		7	51.8	124	1.29	6 / 6
		1.4	60		8	48.7	47	0.69	6 / 6
	94	1.8	0	97	9	73.9	1480	14	2 / 2
		1.7	0		10	67.4	933	7.76	6 / 6
		1.7	0	104	11	72.5	443	3.17	6 / 6
		1.7	180		12	73.8	301	2.87	6 / 6
93 / 845	88	1.6	0	97	13	132.8	165	1.9	6 / 6
		1.5	30		14	45.2	23	0.86	6 / 6
		1.1	60		15	-	-	-	0 / 6
		0.7	90		16	-	-	-	0 / 6
		1.4	0		17	37.9	11	0.06/1.12	6 / 6

Test	PD occurrence during first five cycles	PD occurrence under transients	Current density
1	1a) 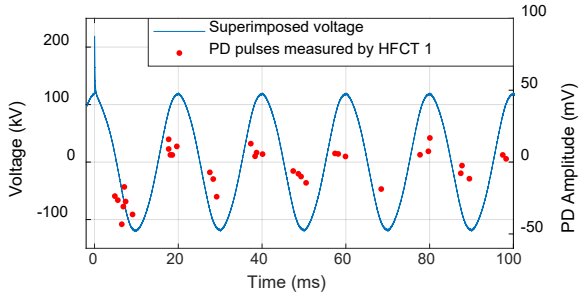	1b) 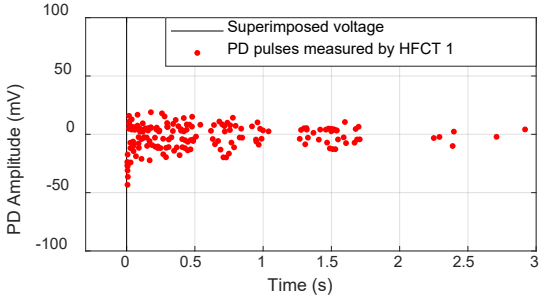	1c) 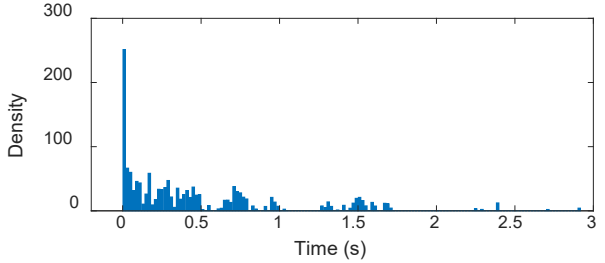
2	2a) 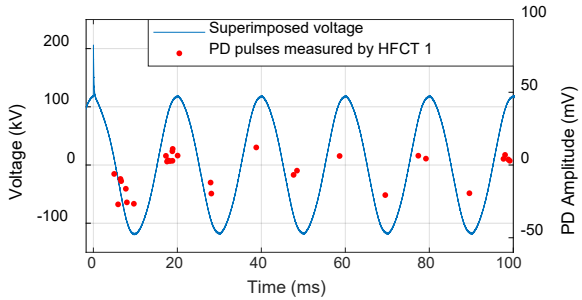	2b) 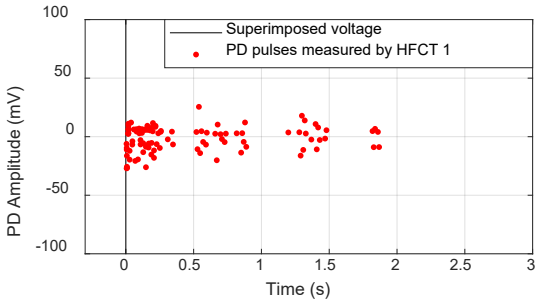	2c) 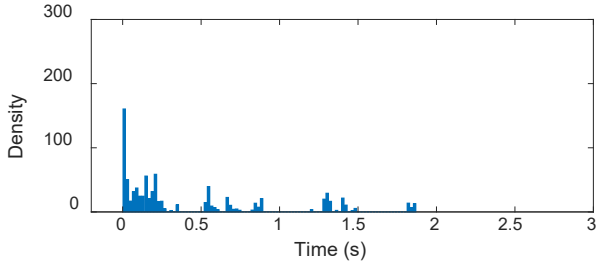
3	3a) 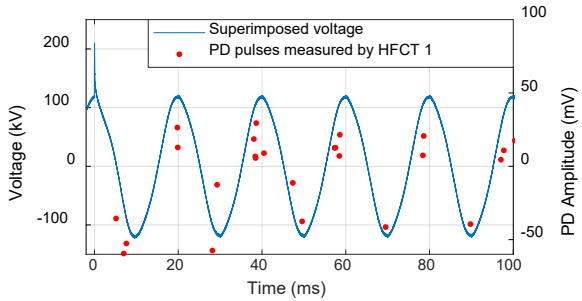	3b) 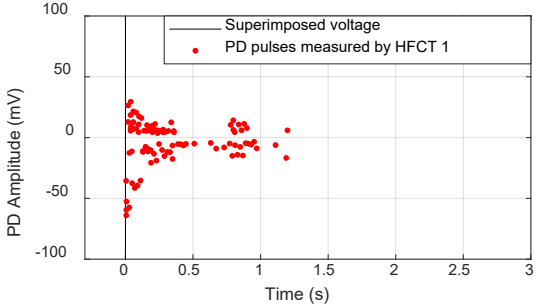	3c) 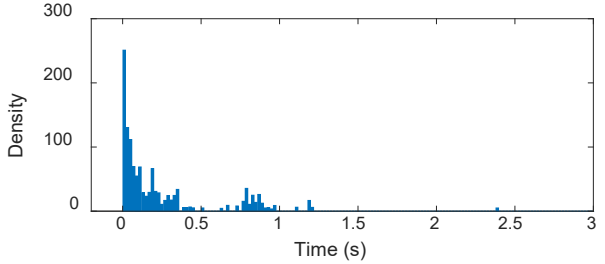

Test	PD occurrence during first five cycles	PD occurrence under transients	Current density
4	4a) 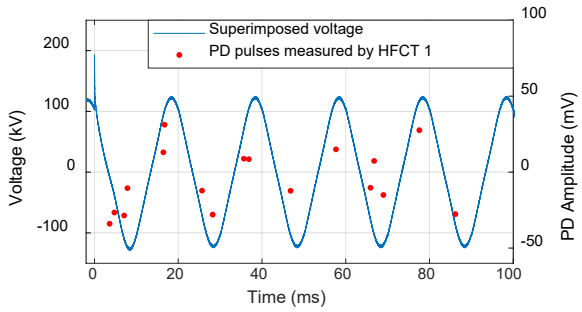	4b) 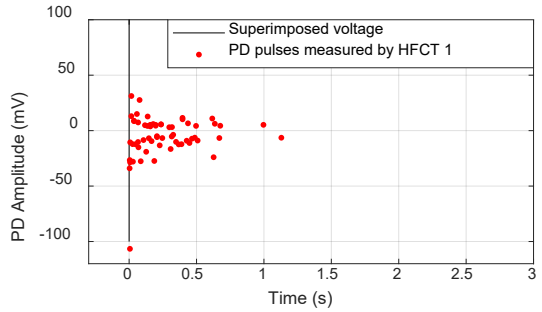	4c) 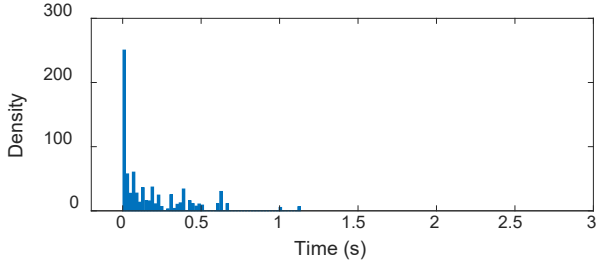
5	5a) 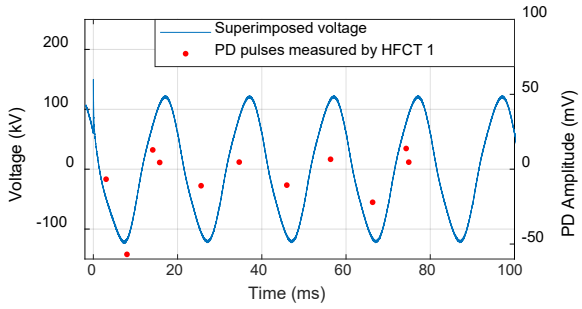	5b) 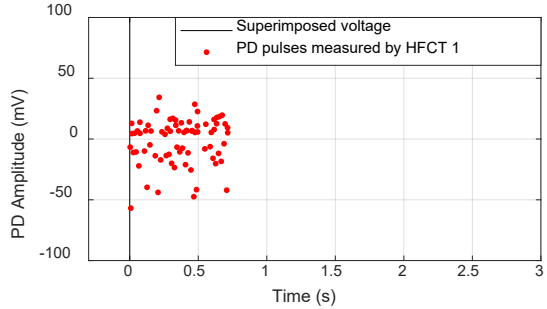	5c) 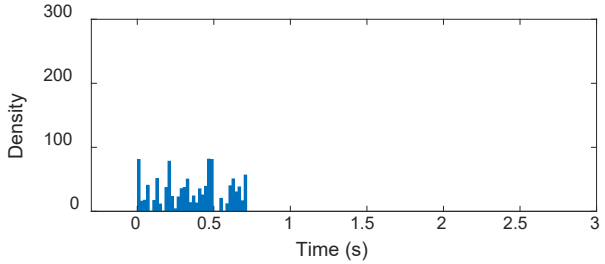
7	7a) 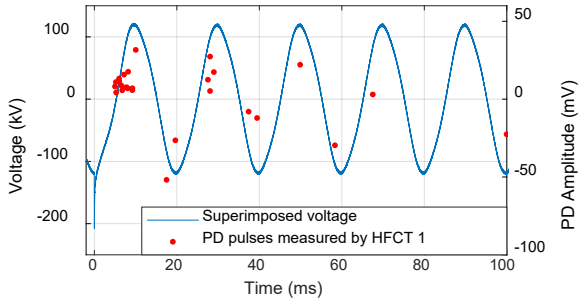	7b) 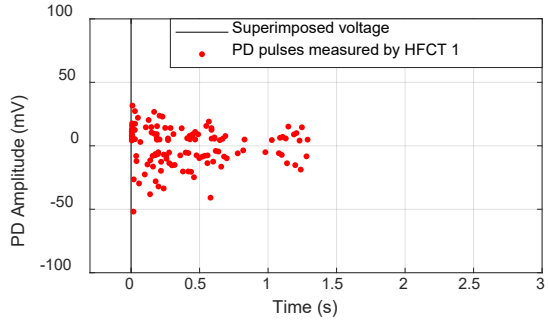	7c) 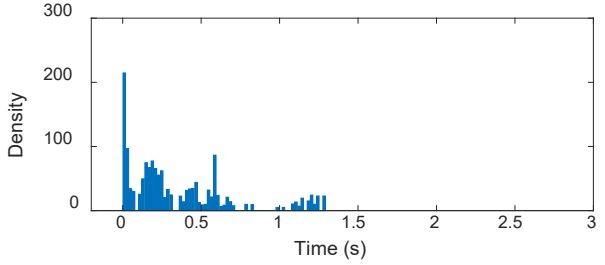

Test	PD occurrence during first five cycles	PD occurrence under transients	Current density
8	8a) 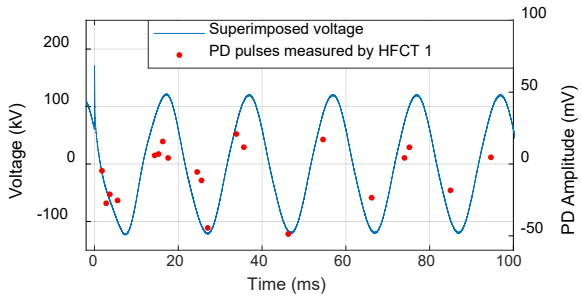	8b) 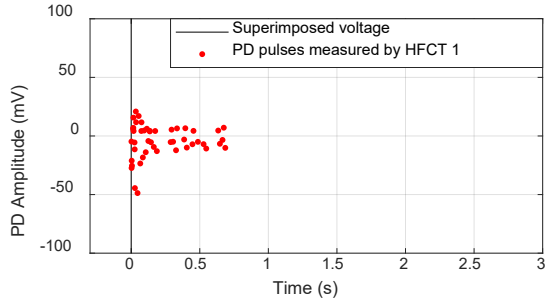	8c) 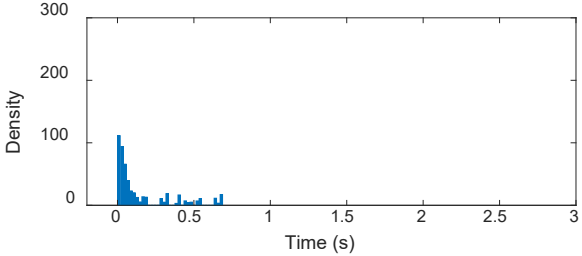
9	9a) 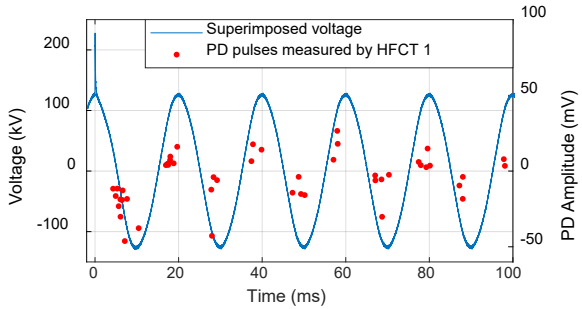	9b) 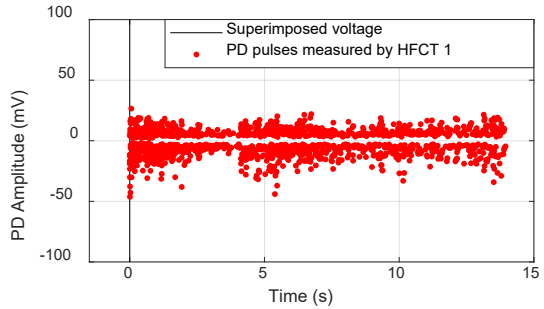	9c) 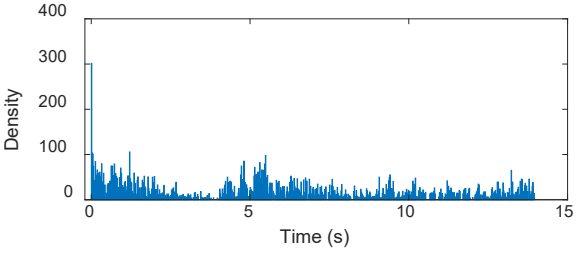
10	10a) 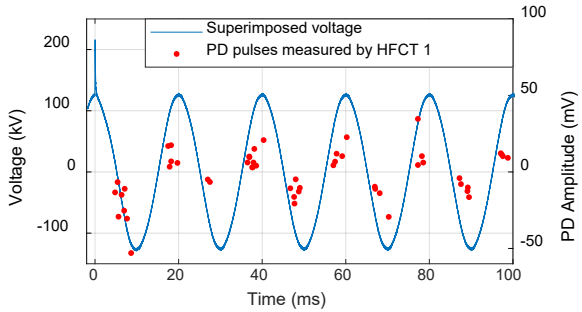	10b) 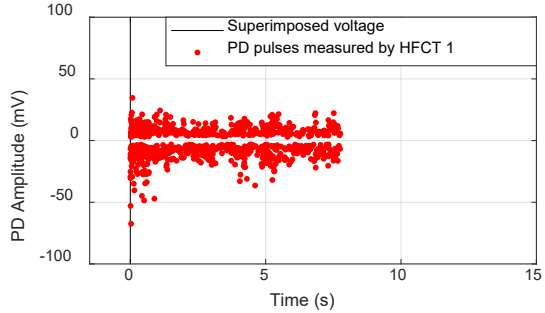	10c) 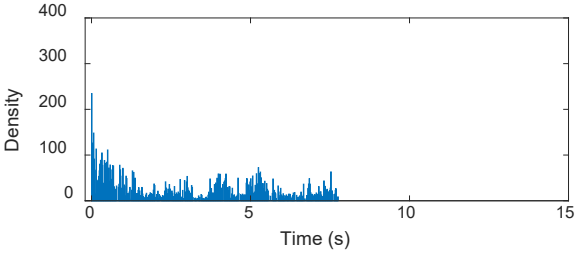

Test	PD occurrence during first five cycles	PD occurrence under transients	Current density
11	11a) 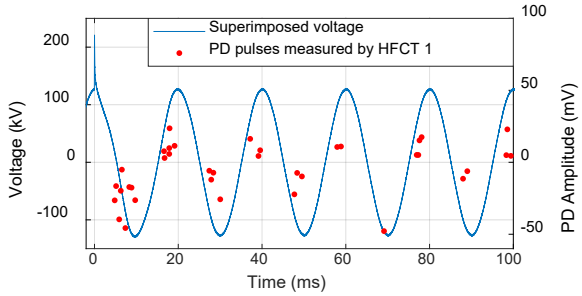	11b) 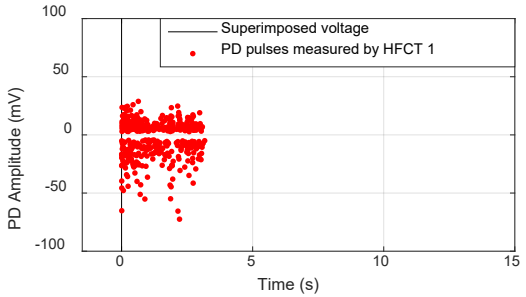	11c) 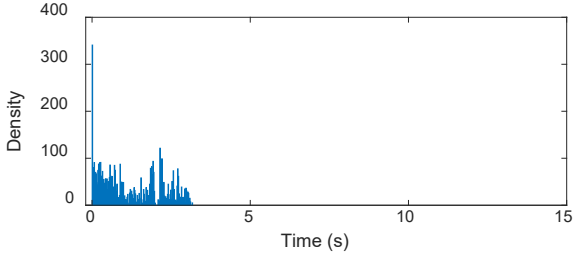
12	12a) 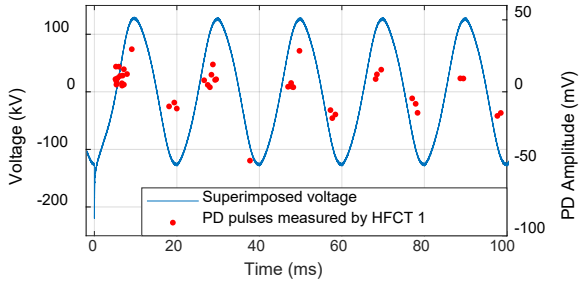	12b) 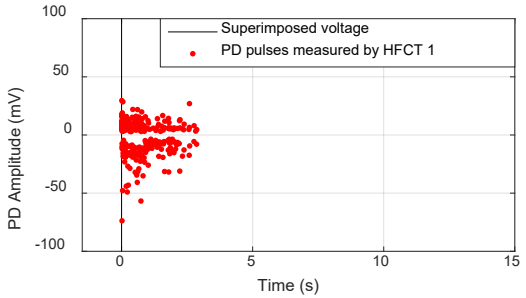	12c) 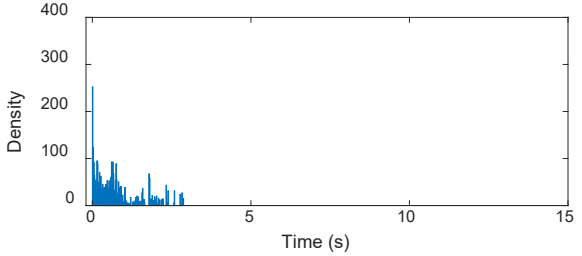
13	13a) 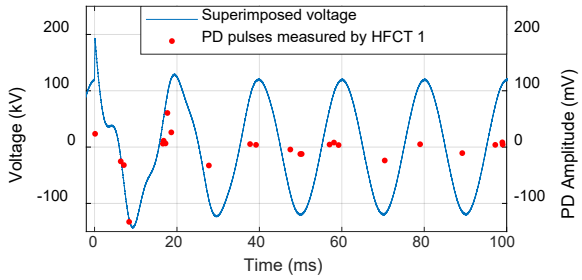	13b) 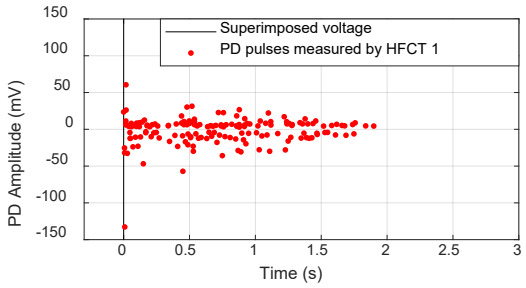	13c) 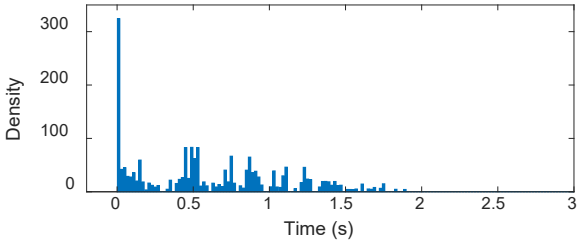

Test	PD occurrence during first five cycles	PD occurrence under transients	Current density
14	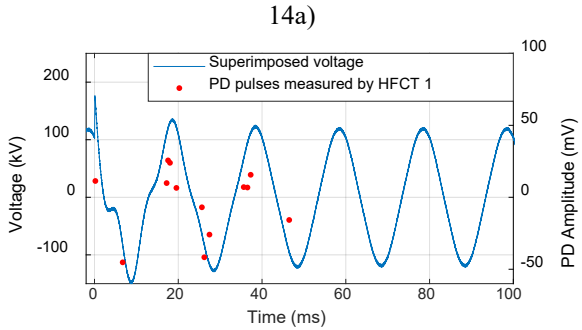	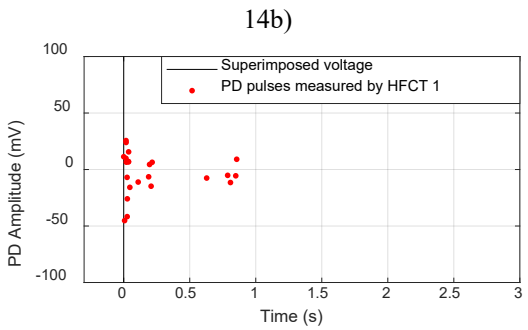	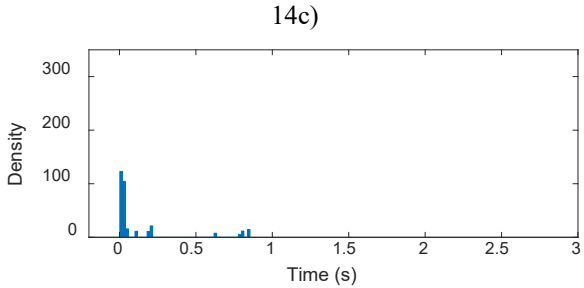
17	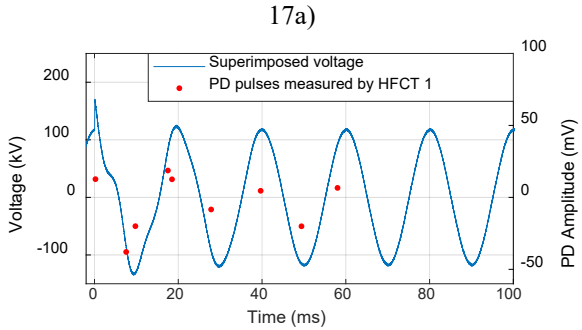	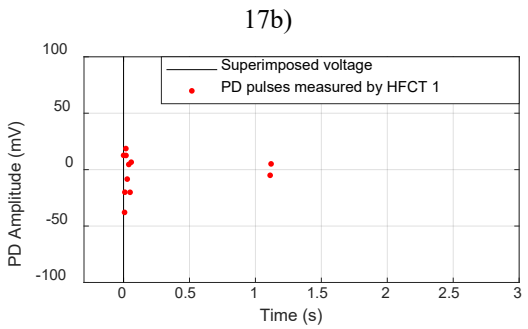	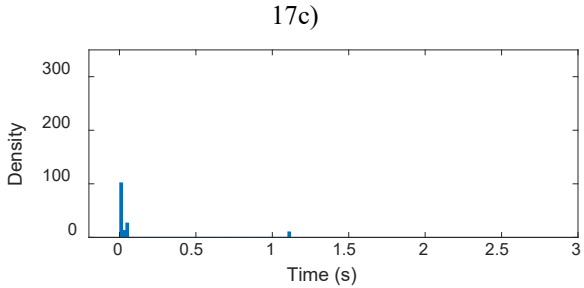

Figure 7.9: Measurement results of PD under transients (test 6, test 15 and test 16 are not shown in the figure since there were no PD observed).

Partial discharge initiation under superimposed transients

In most of the tests, partial discharges were initiated by the superimposed transients and persisted under AC voltage for a certain period of time. Although the PD behaviour is different for different transient waveforms, the principle of the PD initiation is similarly related to the electric field conditions within the defect. Test 13 with long impulse superimposed and test 2 with short impulse superimposed are to be described in details in the following.

Figure 7.9-13 depicts the measurement result in test 13. Since the applied impulse has long front time, it was able to observe the main discharge, which initiated as soon as the impulse was applied (Figure 7.9-13a). When the voltage turned to the negative cycle, several negative discharges occurred. The observed main discharge and the first negative discharge show their TRPD pulse shapes in Figure 7.10.

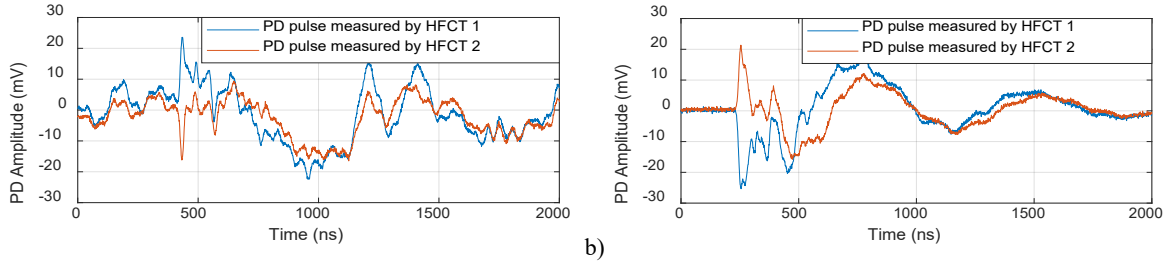

Figure 7.10: TRPD pulse shapes in test 13: a) the first main discharge, b) the first negative discharge.

The physical process of PD initiation determined by the electric field condition within the defect is described in Figure 7.11. Without considering the charge decay and the trapped charges (Figure 7.11a), the first main discharge initiates as soon as the local field E_i reaches the inception field E_{inc} at the impulse rising phase. After the discharge process, the charges deposited on the defect surface creates an opposite E_q, which deviates E_i from the background field E_c. When the voltage turned to the negative cycle, very soon E_i reaches the negative inception field $-E_{inc}$ and the negative discharges occur. After the positive discharge occurred in the next positive cycle, E_i regresses to E_c and no more PD occurs.

In practice, the charges left on the defect surface decay with time before the next discharge event occurring. Thus, instead of being constant, the created E_q decreases. This will influence the resulting E_i and PD occurrence. Considering this charge decay (Figure 7.11b), following the negative discharges in the first negative cycle, two positive discharges occur in the positive cycle and a negative E_q is left. With the decreasing E_q, E_i could reach the $-E_{inc}$ again leading to another discharge. And then the discharges reoccur. This is in accordance with the observation in the test (Figure 7.9-13a). Moreover, apart from the charges deposited on the defect surface, there are also charges that trapped on the surface with a certain energy level. If they obtain enough energy, they could escape from the traps and become free charges, which are potential first electrons for partial discharges to occur. If they stay in traps on the surface, they may also create a tiny field E_q which keeps E_i deviating from E_c.

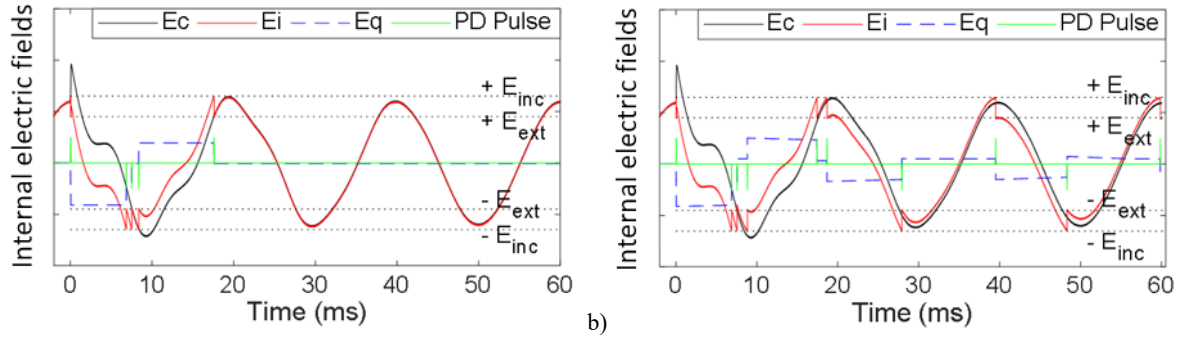

Figure 7.11: Schematical electric field conditions in test 13: a) without considering charge decay and the trapped charges, b) with considering charge decay and the trapped charges.

In test 13, the PD activity lasted for around two seconds. The PD extinction might be caused by the lack of the first free electron and insufficient local field. With more PDs occurring in the defect, the charges will increase the conduction of the defect surface, which leads to a faster charge decay. With faster charge decay, the created E_q after a PD event will decrease faster so that no more free charges are available as the first free electron. Without the E_q created by the deposited charges, the tiny field created by the trapped charges is not sufficient to drive E_i reaching E_{inc}. As a consequence, discharge cannot reoccur.

In test 2, the superimposed impulse has a short front time of 3 µs, which is within the dead zone of the PD measuring system. Therefore, it is not possible to detect main discharges during the impulse. As shown in (Figure 7.9-2a), the first detected PD is in the negative cycle. The main discharge, which is supposed to occur, can be seen from the analytical electric field condition (Figure 7.12). Without considering the charge decay (Figure 7.12a), main discharges initiate when the impulse is applied. During the first negative cycle, discharges reoccur for several times. Since no charge decay is considered, the field created by charges E_q keeps constant between every two PD pulses, and approximately reaches to zero after several PDs. With such tiny E_q, the local field E_i cannot reach the inception field E_{inc}. Thus PD extinguishes. If considering the charge decay (Figure 7.12b), the field created by charges E_q decreases between every two PD pulses. Due to the slow charge decay and the very short interval between every two PDs, the change in E_q is not obviously shown in the figure. However, after several PDs, the accumulated charge decay processes result in a positive E_q, which makes the local field E_i reach the inception field E_{inc}. Consequently, PD persist under AC voltage. Similar to the case in test 13, the PD activity lasted for around two seconds.

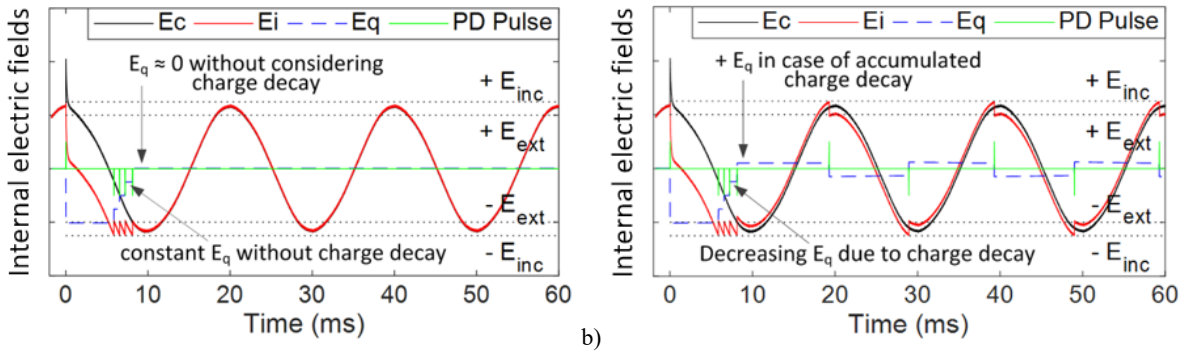

Figure 7.12: Schematical electric field conditions in test 2: a) without considering charge decay and the trapped charges, b) with considering charge decay and the trapped charges.

Since the partial discharge process is a dynamic process, and the real field conditions in the defect are influenced by many other factors, such as the defect dimension and shape, the gas composition in the defect, the aging condition of the insulation etc., the analytical electric field conditions cannot completely reveal the real field conditions within the defect. However, they are very helpful for understanding the probable physical process of partial discharges under the transients.

The results presented in Table 7.5 and Figure 7.9 show that, the superimposed transients could initiate partial discharges in the cable system. After the transient, the PD behaviour is influenced by the ongoing AC voltage which determines the background field E_c, as well as the surface charges left by previous discharges process which determines the E_q. The influence of different waveforms on the PD behaviour will be discussed in the following section.

Influence of different Ratios

In test 1 (Figure 7.9-1) and test 2 (Figure 7.9-2), the short impulses with T_f / T_h = 3 / 91 µs were superimposed on the same AC voltage of 88 kV_{rms} at 0° with different *Ratios* of 1.8 and 1.7 respectively. The PDIV were measured before each test as 97 kV_{rms}. As discussed before, partial discharges were supposed to initiate during the impulse. However, due to the dead zone of the PD measuring system, only PDs that occurred beyond the dead zone are detectable. This is why we could observe PDs only from the first negative cycle after the impulses. In test 1, the number and magnitude of PDs which occurred during the first cycle right after the impulses are relatively higher than that in test 2 (Figure 7.9-1a and Figure 7.9-2a). The maximum PD magnitudes as shown in Table 7.5 occurred in the first cycle in both tests. With time, both the PD magnitude and the PD number per cycle, i.e. the PD repetitive rate, decrease until PD extinguished. This is also seen in the PD density pattern (Figure 7.9-1c and Figure 7.9-2c). Due to the large number of PD occurred and the high magnitude of the occurred PDs, the PD densities of the first cycle in test 1 is relatively higher than in test 2. After the first cycle, the densities firstly decrease dramatically and then tenderly with time. In both tests, the PD activities lasted for a few seconds. In test 1 under waveform with higher *Ratio* of 1.8, a higher density is observed of the first cycle compared to that in test 2. Moreover, the PD activity lasted longer (longer duration) and more PDs occurred (larger PD number) during this process. Such difference in PD behaviour is seen as a result of different field conditions caused by the different *Ratios* even though the different is small. This is illustrated in (Figure 7.13). With higher *Ratio*, a larger impulse is superimposed on AC voltage, which results in a longer period of time during which the applied voltage is higher than the PDIV. This gives more chances for more PDs to occur in a short time. In addition, those consecutively occurring PD events would generate more charges which will contribute to a larger E_q. This would further lead to a larger E_i and therefore to more PD events. As a consequence, more charges are accumulated before decaying and recombination. Those charges enable PD activity to persist for a longer time under AC voltage. To sum up, the impulse determines the early initiated PDs, especially during the first cycle after the impulse. Those early initiated PDs further influence the PD behaviour under AC voltage.

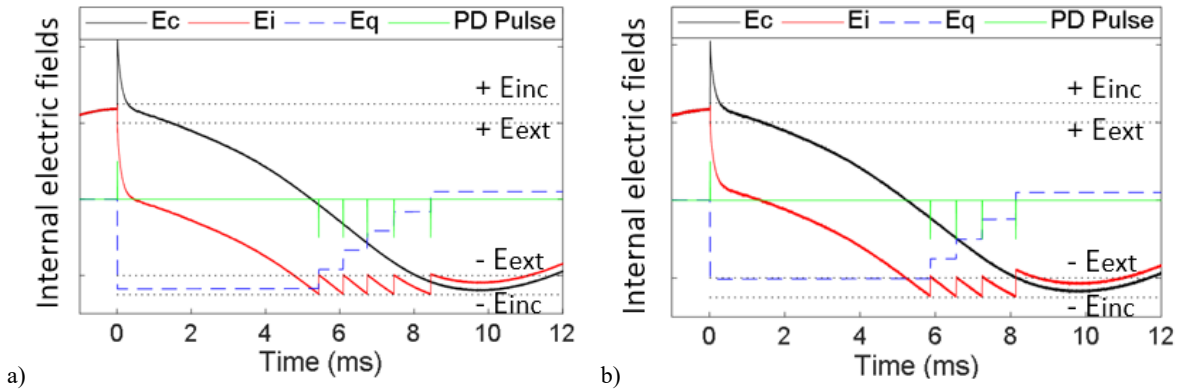

Figure 7.13: Schematical electric field conditions in test 1 and test 2 with different *Ratios*: a) test 1, *Ratio*=1.8, b) test 2, *Ratio*=1.7.

Similar effect of *Ratio* on partial discharge are observed with higher AC voltage in test 9 vs. test 10, and with longer impulses in test 13 vs. test 17. In test 9 and test 10 (Figure 7.9-9 and Figure 7.9-10), the short impulses were applied on an AC voltage of 94 kV_{rms} with *Ratio* of 1.8 and 1.7 respectively. With *Ratio* of 1.8, the PD density is higher both in the first cycle and in the AC cycles later. In total, more PDs occurred and the PD activity lasted longer. In test 13 and test 17 (Figure 7.9-13 and Figure 7.9-17), longer impulses with T_f / T_h = 93 / 845 µs were applied on AC of 88 kV_{rms}. Main discharges are observed during the impulse. With *Ratio* of 1.4 in test 17, very few PDs occurred, resulting in a small and short PD density pattern, a small PD number and duration in total.

Influence of different phase angles

In test 3 to test 6, the same impulses were superimposed on the AC voltage at phase angles of 0°, 30°,60° and 90° respectively. This results in different *Ratios* as shown in Table 7.5. When the impulse was applied at 0° in test 3 and at 30° in test 4, PD were always initiated by the impulse for all the repeated six tests (PD occurrence = 6/6). PD occurred in test 3 lasted slightly longer than that in test 4, and the PD density is also slightly higher than that in test 4 (Figure 7.9-3 and Figure 7.9-4). However, when the impulse was applied at 60° in test 5, in only one out of six tests (Figure 7.9-5) PDs occurred (PD occurrence = 1/6). And with 90° in test 6, no PD were initiated by the impulses among all the repeated tests (PD occurrence = 0/6).

Considering the analytical electric field perceptions, although the field conditions are slightly different under waveforms with 0° (Figure 7.14a) and 30° (Figure 7.14b), they cause similar PD events during the first cycle after the impulses. With angle of 60°, less PDs occurred (Figure 7.14c). And with angle of 90°, no PD could occur (Figure 7.14d).

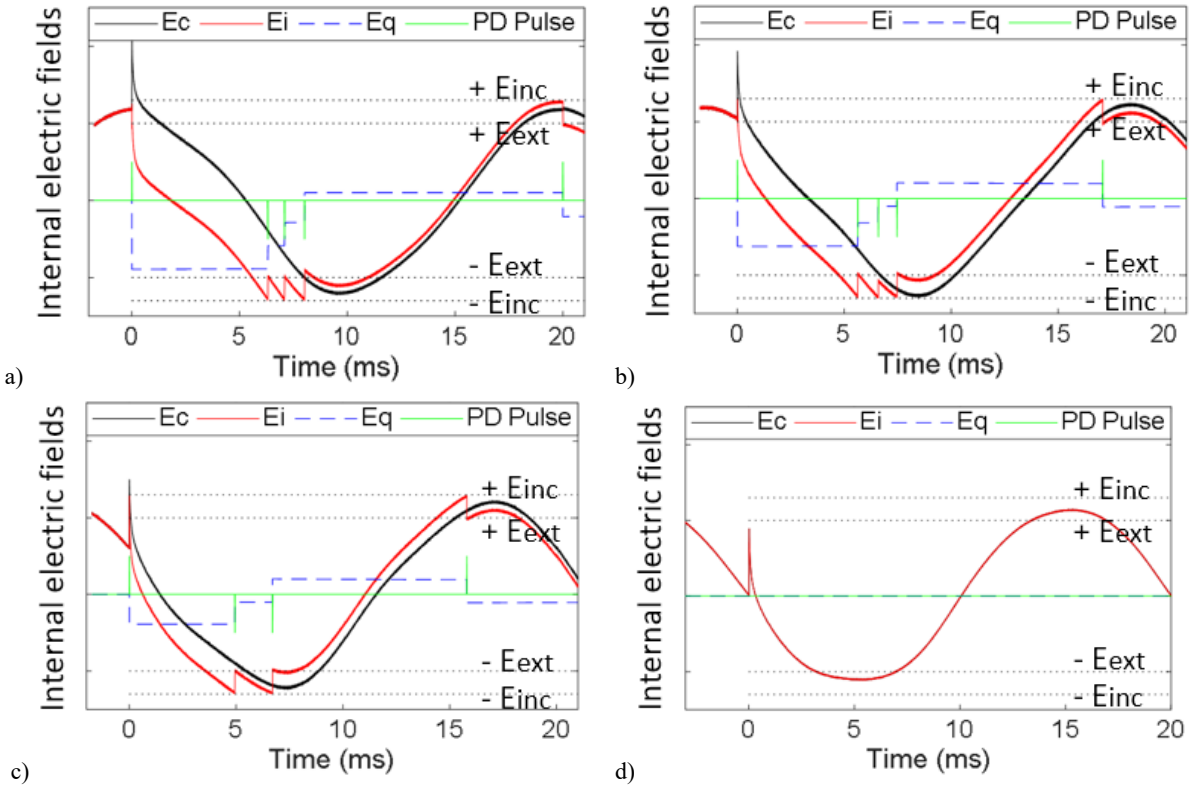

Figure 7.14: Schematical electric field conditions in test 3 to test 6 with different phase angles: a) test 3, φ=0°, b) test 4, φ=30°, c) test 5, φ=60°, d) test 6, φ=90°.

In test 3 to test 6, both the phase angle and the *Ratio* vary. Between these two parameters, we assume that the *Ratio*, more precisely the overvoltage value, is dominantly affecting the PD occurrence. This is illustrated in (Figure 7.15). For all the four tests, the PDIV was measured the same as 104 kV_{rms}. When the impulse was applied at a larger phase angle, a smaller peak value will be obtained. Consequently, the period of time that the voltage being higher than PDIV is shorter, or the voltage even cannot reach the PDIV. In this case, PD will not, or only have small chance to occur. This is what has been observed in test 5 and test 6. It is worth noting that, with 60° the overvoltage also exceeds the PDIV for a very short time in Figure 7.15, which is still supposed to initiate PDs. However, it is quite possible in practice that the first free electron for PD initiation cannot be available during this short time, or the local field deviates from the background field. Then PD missed the chance to initiate. Thus, for only one out of six tests PDs occurred in test 5.

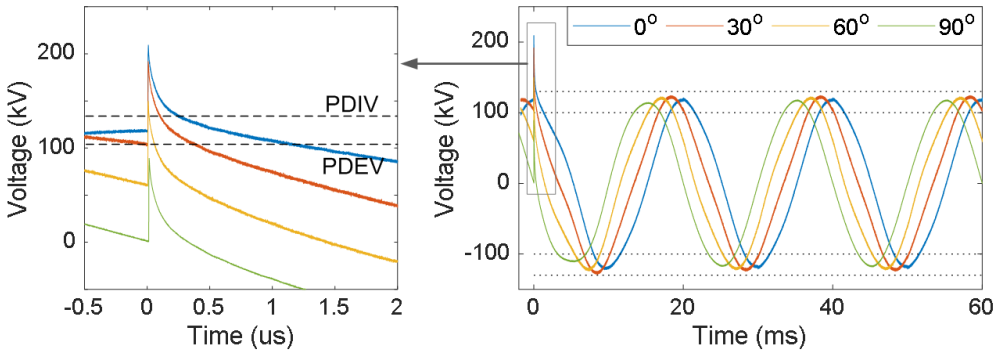

Figure 7.15: Overvoltage vs. PDIV in test 3 to test 6.

In order to further prove the assumption that the overvoltage value is the dominant parameter of PD occurrence, in test 8 the impulse was applied at the same phase angle of 60° as in test 5, while the resulting *Ratio* is of 1.4 being higher than that of 1.2 in test 5. In this case, PD were observed in all of the six tests (PD occurrence = 6/6). One measurement is shown in Figure 7.9-8. Hereby we can conclude that, the dominant parameter which influences the PD occurrence is the *Ratio*, or the overvoltage value.

The exactly same phenomenon was observed in test 13 to test 16 with longer impulses. PDs were always initiated (PD occurrence = 6/6) by the impulses when they were applied at 0° and 30°, while no PD was observed with the phase angles of 60° and 90° (PD occurrence = 0/6). PD that occurred in test 13 lasted longer than those in test 14, and the PD density is also much higher than that in test 14 (Figure 7.9-13 and Figure 7.9-14).

Influence of different PDIV values

The voltage waveforms applied in test 2 and test 3 were exactly the same, while the PDIV values measured before the tests were different. With lower PDIV of 97 kV_{rms} in test 2, it is easier for the voltage to reach the PDIV value. Therefore, more PDs were initiated in the first cycle but with lower amplitude (Figure 7.9-2b). The PD density is hereby lower (Figure 7.9-2c). The analytical electric field condition is seen in Figure 7.13b. However, the PD activity lasted longer (Figure 7.9-2a). With higher PDIV value, less PDs with higher amplitude occurred. The PD density is higher but the PD activity lasted shorter. The analytical electric field condition is seen in Figure 7.14a.

Similar phenomenon is observed in test 10 (Figure 7.9-10) and test 11 (Figure 7.9-11), where the AC voltage for both tests were set as 94 kV_{rms}.

Influence of different AC levels

If the PDIV value is kept the same, with all the other parameters the same but higher AC voltage, it is also easier for the voltage to reach the PDIV value and then initiate more PDs. The effect of AC level can be seen in test 1 vs. test 9, test 2 vs. test 10, and test 3 vs. test 11. In each pair of tests, under the waveform with higher AC voltage level, more PDs with higher amplitude initiated in the first cycle, the obtained PD densities are higher, and the PD activities lasted for longer time. The analytical field conditions in test 3and test 11 are seen in Figure 7.14a and Figure 7.16.

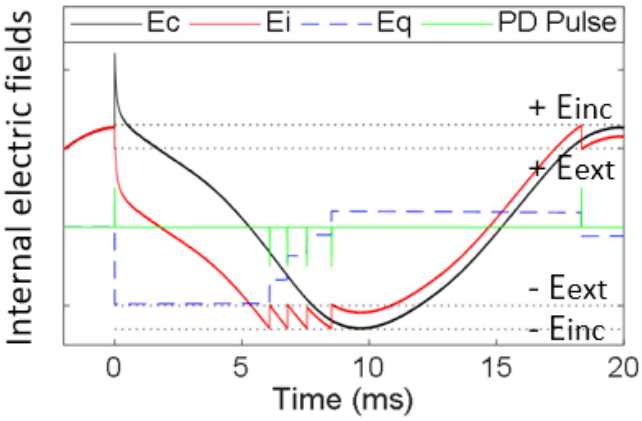

Figure 7.16: Schematical electric field conditions in test 11 with higher AC=94 kV_{rms}

Influence of different impulse polarities

In test 7, the same impulse as in test 3 was applied but with negative polarity and on the negative AC crest. Besides more PDs occurring in test 7, similar PD behaviour has been observed as in test 3. In test 11 and test 12 with higher AC voltage, the PD behaviour under positive impulse and negative impulse are similar as well. As a conclusion, the polarity of the impulse will not have an impact on the PD behaviour.

Uncertainty in PD data analysis

There might be errors in the PD measurement results given in Table 7.5 which might arise in the PD data analysis process. Usually, a single PD event was captured as one PD event by the two HFCT sensors as shown in Figure 7.10. However, it also happened that several PD events occurred consecutively with very short time interval, which was still acquired as one signal. Figure 7.17a shows one captured PD signal in test 11, in which actually three PD events occurred. When processing the PD data, these three PD events were regarded as one single PD event. In this way, another two PDs were missed, which brings errors to the PD measurement results. Figure 7.17b depicts another example measured in test 7, where two PD events occurred in series. Another type of error is caused by the misreading of the PD amplitude. As shown in Figure 7.17c which was measured in test 14, the small PD signal is superimposed on the relatively large disturbance signal. Such PD event can be easily missed, or its amplitude can be mistaken.

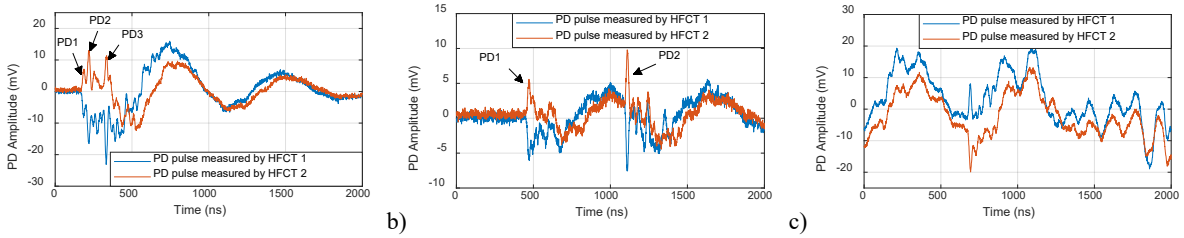

Figure 7.17: PD signals which may cause errors in PD parameters: a) PD occurred consecutively in test 11, b) PD occurred in series in test 7, c) PD signal superimposed on disturbance signal in test 14.

7.2.3 Case study of defect Type B

In the last section 7.2.2, PDs were investigated under superimposed voltages with a defect which can pass the maintenance test. In this section, the defect which can pass the commissioning test is investigated.

With the defect dimension of 6 mm, the artificial defect generates partial discharges at voltage above 1.7 U_0 and the partial discharge extinguish at voltage at 1.5 U_0. No partial discharge is detected at 1.5 U_0. This was performed following the PD test procedure given in section 3.2.5 and Figure 3.10. Such defect will pass the PD test in the after-laying commissioning tests and will be subjected to the operating voltage as described in section 3.2.5. The question is then, whether partial discharge will also initiate within such defect under superimposed transient situation as discussed in section 7.2.2. To answer this question, the same tests were performed on the HV cable system under the waveform shown in Figure 6.7b and with the test procedure given in section 7.2.1 (Figure 7.8). The AC voltage was set as the operating voltage of 87 kV_{rms}. Short impulses with T_f / T_h = 3 / 91 µs were superimposed on the AC voltage at the AC crest (φ=0°). The total peak value of the overvoltage V_{peak} increased stepwise. That is, the *Ratio* increased from 1.8 to 2.1. For each voltage, the measurement was repeated for six time. The PD measurement results are given in Table 7.6. In all the tests, no PD was detected being initiated by the superimposed transients. However, we could not conclude that no PD was initiated by the superimposed transients. It is possible that main discharges occurred, which however, were within the dead zone so that they cannot be detected. Or there is a probability that PDs could be initiated, which mean more measurements are desired for statistical purpose.

Table 7.6: Tests on HV cable under superimposed voltages with PD that pass after-laying commissioning tests.

T_f / T_h [µs]	AC [kV_{rms}]	V_{peak} [kV]	$\mathbf{Ratio} = \frac{V_{peak}}{V_{ACpeak}}$	φ [°]	PD
3 / 91	87	226	1.8	0	No
		235	1.9		No
		245	2.0		No
		256	2.1		No

7.3 Conclusions

Partial discharges in an artificial defect in a HV cable joint under superimposed transients were investigated by using the dedicated experimental set-up, which has been proposed and verified in chapter 6. The HV cable joint with different defect dimensions – different outbound displacements of cable - was subjected to different test voltages, as shown in Table 7.7, summarizing the tests and defect information.

Table 7.7: Summary of impulse tests and superimposed tests on HV cable system with different defect dimensions.

Defect dimensions D [mm]	PDIV [kV_{rms}]	PDEV [kV_{rms}]	Tests	AC levels [kV_{rms}]	Applicable tests with their PD pass criterion
7	104/97	90	Impulse voltages	-	Maintenance test at overvoltage: No detectable PD at $1.1U_0$ for cables > 15 years
			Superimposed voltages	87	
6	150	139	Superimposed voltages	87	Commissioning test at overvoltage: No detectable PD at $1.5U_0$

PD measurement results obtained from the pure impulse tests with the defect dimension of 7 mm (section 7.1) show that:

- Impulse voltage can initiate partial discharges with sufficient voltage level. Several main discharges initiated during the front time of the impulses. More reverse discharges occurred during the tail time of the impulses until the impulse finished.
- For the impulse voltages with the same shape (T_f/T_h), the higher the peak value, the earlier PD would initiate and the more PDs would occur during the entire impulse. While for the impulse voltages with the same peak value and different shapes, the shorter the impulse, the earlier PD would initiate. However, the wave shape doesn't influence the number of PD occurred. As a conclusion, however based on one cable model, the peak value of impulse voltage has more significant effect on partial discharges than the impulse shape. Thus, impulse voltage with high peak value needs more attention.

PD measurement results obtained from the defect dimension of 7 mm - which can pass the maintenance tests - under different superimposed transients (section 7.2.2) show that:

- Partial discharges can be initiated by the superimposed transients under certain conditions. When the impulse was applied, main discharges with the same polarity as the impulse were firstly initiated during the front time of the applied impulse. After the impulse finished, the initiated PDs were sustained by the AC voltage.
- The parameters of the superimposed transients have influences on the PD behaviour: the higher the peak overvoltage value, in other word the *Ratio*, the more numbers of PDs occur which would persist for a longer time under AC voltage. When the same impulse was superimposed on the AC voltage with a certain phase angle, the larger the phase angle (the farther the impulse is from the AC crest), the less probability PDs would occur and the less numbers of PDs would occur. With higher PDIV, less PDs with higher amplitude occurred. And higher AC voltage level may lead to more PDs with higher amplitude initiated in the first cycle and longer duration of PD activities. The polarity of the impulse does not have an impact on the PD behaviour.

The influence from the superimposed transients on PD behaviour can be explained by the electric field conditions within the defect under certain assumptions. Basically, the overvoltage of the impulse will

initiate a group of PDs with higher number and magnitude during the first cycle, which leave many charges on the defect surface and cause a change in the electric field condition. The generated charges will increase the probability of PD occurrence by contributing to the local field and providing free electrons. This will further influence the PD activity persisting under AC voltage. Different superimposed transients result in different situations of the first initiated PDs, and therefore the later PD behaviour.

PD measurement results from the defect dimension of 6 mm - which can pass the after-laying commissioning tests - under different superimposed transients (section 7.2.3) show that:

- No partial discharge was detected under the superimposed transients with the *Ratio* varying from 1.8 to 2.1. However, based on only one cable model, we cannot conclude that, with such defect partial discharge cannot be initiated by the superimposed transients. Due to the limitation of the test, the transient voltage was not further increased. It is possible that partial discharge will be initiated by a larger transient. Nevertheless, a transient with overvoltage higher than $2.1U_0$ rarely occurs in the reality, which also reduces the risk of PD initiation if such defect exists in the cable insulation.

Chapter 8

Conclusions and Recommendations

Based on our investigations in the foregoing chapters, conclusions on our main objective as formulated in section 1.3 are summarized in section 8.1 by first addressing what has been found regarding our research questions, next followed by the overall conclusion. Section 8.2 describes what remained beyond the scope of this thesis but is advised as recommendation for future work.

8.1 Conclusions

This section summarizes the answers based on the investigations in the foregoing chapters, thereby first citing the research question.

1. **What are the possible transient situations in the power system, e.g. in mixed overhead line and cable systems?**

Transients occurred in the power system are usually the results of switching operations or lightning strikes. We couldn't have collected the possible transient situations occurring in the HV system nowadays. However instead, we have collected the possible transients occurred in the Dutch 380 kV mixed overhead line and cable system. Simulations and field measurement results (Chapter 2) show that, transients as in the mixed overhead line and cable system can lead to overvoltage followed by oscillations at high frequencies.

The transients applied in the measurements were simplified due to experimental facilities, but they still incorporate the characteristics of the simulated and measured transients.

2. **What are the typical insulation defects occurring in cable accessories? How to design and prepare a proper HV research object that can incorporate the characteristics of the defects and possible problems brought by the defects?**

The dominating insulation defects are in the cable accessories, mainly located at the XLPE interface, caused by handling problems during installation (chapter 3). Many of the defects at interface - such as air gap, insulation damages, semi-conductive layer problems - will cause partial discharges. To replicate those typical defects in the cable models has research limitations. However, it is possible to simulate

defect conditions by creating artificial defects in the joint of the cable model, which can surely generate partial discharges. For MV cable models, we could create artificial defects by inserting a metal wire and a plastic tie-wrap strip into the joints along the interface. The former defect led to a small void most probably at the tip of the metal wire at the interface. The latter one led to air gaps along the interface. The measured PRPD patterns confirmed that these two defects generated internal discharges and surface discharges respectively. For the HV cable model, we created the artificial defect by moving the cable out of the joint over a small distance, thereby generating partial discharges. In the experiments this defect could be adjusted in dimension, and generate partial discharges with different PDIV and PDEV.

3. **How to investigate the effects of superimposed voltages on breakdown of a cable insulation by HV experiments? What are the effects?**

To investigate the effects of superimposed voltages on breakdown of cable insulation, polymeric material samples were prepared. A breakdown set-up was implemented to generate and apply the superimposed voltages to the material samples, and to measure the breakdown voltages under each testing voltage.

Our experiments show that, the superimposed voltages lead to lower breakdown strength in insulation materials compared to pure AC voltage (chapter 4). The breakdown strengths of small-scale XLPE material samples are much higher under DC voltage than under AC voltage (more than two times). The higher the AC frequency, the lower the breakdown strength. This might be caused by the increasing dielectric power losses with the increasing frequency. Under superimposed voltage waveforms, consisting of a high frequency sine wave in superposition with the 50 Hz AC voltage, insulation samples break down at lower AC voltage when the superimposed sine wave has larger amplitude.

Our experiments are limited to AC voltage with frequencies up to 2.5 kHz and superimposed waveforms. Moreover, the material samples were tested without creating defects on them.

4. **How to investigate the effects of transients on partial discharge behaviour of the cable insulation system by HV experiments? What are the effects?**

To investigate the effects of transients on partial discharge behaviour in MV and HV cables, cable models were prepared as test object consisting of cable and accessories, and artificial defects were created in the cable joints. An experimental set-up was implemented to generate and apply the superimposed transient voltages on the cable models, and to measure PD signals during the transients. The acquired PD data were analysed and presented in phase-resolved PD patterns (PRPD) and time-resolved PD pulses (TRPD) for interpretations (Chapter 5 and 6). The MV cable model was tested under superimposed transients. The HV cable model was subjected to both impulses and superimposed transients, which are realistic transients occurring in practice.

Our experiments confirmed that superimposed transients do initiate partial discharges in MV and HV cable accessories, under certain voltage conditions and defect dimensions. The experiment with MV cable models (Chapter 5) shows partial discharges were initiated by the transients during the impulse period. When the transients stopped and the voltage went back to normal AC voltage, different PD scenarios were observed as: extinction, intermittent recurrence and persistence. In addition, the closer the AC level of the superimposed voltage to the PDIV and the further from the PDEV, lesser superimposed voltages are needed to trigger PDs, and the triggered PD activities become more active and sustained.

The experiments with the HV cable model stressed by pure impulse voltage (chapter 7) show that for positive impulse voltage, PDs firstly initiate during the front time with positive polarity, which are

recognized as main discharges, and secondly appear during the tail time with negative polarity, which are referred to as reverse discharges. The experiment with the HV cable model with an artificial defect of a dimension fulfilling the requirements of supposedly a maintenance test used for cables in service, shows that partial discharges were initiated by the superimposed transients during the impulse moment when the transient overvoltage is larger than 1.4 U_0. The initiated PDs can persist for a certain period of time up to more than ten seconds after the voltage returns to AC operating level. The shape of the superimposed wave, including the peak overvoltage value, the AC voltage level, the phase angle at which the impulse is applied, has measurable influence on the PD behaviour in the sense of the number, the probability and the duration of PD occurrence, as well as the PD amplitude. With a defect dimension which allows a new cable to pass the after-laying commissioning tests, no partial discharge was detected under the superimposed transients with an overvoltage up to 2.1 U_0.

The influence of the superimposed transients on PD behaviour are related to several factors including the local electric field conditions, the availability of the initiatory electron, the charges deposited on the defect surface and in the traps, the charge decay process, and the aging status of the insulation. Basically, the overvoltage of the impulse will firstly initiate a group of PDs. The discharge process deposits charges on the defect surface, which feeds PD activity persisting under AC voltage.

Due to the limitation of the test circuit, the applied transient voltages can hardly be further increased. Only a few tests with overvoltage of the superimposed transients up to 2.1 U_0 could be performed on the cable model as required for new cable, however to consolidate conclusions more investigation is needed.

5. What kind of diagnostic knowledge should be acquired to obtain an early warning of the onset of partial discharges or degradation activated by transients, which can be used for power cable condition monitoring?

The cable model experiments show that artificially introduced hidden defects can become PD active due to transients superimposed on the AC nominal voltage. In HV laboratory conditions such PD activity was detectable, which in principle provides an early warning sign of degradation of a hidden defect. However, for detection of such PD during transients in the power system a field monitoring technology is still lacking. Preferably, PD measurements as in the lab need to be performed during transient situations in the power system. In case transients occur in the power system when the voltage is operating at a higher level up to 1.1 U_0, it was shown that the initiated partial discharges persisted longer under AC voltage after the transient stopped. Such transient situations deserve special attention for possible PD occurrence.

The above conclusions are drawn from the PD measurements on cable models simulating worse case defects. Also, experiments were carried out under laboratory conditions, which means the conclusions have certain limitations, as for example the transient waveforms are not exactly the same as in practice, and the transient overvoltage value that can be reached is limited. Moreover, the critical overvoltage values can be different in the field, since the real transients in field are more complex. However, our findings provide preliminary diagnostic knowledge to extend cable condition assessment with involving the effects of transients.

Overall Objective: to detect, reveal and understand the effects of transients on partial discharge phenomena and breakdown in high voltage cable insulation, which could potentially lead to an unexpected insulation failure.

Wrapping up the answers to all questions above, a better understanding of partial discharge behaviour in cable models under superimposed transients and of breakdown in insulation material samples under superimposed voltages has been achieved. In cable models we have detected partial discharges, which initiated under transient conditions only. It has been observed partial discharge behaviour dependent on the shape of the transients, and PDs can persist when the AC voltage condition returns. Moreover, the breakdown experiments on XLPE insulation samples show that the higher frequency sinusoidal voltages as well as the superimposed voltages cause lower breakdown strengths.

There are still subjects that have not completely been resolved such as: partial discharges and breakdown under other types of transients of more realistic defects, the PD patters collection for each type of defect under transients, the PD detection under transients in the field. To address these issues, some advices are proposed in the next section for future work and general recommendations.

8.2 Future Work and Recommendations

In view of the current project limitations we focused on one of the most prominent realistic defects located in the HV cable joint interface. However, with the changing conditions of the cable network in mind, it is advised to extend the knowledge build-up by including more transients as observed in practice and also other potentially detrimental defects, which occur in the insulation structures in the cable, the joints and terminations.

Experiments have shown that, partial discharges are initiated in the cable and accessories by transient situations. In some cases, the initiated PD extinguish soon while in other cases they are sustainably occurring. For condition monitoring it would be of interest to collect and build up a ‘database’ of all the possible PD characteristics or patterns under each possible transient situation.

The implemented PD measurements are suitable for laboratory tests. It is of interest to transfer the knowledge and diagnostic technique from laboratory to field circumstances, where, the noise and signal attenuation are the main issues and challenges to be addressed.

As extension to our research the following recommendations are given:

PDs which only occur at the impulse moment are difficult to be detected by common monitoring systems. Therefore, the development of a monitoring system which is able to measure PDs under an impulse transient within microseconds scale, is advised.

The PDs initiated by transients may not lead to breakdown immediately, but can accumulate insulation degradation. In particular, the PDIV may get decreased, which will cause more PD occurrence and accelerate the degradation. Moreover, such intermittent PDs can switch to sustained PDs, which damage the cable insulation. Therefore, it is important to monitor PDs when there is a transient (if known, such as switching actions) if possible, or to localize if such defects above PDIV exist.

The old cable systems, which have been exposed to aging process, could be more sensitive to transient situations. Even though a cable system has passed the maintenance tests, it is still quite possible that there are hidden defects existing in the system. When cable system encounters a transient situation, partial discharge can be initiated and reoccur. In this sense, it is still under discussion whether the maintenance tests criteria are properly set or need more adjustments.

Our research did not include field validation due to project limitations in time and financing. However, considering that our research shows that transients ignite sustaining PDs at artificial defect locations in joints, it is recommended that the cable owners to validate by non-destructive PD measurements in the field if such detrimental defect sites can be located in HV cables, which are known to be exposed to switching or other transient impulses. Our assembled knowledge about transient PD events obtained by our research may serve the cable owner's asset management to take preventive measures to avoid unexpected cable insulation failures.

Appendix

Table A.1: Setting of Marx impulse generator for generating different test impulses.

Waveform	C_{load} [nF]	Test	Impulse characteristics		Value/setting of each stage		
			T_f [µs]	T_h [µs]	C [nF]	R_f [Ω]	R_h [Ω]
Impulse	4.25	1	3	56	500	Stage 1-5: 35	Stage 1-5: 137
		2	3	2000		Stage 1-5: 35	Stage 1-5: 6000
		4	300	2650		Stage 1-5: 3400	Stage 1-5: 6000
Superimposed voltage	2.25	3	3	91		Stage 1-5: 35	Stage 1-5: 137
		5	93	714		Stage 1: 500, Stage 2-5: 35	Stage 1: 1325, Stage 2-5: 2170
		6	93	845		Stage 1: 500, Stage 2-5: 35	Stage 1-3: 137, Stage 4-5: 6000

Abbreviations and Symbols

γ	the gas combination in the cavity
β	the shape parameter in Weibull analysis, also known as the Weibull slope
$\emptyset_{rad}$	the ionizing quantum flux density regarding an air filled cavity
C_{rad}	the volume ionization parameter in the cavity
d	gas density in the cavity
p	gas pressure in the cavity
η	the scale parameter in Weibull analysis
ρ	correlation coefficient in Weibull analysis
σ_s	the surface conductivity
r_c	the equivalent radius of the circumference of the conducting surface
τ_{dc}	RC decay time constant
ε_0	permittivity
ϕ	phase angle of superimposed impulse on AC voltage
ω	Angular frequency (rad/s)
C	Capacitance in farad (F)
C_b	blocking capacitor
C_d	filtering capacitor for low-pass filter
C_k	coupling capacitor

C_{load}	load capacitance
E	the breakdown strength
E_c	electric field
E_{ext}	extinction field of PD
E_i	local electric field
E_{inc}	inception field of PD
$F(E)$	the cumulative probability of breakdown using Weibull analysis
E_q	electric field created by charges
H_n	the pulse count distribution
H_n'	the average pulse count distribution
l	void dimension
P	Dielectric power losses in watt (W)
R_d	filtering resistor for low-pass filter
R_f	front resistor for generating impulses
R_{h_LI}	tail resistor for generating lightning impulses
R_{h_SI}	tail resistor for generating switching impulses
t_{delay}	PD inception delay time
$tan\delta$	loss tangent or dissipation factor
T_f	front time of impulse
T_h	time to half value of impulse
U	Voltage in volt (V)
V_{ACpeak}	AC peak value
V_{peak}	peal value of transient overvoltage
AC	alternating current
DC	direct current
DSO	distribution system operator
HFCT	high frequency current transformer
HV	high voltage
MD	main discharges

MV	medium voltage
OHL	overhead line
PD	partial discharge
PDIV	PD inception voltage
PDEV	PD extinction voltage
PRPD	phase-resolved PD
Ratio	Total voltage peak to AC voltage peak ratio
RD	reverse discharges
SG	spark gap
TRPD	time-resolved PD
TVS	transient voltage suppressor
TSO	transmission system operator
UGC	underground cable
VD	voltage divider
XLPE	cross-linked polyethylene

Bibliography

[1] CIGRÉ WG C4.502, “Power system technical performance issues related to the application of Long HVAC cables,” Technical Brochure 556, Paris, October 2013.

[2] CIGRÉ WG B1.30, “Cable systems electrical characteristics,” Technical Brochure 531, Paris, April 2013.

[3] CIGRÉ WG B1.10, “Update of service experience of HV underground and submarine cable systems,” Technical Brochure 379, Paris, April 2009.

[4] CIGRÉ WG B1.07, “Statistics of AC underground cables in power networks,” Technical Brochure 338, Paris, December 2007.

[5] CIGRÉ WG B1.47, “Implementation of long AC HV and EHV cable systems,” Technical Brochure 680, Paris, March 2017.

[6] O. Ongkiehong and S. Eos, “Description of the state under the Dutch energy research program,” EOS (Energie Onderzoek Strategie), September 2006.

[7] V. Maanen, D. Gl, and S. Meijer, “Failures in underground power cables – return of experience,” in 9th International Conference on Insulated Power Cables, Jicable'15, Versailles 21-25 June, 2015.

[8] CIGRÉ B1.22, “Cable Accessory Workmanship on Extruded High Voltage Cables,” Technical Brochure 476, Paris, October 2011.

[9] C. Zhou, H. Yi, and X. Dong, “Review of recent research towards power cable life cycle management,” *High Volt.*, vol. 2, no. 3, pp. 179–187, 2017.

[10] C. Zhou, X. Jing, Z. Tang, W. Jiang, B. Alkali, and J. Yu, “Statistical Approaches for Analysis of Failure Data in Power Cables,” p. 9.

[11] J. Densley, “Ageing mechanisms and diagnostics for power cables - an overview,” *IEEE Electr. Insul. Mag.*, vol. 17, no. 1, pp. 14–22, Jan. 2001.

[12] R. A. Hartlein and R. N. Hampton, “Cable Diagnostic Focused Initiative,” DOE/CH/11237-Final Report, 1004068, Dec. 2010.

[13] G. Hoogendorp, “Steady State and transient behavior of underground cables in 380 kV transmission grids,” Delft University of Technology, 2016.

[14] R. Hartlein *et al.*, “Applying Diagnostics to Enhance Cable System Reliability (Cable Diagnostic Focused Initiative, Phase II),” 1255949, Feb. 2016.

[15] CIGRÉ WG B1.05, “Transient voltages affecting long cables,” Technical Brochure 268, April 2005.

[16] H. Khalilnezhad, “Technical Performance of EHV Power Transmission Systems with Long Underground Cables,” Delft University of Technology, 2018.

[17] F. Barakou, “Investigation of the impact of EHV underground power cables on the resonant and transient grid behavior.” Technische Universiteit Eindhoven, 2018.

[18] CIGRÉ, WG B1.09, *“Remaining Life Management of Existing AC Underground Lines,”* Technical Brochure 358, Paris, October 2008.

[19] K. Abdolall, A. J. Vandermaar, M. Stephens, and D. Tarampi, “Effects of testing on service aged XLPE cables,” in *2015 IEEE Electrical Insulation Conference (EIC)*, 2015, pp. 93–97.
[20] L. Cao and S. Grzybowski, “Accelerated aging study on 15 kV XLPE and EPR cables insulation caused by switching impulses,” *IEEE Trans. Dielectr. Electr. Insul.*, vol. 22, no. 5, pp. 2809–2817, Oct. 2015.
[21] L. Xu *et al.*, “The degradation of 10kV XLPE cable accessories under switching impulses,” in *2018 12th International Conference on the Properties and Applications of Dielectric Materials (ICPADM)*, 2018, pp. 463–466.
[22] L. Cao, A. Zanwar, and S. Grzybowski, “Electrical aging phenomena of medium voltage EPR cable energized by ac voltage with switching impulses superimposed,” in *2011 IEEE Electric Ship Technologies Symposium*, 2011, pp. 353–356.
[23] R. J. Densley and B. Salvage, “Partial Discharges in Gaseous Cavities in Solid Dielectrics under Impulse Voltage Conditions,” *IEEE Trans. Electr. Insul.*, vol. EI-6, no. 2, pp. 54–62, Jun. 1971.
[24] R. J. Densley, “Partial Discharges in Electrical Insulation under Combined Alternating and Impulse Stresses,” *IEEE Trans. Electr. Insul.*, vol. EI-5, no. 4, pp. 96–103, Dec. 1970.
[25] X. F. Zhao, X. Yao, Z. F. Guo, Y. Y. Wang, J. H. Li, and Y. M. Li, “Partial discharge characteristics and mechanism in voids at impulse voltages,” *Meas. Sci. Technol.*, vol. 22, no. 3, p. 035704, Mar. 2011.
[26] CIGRÉ, WG B1.09, “Remaining Life Management of Existing AC Underground Lines, ” Technical Brochure 358, Paris, October 2008.
[27] CIGRÉ WG B1.04. “Maintenance for HV Cables and Accessories.” Technical Brochure 279, Paris, August 2005.
[28] CIGRÉ WG B1.29, “Guidelines for maintaining the integrity of XLPE transmission cable accessories,” Technical Brochure 560, Paris, December 2013.
[29] J.J. Smit, E. Gulski, and E. Pultrum, “PD Fault Analysis of SIR-based Cable Terminations，Proceedings of the 10th International Symposium on High Voltage Engineering, ISH1997, Montreal, Canada, August 25-29, 1997. .
[30] Mousavi Gargari, S (Shima), “Pattern recognition and knowledge extraction for on-line partial discharge monitoring with defect location.” Technische Universiteit Eindhoven, 2012.
[31] CIGRÉ, WG 21.06, “Accessories for HV Cables with Extruded Insulation, ” Technical Brochure 177, Paris, February 2001.
[32] CIGRÉ WG B1.21. “Third-party damage to underground and submarine cables.” Technical Brochure 398, Paris, December 2009.
[33] IEC 60505, “Evaluation and qualification of electrical insulation systems,” April 2017.
[34] L. A. Dissado and J. C. Fothergill, *Electrical Degradation and Breakdown in Polymers*. IET, 1992.
[35] CIGRÉ, Joint Task Force 21/15, “Interfaces in Accessories for Extruded HV and EHV cables, ” Technical Brochure 210, Paris, August 2002.
[36] IEC 60505-2004, “Evaluation and qualification of electrical insulation systems” October 2004.
[37] S. Boggs and J. Densley, “Fundamentals of partial discharge in the context of field cable testing,” *IEEE Electr. Insul. Mag.*, vol. 16, no. 5, pp. 13–18, Sep. 2000.
[38] IEC 60505 Annex A, “Evaluation and qualification of electrical insulation systems” December 2010.
[39] “F. H. Kreuger, Industrial High Voltage-Vol. I, Delft University Press, Delft, The Netherlands, 1991.”.
[40] L. A. Dissado and J. C. Fothergill, *Electrical Degradation and Breakdown in Polymers*. IET, 1992.
[41] U. Fromm, “Partial discharge and Breakdown Testing at High DC Voltage.” Ph.D. dissertation, Delft University Press, 1995.
[42] “F. H. Kreuger, Industrial High Voltage-Vol. II, Delft University Press, Delft, The Netherlands, 1992.” .
[43] CIGRÉ WG A1.39, “Dielectric dissipation factor measurements on new stator bars and coils.” Technical Brochure 769, Paris, June 2019 .
[44] “IEEE Recommended Practice for Measurement of Power Factor Tip-Up of Electric Machinery Stator Coil Insulation,” *IEEE Std 286-2000*, pp. i–29, 2001.
[45] S. A. Boggs, “Partial discharge. III. Cavity-induced PD in solid dielectrics,” *IEEE Electr. Insul. Mag.*, vol. 6, no. 6, pp. 11–16, Nov. 1990.

[46] P. H. F. Morshuis, “Partial Discharge Mechanisms - Mechanisms leading to breakdown, analyzed by fast electrical and optical measurements” Ph.D. dissertation, Delft University Press, 1993.
[47] S. A. Boggs, “Partial discharge: overview and signal generation,” *IEEE Electr. Insul. Mag.*, vol. 6, no. 4, pp. 33–39, Jul. 1990.
[48] L. Niemeyer, “A generalized approach to partial discharge modeling,” *IEEE Trans. Dielectr. Electr. Insul.*, vol. 2, no. 4, pp. 510–528, Aug. 1995.
[49] F. Gutfleisch and L. Niemeyer, “Measurement and simulation of PD in epoxy voids,” *IEEE Trans. Dielectr. Electr. Insul.*, vol. 2, no. 5, pp. 729–743, Oct. 1995.
[50] G. C. Crichton, P. W. Karlsson, and A. Pedersen, “Partial discharges in ellipsoidal and spheroidal voids,” *IEEE Trans. Electr. Insul.*, vol. 24, no. 2, pp. 335–342, Apr. 1989.
[51] I. W. McAllister, “Partial discharges in spheroidal voids. Void orientation,” *IEEE Trans. Dielectr. Electr. Insul.*, vol. 4, no. 4, pp. 456–461, Aug. 1997.
[52] M. Gamez-Garcia, R. Bartnikas, and M. R. Wertheimer, “Synthesis Reactions Involving XLPE Subjected to aartial Discharges,” *IEEE Trans. Electr. Insul.*, vol. EI-22, no. 2, pp. 199–205, Apr. 1987.
[53] E. Cartier and P. Pfluger, “Detection of Hot Electron-Induced Radiation Damage in Organic Dielectrics by Exoelectron Emission from Thin Films,” *IEEE Trans. Electr. Insul.*, vol. EI-22, no. 2, pp. 123–128, Apr. 1987.
[54] H.-R. Zeller, T. Baumann, E. Cartier, H. Dersch, P. Pfluger, and F. Stucki, “The physics of electrical breakdown and prebreakdown in solid dielectrics,” in *Festkörperprobleme 27*, Springer, Berlin, Heidelberg, 1987, pp. 223–240.
[55] R. M. Eichhorn, *Engineering Dielectrics Volume Iia Electrical Properties of Solid Insulating Materials: Molecular Structure and Electrical Behavior*. ASTM International, 1983.
[56] H.- Burgener and K. Frohlich, “Probability of partial discharge inception in small voids,” in *2001 Annual Report Conference on Electrical Insulation and Dielectric Phenomena (Cat. No.01CH37225)*, 2001, pp. 298–302.
[57] T. Tanaka, “Internal Partial Discharge and Material Degradation,” *IEEE Trans. Electr. Insul.*, vol. EI-21, no. 6, pp. 899–905, Dec. 1986.
[58] E. C. Rogers, “The self-extinction of gaseous discharges in cavities in dielectrics,” *Proc. IEE - Part Power Eng.*, vol. 105, no. 24, pp. 621–630, Dec. 1958.
[59] M. Gamez-Garcia, R. Bartnikas, and M. R. Wertheimer, “Synthesis Reactions Involving XLPE Subjected to Partial Discharges,” *IEEE Trans. Electr. Insul.*, vol. EI-22, no. 2, pp. 199–205, Apr. 1987.
[60] P. H. F. Morshuis and F. H. Kreuger, “Transition from streamer to Townsend mechanisms in dielectric voids,” *J. Phys. Appl. Phys.*, vol. 23, no. 12, pp. 1562–1568, Dec. 1990.
[61] M. Gamez-Garcia, R. Bartnikas, and M. R. Wertheimer, “Modification of XLPE exposed to partial discharges at elevated temperature,” *IEEE Trans. Electr. Insul.*, vol. 25, no. 4, pp. 688–692, Aug. 1990.
[62] P. H. F. Morshuis and F. H. Kreuger, “The evolution of the discharge mechanism in a dielectric bounded cavity due to surface effects,” in *[1991] Proceedings of the 3rd International Conference on Properties and Applications of Dielectric Materials*, 1991, pp. 672–675 vol.2.
[63] P. H. F. Morshuis, “Degradation of solid dielectrics due to internal partial discharge: some thoughts on progress made and where to go now,” *IEEE Trans. Dielectr. Electr. Insul.*, vol. 12, no. 5, pp. 905–913, Oct. 2005.
[64] K. D. Wolter, J. Tanaka, and J. F. Johnson, “A Study of the Gaseous Degradation Products of Corona-Exposed Polyethylene,” *IEEE Trans. Electr. Insul.*, vol. EI-17, no. 3, pp. 248–252, Jun. 1982.
[65] K. D. Wolter, J. F. Johnson, and J. Tanaka, “Degradation Product Analysis for Polymeric Dielectric Materials Exposed to Partial Discharges,” *IEEE Trans. Electr. Insul.*, vol. EI-13, no. 5, pp. 327–336, Oct. 1978.
[66] P. Dejean, N. Foulon, M. Goldman, and H. Dejean, “Chemical aspects of the ageing of solid insulating materials submitted to partial discharges,” in *[1992] Proceedings of the 4th International Conference on Conduction and Breakdown in Solid Dielectrics*, 1992, pp. 181–185.

[67] M. Goldman, A. Goldman, and J. Gatellet, “Physical and chemical aspects of partial discharges and their effects on materials,” *IEE Proc. - Sci. Meas. Technol.*, vol. 142, no. 1, pp. 11–16, Jan. 1995.
[68] P. Morshuis, “Assessment of dielectric degradation by ultrawide-band PD detection,” *IEEE Trans. Dielectr. Electr. Insul.*, vol. 2, no. 5, pp. 744–760, Oct. 1995.
[69] J. T. Holboll and M. Henriksen, “Partial discharge patterns and surface deterioration in voids in filled and unfilled epoxy,” in *Conference Record of the 1992 IEEE International Symposium on Electrical Insulation*, 1992, pp. 354–358.
[70] A. Pedersen, G. C. Crichton, and I. W. McAllister, “The theory and measurement of partial discharge transients,” *IEEE Trans. Electr. Insul.*, vol. 26, no. 3, pp. 487–497, Jun. 1991.
[71] J. Densley, T. Kalicki, and Z. Nodolny, “Characteristics of PD pulses in electrical trees and interfaces in extruded cables,” *IEEE Trans. Dielectr. Electr. Insul.*, vol. 8, no. 1, pp. 48–57, Feb. 2001.
[72] IEC 60270. “High-voltage test techniques - Partial discharge measurements”, March, 2001.
[73] CIGRÉ WG 21.16, “Partial Discharge Detection in installed HV extruded cable systems” Technical Brochure 182, Paris, April 2001.
[74] E. Gulski, J. J. Smit, and F. J. Wester, “PD knowledge rules for insulation condition assessment of distribution power cables,” *IEEE Trans. Dielectr. Electr. Insul.*, vol. 12, no. 2, pp. 223–239, Apr. 2005.
[75] M. Fenger, “Experiences with commissioning testing of HV EHV cable systems: The influence of voltage level and duration for identifying life limiting defects,” in *2012 IEEE International Symposium on Electrical Insulation*, 2012, pp. 242–249.
[76] G. C. Stone, “Partial discharge diagnostics and electrical equipment insulation condition assessment,” *IEEE Trans. Dielectr. Electr. Insul.*, vol. 12, no. 5, pp. 891–904, Oct. 2005.
[77] CIGRÉ WG B1.28, “On-site partial discharge assessment oh HV and EHV cable systems”, Technical Brochure 728, Paris, 2013.
[78] CIGRÉ WG D1.33, “High-voltage on-site testing with partial discharge measurement”, Technical Brochure 502, Paris, June 2012.
[79] F. J. Wester, “Condition Assessment of Power Cables using Partial Discharge Diagnosis at Damped AC Voltages,” Ph.D. dissertation, Delft University, 2004.
[80] CIGRÉ WG B1.28, “On-site partial discharge assessment on HV and EHV cable systems”, Technical Brochure 728, Paris, May 2018.
[81] J. C. Chan, P. Duffy, L. J. Hiivala, and J. Wasik, “Partial discharge. VIII. PD testing of solid dielectric cable,” *IEEE Electr. Insul. Mag.*, vol. 7, no. 5, pp. 9–16, Sep. 1991.
[82] E. Lindell, T. Bengtsson, J. Blennow, and S. M. Gubanski, “Measurement of partial discharges at rapidly changing voltages,” *IEEE Trans. Dielectr. Electr. Insul.*, vol. 15, no. 3, pp. 823–831, Jun. 2008.
[83] A. Rodrigo Mor, L. C. Castro Heredia, D. A. Harmsen, and F. A. Muñoz, “A new design of a test platform for testing multiple partial discharge sources,” *Int. J. Electr. Power Energy Syst.*, vol. 94, pp. 374–384, Jan. 2018.
[84] CIGRÉ WG D1.33, “Guidelines for Unconventional Partial Discharge Measurements”, Technical Brochure 444, Paris, December. 2010.
[85] IEC/TS-62478 - Ed 1.0, “High Voltage Test Techniques—Measurement of Partial Discharges by Electromagnetic and Acoustic Methods”, August, 2016.
[86] A. Rodrigo, P. Llovera, V. Fuster, and A. Quijano, “High performance broadband capacitive coupler for partial discharge cable tests,” *IEEE Trans. Dielectr. Electr. Insul.*, vol. 20, no. 2, pp. 479–487, Apr. 2013.
[87] IEC/TS 61934 - Ed 2.0, “Electrical insulating materials and systems--electrical measurement of partial discharges (PD) under short rise time and repetitive voltage impulses”, 201.
[88] N. Hayakawa, Y. Yoshitake, N. Koshino, T. Ueda, and H. Okubo, “Impulse partial discharge characteristics and their mechanisms under non-uniform electric field in N/sub 2//SF/sub 6/ gas mixtures,” *IEEE Trans. Dielectr. Electr. Insul.*, vol. 12, no. 5, pp. 1035–1042, Oct. 2005.
[89] H. Ji, G. Ma, C. Li, Z. Pang, and S. Zheng, “Influence of voltage waveforms on partial discharge characteristics of protrusion defect in GIS,” *IEEE Trans. Dielectr. Electr. Insul.*, vol. 23, no. 2, pp. 1058–1067, Apr. 2016.

[90] J. Deng *et al.*, "Partial discharge characteristics of uniform gap in oil-impregnated paper insulation under switching impulse voltage," *IEEE Trans. Dielectr. Electr. Insul.*, vol. 23, no. 6, pp. 3584–3592, Dec. 2016.
[91] L. Zhang, X. Han, and J. Li, "Partial discharge detection and analysis of needle-plane defect in SF6 under negative oscillating lightning impulse voltage based on UHF method," *IEEE Trans. Dielectr. Electr. Insul.*, vol. 24, no. 1, pp. 296–303, Feb. 2017.
[92] M. Ren, M. Dong, R. Ye, and Y. Liu, "Partial discharge test under standard oscillating impulses on a gas-insulated bus with artificial metal particle defects on the insulator surface," *IEEE Trans. Dielectr. Electr. Insul.*, vol. 23, no. 6, pp. 3593–3601, Dec. 2016.
[93] V. R Garcia-Colon, J. A. Estrada García, W. K. Ley Cotoc, E. Betancourt Ramirez, "Development of Ultra Wide Band Partial Discharge Sensors for Power Transformer Winding Insulation." *Cigre Session* 2008, paper D1-211.
[94] H. A. Illias, M. A. Tunio, H. Mokhlis, G. Chen, and A. H. A. Bakar, "Experiment and modeling of void discharges within dielectric insulation material under impulse voltage," *IEEE Trans. Dielectr. Electr. Insul.*, vol. 22, no. 4, pp. 2252–2260, Aug. 2015.
[95] N. Hayakawa, R. Yamaguchi, Y. Ukai, H. Kojima, F. Endo, and H. Okubo, "Partial discharge activities under AC/impulse superimposed voltage in LN2/polypropylene laminated paper insulation system for HTS cables," *J. Phys. Conf. Ser.*, vol. 234, no. 3, p. 032020, Jun. 2010.
[96] R. Nikjoo, N. Taylor, and H. Edin, "Effect of superimposed impulses on AC partial discharge characteristics of oil-impregnated paper," *IEEE Trans. Dielectr. Electr. Insul.*, vol. 23, no. 6, pp. 3602–3611, Dec. 2016.
[97] T. R. Blackburn, B. T. Phung, and Z. Hao, "On-line partial discharge monitoring for assessment of power cable insulation," in *Proceedings of 2005 International Symposium on Electrical Insulating Materials, 2005. (ISEIM 2005).*, 2005, vol. 3, pp. 865-868 Vol. 3.
[98] D. A. Nattrass, "Partial discharge measurement and interpretation," *IEEE Electr. Insul. Mag.*, vol. 4, no. 3, pp. 10–23, May 1988.
[99] N. H. Ahmed and N. N. Srinivas, "On-line partial discharge detection in cables," *IEEE Trans. Dielectr. Electr. Insul.*, vol. 5, no. 2, pp. 181–188, Apr. 1998.
[100] E. Gockenbach and W. Hauschild, "The selection of the frequency range for high-voltage on-site testing of extruded insulation cable systems," *IEEE Electr. Insul. Mag.*, vol. 16, no. 6, pp. 11–16, Nov. 2000.
[101] W. Li, J. Li, F. Zhou, S. Wang, H. Li, and S. Li, "The effect of frequency on the breakdown of XLPE cable insulation with artificial defects," in *2012 Annual Report Conference on Electrical Insulation and Dielectric Phenomena*, 2012, pp. 375–378.
[102] J. C. Das, *Transients in Electrical Systems - Analysis, Recognition, and Mitigation*. McGraw-Hill Companies, 2010.
[103] Z. Wang, L. Pang, T. Wang, H. Yang, Q. Zhang, and J. Li, "Breakdown characteristics of oil-paper insulation under lightning impulse waveforms with oscillations," *IEEE Trans. Dielectr. Electr. Insul.*, vol. 22, no. 5, pp. 2620–2627, Oct. 2015.
[104] IEC 60243-1, "Electric strength of insulating materials - Test methods - Part 1: Tests at power frequencies," July, 2013.
[105] IEC 60243-2, "Electric strength of insulating materials - Test methods - Part 2: Additional requirements for tests using direct voltage," February, 2014.
[106] R. B. Abernethy, *The new Weibull handbook: reliability & statistical analysis for predicting life, safety, risk, support costs, failures, and forecasting warranty claims, substantiation and accelerated testing, using Weibull, Log normal, Crow-AMSAA, Probit, and Kaplan-Meier models*. North Palm Beach, Fla.: R.B. Abernethy, 2008.
[107] IEC 62539, "Guide for the statistical analysis of electrical insulation breakdown data," August, 2007.
[108] "(Replaced) IEEE Guide for the Statistical Analysis of Electrical Insulation Breakdown Data," *IEEE Std 930-2004 Revis. IEEE Std 930-1987*, pp. 1–41, Apr. 2005.
[109] E. Gulski, "Computer-aided recognition of partial discharges using statistical tools," Delft University Press, Delft, 1991.

[110] M. Hikita, K. Yamada, A. Nakamura, T. Mizutani, A. Oohasi, and M. Ieda, "Measurements of partial discharges by computer and analysis of partial discharge distribution by the Monte Carlo method," *IEEE Trans. Electr. Insul.*, vol. 25, no. 3, pp. 453–468, Jun. 1990.
[111] P. Chowdhuri *et al.*, "Review of research on nonstandard lightning voltage waves," *IEEE Trans. Power Deliv.*, vol. 9, no. 4, pp. 1972–1981, Oct. 1994.
[112] IEC 60885-3, "Electrical test methods for electric cables-part 3: test methods for PD measurements on lengths of extruded power cables," June, 2015.
[113] "Partial discharges software - PDflex: PD parameters and clustering," *PDFlex - Unconventional partial discharge analysis*. [Online]. Available: http://pdflex.tudelft.nl/. [Accessed: 28-Aug-2018].
[114] A. R. Mor, L. C. C. Heredia, and F. A. Munoz, "Estimation of charge, energy and polarity of noisy partial discharge pulses," *IEEE Trans. Dielectr. Electr. Insul.*, vol. 24, no. 4, pp. 2511–2521, 2017.
[115] A. R. Mor, P. H. F. Morshuis, and J. J. Smit, "Comparison of charge estimation methods in partial discharge cable measurements," *IEEE Trans. Dielectr. Electr. Insul.*, vol. 22, no. 2, pp. 657–664, Apr. 2015.
[116] F. J. Wester, E. Guilski, and J. J. Smit, "Detection of Partial Discharges at Different AC Voltage Stresses in Power Cables," *IEEE Electr. Insul. Mag.*, vol. 23, no. 4, pp. 28–43, Jul. 2007.
[117] "Prysmian HVC LR 220 kV Cable." [Omline]. Available: https://www.prysmiangroup.com/en.
[118] "On-line Partial Discharge Products and Test Services | HVPD." [Online]. Available: https://www.hvpd.co.uk/. [Accessed: 08-Mar-2019].
[119] X. Hu, W. H. Siew, M. D. Judd, and X. Peng, "Transfer function characterization for HFCTs used in partial discharge detection," *IEEE Trans. Dielectr. Electr. Insul.*, vol. 24, no. 2, pp. 1088–1096, Apr. 2017.
[120] A. R. Mor, F. A. Muñoz, J. Wu, and L. C. C. Heredia, "Automatic partial discharge recognition using the cross wavelet transform in high voltage cable joint measuring systems using two opposite polarity sensors", International Journal of Electrical Power & Energy Systems, vol. 117, May 2020.
[121] CIGRÉ WG D1.33, "Guidelines for Unconventional Partial Discharge Measurements", Technical Brochure 444, Paris, December. 2010.

List of Publications

Journal papers

[1] J. Wu, A. Rodrigo Mor, J. J. Smit, “Partial discharges activated by impulses and superimposed voltages in a high voltage cable model”, International Journal of Electrical Power & Energy Systems, submitted in Feb. 2020.

[2] J. Wu, A. Rodrigo Mor, P. V. M. van Nes, J. J. Smit, “Measuring method for partial discharges in a high voltage cable system subjected to impulse and superimposed voltage under laboratory conditions”, International Journal of Electrical Power & Energy Systems, vol. 115, Feb. 2020.

[3] J. Wu, A. Rodrigo Mor, J. J. Smit, “The effects of superimposed impulse transients on partial discharge in XLPE cable joint”, International Journal of Electrical Power & Energy Systems, vol. 110, Sept. 2019, pp. 497-509.

[4] A. R. Mor, F. A. Muñoz, J. Wu, and L. C. C. Heredia, “Automatic partial discharge recognition using the cross wavelet transform in high voltage cable joint measuring systems using two opposite polarity sensors”, International Journal of Electrical Power & Energy Systems, vol. 117, May 2020.

[5] L. C. C. Heredia, A. R. Mor, and J. Wu, “Method for Recognition of Partial Discharge Signals in Impaired Datasets Using Cumulative Energy Signatures”, International Journal of Electrical Power & Energy Systems, submitted in Jan. 2020.

Conference papers

[1] J. Wu, P. V. M. van Nes, A. Rodrigo Mor, J. J. Smit, "Partial Discharges in XLPE Insulated Cable under Superimposed Transient Voltages". In *IEEE 37th Electrical Insulation Conference (EIC)*, Calgary, Canada, Jun. 2019.

[2] J. Wu, L. C. Castro Heredia, A. Rodrigo Mor, J. J. Smit, "Partial Discharges at Artificial Defects in XLPE Cable Accessories under Superimposed Transients". In *2018 IEEE International Conference on High Voltage Engineering and Application (ICHVE)*, Athens, Greece, Sept. 2018.

[3] J. Wu, H. Jin, A. Rodrigo Mor, J. J. Smit, "Effects of Transients on Breakdown of XLPE Cable Insulation". In *20th International Symposium on High Voltage Engineering (ISH)*, Buenos Aires, Argentina, Sept. 2017.

[4] J. Wu, H. Jin, A. Rodrigo Mor, J. J. Smit, "The effect of frequency on the dielectric breakdown of insulation materials in HV cable systems". In *2017 International Symposium on Electrical Insulating Materials (ISEIM)*, Toyohashi City, Japan, Sept. 2017.

[5] H. Jin, I.-A. Tsekmes, J. Wu; A. Rodrigo Mor, J. J. Smit, "The effect of frequency on the dielectric strength of epoxy resin and epoxy resin based nanocomposites". In *2017 International Symposium on Electrical Insulating Materials (ISEIM)*, Toyohashi City, Sept. 2017.

[6] Khalilnezhad, H., Barakou, F., Kandalepa, N., Wu, J., Wu, L., Popov, M., Steennis, E.F., Wouters, P.A.A.F., Mousavi Gargari, S., Bos, J.A., de Jong, J.P.W., Jansen, C.P.J., Smit, J., and Kuik, R. (2016). Shunt compensation sizing, reliability analysis, and condition monitoring measurements and simulations for an EHV mixed OHL-Cable connection. In *CIGRE*, *C4-304*, Paris, France.

Award

The IEEE Caixin Sun and Stan Grzybowski Best Student Paper Award, for "Partial Discharges at Artificial Defects in XLPE Cable Accessories under Superimposed Transients", In *2018 IEEE International Conference on High Voltage Engineering and Application (ICHVE)*, Athens, Greece, Sept. 2018.

Acknowledgements

I always feel I am so lucky, that I have met many people who are helping, protecting, supporting and guarding me in their own way, in or out of my sight. Without them, I will never be able to become who I am now. At this moment when I am finalizing an important stage of my life, my mind gathers up bits of the past time. Here I want to express my thankfulness to those people.

First of all, I would like to thank my promotor prof. Johan Smit, for accepting me as your last PhD student and guiding me all through my PhD process. You spent a lot of effort on guiding and supervising my work. For that we usually had millions of discussions, which helped me to have a lot of critical thinkings and better understanding of my work. The first time I got challenged in the progress meeting, the first time I presented my work in the conference and the first time I got award, you were always there standing for me and watching me growing up. Not only about work, we also talked about life, news etc. I sincerely feel appreciated that I could have you as my promoter.

Next, I would like to give my great gratitude to my daily supervisor and co-promotor dr. Armando Rodrigo Mor. Armando, forgive me that I don't have enough words to thank you. Without you I wouldn't have completed my PhD work. You always gave me enough space to make mistakes and progress, respect my ideas and support my way of doing research. On the other hand, you were always there whenever I had questions or problems. You reminded me and gave me suggestions on time when I was confused or in a wrong direction. You encouraged me to be confident, to believe myself. I want to become a reliable engineer or scientist as you, so that the society can trust my decisions.

Ir. Paul van Nes, my special thanks to you. I got your support since I started my practical work in the HV laboratory. Especially at the most difficult and critical moment of my PhD work, you decided to help me with my HV tests, even giving up your holiday time. When I was worried about the measurement results, you encouraged me by sharing your experience and your fruits. A million thanks for your effort, your time and caring.

I would like to thank prof. Pavol Bauer for being my promotor. You always kept tracking on my working progress, caring about my working situation and gave me advises. Also, you gave me valuable comments on my work. Thank you for these all.

I would also like to thank prof. dr. ing. R. Plath, prof. dr. ir. F. Garnacho Vecino, dr. ir. Shima Mousavi Gargari and prof. dr. Rob Ross as being the committee members in my PhD defense. Thanks for your time spent on my thesis and all of the comments you provided to me. Especially I want to thank to the latter two. It is a great appreciation that I could get chance to discuss with you in the 380 kV Randstad Cable progress meetings. Thank you for sharing your knowledge, experience and opinions, which brought me a lot of inspirations. Also, many thanks to prof. ir. Peter Vaessen who accepted to be the reverse member. Thank you for your wise comments as well as the fruitful discussions we have ever had. They are really helpful.

I would like to thank all my colleagues in the HV lab. Thank you Radek Heller, Wim Termorshuizen and Remko Koornneef. With your assistance and support, I could finish my experimental works in lab. I would especially like to thank Luis Carlos. You helped me a lot with my tests. Whenever I was stuck and needed help, I can reach you and you were always there helping me patiently or offering me advises. As being friends in life, you believe me, support me and encourage me to go further. You shared so many valuable minds with me. I will always keep them. Thank you so much for your support and caring.

I would like to thank TenneT TSO B.V. for the financial and technical support. Also, I would like to thank dr. Fani Barakou and prof. Peter Wouters from Eindhoven University of Technology, and prof. Fred Steennis from DNV GL. Thank you for all the information and advises you provided to me.

I started to work at DNV GL at the stage that I was finalizing my PhD thesis. Handling work and thesis together was not easy. I want to take this change to express my thankfulness to my DNV GL colleagues, especially Edward Nagel, Ebbo de Meulemeester and Cornelis Plet. You helped me to settle down in my work, and also support me to finish my PhD work.

To lovely Sharmila, you have assisted me on work in every aspect. You are so friendly and enegetic, which always cheered me up. Thank you for what you have done for me.

I want to take this chance to thank dr. Peter Morshuis. You encouraged me to be courageous, to explore the HV world as much as possible. I always keep that in my mind. I admire your professionalism in both HV engineering, and cooking. Thank you very much!

To my awesome colleagues from the HV group, thank you for all the discussions and jokes in and out of working time. Alessandro, we started to share office four years ago and even now. During which time you offered me your help, cares and jokes. Fabio, with your intelligence and wisdom you have shared many ideas and advises with me related to work and other things. Guillermo, working or having fun with you will never be bored. Djurre, you are so open and willing to share, to try new things. I enjoyed listening to your music and talking to you. It is too short time being colleague with you. Thanks to all of you, cool guys, my friends, for all. The same thankfulness goes to other colleagues: Mohamad, Babak, Andreas, Dhanashree. Thank you for your time, your advises and your caring for me!

To my new friends I met after I came to the Netherlands. Joe, my lovely chef, I won't enjoy my PhD life without you, your wonderful food and pictures. Dhiradj, it is always nice talking to you and seeing you enjoy my food. Thanks to all of you for the time you shared with me for cooking, eating, talking or just sharing. Qikai, thank you for introducing this PhD position to me and offering your apartment. Huifei, thank you for helping me on work during my first stage of PhD, and the nice time with you and Pieter in enjoying the life! Lukasz, you have given me many good recommendations and encouragements. Thank you for sharing your wisdom and time with me! Also, I want to thank Alex and Roman for your help and advises, although we even haven't worked together. My sweetest Antonella,

you are the first one who helped me to get familiar with my working environment and brought me to enjoy my life in Delft. You will always be the angel in my heart.

To my old friends, who have accompanied me for a long time and are so important in my life. Yusi, we have known each other for more than 16 years since high school. It must be a magic we are still next to each other in the Netherlands far from our homes, and could help each other. Thank you for supporting me during my difficult times and all the concerns with me. Zhen, how can I express all of my thankfulness to you... Since we met 9 years ago, you have brought so much to my life. You are so kind, considerable, positive and brave. Those are all I want to, am trying to and have learnt from you. You care about me and my life, and always support me with your wisdom and accompany. Thank you! Also, my great thankfulness to my other friends: Lin, Shiliang, Jingxin, Qi, Xiao, Renlin, Yifei, Rui... We spent the most beautiful time for Master. Thanks for all of this!

A big thanks goes to a very special person in my life, Jianning. You are always there no matter what, supporting me both in work and life. You are the kindest person I have ever met. I have learned a lot from you, as being responsible to work, being tolerant to people, being a better person. Thank you for sharing your time and ideas with me, for all you have done for me.

The last but not the least, I want to thank my parents and my family. Thank you for bringing me to the world, for educating me as a strong and kind person, for believing in me and for supporting me endless no matter when, where, what and how. Without you, I couldn’t become what I am now. No matter where I am, I know you are always standing by me, and I will always be there standing by you. Thanks, papa and mama!

Curriculum Vitae

Jiayang Wu was born on 5th August 1988 in Nanjing, China. She received her BSc degree in the department of Electrical Engineering from the Southeast University, Nanjing, China, in 2010. In the same year, she started her Master program in Electrical Engineering, Information Technology and Computer Engineering at RWTH Aachen University of Technology, Aachen, Germany and received her MSc degree in electrical power engineering in 2013. In 2015, she joined the Electrical Sustainable Energy Department at Delft University of Technology, the Netherlands, as a Ph.D candidate. Her research topic is “Effects of Transients on High Voltage Cable Insulation”. Since October 2019, she became a consultant in Transmission and Distribution Technology group in DNV GL, Arnhem, the Netherlands.